Purinergic signalling in osteosarcoma

Luke Tattersall

Thesis submitted in accordance with the requirements of The University of Sheffield for the degree of Doctor of Philosophy.

Department of Oncology & Metabolism

Faculty of Medicine, Dentistry & Health

Date: January 2019

Acknowledgements

The work carried out in this thesis would not have been possible without the help of many people over the last 3 years.

I would like to express my appreciation and gratitude to my PhD supervisors Professor Allie Gartland and Dr Shelly Lawson. Thank you for the opportunity to carry out this research, for all the support, encouragement, advice, guidance, patience, belief in me and everything you have taught me. Thank you for always pushing me forward more, caring about me and my career goals and developing me as a scientist by providing me with all the opportunities available, this has led to many unforgettable life experiences for me.

I would like to thank Dr Karan Shah for his support and everything he has taught me, but mainly for always pushing me hard to progress and develop as a scientist. Professor Dominique Heymann for all his advice and resources for the project. Dr Elena Adinolfi, Professor Francesco Di Virgilio and their lab groups for hosting me in Ferrara Italy. I would also like to thank members of the Gartland Bone Group, SMaRT group and friends within the department of Oncology and Metabolism that have contributed towards having such an enjoyable PhD experience.

I would like to acknowledge and thank the Bone Cancer Research Trust for the funding of the project, and all their hardworking supporters that make this research possible.

My final thanks go to my close friends (particularly Jake and Brad), my girlfriend and my parents Julie and Michael and brothers Josh and Charlie for all their encouragement and support but mainly for listening to me talk endlessly about science over the duration of the PhD.

Statement of Attribution

I, Luke Tattersall, confirm that the work submitted in this thesis is my own work, any information originating from other sources has been indicated. I would also like to acknowledge the following people for their contribution to the data in this project:

Mr Darren Lath for the sectioning of the mice bones and TRAP staining/quantification of them.

Mr Alex Williamson for his assistance with the *in vitro* MNNG-HOS cell work.

Summary

Osteosarcoma (OS) is the most common type of primary bone cancer affecting adolescents and children attributed to rapid bone growth and turnover, it is a rare incurable and often fatal disease. Current treatments include standard chemotherapy, limb salvage surgery or amputation. Survival statistics have remained constant with no advances in treatments options for decades. Patients with metastasis continue to have a poor 5-year survival rate of around 20%. This highlights an urgent need for development of novel therapeutic strategies for the treatment of OS.

Purinergic signalling, involves extracellular nucleotides binding to purinergic receptors and has been found on osteoblasts with different functions including differentiation, apoptosis and bone remodelling. They are also highly expressed on many cancers. ATP is at a high concentration in the tumour microenvironment, yet absent from surrounding healthy tissue. ATP can modify the tumour microenvironment in favour of cancer growth and potentially result in disease progression. The P2X7 receptor (P2X7R) is a ATP gated ion channel which has received an increasing amount of attention due to evidence of its overexpression and function in carcinogenesis of a range of different tumours. Studies exploring the role of the P2X7R in OS are limited.

In this thesis the hypothesis that the P2X7R and related splice variants play a role in OS progression and metastasis and it's potential as therapeutic target has been tested both *in vitro* and *in vivo.*

Contents

List of Figures

List of Tables

List of Abbreviations

ALP	**Alkaline phosphatase**
AUC	**Area under the curve**
BBG	**Brilliant blue G**
BzATP	**Benzoyl ATP**
CRISPR	**Clustered regularly interspaced short palindromic repeats**
CT	**Computed tomography**
Da	**Daltons**
DMSO	**Dimethyl sulfoxide**
EDA	**Experimental design assistant**
EDTA	**Ethylenediaminetetraacetic acid**
FBS	**Foetal bovine serum**
GPCRs	**G protein coupled receptors**
HBSS	**Hank's balanced salt solution**
HDMTX	**High-dose methotrexate**
IHC	**Immunohistochemistry**
IP	**Intraperitoneal**
KN-62	**1-N,O-bis(5-isoquinolinesulfonyl)-N-methyl-l-tyrosyl-4-phenylpiperazine**
LDH	**Lactate dehydrogenase**
MAP	**High-dose methotrexate, doxorubicin and cisplatin**

MDT	**Multidisciplinary team**
MMP	**Matrix metalloprotease**
MNNG	**N-methyl-N'-nitro-N- nitrosoguanidine**
MSC	**Mesenchymal stem cells**
MTS	**[3-(4, 5-dimethylthiazol-2-yl)-5-(3-carboxymethoxyphenyl)-2-(4-sulfophenyl)-2H-tetrazolium**
oATP	**Oxidized ATP**
OPG	**Osteoprotegerin**
OS	**Osteosarcoma**
P2X7R	**P2X7 receptor**
PBS	**Phosphate buffer saline**
PBST	**PBS-tween**
PCR	**Polymerase chain reaction**
PDOX	**Patient-derived orthotopic xenograft**
PET	**Polyethylene terephthalate**
PMS	**Phenazine methyl sulphate**
PPADS	**Pyridoxal phosphate-6-azophenyl-2-4-disulfonic acid**
qPCR	**Quantitative PCR**
RANKL	**Receptor activator of nuclear factor Kappa-B ligand**
Rb	**Retinoblastoma protein**
ROI	**Region of interest**

RT	**Reverse transcription**
RT-ve	**Reverse transcription negative**
RT+ve	**Reverse transcription positive**
TBE	**Tris-borate-EDTA**
TRAP	**Tartrate-resistant acid phosphate**
VEGF	**Vascular endothelial growth factor**
ΔCT	**Delta cycle threshold**

Chapter 1 – Introduction

1.1 Introduction to OS

Cancer defines a diverse range of different diseases with various traits, prognosis, treatment regimens and survival outcomes. Although diverse, a central aspect of cancer biology is that they must have common “hallmarks” that facilitate growth and metastasis. Six essential hallmarks were originally described, these include: self-sufficiency in growth signals, Insensitivity to growth-inhibitory (antigrowth) signals evasion of programmed cell death (apoptosis), limitless replicative potential, sustained angiogenesis, and tissue invasion and metastasis (Hanahan & Weinberg, 2000). After further progression in the cancer field four hallmarks were then added to include: reprogramming of energy metabolism, evading immune destruction, genomic instability and tumour promoting inflammation (Hanahan & Weinberg, 2011). These hallmarks provide information about the underlying complex process that cancer cells acquire and have aided in the development of effective therapeutics. As many different cancers exist they are determined based on their tissue of origin, and whether they are benign or malignant. OS is a rare and orphan malignant tumour of mesenchymal origin with highly heterogeneous subtypes. OS mainly affects children and adolescences and has two peak incident ages being described at 18 and 60 years of age with males affected more than females (Mirabello *et al*., 2009). In 80% of cases OS affects the limbs (Figure 1.1), in particular the long bones, which can be attributed to rapid bone growth and turnover during adolescence (Savage & Mirabello, 2011). The remainder of cases occur in the axial skeleton (Longhi *et al.,* 2006) and in rarer cases the jaw (Baumhoer *et al.,* 2014) or the hand (Pradhan *et al.,* 2015). Worldwide incidence occurs at a rate of approximately 1-5 cases per million people per year (Mirabello *et al.,* 2009) and these tumours represent < 0.2% of malignant tumours registered in the EUROCARE database (Stiller *et al*., 2001).

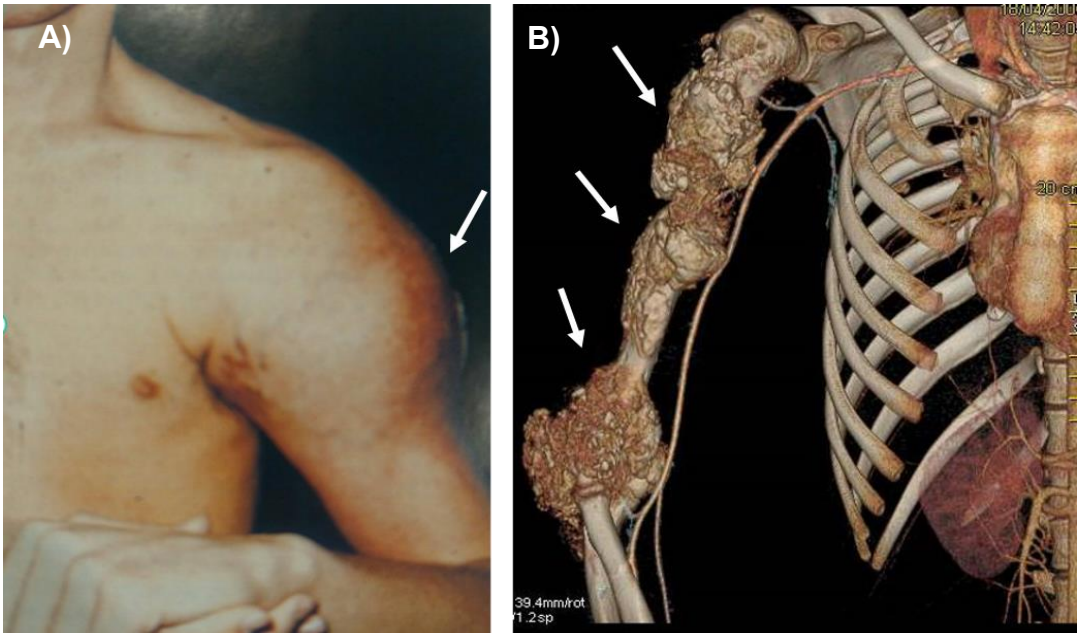

Figure 1.1: A palpable OS tumour occurring in the limb of a patient. A) An OS of the left proximal humerus showing a prominent tumour palpation in a 21-year-old male. Image adapted from Atlas of Diagnostic Oncology (Skarin, & Canellos, 2002) used with permission under the terms of the creative commons attribution licence (CC-BY). **B)** A computer tomography (CT) scan showing an OS tumour. Image courtesy of Professor Dominique Heymann (Sheffield University, UK, INSERM, France) from the cover of Bone Cancer (Ed Heymannn D, academic press 2010) used with permission. Arrows indicate the tumour palpation and the outgrowth of the tumour mass in the bone.

OS cells originate from mesenchymal stem cells (MSC) of the osteoblastic differentiation pathway, and as such OS cells express typical markers of osteoblast cells (alkaline phosphatase, osteocalcin and/or bone sialoprotein) and the resultant tumour is characterized by the presence of a mineralized osteoid-type matrix produced by the OS cells. Several OS subtypes exist (Figure 1.2) and the type depends upon at what stage of differentiation the oncogenic event occurs (Heymann & Rédini, 2011). An osteoblastic subtype is seen with the most differentiated cells. In this case, OS cells produce large quantities of osteoid matrix. This is organized in a complex trabecular structure, often external to the normal bone and described as a “sunburst” pattern (due to expansion of the tumour, mineralization and formation of periosteal spicules or “streamers”) when seen on radiography. A chondroblastic OS subtype results from mutations in less differentiated cells, where OS cells produce a more cartilaginous matrix in addition to the osteoid matrix as is reminiscent of endochondral

ossification. A fibroblastic OS arises from the least differentiated OS cells and gives a morphology reminiscent of fibroblastic matrix tissue

1.2 OS aetiology and risk factors

Whilst between 10% and 15% of OS cases have an identifiable potential cause, the majority of cases are of unknown aetiology. Certain risk factors have been suggested including bone infarct, osteochondroma, Paget's disease, and previous irradiation (Gerrand *et al.,* 2016). The rapid bone growth and turnover that occurs during adolescence, especially at the metaphysis of long bones, may explain the association with the frequent occurrence of OS at these sites and stages of development. Tall stature has also been suggested to be a predisposing factor, with OS patients being significantly taller than the average population, particularly those with OS occurring in the femur, the largest and quickest growing bone, compared with occurrence at other sites (Cotterill *et al.,* 2004).

1.3 Inherited disorders associated with OS

A number of genetic risk factors for OS are known, with several cancer predisposing

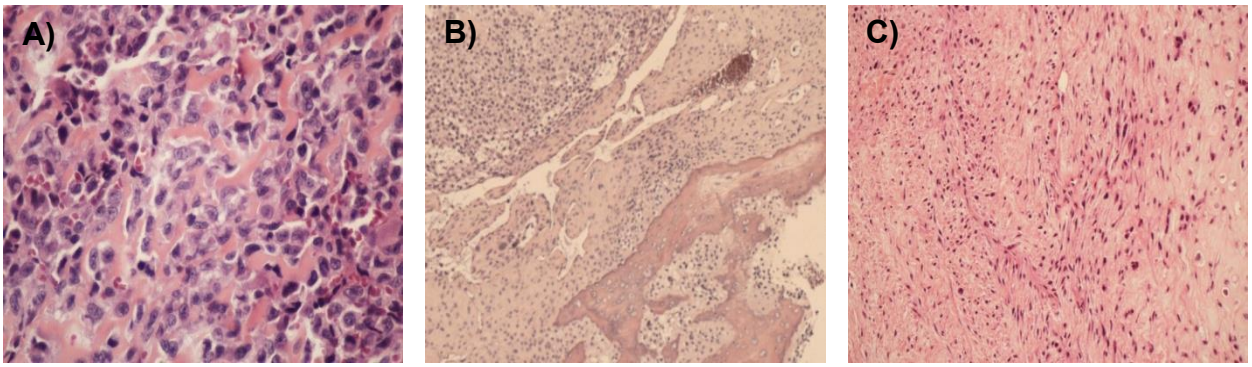

Figure 1.2: The three main histological subtypes of conventional OS. A) Osteoblastic OS **B)** Chondroblastic OS **C)** Fibroblastic OS. Images courtesy of Dr M.F. Heymann (Institut de Cancerologie, Nates, France) used with permission.

syndromes and inherited disorders being associated with increased rates of OS (Table 1.1). Li-Fraumeni syndrome (so named in recognition of the researchers who characterized the families with high rates of sarcomas and other cancers in 1969 (Li & Fraumeni, 1969) is caused by an autosomal dominant germline mutation in *TP53* which encodes the p53 protein. p53 is a well-known regulator of cell proliferation and apoptosis-induced cell death, and as such is critical for normal cell growth. Mutations

in *TP53* result in the loss of its tumour suppressor function and thus oncogenic transformation. Many, but not all, OS cases have a mutation in *TP53,* which is thus considered a risk factor. However, *TP53* mutations do not correlate with clinical outcome in high grade OS and cannot effectively be used as a prognostic marker for metastasis development or response to chemotherapy (Wunder *et al.,* 2005). Hereditary retinoblastoma is caused by a mutation in *RB1*, the gene that encodes Retinoblastoma protein (Rb). Rb interacts with E2F transcription factors to regulate the cell cycle and is also involved in normal differentiation processes. Mutation in *RB1* results in loss of the tumour suppressor activity and its inactivation is a common characteristic of a range of cancers (Weinberg, 1995). In patients with *RB1* mutations OS is the most commonly occurring tumour, aside from retinoblastoma itself. A 500-fold increase is observed in the risk of OS development in people with *RB1* mutations compared to the general population. Aside from inherited inactivation, sporadic cases of OS mutations in *RB1* occur in 60% of cases (Thomas *et al.,* 2001). A meta-analysis of 12 studies with 461 patients concluded that *RB1* mutations can be a prognostic marker for OS, as loss of Rb correlated with an increase in metastasis and mortality, with a decrease in response to chemotherapy (Ren & Gu, 2015). These inherited disorders, as well as the others listed in Table 1.1, which include three germline mutations in DNA helicase genes, only explain a very small proportion of the incidence of OS. Indeed, the vast majority of OS cases are complex and have inconsistent genetic alterations. Known tumour suppressor genes undergo deletions and mutation events, whilst for established oncogenes gains of portions of chromosomes are found in OS (Martin *et al.,* 2012). Although the majority of these chromosome lesions in OS occur in known cancer genes, they can still contribute towards understanding why OS can occur.

Table 1.1: Common genetic conditions in which OS can occur.

Genetic conditions predisposing to OS development	Chromosome location	Abnormality
Li-Fraumeni syndrome	17p13.1	Rearrangement
Hereditary retinoblastoma	13q14.2	Deletion
Rothmund-Thomson syndrome	8q24.3	Rearrangement
Bloom syndrome	15q26.1	Rearrangement
Werner syndrome	8p12	Rearrangement
Rapadilino	8q24.3	Rearrangement
Diamond–Blackfan anaemia	Numerous	Deletion/Rearrangement

1.4 Symptoms, diagnosis and treatment

The most common symptom of OS is pain, with other symptoms such as swelling/lumps and tenderness, stiff joints, an unexplained limp and bone fractures occurring later (Taran *et al.,* 2017). Patients usually only seek medical attention after an event such as a trauma or vigorous exercise. Given that the annual incidence of OS is 7.9 per million (~380 people diagnosed in England per year), the likelihood of a general practitioner ever seeing a patient with OS in their working life time is extremely low (Gerrand *et al.,* 2016). This often means that delays occur in the diagnosis of OS and the duration of symptoms is on average 3 months, although patients can have persisted with symptoms for several months or even years before a diagnosis is made. A diagnosis can be missed by GPs as pain is attributed to growing pains or trauma such as a sprain or fracture. However, pain that gradually increases in intensity, and bone pain at night should always be considered as “red flag symptoms” that require investigation for potential OS. A variety of procedures should be used for diagnosis starting with a plain X-ray. Any feature of bone destruction, bone formation and periosteal or soft tissue swelling are suggestive of OS, with urgent referral to a bone multidisciplinary team (MDT) and magnetic resonance imaging and CT scans

subsequently required (Oryan *et al.,* 2015). However, a normal x-ray cannot definitively rule out OS and further investigations should also be done following red flag symptoms. Additionally, in older patients, more extensive investigations with a whole body positron emission tomography scan often used to rule out metastatic bone cancer. In order for a definitive OS diagnosis to be made, an invasive biopsy must be performed by an experienced oncologist or pathologist, with histology performed on the sample to evaluate stage and prognosis. Different biopsy types include: fine-needle aspiration, percutaneous core-needle biopsy and incisional biopsy. The choice of which to use is dependent upon tumour size and location (Errani *et al.,* 2013). Although there is some dispute regarding which biopsy is the optimal to diagnose bone cancers, a recent study concluded that percutaneous core needle biopsy should be the first line diagnostic test when OS is suspected. This is where a section of tissue is removed to be examined as oppose to fine needle aspiration which only removes a small amount of cells and an incisional biopsy which requires open surgery. The study found percutaneous core needle biopsy had a 93% sensitivity, 100% specificity, 100% positive predictive value and 99.9% negative predictive value in 73 patients (Taupin *et al.,* 2016). Percutaneous core needle biopsies present numerous advantages over open surgical biopsies which can have a range of complications such as seromas, infections and bone fractures (Taupin *et al.,* 2016; Errani *et al.,* 2013). In addition to a patient's full history and imaging, biochemical laboratory testing of blood and urine is done. It is generally normal, with the exception of raised alkaline phosphatase (ALP), lactate dehydrogenase (LDH) levels and erythrocyte sedimentations rates which are of prognostic value in OS.

Treatment options and survival rates for OS have not changed very much in the past 30 years unfortunately. Within the UK, OS patients should be referred to and seen by a fully accredited bone sarcoma MDT under the 2-week wait pathway. Treatment options should then be discussed by the MDT with a surgeon, radiologist, pathologist and oncologist (Gerrand *et al.,* 2016). In nearly all cases, surgery is required to remove the primary tumour, surgical intervention should aim to remove the tumour completely, with wide margins. Whereas amputation was the only surgical option 30 years ago, limb salvage surgery has now become possible through technological and surgical advancements. Limb salvage surgeries include endoprosthetic replacement, biological reconstruction using allografts or autografts, or a combination of both. For

tumours around the knee (in the distal femur or proximal tibia) rotationplasty can be used (Ando *et al.,* 2013). This is where the affected bones are removed, the lower part of the tibia and ankle preserved, rotated through 180 degrees and attached to the femoral stump to function as a “knee” joint. Whilst this type of procedure is relatively rare, and has major cosmetic and psychological disadvantages, it does offer more functional advantages to the growing child, which have been shown to extend into adulthood (Benedetti *et al.,* 2016, Potter, 2016).

In addition to curative surgery, chemotherapy-based treatments are also given to OS patients. This regimen remains largely the same as the first adjuvant chemotherapy treatment used in 1970, with Doxorubicin and Methotrexate being the main drugs of choice, with Cisplatin and Ifosfamide later added (Ando *et al.,* 2013). This toxic cocktail of DNA intercalators, DNA/RNA synthesis inhibitors and alkylating agent improved the 5-year disease-free survival of OS patients to over 70% (Bacci *et al.,* 2002). Further attempts were made in the late 1970’s to improve treatment by the introduction of neoadjuvant chemotherapy (chemotherapy before surgery). As well as reducing the tumour burden, this gave the perceived advantage of being able to histologically determine the response of the tumour to the chemotherapy, so that post-operative therapy could be tailored. Since then, neoadjuvant therapy has become the standard treatment for OS patients – with the UK guidelines indicating 10 weeks of neoadjuvant induction chemotherapy with high-dose Methotrexate (HDMTX), Doxorubicin and Cisplatin (MAP) before surgical intervention, followed by adjuvant chemotherapy (Gerrand *et al.,* 2016). However, the actual benefit of this regime is not proven. In a controlled study performed to formally assess whether neoadjuvant chemotherapy in addition to surgery and adjuvant chemotherapy was better than surgery and adjuvant surgery alone, no significant difference was found for event-free survival rates between treatment groups (Goorin *et al.,* 2003). The advantage of this type of therapy is that there is often a rapid improvement of symptoms and earlier treatment of micro-metastatic disease. Most OS patients are thought to have microscopic metastasis at the time of diagnosis, as evidenced by the low survival rate previously observed in patients without chemotherapy treatment, and the fact that up to 90% develop recurrent metastasis when treated with surgical resection (Taran *et al.,* 2017). Unfortunately, there are numerous side effects to the chemotherapy used in OS such as: alopecia, hypersensitivity reactions, nausea, vomiting, immunosuppression,

nephrotoxicity, neurotoxicity and cardiomyopathy (Minotti *et al*., 2004, Florea & Büsselberg, 2011). Additionally, there could be an issue with regards to future fertility, affecting both males (Schrader *et al.,* 2001) and females (Blumenfeld, 2012) and which is often overlooked or not discussed.

1.5 Prognosis

Whilst it is difficult to predict a patient's response to treatment, the stage, location and metastasis of the OS at time of diagnosis are major prognostic factors and determine the grade of the tumour. The higher the grade the lower the chance a patient will live disease-free beyond 5 years. Metastasis is a major clinical problem and refers to the spread of cancer cells to distant organs, and can be present at diagnosis. It is a complex process of events which can be divided into different stages: invasion through extracellular matrix, invasion into blood and lymphatic vessels, survival in the circulation or lymphatics, extravasation into secondary distant tissue and colonisation and survival in the new environment. Many drug successfully target the primary tumour but not the disseminating metastatic cells which have increased heterogeneity (Chiity *et al*., 2018, Zhu *et al.,* 2013, Posthumadeboer *et al.,* 2011, Hanahan & Weinberg, 2011). Obvious overt metastasis at presentation, tumours located in the proximal extremities or in the axial skeleton, high serum levels of ALP and LDH, old age and high body mass index are all associated with poor prognosis. Recurrence of OS reduces the long-term survival rates to ~30%, with early relapse and distant non-lung metastases associated with the poorest prognosis (Gelderblom *et al.,* 2011). Another indicator of poor prognosis is chemoresistance, a major issue in OS due to heterogeneity of the disease as well as the multitude of mechanisms that have been reported to mediate chemoresistance in OS cells (He *et al.*, 2014). In order to improve prognosis and overcome some of these issues in OS, a number of laboratory based pre-clinical models have been developed to recapitulate the OS disease. These can be utilised both *in vitro* and *in vivo*.

1.6 Pre-clinical OS models

1.6.1 *In vitro* models

Representative models of OS are an important tool that have contributed a substantial amount of knowledge about a wide range of OS characteristics and are often used as

the first step when trying to identify new therapeutic targets. Both human and murine *in vitro* immortalized cell lines exist, originally isolated from OS patients and murine OS models respectively; these cell lines have been extensively characterized and used for many years (Table 1.2).

Table 1.2: Commonly used human OS cell lines and their characteristics.

Cell line	Year	Gender	Age	Phenotype	ALP activity	Tumourgenicity *in vivo*	Pulmonary metastasis	References
U2OS	1964	Female	15	Very early osteoblast/ fibroblastic	Low	Low	No	(Pautke *et al.,* 2004, Orimo *et al.,* 2008, Pontén & Saksela, 1967)
SaOS-2	1973	Female	11	Mature osteoblast	High	Low	Rare	(Pautke *et al.,* 2004, Fogh *et al.,* 1977, Czekanska *et al.,* 2012)
MG-63	1977	Male	14	Immature osteoblast	Low	Low	No	(Clover & Gowen, 1994, Heremans *et al.,* 1978, Czekanska *et al.,* 2012)
HOS-Te85	1971	Female	13	Immature osteoblast	Low	No	No	(Clover & Gowen, 1994, McAllister *et al.,* 1971)
KHOS/NP	1975	Female	13	Osteolytic/osteogenic	Low	Yes	Yes	(Rhim *et al.,* 1975b, Uluçkan *et al.,* 2015)
MNNG-HOS	1975	Female	13	Osteolytic/osteogenic	Low	Yes	Yes	(Rhim *et al.,* 1975a, Uluçkan *et al.,* 2015)
143B	1979	Female	13	Osteolytic	Low	Yes	Yes	(Campione-Piccardo *et al.,*1979).

1.6.2 Human derived cell lines

The first human cell line used was U2OS in 1964, isolated from the tibia of a 15-year-old female (Pontén & Saksela, 1967) and was followed by the HOS-Te85 OS cell line derived from a 13 year old female in 1971 (McAllister *et al.,* 1971), the SaOS-2 cell line derived from an 11 year old female (Fogh *et al.,* 1977) and the MG-63 cell line derived from a 14 year old male (Heremans *et al.,* 1978). The MNNG-HOS, KHOS and 143B OS cell lines are all derivatives of the HOS-Te85 parental OS cell line. MNNG-HOS OS cells were created by chemically transforming HOS-Te85 OS cells with 0.01 µg/mL N-methyl-N'-nitro-N- nitrosoguanidine (MNNG) (Rhim *et al.,* 1975a). The KHOS OS cell line was formed by transforming the HOS-Te85 parental OS cell line with the Kirsten murine sarcoma virus (Rhim *et al.,* 1975b, Carloni *et al.,* 1988) and the 143B OS cell line is a K-Ras oncogene transformed HOS-Te85 derivative (Campione-Piccardo *et al.,*1979). When comparing *in vitro* characteristics of these HOS derivatives, the 143B OS cell line has the highest rate of proliferation and cell migration, is the least adherent, and forms the most colonies in a type I collagen suspension. The MNNG-HOS OS cell line is not as aggressive as 143B, but is more aggressive than the HOS-Te85 OS parental cell type, which displays the least aggressive characteristics (Luu *et al.,* 2005).

Although originating from an OS patient, SaOS-2 OS cells have been extensively used as an *in vitro* model of “normal” osteoblast behaviour and represent a mature osteoblast phenotype with high ALP activity (Czekanska *et al.,* 2012). Derivatives of SaOS-2 OS cells have different characteristics and are known as SaOS-LM2 to SaOS-LM7; these were isolated from the lung metastasis of SaOS-2 OS cells previously injected into the tail vein of mice (Jia *et al.,* 1999) and therefore represent a metastatic phenotype. When comparing the parental SaOS-2 OS cell line to the SaOS-LM5 and SaOS-LM7 metastatic variants, the derivatives have a similar level of ALP activity and response to chemotherapeutics, but are less adhesive and have smaller morphology with higher nuclear instability which likely contributes to their metastatic phenotype (Muff *et al.,* 2007).

1.6.3 Rodent derived cell lines

Most murine-derived cell lines originate from spontaneous mouse tumours; the Dunn cell line is an osteogenic cell line with high ALP activity (Muff *et al.,* 2012) and was established from a tumour in the tail of a C3H mouse (Dunn & Andervont, 1963). LM8 (lung metastatic variant 8) is derived from Dunn cells and was developed by inoculating the Dunn parental cell line into the tail vein of C3H mice and collecting the pulmonary metastasis; these cells were then grown in culture and again injected into the tail vein of C3H mice. This *in vivo* passage of the cells was repeated 8 times until lung metastasis occurred with 100% efficiency in the mice. When the parental Dunn and LM8 cells were then compared *in vitro,* the results demonstrated that LM8 cells grew faster, and had higher vascular endothelial growth factor (VEGF) expression, matrix metalloprotease (MMP) activity, invasiveness, and ALP activity (Asai *et al.,* 1998). Further cell lines were developed from a spontaneous OS originating in the distal femur of an 894-day-old female BALB/c mouse. Thirty-six single cell clones were grown *in vitro*, from which 5 cell lines were established (known as K7, K8, K12, K14 and K37). These were selected to be representative of the different cells growing in culture based on morphology. Further analysis demonstrated that there were additional differences as K7 cells had the highest rate of growth, while K12 cells had the largest ALP activity (Schmidt *et al.,* 1988). A derivative of the K7 cell line called K7M2 was established by injecting the K7 parental cell line into the proximal tibia of a BALB/c mouse and collecting the pulmonary metastasis. This was then implanted again into the tibia of a mouse and collected, and the "*in vivo* passaging" was repeated until establishment of the highly metastatic cell line (Khanna *et al.,* 2000).

The MOS-J OS cell line was established from a spontaneous chondroblastic OS from the right femur of a C57BL/6J mouse. This cell line displays features *in vitro* which are characteristics of osteoblasts, for example high ALP activity and calcium deposition along with the ability to promote osteoclast differentiation (Joliat *et al.,* 2002).

Unlike the previously discussed murine cell lines, rat OS cell lines were predominantly established through radiation exposure. One of the most common rat OS cell lines UMR-106 was developed through the serial injection of ^{32}-P into Sprague-Dawley rats (Martin *et al.,* 1976). UMR-106 cells are an osteogenic cell line with osteoblast

morphology, and display high ALP activity and adenylate cyclase activation in response to parathyroid hormone (Partridge *et al.,* 1983).

1.6.4 Advantages and limitations of *in vitro* OS models

Immortalized cell lines possess a range of advantages; they have been used for a long period of time and are able to be stored frozen, enabling generations of researchers to continue vital *in vitro* research across various laboratory groups. They are relatively cheap, don't have any ethical considerations and can be manipulated to cover a range of experimental conditions precisely as intended, e.g. regulation of temperature, pH and oxygen levels. Additionally, individual characteristics of the OS cell lines (e.g. migration, invasion, gene expression, and angiogenesis) can be investigated either alone or in combination with other constituents of the tumour microenvironment such as the cell matrix or interactions with other cell types. A final advantage is that they decrease the use of animals used for research purposes.

However, comprehensive *in vitro* modelling of a complicated disease like OS is limited. This is due to constant progression and changes caused by intricate interactions with various components of the bone and tumour microenvironment – *in vitro* cell lines fail to recapitulate this. Indeed the SaOS-2 derived LM7 and LM2 cell lines display a poor correlation of gene expression *in vitro* compare to *in vivo* (Lisle *et al.,* 2008). Additionally, there is a high chance of genetic diversity within a cell population due to cells being in culture for several years leading to differences in results across the years and even across laboratories. Finally, there are additional considerations for *in vitro* cell use, for example, contamination can occur easily with bacteria, mycoplasma, or other cell lines, again affecting the results. Therefore, whole animal models of OS are ultimately needed.

1.6.5 *In vivo* OS models

Animal models provide substantial information towards understanding OS behaviour and progression along with the ability to test pre-clinical compounds as potential new therapeutics. An animal model must therefore be representative of the course of the OS disease; this has remained challenging as OS is complex and diverse, and its pathology is not completely understood. No single OS model fully represents the clinical aspects of the disease and a variety of different approaches have been used

to model OS including: spontaneous cases induced through animal exposure to radiation, human and murine cell injection, xenotransplantation, and genetically modified mouse models (Guijarro *et al.,* 2014, Janeway & Walkley, 2010). Early models used techniques that involved implanting radiation into animals. For example, in the early 1970's ^{32}P-impregnated polyvinyl chloride discs were inserted into the distal femoral metaphysis of rats, but only a 28% incidence rate occurred after 18 months (Cobb, 1970). The process of using radiation has various limitations: the optimum dose for a suitable time period that induces OS is hard to establish, too low a dose doesn't have a high enough incidence, whilst multiple OS tumours in different and unpredictable locations occur with too much radiation (Cobb, 1970).

1.6.6 Genetically engineered murine models of OS

Transgenic mouse models can be designed to demonstrate and study a genetic initiating and driving event for a disease. However, in the case of OS, a genetically engineered model may not fully replicate the genetic diversity seen in OS, although this type of model does demonstrate characteristics similar to human OS. One of the earliest transgenic models of OS is the c-*fos* overexpressing mouse; c-*fos* is important in a variety of cell processes such as cell growth, differentiation, transformation, and regulation of specific gene expression. Mice lacking c-*fos* expression develop osteopetrosis, however, c-*fos* is also considered a proto-oncogene (Wang *et al.,* 1995) and is a target for transcriptional stimulation by p53 (Elkeles *et al.,* 1999). Overexpression of c-*fos* in osteoblast cells led to OS with a 100% success rate in the founder mice. The cells lines established from the tumours express high levels of type I collagen, ALP, and osteopontin/2ar however, osteocalcin/BGP expression was either low or absent (Grigoriadis *et al.,* 1993). Since this period, other transgenic models have been developed that capitalize on the role that loss of function of p53 and Rb play in OS pathogenesis. Transgenic mice models were developed in Osterix-Cre mice where conditional deletion of p53 or Rb alleles lead to OS pathogenesis with similar characteristics to human OS such as gene expression signatures, histology, and metastatic behaviour (Walkley *et al.,* 2008).

1.6.7 Human xenograft murine models of OS

Various human OS cell lines are capable of forming OS tumours *in vivo* in immune-deficient mice (a lack of immune system being required to prevent the rejection of the human cells) using different inoculation sites and techniques. The first study to asses HOS-Te85, MNNG-HOS and 143B OS cells using intratibial injection found graded difference between the cell lines. HOS-Te85 OS cells were both none tumourigenic and none metastatic, MNNG-HOS OS cells were tumourigenic with tumours being predominantly osteolytic and showing some pulmonary metastasis. The 143B were the most aggressive being both tumourigenic, again with tumours being predominantly osteolytic, and displaying high levels of pulmonary metastasis (Luu *et al.,* 2005). SaOS-2 cells tumourigenicity can vary, but when tumours do form they have an osteoblastic phenotype (Gvozdenovic *et al.,* 2013). The method of injection used can affect the growth of the cells, for example when injected subcutaneously or intramuscularly no tumours occur (Mohseny *et al.,* 2011), however, when injected with an intratibial injection in BALB/c nude mice, tumours will form (Lin *et al.,* 2014).

Within our laboratory a paratibial injection of OS cells is utilized. This procedure scratches the surface of the tibia just before injection of the cells close to the periosteum.

1.6.8 Syngeneic murine models of OS

Of the previously discussed murine OS cell lines, many are used as *in vivo* models (Table 1.3), and are predominantly divided into the parental cell line and its more metastatic derivative. The K7 cell line, when injected either paratibially or intraosseously develops osteolytic tumours with rare pulmonary metastasis (Schmidt *et al.,* 1988), whilst its derivative, K7M2, forms pulmonary metastasis in 90% of mice (Khanna *et al.,* 2000). The Dunn cell line and its derivative LM8, both form primary tumours when injected either subcutaneously, intraosseously or intravenously; however, the Dunn cell line only forms micrometastases whereas the LM8 is highly metastatic in 100% of mice (Dunn & Andervont, 1963; Asai *et al.,* 1998). The MOS-J cell line displays a chondroblastic OS subtype and forms primary tumours when injected paratibially or intraosseously with an osteogenic phenotype (Joliat *et al.,*

2002). Intramuscular injection of 4×10^6 MOS-J cells results in tumours in contact with the tibia approximately 8 days later (Gobin *et al.,* 2014).

The only commercially available rat OS cell line that is capable of forming tumours *in vivo* is UMR-106. When 1×10^6 UMR-106 cells are injected directly into the rat femur, there is a 100% yield of tumour formation and pulmonary metastasis. Histologically the tumours from the UMR-106 cell line represent a poorly differentiated OS (Yu *et al*., 2009).

Table 1.3: Commonly used rodent OS cell lines and their characteristics.

Cell line	Animal	Year	Phenotype	Tumourgenicity *in vivo*	Pulmonary metastasis	References
Dunn	Mouse	1963	Osteogenic	Yes	Yes/Rare	(Dunn & Andervont, 1963)
LM8	Mouse	1998	Osteogenic	Yes	Yes	(Asai *et al.,* 1998)
K7	Mouse	1988	Osteolytic	Yes	Yes/Rare	(Schmidt *et al.*, 1988)
K7M2	Mouse	2000	Osteolytic	Yes	Yes	(Khanna *et al.,* 2000)
MOS-J	Mouse	2002	Chondroblastic	Yes	Yes	(Joliat *et al.,* 2002)
UMR-106	Rat	1976	Osteogenic	Yes	Yes	(Martin *et al.,* 1976) (Partridge *et al.*, 1983)

1.6.9 Canine models of OS

OS is the most frequent bone tumour in dogs with incidence rate 27 times higher than in humans (Simpson *et al.,* 2017) and in particular in large breeds such as St. Bernard's and Rottweilers (Misdorp, 1980). Human and canine OS have many similarities: they share the same environmental factors, males are affected more often

than females, it mainly occurs in the long bones, metastasis to the lungs occurs, the pathogenesis is unknown, and treatment regimens are similar (Rowell *et al.,* 2011). Canines have previously been used in OS research as they were originally used in clinical trials on limb salvage techniques, and many of those techniques developed are now commonly used in humans (Rowell *et al.,* 2011). Additionally, a canine cell line called D-17 is commercially available and was derived from the lung metastasis of a poodle in 1969 (LaRue *et al.,* 1989). More recently, researchers, veterinary practitioners and dog owners are taking advantage of the fact that naturally occurring OS in dogs is closely related to human OS. Owners tend to be heavily invested in their pet's wellbeing and they often seek the best treatments for their pets, should they be diagnosed with OS. Thus, canine OS can be used as a valid clinical model for new therapeutics, with the potential for adequately sized clinical trials to be performed due to the large population sizes (Fenger *et al.,* 2014).

1.6.10 Zebrafish models of OS

Results of sequencing of the zebrafish genome showed that approximately 70% of human genes have at least one obvious zebrafish orthologue and can therefore model various diseases (Howe *et al.,* 2013). This combined with the ability to easily and rapidly produce transgenic zebrafish models means that they are an attractive model, and have increasingly been used in the cancer research field to complement murine and *in vitro* models. In addition, the use of zebrafish to study bone development and disease has dramatically increased in recent years and has proven important for validating candidate human disease genes (Luderman *et al.,* 2017; Spoorendonk *et al.,* 2010).

Zebrafish models have a number of advantages: studies involving zebrafish embryos have fewer ethical implications, are very inexpensive, and are able to produce hundreds of embryos in one mating, which grow fast and can be easily imaged due to transparency or with fluorescent reporters. The main disadvantages of zebrafish models are due to problems with sectioning tissue due to size, a lack of antibodies to their proteins, and leakage of injected cells (Brown *et al.,* 2017).

Development of zebrafish models to study OS are limited and are still emerging, one reason for this is due to the high genetic variability of the disease, meaning a

transgenic strain is difficult to achieve. The effects of MNNG, which was used to transform HOS-Te85 OS cells, on tumour induction in different ages of zebrafish demonstrated the zebrafish were more sensitive when treated as embryos rather than when older, and MNNG predominantly produced tumours of mesenchymal histology including chondromas and various sarcomas except OS (Spitsbergen *et al.,* 2000). More recently, parental mouse mesenchymal stem cells (MSCs) or transformed oncogenic MSCs, which are more comparable to OS, were injected into zebrafish and whole genome expression analysis was performed. The results from the zebrafish embryo experiments complemented the earlier *in vivo* mice studies and showed that angiogenesis and migration-related genes were upregulated in the transformed MSCs, further validating the zebrafish as a model for OS (Mohseny *et al.,* 2012).

1.6.11 Advantages and limitations of common *in vivo* OS models

In vivo approaches used to model OS have various advantages over *in vitro* cell lines, the main advantage being that the *in vivo* model provides a more representative environment, as it involves a living, integrated system. The *in vivo* approach allows interactions with other components of the host and tumour microenvironment to be involved rather than a single cell line, which can affect results and response to therapeutics. Disadvantages of *in vivo* models include ethical considerations, high costs compared to *in vitro* cell work, and a higher level of technical skill required to perform the studies.

Within the *in vivo* approaches previously discussed, there are several advantages and limitations. Human xenograft murine models form OS in a short time frame and are reproducible across many different laboratories. However, they use cell lines, which are genetically similar, whereas OS in patients is a highly diverse disease. Human xenografts are also performed in immunocompromised mice and therefore do not recapitulate the immune response and are less useful for immunoncology research. Syngeneic models have the advantage of having the host and tumour cells of the same species, with a functional immune response providing a realistic environment. However, results from studies of murine cell lines are often difficult to translate to humans, and the results can be controversial and/or opposing (Dass & Choong, 2007 Piperno-Neumann *et al.,* 2016).

1.6.12 Patient-derived orthotopic xenograft (PDOX) murine model of OS

PDOXs are a novel preclinical model of OS. The technique uses patient-derived tumour samples and surgically grafts them to an immunocompromised mouse, which then develops into an OS model. Development of one OS PDOX model used tissue from a 17-year-old female with OS of the right femur, which then relapsed 24 months after the initial diagnosis with new tumours in the right tibia, both lungs and the mediastinum. The xenograft was established by drilling into the tibia of BALB/c nude mice and inserting a 1 mm^3 tumour fragment into the bone marrow. The resultant tumour was then passaged in mice a further 2 times; during this *in vivo* passaging, increased tumourgenicity was observed, as the time to tumour development reduced from 40 days to 20 days. The patient tumour was also grown in culture to develop a primary cell line called OS-RH-2011/5, which was similarly passaged into mice twice, with 100% tumour take at 2 weeks (Blattmann *et al*., 2015). When the genetic and histological parameters of the xenograft, primary cell line and initial tumour were analysed and compared, they were found to display similarity to each other and to the initial patient's tumour, demonstrating a model that closely resembles the initial OS. Interestingly, there were differences in the subcutaneous and orthotopic tumours. A limitation of this initial study was that pulmonary metastasis was not detected until 60 days after implantation. A recent study analysed 15 different solid tumour PDOX's including OS; a total of 31 samples were injected with a take rate of 49%. Using whole-genome sequencing and whole-exome sequencing, the study matched the patient tumour with the xenograft tumour and of all the tumours analysed, OS had the best clonal preservation (Stewart *et al.,* 2017). This was also shown to be the case when xenografts were compared to primary tumours morphologically. (Mayordomo *et al.,* 2010).

A major problem with current OS treatment is that response to the different drugs varies and is hard to predict. In addition to providing a useful model to study OS behaviour, PDOX's provide a platform for drug screening and to predict response to chemotherapy (Bruheim *et al.,* 2004, Igarashi *et al.,* 2017, Stebbing *et al.,* 2014). PDOXs possess a range of advantages as a research tool including recapitulating the clinical characteristics, screening for chemotherapy resistance, and potentially offering the opportunity for personalized OS treatment. However, there are also some

limitations: low patient tumour source availability due to low incidence of the disease, the need for immunocompromised rather than immunocompetent mice, long time frames, the required high level of technical skill, and required patient consent. They also often fail to establish *in vivo,* which could potentially be due to treatments the patient has already received.

Ultimately, the choice of OS model used should be carefully considered and dependent on the research questions but will invariably be limited by the laboratories resources and skill sets. However, it is best to use a number of pre-clinical models to fully validate any new target or drug, and to maximize the chance of it making it to clinical trials and patient use for OS. In this thesis both an *in vitro* model and *in vivo* model has been utilised and will enable both the OS tumour and the OS bone microenvironment to be targeted to potentially identify a novel treatment for OS.

1.6.13 The need for new treatments in OS

Studies aiming to improve the prognosis for OS patients are currently ongoing, encompassing a range of different approaches and techniques. The high amount of heterogeneity in OS tumors, as well as the rarity of the disease has limited therapeutic developments and novel breakthroughs, meaning that treatments for OS have remained the same since around the 1970s (Saraf *et al.,* 2018), with the 5-year survival rate of OS patients remaining unchanged over the last 30 years or more (Gerrand *et al.,* 2016). As well as targeting the cancer cells in OS, consideration for the microenvironment the cells reside in is of paramount importance in understanding the disease initiation and progression. ATP is a major constituent of both the bone and tumour microenvironment (Rumney e*t al.,* 2012, Di Virgilio & Adinolfi, 2017) with the process of purinergic signalling found to influence many aspects of the bone microenvironment (Agrawal & Gartland, 2013) and the growth of many different cancers (Di Virgilio & Adinolfi, 2017) Therefore, targeting purinergic signalling in OS could provide a new therapeutic option.

1.7 Purinergic Signalling historical overview

The first study recognising the physiological action of extracellular purines was published in 1929. In this study adenine extracts from various tissue were found to regulate cardiac rhythm and blood vessel pressure (Drury & Szent-Györgyi, 1929).

However, it wasn't until 1972 that Professor Geoffrey Burnstock devised the term 'Purinergic' and showed that ATP could act as an extracellular messenger responsible for nonadrenergic, non-cholinergic transmission in the gut and bladder (Burnstock, 1972). The purinergic hypothesis was met with initial resistance as ATP was already an accepted intracellular energy source. It was therefore considered unlikely such a molecule would also be involved in extracellular signalling. Since this initial period, ATP acting as a neurotransmitter and extracellular messenger is now widely accepted and implicated in many different physiological processes and pathological conditions.

It would however be another 20 years after the finding that ATP could act as an extracellular messenger before the receptors were cloned and characterised, starting with the P1 receptors for adenosine (Burnstock, 2012). After this came the $P2Y_1$ receptor (Webb *et al.,* 1993) and $P2Y_2$ receptor originally termed P2U (Lustig *et al.,* 1993); the first P2X receptors were characterised the year after those (Brake *et al.,*1994, Valera *et al.,*1994). After the initial classification into P1 and P2 receptors and then the many new receptors were discovered which meant a subdivision into P2Y and P2X with the nomenclature clearly defined based on agonist potency, signal transduction and molecular structure (Abbracchio & Burnstock, 1994).

1.7.1 Purinoceptors

The P1 (adenosine) receptors are G-protein coupled receptors (GPCRs) and have 4 subtypes. P2 receptors are subdivided into P2Y GPCRs of which there are 8 human subtypes and P2X ligand gated ion channels of which there are 7 subtypes (Table 1.4).

Table 1.4: Purinergic receptor physiology, agonist and subtypes

Receptor	Type	Agonist	Subtypes
P1	GPCR	Adenosine	A_1, A_2A, A_2B, A3
P2Y	GPCR	ATP, ADP, UTP	$P2Y_1$, $P2Y_2$, $P2Y_4$, $P2Y_6$, $P2Y_{11}$, $P2Y_{12}$, $P2Y_{13}$, $P2Y_{14}$
P2X	Ligand-gated ion channels	ATP	P2X1, P2X2, P2X3, P2X4, P2X5, P2X6, P2X7,

P2Y G-protein coupled receptors all have seven hydrophobic transmembrane regions consisting of three extracellular and 3 intracellular loops, they each contain an N terminus and intracellular C terminus which has the protein kinase binding motif. P2Y receptors form homo and heterodimers similar to GPCRs (Kugelgen & Hoffmann, 2016). The P2X ligand gated ion channels were first cloned in 1994 and range from 388 to 595 amino acids which form both homo and heterotrimeric receptors. Structurally they contain two hydrophobic transmembrane domains capable of spanning the plasma membrane, with intracellular amino and carboxyl terminals and a large extracellular loop containing ~280 amino acids and 10 cystine residues capable of forming disulfide bridges to stabilize the protein structure. ATP binds to this extracellular region and three molecules are required to activate the channel, upon activation of the channel cells become permeable to various small ions such as Na+ and Ca^{2+} (North, 2002). Of particular interest in this thesis is the P2X7R.

The P2X7R, although having some related sequence and functional characteristics to other P2X ion channels, is quite distinct. The P2X1–P2X6 subunits are 379–472 amino acids long, however, the P2X7R monomeric subunit is the largest of the P2X family with 595 amino acids (Syed & Kennedy., 2012). This is due to a much longer carboxyl terminal (Bartlett *et al.*, 2014, Syed & Kennedy., 2012) amongst P2X receptors the C terminal has approximately 40-50% similarity with the P2X7 the most dissimilar (North 2002., Syed & Kennedy 2012). The mechanism of P2X7R pore formation has two different proposed hypothesises, one is that a conformational change occurs dilating the P2X7R itself, thereby allowing larger molecules through. The second is that the pore is a separate distinct molecular structure or recruits a secondary complex activated by P2X7R (Young & Górecki, 2018, Alberto *et al.,* 2013, Pelegrín, 2011), pannexin hemi-channels have been suggested to play this role (Alberto *et al*., 2013).

In addition to the full length P2X7R, termed P2X7RA, nine different human P2X7R splice variants have been discovered and termed P2X7RB-P2X7RJ. Of these splice variants P2X7RB is unique in that it retains its ability to act as a functional ion channel (Feng *et al.,* 2006, Cheewatrakoolpong *et al.,* 2005) and shares a similar tissue distribution as the full length receptor (Sluyter & Stokes, 2011). P2X7RB preserves an intron between exons 10 and 11, this causes the insertion of a stop codon which eliminates translation of the last 249 amino acids of the C terminus and the addition of

an extra 18 amino acids after residue 346. These alterations still enable receptor stimulation by ATP or Benzoyl ATP (BzATP) but P2X7RB lacks the typical P2X7R pore formation response (Adinolfi *et al.*, 2010), it therefore displays a non-functional phenotype. Non-functional P2X7Rs have been found to be essential for tumour cell growth (Gilbert *et al.,* 2019). P2X7RA and P2X7RB share the same antagonists (Giuliani *et al.* 2014) with various companies developing them for a wide range of applications. First generation P2X7R antagonists include: Reactive Blue 2, Suramin and derivatives, Coomassie Brilliant Blue G (BBG), pyridoxal phosphate-6-azophenyl-2-4-disulfonic acid (PPADS), 1-N,O-bis (5-isoquinolinesulfonyl)-N-methyl-l-tyrosyl-4-phenylpiperazine (KN-62), and oxidized ATP (oATP) (Young & Górecki, 2018). Second generation P2X7R antagonists have increased specificity and include tetrazoles such as A438079 and cyanoguanidines such as A740003 both produced by Abbott Labs, GSK314181A produced by GalaxoSmithKline and AZ11645373 produced by AstraZeneca with the latter two blood brain barrier permeable. These have further been followed by AZD9056 (AstraZeneca) and CE-224,535 (Pfizer) (Young & Górecki, 2018).

1.7.2 Purinergic signalling in the musculoskeletal system

Purinergic signalling has been found throughout the musculoskeletal system with both P1 and P2 receptors expressed on bone cells (Orriss, 2015). MSCs differentiate into osteoblasts, and have been found to be influenced through selective purinergic receptors involved in proliferation and differentiation as interestingly MSCs spontaneously expel ATP (Kaebisch *et al.,* 2015).

Purinergic receptors have also been found to be expressed on human OS cell lines SaOS2 and Te85, and also primary human bone derived cells. However, the Te85 OS cells were found to have no functional receptor despite having P2X7R expression at the mRNA level, demonstrating receptor expression is related to the stage of cell differentiation (Gartland *et al*., 2001). Using rat calvarial osteoblasts it was demonstrated that P2XR expression shifted to P2YR expression through differentiation in culture (Orriss *et al.,* 2006). There is also P2X7R and P2X4R expression in SaOS2 and MG63 OS cell lines which both demonstrated pore formation (Alqallaf *et al*. 2009). Studies using the human MG63 OS cell line found that DNA

synthesis can be mediated via extracellular ATP acting on P2XR but not P2YR, subsequently increasing cell proliferation (Nakamura *et al*., 2000).

Effects of purinergic signalling in osteoclasts have been demonstrated, interleukin 6 which is involved in osteoclast formation, was increased in response to ATP acting on P2YR thus demonstrating the role of purinergic signalling on bone remodelling (Ihara *et al.,* 2005). It has been additionally demonstrated that ATP did not directly increase resorption by acting on osteoclasts, but rather through increasing expression of receptor activator of nuclear factor Kappa-B ligand (RANKL) which then had a synergistic effect of increasing osteoclast resorption (Buckley *et al.,* 2002). Other effects of purinergic receptors on osteoclasts have since been established with multiple P2XR and P2YR expressed on osteoclasts (Orriss *et al.,* 2010). Osteoclasts express P2X7R that is functionally active and contributes towards the initial cell linage commitment. Blocking the receptor prevented the fusion of osteoclast precursors forming larger atypical differentiated multinucleated osteoclasts (Gartland *et al.,* 2003).

The role of purinergic signalling in these different bone cells has clearly made significant advancements since its initial discovery, with the identification of a range of functions that may potentially provide therapeutic targets for a variety of bone disorders. The effects of purinergic receptors including both P2Y and P2X receptors in the musculoskeletal system are summarised in Table 1.5. The effect specifically by P2X7R in the musculoskeletal system *in vitro* are summarised in Table 1.6 and P2X7R KO models in Table 1.7 (Agrawal & Gartland, 2013). Many studies routinely use OS cell lines as a model for osteoblasts to investigate purinergic signalling in bone, their interaction in an oncogenic setting is still unclear. This therefore warrants more in-depth studies to be carried out with the potential to identify novel prognostic markers and therapeutic options for OS.

Table 1.5: P2 receptor expression, function and phenotype in the musculoskeletal system. Adapted with permission under the terms of the creative commons attribution licence (CC-BY). *Gene* (Lenertz *et al*., 2015), with additional information included (Kanaya *et al.,* 2016, Orriss *et al.,* 2011, Orriss & Arnett, 2012, Hoebertz *et al.,* 2002).

Receptor	Agonist	G-protein coupling	Function, expression and phenotype	References
P2X1	ATP		Negative regulation of bone mineralization	Von Kugelgen (2006)
P2X2	ATP		Expressed in femoral bone tissue and bone marrow cells from mice	Kanaya *et al., (*2016)
P2X3	ATP		Expressed in human MSCs	Nicolaidou *et al*., (2012)
P2X4	ATP		SNP associates with an increased risk for osteoporosis	Spangrude *et al*., (1988)
P2X5	ATP		Expressed in human MSCs and osteoblasts	Nicolaidou *et al*., (2012)
P2X6	ATP		Upregulated in adipocytes, low expressed in osteoblasts	Nicolaidou *et al*., (2012)
P2X7	ATP		Important role in bone development and homeostasis (full P2X7R function can be found in Table 1.6 and 1.7)	Pittenger *et a*l., (1999), Sitcheranet *et al., (*2003), Solle *et al., (*2001), Sun *et al., (*2013), Syberg *et al., (*2012) Takahashi *et al.,* (1988) Thaler *et al*., (2014)
P2Y1	ADP	Gq/11	Expressed on both osteoblasts and osteoclasts. Modulates osteoblast responses to systemic factors Increases ATP release and *c-fos* expression. Decreased bone mass in P2Y1-/- mice.	Orriss *et al., (*2011), Orriss & Arnett, (2012), Wagner, (2010)
P2Y2	ATP, ADP	Gq/11	Expressed on both osteoblasts and osteoclasts. Expression increases with osteoblast differentiation. Increased bone mass in P2Y2-/- mice	Orriss *et al., (*2011), Wagner, 2010)
P2Y4	UTP	Gi & Gq/11	No P2Y4 mRNA expression in rat osteoblasts	Hoebertz *et al., (*2002)
P2Y6	UDP	Gq/11	Decreased bone resorption in P2Y6-/- mice	Wang *et al., (*2012)
P2Y11	ATP	Gs and Gq/11	Expressed on human osteoclasts	Orriss & Arnett, (2012)
P2Y12	ADP	Gi	Important mediator of normal bone maintenance, Receptor inhibition by Clopidogrel causes reduced proliferation, differentiation, and function.	Orriss & Arnett, (2012), Wang *et al*., (2014), Weissman, (2000)
P2Y13	ADP	Gi	Decreased bone formation and bone resorption in P2Y13-/- mice, Decreased trabecular bone, osteoclast numbers, and rate of bone remodeling. Resistant to ovariectomy-induced bone loss	Orriss & Arnett, (2012), Wagner, (2010)
P2Y14	UPD-glucose	Gi	Expressed on mouse osteoclasts and primary rat osteoblasts	Orriss & Arnett, (2012)

Table 1.6: P2X7R effects on bone cells. Used with permission under the terms of the creative commons attribution licence (CC-BY). *Journal of Molecular Endocrinology* BioScientifica (Agrawal & Gartland, 2013).

Lineage	Stage	Species/Source	Stimulus	Downstream signalling	Function	References
Osteoblast	Progenitors	Human/MSCs	Shockwave treatment or agonist application	P38 MAPK activation, and c-Fos and c-Jun mRNA transcription PKC and Rho-associated kinase activation	Enhanced osteogenic differentiation and mineralisation	Sun et al. (2013) and Noronha-Matos et al. (2014) Panupinthu et al. (2008).
			Agonist application	Production of LPA metabolites		
	Mature	Rat/Calvariae	Agonist application	Hydrolysis of extracellular nucleotides to pyrohosphate	Increased osteoblast differentiation and matrix mineralisation	Orriss et al. (2012) and Orriss et al. (2013) Li et al. (2005), Panupinthu et al. (2007), Liu et al. (2008),Okumura et al (2008), Panupinthu et al. (2008),Gavala et al (2010),Genetos et al (2011), and Grol et al (2012)
				Production of lipid mediators		
		Mouse/primary and cell lines		Induction of transcription factor FosB/AP-1	Reduced bone mineralisation	
				Sustained proto efflux and PKC activation		
				Fluid shear-stress-induced nuclear accumulation of NF-kB	Increased osteoblast differentiation and matrix mineralisation	
		Human/primary and cell lines	Agonist application	Reversible plasma membrane blebbing		Gartland et al (2001) and Alqallaf et al (2009),
				Extensive plasma membrane blebbing	Cell apoptosis	
Osteocyte		Mouse/cell line	Fluid shear stress	Contradictory evidence for PGE_2	Mechanotransduction	Yoshida et al (2002), Cherian et al (2005)and Li et al (2007)
Osteoclast	Progenitors	Mouse/HSCs	Agonist application	Reduction in Notch expression	Increased differentiation into myeloid cells	Barbosa et al (2011)
	Precursors	Mouse/primary cells and RAW 264.7	Knockdown	Prevents NF-kB nuclear localisation, PKC translocation down regulation of NFATc1,cathespin K,TRAP,AT6v0d2,cSrc.c-Jun and Car2, and suppression of the prosteoclastic effect of LPA	Inhibition of cell fusion. Reduction in osteoclast formation and activity	Korcok et al (2004),Armstrong et al. (2009) and Hwang et al (2013)
		Human/Peripheral blood	Pharmacological blockade		Inhibition of cell fusion	Gartlland et al (2003a),Agrawal et al (2010) and Pallegatti et al (2011)
			Agonist application	Prevents ATP release via P2X7R pore		Miyazaki et al (2012)
		Mouse/primary cells				
	Mature		Agonist application or P2X7R transfection	Disruption of osteoclastic cystoskeleton via mitochondria energy regulation	Decreased osteoclast survival and bone resorption	
		Human/peripheral blood and HEK293	Agonist application	Activation of NFATc1	Increase in proliferation in serum-free conditions and resistance to apoptosis in transfectants	Adinolfi et al (2009) and Agrawal & Gartland (2011)
		Human peripheral blood		Reorganisation of cytoskeleton and secretion of lytic granules and osteoclast-matrix attachment site	Increase bone resorption	Hazama et al. (2009)

Table 1.7: Bone phenotype of existing P2X7R KO mice models. Imaged used with permission under the terms of the creative commons attribution licence (CC-BY). Journal of Molecular Endocrinology BioScientifica (Agrawal & Gartland, 2013).

Model	Sex examined	Bone strength measurement	Histomorphometric analysis	Remarks	Reference
Pfizer KO	Males and females (overall reduced bone mass)	Low BMC in trabecular, cortical and total bone, smaller bone diameters decreased periosteal and endocortical circumferences in femora.	Decreased periosteal bone formation (mineralising surface, bone formation rate) with an increase in parameters of bone resorption (osteoclast number, percentage osteoclast surface).	Reduced osteogenesis in response to mechanical loading, impaired fracture repair.	Ke *et al.,* (2003), Li *et al.,* (2005, 2009)
GSK KO	Females (no overall overt skeletal phenotype)	Unchanged BMD, increase in cortical thickness	No significant difference in cancellous bone volume in tibia, no significant difference in the number of osteoclasts in femora.		Gartland *et al.,* (2003)
C57Bl/6 KO (451L allele)	Females	Increase in whole body BMD, increase in bone strength.	Significant increase in trabecular thickness in the tibia and vertebrae.		Syberg *et al.,* (2012)
BALB/cJ KO (P451 allele)	Females	High total BMD, BMC and bone area, increased femoral strength.	Reduced serum CTX, ALP and no changes in osteocalcin.	C57Bl/6 WT carrying the naturally occurring 541L allele has lower BMD, femoral strength and concentration of bone markers compared with BALB/cJ WT. In addition, lower markers for bone formation and resorption in the C57Bl/6 WT vs BALB/cJ WT.	Syberg *et al.,* (2012)

1.7.3 Purinergic signalling and cancer

Given that purinergic receptors are found on the majority of cell types in humans (Burnstock, 2017) with a variety of functions, as previously discussed, there is likely a role in pathophysiological conditions. Extensive studies are now discovering how the surrounding tumour microenvironment can influence tumour characteristics. ATP is at a high concentration in the tumour microenvironment (Adinolfi, 2013, Qiu *et al*., 2014) yet absent from surrounding healthy tissue (Pellegatti *et al*., 2008), and potentially implicates purinergic signalling with cancer development and progression to metastasis. The therapeutic targeting of these receptors hasn't been explored to its full potential (Burnstock, 2017). This could be due to some contentious views and discrepancies in the role that purinergic receptors play in cancer.

Treatment of cancer with intravenous ATP infusions was suggested to improve quality of life of patients by preventing weight and muscle loss, this was found to be the case in a clinical trial of advanced non-small lung cell lung cancer, where 28 patients received ATP (Agteresch *et al*., 2000). However, this study has various limitations, for example quality of life measurement is subjective and self-reported and could be linked to the patients knowing that they were receiving a treatment as the study wasn't blinded. The empirical evidence presented actually demonstrated only a small difference in mean quality of life scores with additional weight loss prevention only minimal. The difference in initial weight and weight gain wasn't measured at baseline which could mean the data just naturally varies amongst participants. Over half the participants either passed away or dropped out, therefore data could potentially be biased as the ones dropping out or facing death are the participants most likely to report a lower quality of life score. A second study concluded that ATP could safely be administered in a home setting in advanced cancer patients, despite reporting 192 different side effects from the procedure (Beijer *et al.* 2007).

The above studies may just be demonstrating the effects on different systems in general, as ATP is a major constituent of the tumour microenvironment and consequently a direct effect on tumour physiology would be expected (Qiu *et al.,* 2014, Adinolfi 2013). ATP has been found to be significantly higher than surrounding healthy tissue (Pellegatti *et al.,* 2008). ATP depletion in combination with anti-cancer therapy

was found to cause a significant reduction in breast tumour size and in some instances complete regression in mice (Martin *et al.,* 2000).

Due to the dual nature of the P2X7R it can cause an increase in cell proliferation with low tonic amounts of ATP present. However, high concentrations of ATP were capable of decreasing cell number in human cutaneous squamous cell carcinoma A431 cells (Greig *et al.,* 2003). This was thought to be due to P2X7R, as it has the ability to form a larger pore at higher concentrations of ATP, this would cause an influx of intracellular Ca^{2+} ions and hence activate cell death pathways. Furthermore, one study found that the melanoma cell line A375 expressed P2X7R with its activation causing a decrease in cell number through apoptosis (White & Butler, 2005).

There is evidence suggesting purinergic receptors are found and implicated in cancer as P2X7R is found to be present on a variety of malignant cells (Di Virgilio *et al.,* 2009). P2X7R expression increases invasiveness *in vivo* in HEK-293 tumours (Adinolfi *et al.,* 2012). In pancreatic ductal adenocarcinoma overexpression of P2X7R causing increased proliferation, invasiveness and survival, treatment against P2X7R with an allosteric inhibitor (AZ10606120) reduced these characteristics (Giannuzzo *et al.,* 2015). In addition, P2X7R has been shown to trigger the release of growth factors for cells increasing proliferation in neuroblastoma (Di Virgilio *et al.,* 2009).

1.7.4 Purinergic signalling in bone cancer

With regards to bone cancer itself, despite the fact that purinergic signalling has a variety of known functions on bone cells and implications in cancer, research concerning bone cancer is limited. Interestingly the chromosome location of P2X7R is 12q24 (Sluyter & Stokes, 2011). One study reported that chromosome 12 abnormalities are common in mesenchymal tumours with overexpression of 12q sequences particularly in OS (Gisselsson *et al.,* 2002). This correlates P2X7R and OS onset and development.

Studies mainly focus on metastasis to bone and the subsequent bone pain experienced. By blocking P2X3R involved in pain regulation, mice injected with mammary carcinoma cells in the tibia experienced less pain (Kaan *et al.,* 2010, Wu *et al.,* 2012). P2X7R in OS has initially been investigated, in one study 54 advanced stage IV OS patient tissue samples were analysed using P2X7R antibodies and found

that over 80% of the samples had the P2X7R present (Giuliani *et al.,* 2014). However, this is yet to be confirmed on a larger scale or on samples that include tumours at different stages of the disease to fully demonstrate P2X7R involvement in aggressiveness and progression of OS.

The same study then subsequently transfected P2X7R variants into Te85 OS cells. The results indicated that that having a truncated B isoform led to a greater increase in cell proliferation and higher cell density, although transfection with any P2X7R into the Te85 OS cell line resulted in increased cell growth (Giuliani *et al.,* 2014). Nuclear factor of activated T cells complex (NFATc1) was found to have a greater increase in expression when P2X7R was present, this has a role in osteoblast proliferation and bone growth and could explain the increased growth rate. Additionally, stimulation with BzATP increased proliferation in all transfected clones through stimulating P2X7R. RANK-L expression was reduced suggesting a role in altered bone remodelling which is a common trait in OS, again demonstrating how P2X7R expression can alter bone cell behaviour. The findings of this study support the role of P2X7R in OS pathogenesis (Giuliani *et al.,* 2014) and contradicts the findings of decreased cell proliferation in other cancers through activation of apoptosis (White & Butler, 2005). Finally, the study provides initial data to build on with regards to the role of P2X7R in OS.

1.8 Summary and hypothesis

A harsh treatment regime exists for OS patients including amputation, chemotherapy and limb salvage surgery, which hasn't changed for a number of years. This is similar for the survival statistics of this often fatal disease. The evidence for purinergic receptors involvement in other cancers is well documented, as is its role in bone cell function. Currently purinergic receptor antagonists have been found to be safe and well tolerated in humans (Silverman *et al.,* 2008) in a clinical trial for rheumatoid arthritis. Therefore, if OS can be treated with P2X7R antagonists, there could potentially be a quick transition from the bench to benefiting patients directly.

The proposed hypothesis to be tested is that **P2X7R plays a role in the development of OS**, **which can be exploited as a therapeutic target.** To test this hypothesis this thesis has a number of objectives:

- To determine the functional characteristics of the P2X7R variants in OS cells, this will be achieved using end-point PCR, qPCR, calcium assays, and pore formation assays.
- To determine the effect of P2X7R expression and antagonism on OS cell proliferation using an MTS assay.
- To determine the effect of P2X7R expression on OS cell adhesion to type 1 collagen.
- To determine the effect of P2X7R expression on OS cell migration using a scratch assay.
- To determine the effect of P2X7R expression on OS cell invasion using transwells.
- To form a suitable OS *in vivo* model for targeting of the P2X7R.
- To determine if P2X7R expression and antagonism can affect the primary OS tumour size *in vivo* using calliper measurements.
- To determine if P2X7R expression and antagonism can affect the histology of the OS tumours by H&E staining.
- To determine if P2X7R expression and antagonism affects proliferation and cell death *in vivo* using Immunohistochemistry (IHC).
- To determine if P2X7R expression and antagonism affects the bone phenotype using micro-CT analysis.
- To determine if P2X7R expression and antagonism affects the osteoclast number at the tumour-bone interface.
- To determine if P2X7R expression and antagonism affects OS pulmonary metastasis.

Chapter 2 - Materials and Methods

2.1 Cell culture

2.1.1 Cell maintenance and passage

Te85 OS cells were obtained from the laboratory of Professor Jim Gallagher (Liverpool, UK). HEK-293 cells were obtained from the laboratory of Dr Elena Adinolfi (Ferrara, Italy). MNNG-HOS OS cells were provided by Professor Dominique Heymann (Sheffield, UK, INSERM, France). The Te85 OS cell line used is of human origin, specifically a 13-year-old Caucasian female with OS. The MNNG-HOS cell line is a derivative of the Te85 parental OS cell line and has been chemically transformed with 0.01 µg/mL MNNG (Rhim *et al.,* 1975a). The HEK-293 cell line used is of human origin, specifically from human embryonic kidney cells from a healthy aborted foetus (Stepanenko & Dmitrenko, 2015).

Cells lines were defrosted to 37°C and cultured in T75-cm^2 flasks (ThermoFisher scientific, Roskilde, Denmark) in 10 mL DMEM©+Glutamax™ medium (Life Technologies Paisley, UK) containing 10% (v/v) foetal bovine serum (FBS) as a growth supplement with 100 Units/mL penicillin and 100 µg/mL streptomycin antibiotics 1% (v/v) (Life Technologies) (referred to as complete medium). To passage cells, the medium was discarded and cells were washed twice using calcium and magnesium free phosphate buffer saline (PBS) (Life Technologies) Cells were then detached by the addition of 2.5 mL per flask of 0.25% (v/v) trypsin containing 0.01% (v/v) ethylenediaminetetraacetic acid (EDTA) (Sigma, Poole, UK). After detachment by incubating the cells for 5 minutes in a standard 37°C incubator with a 5% CO_2 stream, 10 mL of complete medium was added to inhibit any additional action by trypsin. The cell suspension was then centrifuged at 300g for 5 minutes, the subsequent pellet was resuspended in 1 mL complete medium to then be counted using a trypan blue stain (Sigma) and haemocytometer. Cells were maintained by splitting at 60-70% confluence with a limit of 25 passages. Frozen vials of cell supplies were stored in FBS containing 10% dimethyl sulfoxide (DMSO) and were slowly cooled using a Mr Frosty™ freezing container (ThermoFisher Scientific) at an approximate rate of -1°C/minute. All cell culture work was performed under sterile conditions.

2.1.2 Cell transfections

Te85 OS cells previously used in Professor Gartland's laboratory (Giuliani *et al.,* 2014) have been stably transfected with P2X7R variants including the wild type full length P2X7RA and a truncated P2X7RB isoform. Additionally, Te85 OS cells were transfected with both isoforms to produce a P2X7RAB variant. For the P2X7RA variant G418 (Life Technologies) at a concentration of 0.8 mg/ml was used for selection. For the P2X7RB variant 0.2 mg/ml hygromycin (ThermoFisher Scientific) was used for selection.

MNNG-HOS OS cells were transfected with the mammalian expression vector pcDNA3 (ThermoFisher Scientific) containing a P2X7RB cDNA construct or transfected with an empty mock pcDNA3 vector. Cells were transfected using Lipofectamine® LTX & PLUS Reagent™ kit (ThermoFisher Scientific). 50,000 cells were plated into 6 well plates and left overnight in complete medium. Cells were then changed into OPTI-MEM® reduced serum medium containing PLUS Reagent™ and diluted plasmid DNA. DNA concentration was optimised initially by transfecting with 2, 3 and 4 µg/per well. After a 5-minute incubation at room temperature, Lipofectamine® LTX Reagent was added with a further 30-minute incubation at room temperature. Cells were then left overnight before been changed back in to complete medium and left for a further 48 hours before the addition of 0.2 mg/ml hygromycin.

2.1.3 Measurement of intracellular calcium concentrations

In accordance with the kit instructions, 10 mL Fluo-4 Direct™ calcium assay buffer and 200 µL of a 250 mM probenecid stock solution was added to one bottle of Fluo-4 Direct™ calcium reagent to create a 2X Fluo-4 Direct™ calcium reagent loading solution (Invitrogen, Paisley, UK).

Cells were plated out at a density of 15,000 per well in 96-well plates and left overnight to adhere, the medium was changed into an equal solution of complete medium and the 2X Fluo-4 Direct™ calcium reagent loading solution. Cells were incubated for 1 hour at 37°C before been stimulated with 100 µM BzATP (ThermoFisher Scientific) and then 0.8 µM ionomycin (Sigma, Poole, UK). Calcium concentrations were detected using a FlexStation 3 Multi-Mode Microplate Reader (Molecular Devices,

Sunnyvale USA) with excitation at 490 nm and emission at 525 nm with a cut off wavelength of 515 nm.

2.1.4 P2X7R dependent pore formation (ethidium bromide dye uptake)

Cells were plated out at a density of 15,000 per well in 96-well plates and left overnight to adhere, the medium was then changed to 80 µL Hank's Balanced Salt Solution (HBSS) (ThermoFisher Scientific) and incubated at 37°C with or without 10 µM of the P2X7R inhibitor A740003 (Tocris Biosciences, Bristol, UK) for 1 hour. BzATP was diluted in ultra-pure ethidium bromide (Invitrogen) to a final concentration of 300 µM and 100 µM with 20 µL added to make a final volume of 100 µL. Induction of P2X7R pore formation was then detected on a FlexStation 3 Multi-Mode Microplate Reader at 360 nm excitation and 580 nm emission with a cut off wavelength of 570 nm for 45 minutes after an initial 5-minute baseline reading, with readings taken every 2 minutes.

2.1.5 MTS proliferation assay

Te85 OS cells were seeded at various cell densities of 1250, 2500 and 5000 per well in a 96-well plate in 100 µL phenol-free DMEM (Life Technologies) complete medium. After 24 hours, cells were washed twice with PBS and the medium was changed to medium containing either 0.5%, 2% or 10% FBS medium. At each time-point of day 0, 1, 3, 5 and 7, a previously prepared 1 mL aliquot of [3-(4, 5-dimethylthiazol-2-yl)-5-(3-carboxymethoxyphenyl)-2-(4-sulfophenyl)-2H-tetrazolium, inner salt (MTS), and phenazine methyl sulphate (PMS), mixture in the ratio of 20:1 was diluted in 1:5 in phenol-free DMEM with 100 µL added directly to the 100 µL clear growth medium already in the well to make a total volume of 200 µL. The cells were incubated for 3 hours at 37°C. The absorbance was read at 490 nm using the SpectraMax M5e Microplate Reader (Molecular Devices). For MNNG-HOS cell lines the experiment was performed using the same protocol but using 2500 cells per well. For inhibition studies using Te85 OS cell lines the cells were seeded at 5000 and MNNG-HOS 2500 per well in 0.5% FBS. After 24 hours, cells were treated with 100 µM of A740004 or AZ11645373 P2X7R antagonists and absorbance was read at day 3.

2.1.6 Cell adhesion assay

Type 1 rat tail collagen (Life Technologies) was diluted in distilled water to a concentration of 50 µg/ml. 100 µL was added to the wells of a 96 well plate for 1 hour before removing excess collagen to form a layer along the bottom of the well. 7500 cells per well were then added in medium containing only 0.5% FBS to the collagen coated plate and left for 4 hours at 37°C before washing 4 times with PBS to removed unattached cells. Cells were then lysed using 50 µL lysis buffer (20 mM tris, 0.05 M $MgCl_2$), after 50 µL of diluted Quant-iT™ PicoGreen® dsDNA Reagent was then added to detect the DNA of the lysed remaining cells. Fluorescence was detected and quantified at 485 nm excitation and 530 nm emission with a cut off wavelength of 530 nm using the SpectraMax M5e Microplate Reader.

2.1.7 Cell migration (scratch assay)

The scratch assay was performed in 12 well plates containing 200,000 cells in 2 mL complete medium, once seeded the cells were left overnight to form a confluent monolayer. This was then changed into complete medium containing 5 µg/mL mitomycin C (Sigma) to inhibit cell proliferation, and left to incubate for 2 hours at 37°C. A scratch was then made using a 10 µL pipette tip down the centre of the well. The medium was removed, and the cells were washed twice with PBS to remove the unattached cells made from the scratch. Microscopic images were taken using an EVOS™ FL Auto Imaging System (ThermoFisher Scientific) every 2 hours for a 24-hour period. For low serum experiments the same procedure was performed but in medium containing 0.5% FBS as an alternative to 10% FBS medium. In addition, 10 µM BzATP was used in studies activating the P2X7R again in low 0.5% FBS medium. Scratch assay images were analysed automated using T-scratch software.

2.1.8 Cell invasion

Matrigel (Corning, New York, USA) at a concentration of 1.5 mg/mL was used to form a layer to invade by adding 30 µL to the Corning® FluoroBlok insert to cover the entire surface forming a homogenous layer. The wells were left to set for 2 hours at 37°C. Cells were incubated with 5 µg/mL mitomycin C, to inhibit proliferation, whilst in culture in a T75 flask containing 10 mL complete medium for 2 hours. The cells were then trypsinised, counted and added to the matrigel coated FluoroBlok insert in serum free

medium with the addition of 10 µM BzATP, 10% FBS was used as a chemoattractant in the lower chamber of the well. The FluoroBlok inserts have a light-tight polyethylene terephthalate (PET) membrane which blocks any transmission of light between 400 and 700 nm, therefore any emission from cells in the inserts upper chamber is blocked and only emission from the invaded cells will be detected. To detect these cells, transwell inserts were washed twice in PBS and stained with Calcein AM cell permeant dye (ThermoFisher Scientific) by incubating the inserts in a concentration of 5 µM for 30 minutes at 37°C. The inserts were then washed twice again in PBS and imaged using an EVOS™ FL Auto Imaging System (ThermoFisher Scientific). Images were analysed using Image J (Figure 2.1).

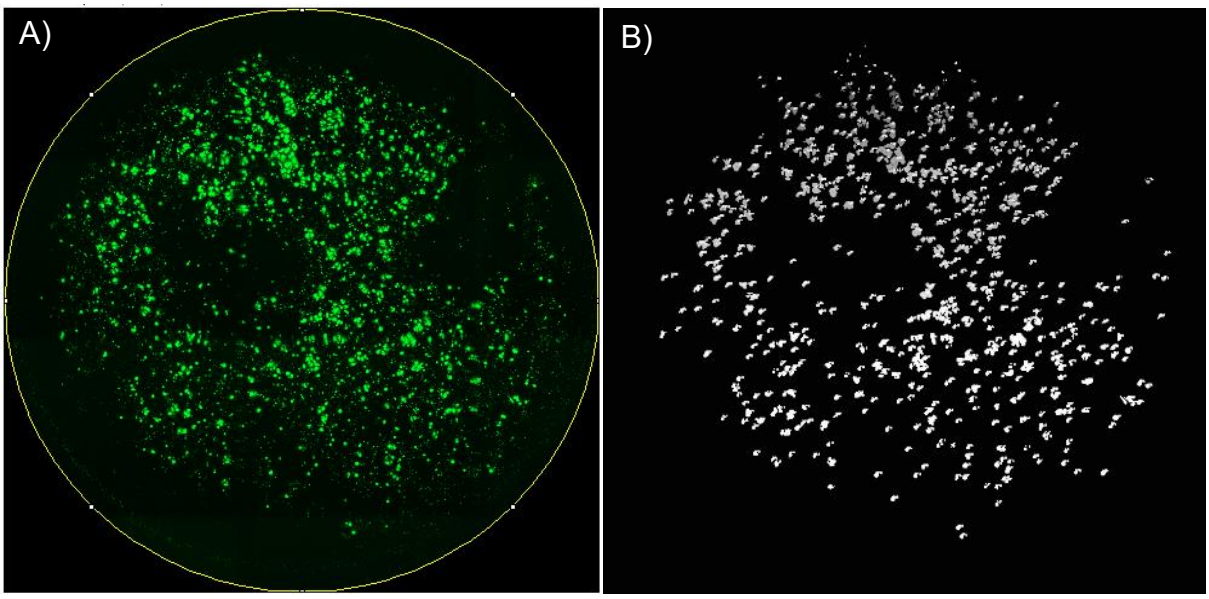

Figure 2.1: Representative example of an analysed invasion transwell. Cells were seeded into the top transwell in FBS free medium containing BzATP and left to invade towards 10% FBS for 24 hours. Cells were then washed with PBS and stained green. **A)** Invaded cells stained with Calcein AM cell permeant dye **B)** Invaded cells analysed using Image J.

2.1.9 P2X7R antagonists

A740003 and AZ11645373 (Tocris Biosciences) are both specific antagonist for P2X7R, with A740003 acting competitively (Honore *et al.,* 2006) and AZ11645373 being allosteric (Michel *et al.*, 2009) they were both dissolved in DMSO to a stock concentration of 10 mM and stored at -80˚C in aliquots.

2.2 Molecular Biology

2.2.1 RNA extraction

RNA was extracted from T75 cell flasks using the ReliaPrep™ RNA Miniprep System kit (Promega, Southampton UK) in accordance with the manufacturers protocol. Firstly 500 µL BL+TG buffer (proprietary buffer provided with the kit) was added to the flask, vigorously pipetted and passed through a 20-gauge needle to fully lyse the cells. Next 170 µL of 100% isopropanol was added and the samples vortexed for 5 seconds. Samples were then loaded into a mini column and centrifuged at 12,000g for 30 seconds. The flow-through solution was then discarded. This step was repeated using 500 µL of an RNA wash solution. A DNAse 1 incubation mix was added to each sample and left at room temperature for 30 minutes. After incubation a column wash solution was added to the mini column containing the samples and was and centrifuged at 12,000g for 15 seconds. Two washes were performed with RNA wash solution firstly adding 500 µL centrifuging at 12,000g for 30 seconds, and then with 300 µL again at 12,000g for 2 minutes. A final elution wash was performed using 50 µL of nuclease free water to collect the RNA.

2.2.2 First strand cDNA synthesis

RNA was reverse transcribed using the Applied Biosystems™ high capacity RNA to cDNA™ Kit (Foster City, CA, USA) in accordance with the manufacturers protocol. 1 µg/µL RNA samples were added to 10.0 µL 2X RT Buffer Mix, 1.0 µL 20X RT Enzyme Mix and made up to 20 µL per reaction with nuclease free water per reaction. For reverse transcription (RT) negative (-ve) samples no RT Enzyme Mix was added to the samples. Samples were kept cool on ice before incubation at 37°C for 60 minutes, followed by 5 minutes at 95°C to heat inactivate the reverse transcriptase, samples were then held at 4°C prior to collection and storage at 4°C.

2.2.3 End-Point Polymerase chain reaction (PCR) primers

End point PCR primers were designed using Pubmed gene sequences (Figure 2.3 & 2.4). P2X7R mRNA expression was determined with two sets of primers for the P2X7R. The first primer set was designed (Table 2.1) early in the gene sequence with the forward primer on the exon boundary between exon 3 and 4 and the reverse

between exon 7 and 8. This N terminal region is present on both the full length and truncated P2X7RB (product length 413 BP). The second primer set was designed further along the gene sequence with the both the forward primer and reverse primer designed to bind to exon 13 (product length 399 BP) this C-terminal region is only present on the full length P2X7RA and thereby unable to be detected in the cells with the truncated P2X7RB (Figure 2.2).

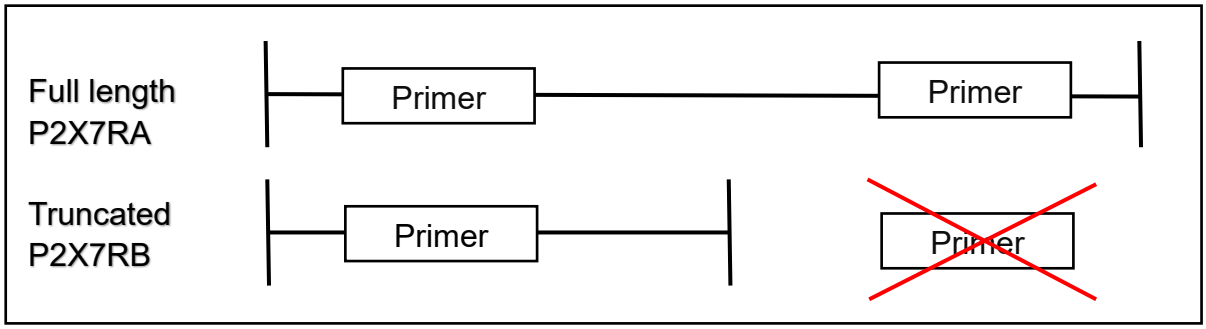

Figure 2.2: Representation of the P2X7R primer design. Two primer sets were designed, one set binds to both the full length P2X7RA and truncated P2X7RB (N-terminal specific), whereas the second set can only bind to the full length P2X7RA (C-terminal specific) as P2X7RB is truncated and missing that region.

GCACACCAAGGTGAAGGGGATAGCAGAGGTGAAAGAGGAGATCGTGGAGAATGGAGTGAAGAAGTTGGTGCACAGTGTCTTTGACACCGCA
GACTACACCTTCCCTTTGCAGGGGAACTCTTTCTTCGTGATGACAAACTTTCTCAAAACAGAAGGCCAAGAGCAGCGGTTGTGTCCCGAGT
ATCCCACCCGCAGGACGCTCTGTTCCTCTGACCGAGGTTGTAAAAAGGGATGGATGGACCCGCAGAGCAAAGGAATTCAGACCGGAAGGTG
TGTAGTGTATGAAGGGAACCAGAAGACCTGTGAAGTCTCTGCCTGGTGCCCCATCGAGGCAGTGGAAGAGGCCCCCCGGCCTGCTCTCTTG
AACAGTGCCGAAAACTTCACTGTGCTCATCAAGAACAATATCGACTTCCCCGGCCACAACTACACCACGAGAAACATCCTGCCAGGTTTAA
ACATCACTTGTACCTTCCACAAGACTCAGAATCCACAGTGTCCCATTTTCCGACTAGGAGACATCTTCCGAGAAACAGGCGATAATTTTTC
AGATGTGGCAATTCAGGGCGGAATAATGGGCATTGAGATCTACTGGGACTGCAACCTAGACCGTTGGTTCCATCACTGCCGTCCCAAATAC
AGTTTCCGTCGCCTTGACGACAAGACCACCAACGTGTCCTTGTACCCTGGCTACAACTTCAGATACGCCAAGTACTACAAGGAAAACAATG
TTGAGAAACGGACTCTGATAAAAGTCTTCGGGATCCGTTTTGACATCCTGGTTTTTGGCACCGGAGGAAAATTTGACATTATCCAGCTGGT
TGTGTACATCGGCTCAACCCTCTCCTACTTCGGTCTGCCCGCTGTGTTCATCGACTTCCTCATCGACACTTACTCCAGTAACTGCTGTCGC
TCCCATATTTATCCCTGGTGCAAGTGCTGTCAGCCCTGTGTGGTCAACGAATACTACTACAGGAAGAAGTGCGAGTCCATTGTGGAGCCAA
AGCCGACATTAAAGTATGTGTCCTTTGTGGATGAATCCCACATTAGGATGGTGAACCAGCAGCTACTAGGGAGAAGTCTGCAAGATGTCAA
GGGCCAAGAAGTCCCAAGACCTGCGATGGACTTCACAGATTTGTCCAGGCTGCCCCTGGCCCTCCATGACACACCCCCGATTCCTGGACAA
CCAGAGGAGATACAGCTGCTTAGAAAGGAGGCGACTCCTAGATCCAGGGATAGCCCCGTCTGGTGCCAGTGTGGAAGCTGCCTCCCATCTC
AACTCCCTGAGAGCCACAGGTGCCTGGAGGAGCTGTGCTGCCGGAAAAAGCCGGGGGCCTGCATCACCACCTCAGAGCTGTTCAGGAAGCT
GGTCCTGTCCAGACACGTCCTGCAGTTCCTCCTGCTCTACCAGGAGCCCTTGCTGGCGCTGGATGTGGATTCCACCAACAGCCGGCTGCGG
CACTGTGCCTACAGGTGCTACGCCACCTGGCGCTTCGGCTCCCAGGACATGGCTGACTTTGCCATCCTGCCCAGCTGCTGCCGCTGGAGGA
TCCGGAAAGAGTTTCCGAAGAGTGAAGGGCAGTACAGTGGCTTCAAGAGTCCTTACTGA

Figure 2.3: The full length P2X7R base pair sequence. Primers were designed that bind early on in the gene sequence highlighted in red, a second set were then designed further along the gene that only bind to the full length P2X7RA shown in green, highlighted in blue is where the P2X7RB truncates.

ATGCCGGCCTGCTGCAGCTGCAGTGATGTTTTCCAGTATGAGACGAACAAAGTCACTCGGATCCAGAGCATGAATTATGGCACCATTAAGT
GGTTCTTCCACGTGATCATCTTTTCCTACGTTTGCTTTGCTCTGGTGAGTGACAAGCTGTACCAGCGGAAAGAGCCTGTCATCAGTTCTGT
GCACACCAAGGTGAAGGGGATAGCAGAGGTGAAAGAGGAGATCGTGGAGAATGGAGTGAAGAAGTTGGTGCACAGTGTCTTTGACACCGCA
GACTACACCTTCCCTTTGCAGGGGAACTCTTTCTTCGTGATGACAAACTTTCTCAAAACAGAAGGCCAAGAGCAGCGGTTGTGTCCCGAGT
ATCCCACCCGCAGGACGCTCTGTTCCTCTGACCGAGGTTGTAAAAAGGGATGGATGGACCCGCAGAGCAAAGGAATTCAGACCGGAAGGTG
TGTAGTGCATGAAGGGAACCAGAAGACCTGTGAAGTCTCTGCCTGGTGCCCCATCGAGGCAGTGGAAGAGGCCCCCCGGCCTGCTCTCTTG
AACAGTGCCGAAAACTTCACTGTGCTCATCAAGAACAATATCGACTTCCCCGGCCACAACTACACCACGAGAAACATCCTGCCAGGTTTAA
ACATCACTTGTACCTTCCACAAGACTCAGAATCCACAGTGTCCCATTTTCCGACTAGGAGACATCTTCCGAGAAACAGGCGATAATTTTTC
AGATGTGGCAATTCAGGGCGGAATAATGGGCATTGAGATCTACTGGGACTGCAACCTAGACCGTTGGTTCCATCACTGCCATCCCAAATAC
AGTTTCCGTCGCCTTGACGACAAGACCACCAACGTGTCCTTGTACCCTGGCTACAACTTCAGATACGCCAAGTACTACAAGGAAAACAATG
TTGAGAAACGGACTCTGATAAAAGTCTTCGGGATCCGTTTTGACATCCTGGTTTTTGGCACCGGAGGAAAATTTGACATTATCCAGCTGGT
TGTGTACATCGGCTCAACCCTCTCCTACTTCGGTCTGGTAAGAGATTCTCTTTTCCATGCTTTAGGAAAATGGTTTGGAGAAGGAAGTGAC
TAA

Figure 2.4: The P2X7RB base pair sequence. Primers were designed that bind early on in the gene sequence highlighted in red.

Table 2.1: Summary of P2X7R primers and their product length

Primers	Forward primer	Reverse Primer	Product size	Tm °C	Annealing temperature °C
P2X7R N-Terminal	TTGTGTCCCGAGTATCCCAC	TCAATGCCCATTATTCCGCC	413	57.6	55
P2X7R C-Terminal	ACCAGAGGAGATACAGCTGC	TACTGCCCTTCACTCTTCGG	399	58.3	55
Beta actin	TGGCACCACACCTTCTACAA	CTATCCCTGTACGCCTCTGG	182	58.7	55

2.2.4 End-Point PCR reaction

The cDNA was amplified using Promega GoTaq Flexi DNA polymerase kit. The reaction mix was as follows: DNA Polymerase (5 u/µL), 5X GoTaq® Reaction buffer, dNTPs (0.2 mM), $MgCl_2$ (1.5 mM) upstream and downstream primer (0.5 µM) and template cDNA (1 µg). The PCR samples were denatured for 2 minutes at 95°C for one cycle, followed by 35 cycles of denaturation at 90°C for 30 seconds, annealing temperature (Table 2.1) for 30 seconds, and extension at 72°C for 30 seconds. A final extension was then performed at 72°C for 5 minutes for one cycle before samples were held indefinitely at 4°C. Successful cDNA synthesis was confirmed by visualising

the amplified products on an electrophoretic gel. No template RT-ve were used in parallel with the RT+ve samples to detect genomic contamination in samples.

2.2.5 Gel electrophoresis

PCR products were identified using gel electrophoresis. A 2% agarose gel was made using 100 mL 1 X Tris-borate-EDTA (TBE) buffer with 2 g agarose (Fisher Scientific, Loughborough, UK) added. This was then microwaved for 2 minutes and left to cool for five minutes. Finally, 3 µL ethidium bromide at a concentration of 500 µg/mL was added for visualisation of the DNA. Gels were run at 200V for 30 minutes and were visualised using a Bio-Rad GelDoc TM XR+ Gel imaging system with a Quantity One software (Bio-Rad Laboratories, Hercules, CA, USA).

2.2.6 TaqMan® Real Time quantitative PCR (qPCR)

Equipment was treated using a UV light hood for 45 minutes prior to performing the reaction which was carried out in a 384 well plate. Each 10 µL reaction consisted of 5 µL 2x Universal Master Mix, 0.5 µL of the Taqman® gene expression assay, 2.5 µL nuclease free water (Applied Biosystems™) and 2 µL cDNA template. Plates were sealed, centrifuged at 300 g for 5 minutes. The qPCR was carried out on an Applied Biosystems 7900HT Real-Time PCR machine. The following Taqman probes were used: Human P2X7R Taqman® gene expression assay, ID: Hs00951600_m1 Catalog: 4351372, human HPRT Taqman® gene expression assay, ID: Hs02800695 Catalog: 1621448.

2.3 *In vivo* studies in murine models of OS

Animal work was carried out at the University of Sheffield Biological Services Unit. The work was performed under the project licence number: PF61050A3 (Professor Alison Gartland) in accordance with UK Home Office regulations and complied with the UK Animals (Scientific Procedures) Act 1986 which was reviewed and approved by the local Research Ethics Committee of the University of Sheffield (Sheffield, UK). Studies were designed using the Experimental Design Assistant (EDA) produced by the National Centre for the replacement, refinement and reduction of animals in research. Animal power calculations were designed in consultation with a statistician from the University of Sheffield School of Maths and Statistics.

2.3.1 Animals

7-9-week-old female BALB/c nude mice (Charles River Margate, UK) were housed under pathogen free conditions. All animals were healthy and pathogen-free at the start of each study and once each study had commenced they were monitored for any unexpected adverse effects. Animals were housed in their respective groups and the numbers per group were determined in consultation with a statistician from the University of Sheffield School of Maths and Statistics. A power calculation was performed, assuming that the mean and SD of 5.6 BV/TV (%) and 1.4 based on the pilot experiment (Chapter 5). A sample size of 10 mice would provide 80% power to see a 25% reduction in to 4.48 BV/TV (%) in the legs given a sham injection, at the 5% significance level. To allow for potential deaths/non-tumour take 12 mice per group were used. Mice were maintained under the same environmentally controlled conditions at room temperature with a 12-hour light/dark cycle, body weight measurements were taken twice a week to monitor health. If the body weight reduced below 20% of that before tumour implantation or tumours reached a mean width of >10 mm in any dimension, then animals were euthanised immediately using schedule 1 procedures.

2.3.2 Establishing a xenograft model of OS (pilot study)

Mice were anesthetized by inhalation of 100% w/v isoflurane (IsoFlo® Zoetis, London, UK) and 2% oxygen before a paratibial injection of 500,000 Te85, Te85+P2X7RA, Te85+P2X7RB, Te85+P2X7RAB, MNNG-HOS, or MNNG-HOS+GFP+LUC OS cell

lines suspended in 20 µL PBS (n= 3 mice/group). An example of an established OS tumour on a mouse limb is shown in Figure 2.5. Mice injected with MNNG-HOS+GFP+LUC and MNNG-HOS naïve OS cells were euthanised after 3 weeks and mice injected with Te85 or Te85 OS cells expressing the P2X7R isoforms were euthanised after 5 weeks by cervical dislocation. Both hind limbs with surrounding tissue remaining intact were collected along with the lungs, all tissue was fixed in 10% neutral buffered formalin at 4°C for 48 hours before been changed into 70% ethanol. Analysis of tumour burden and bone disease were performed as described below.

Figure 2.5: A representative OS tumour growing around a mouse tibia. Mice injected with 500,000 MNNG-HOS naïve OS cells formed palpable tumours after 9 days and after 12 days when 250,000 cells were injected paratibially. Both hind legs were collected for analysis with surrounding tissue left intact to preserve tumour architecture.

2.3.3 Targeting the P2X7RB *in vivo* in the MNNG-HOS model using A740003

Mice were anesthetized by inhalation of 100% w/v isoflurane and 2% oxygen before a paratibial injection of PBS (scratch control, n=12 mice), 250,000 MNNG-HOS (n=36 mice) or MNNG-HOS+P2X7RB (n=36 mice) cells in the left leg only. Mice were then divided into 7 groups (Table 2.2). After 2 days the mice were treated with either vehicle

(PBS+DMSO), Ifosfamide (30 mg/kg) or A740003 (50 µg/kg) administered by intraperitoneal (IP) injection 3 times a week for a total of 3 weeks (9 injections in total).

Table 2.2 Treatment groups in the MNNG-HOS xenograft model of OS.

Cell line	Mouse number	Treatment	Concentration
MNNG-HOS	12	Vehicle	N/A
MNNG-HOS	12	Ifosfamide	30 mg/kg
MNNG-HOS	12	A740003	50 µg/kg
MNNG-HOS+P2X7RB	12	Vehicle	N/A
MNNG-HOS+P2X7RB	12	Ifosfamide	30 mg/kg
MNNG-HOS+P2X7RB	12	A740003	50 µg/kg
Scratched only	12	N/A	N/A

All animals were anesthetized (100% w/v isoflurane and 2% oxygen by inhalation) for cardiac bleeding and euthanised by cervical dislocation. Both the left and right hind limbs were then collected with tissue remaining intact, the lungs were also collected. All tissue was fixed in 10% neutral buffered formalin at 4°C for 48 hours before been changed into 70% ethanol. Analysis of tumour burden and bone disease were performed as described below.

2.3.4 Calliper measurements

Basic calliper measurements were performed at the end of the experiment to determine the size of the tumour on the mouse leg. In addition, measurements were made on the legs *ex vivo* using scanned images from the micro-CT analysis. Tumour width were measured at the widest part of the tumour when the bone was orientated facing the same direction (Figure 2.6).

Figure 2.6: Tumour size measured using a micro-CT scan of the tumour bearing mouse leg. Each mouse was injected with 250,000 cells of either MNNG-HOS or MNNG-HOS+P2X7RB paratibially, suspended in 20 µL PBS. They were then treated with either vehicle, Ifosfamide or A740003 every 2 days for 3 weeks via an IP injection. The mice were euthanised and both legs collected, micro-CT scanned and analysed for the tumour size by measuring the widest part of the tissue. Legs were all orientated facing the same direction.

2.3.5 Micro-CT scanning

Mouse left and right tibia and fibulas were scanned on a Skyscanner micro-CT scanner (1272, Bruker, Belgium) set to take medium sized images (2016 X 1344) using a 0.5 mm aluminium filter and a detection pixel size of 8µm. Images were captured every 0.7°. Scanned images were reconstructed using Skyscan NRecon software (v. 1.6.9, Bruker, Belgium) and datasets were resized using Skyscan CTAn (v. 1.14.4, Bruker, Belgium). The region of interest (ROI) for the total bone volume included both the tibia and fibula and was determined at the top of the bone as soon as the tibia enters the image and femur is excluded, the bottom of the bone was determined at the point where the tibia and fibula meet (Figure 2.7). These regions were then produced by drawing on two-dimensional acquisition images.

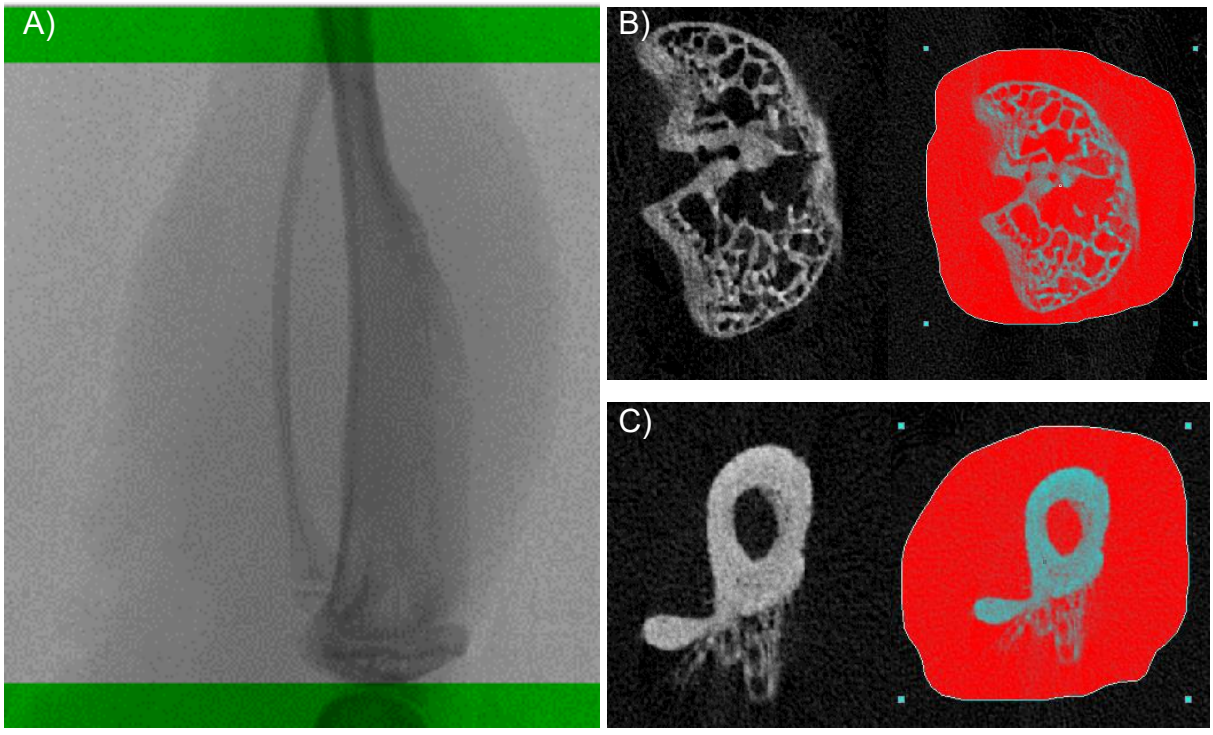

Figure 2.7 Example ROI for analysis of the total bone volume using micro-CT. Each mouse was injected with 250,000 cells of either MNNG-HOS or MNNG-HOS+P2X7RB paratibially. The mice were euthanised and both legs collected, micro-CT scanned and reconstructed. The ROI was drawn on the image around the bone and included both the tibia and fibula in the analysis **A)** Scan image of the full bone **B)** The ROI where the femur ends and tibia begins **C)** The ROI where the tibia and fibula meet.

2.3.6 Bone processing, embedding and sectioning

After micro-CT scanning bones were decalcified in 10% EDTA (20 x bone/leg volume) changing the solution twice a week for 3 weeks, these were then checked using the micro-CT that calcium had been removed. After decalcification tissues were then processed on the Leica TP1020 carousel tissue processor according to the following steps (Table 2.3):

Table 2.3: Bone processing stages on the Leica TP1020

Station	Solution	Time	Vacuum
2	70% Ethanol	2 hours	No
3	70% Ethanol	2 hours	No
4	70% Ethanol	2 hours	No
5	95% Ethanol	2 hours	No
6	95% Ethanol	2 hours	No
7	100% Ethanol	2 hours	No
8	100% Ethanol	2 hours	No
9	Xylene	2 hours	No
10	Xylene	2 hours	No
11	Leica 08605E wax melting point 56ºC	2 hours	Yes
12	Leica Wax (as above)	2 hours	Yes

After processing, the bones were wax embedded at a specific orientation which was the same for each bone. When sectioning, the wax block was first cooled on ice for 15 minutes before being attached to the Leica Microsystems Microtome and sectioned at 5 µm the sections were taken when the tumour was visible and fully exposed then put on to a 45°C water bath to “float” and be picked up using super-frost positively charged

slide. Finally, they were placed in an oven at 37°C to fully adhere to the slides overnight.

2.3.7 Bone histology and IHC- KI-67 and annexin V staining

Wax sections (3 μm) of the left tibiae were dewaxed in xylene, rehydrated through graded alcohols before performing heat mediated antigen retrieval using a water bath at 80°C for 20 min with citrate buffer at pH6 (Abcam, Cambridge, UK). Endogenous peroxidase was blocked with 3% hydrogen peroxide (VWR, Lutterworth, UK) for 30 min at room temperature, washed twice in PBS-tween (PBST) and blocked in 1% Normal goat serum in PBST (Vector Laboratories, Peterborough, UK) for 20 min at room temperature. Primary rabbit anti-human Ki-67 antibody (Abcam 1 mg/ml) or primary rabbit anti-human annexin V antibody (Abcam 1.5 mg/ml) was added to the sections at a dilution of 1:100 for Ki-67 and 1:200 for annexin V. Additionally, rabbit IgG (Abcam 5 mg/ml) was added to the sections at a dilution of 1:500 both in 1% casein. They were incubated for 1 hour at room temperature. After 2 washes in TBST, the sections were treated with biotinylated goat anti-rabbit IgG secondary antibody (Vector Laboratories) at 1:200 in 1% casein for 20 minutes at room temperature. Sections were washed twice in PBST then treated with an ABC kit (Vector Laboratories) for 20 min at room temperature and the bound antibody detected with Impact-DAB substrate-chromagen system (Vector Laboratories) for 5 min at room temperature. The sections were washed in tap water for 3 minutes, counter stained in Gills haematoxylin (VWR, Merck, Birmingham, UK) for 5 seconds, dehydrated through graded alcohols, and cleared with xylene. Coverslips were mounted using DPX. The slides were scanned using a Pannoramic 250 Flash III (3D HISTECH, Budapest, Hungary) and percentage of Ki-67/ annexin V cells quantified using QuPath software (Figure 2.8).

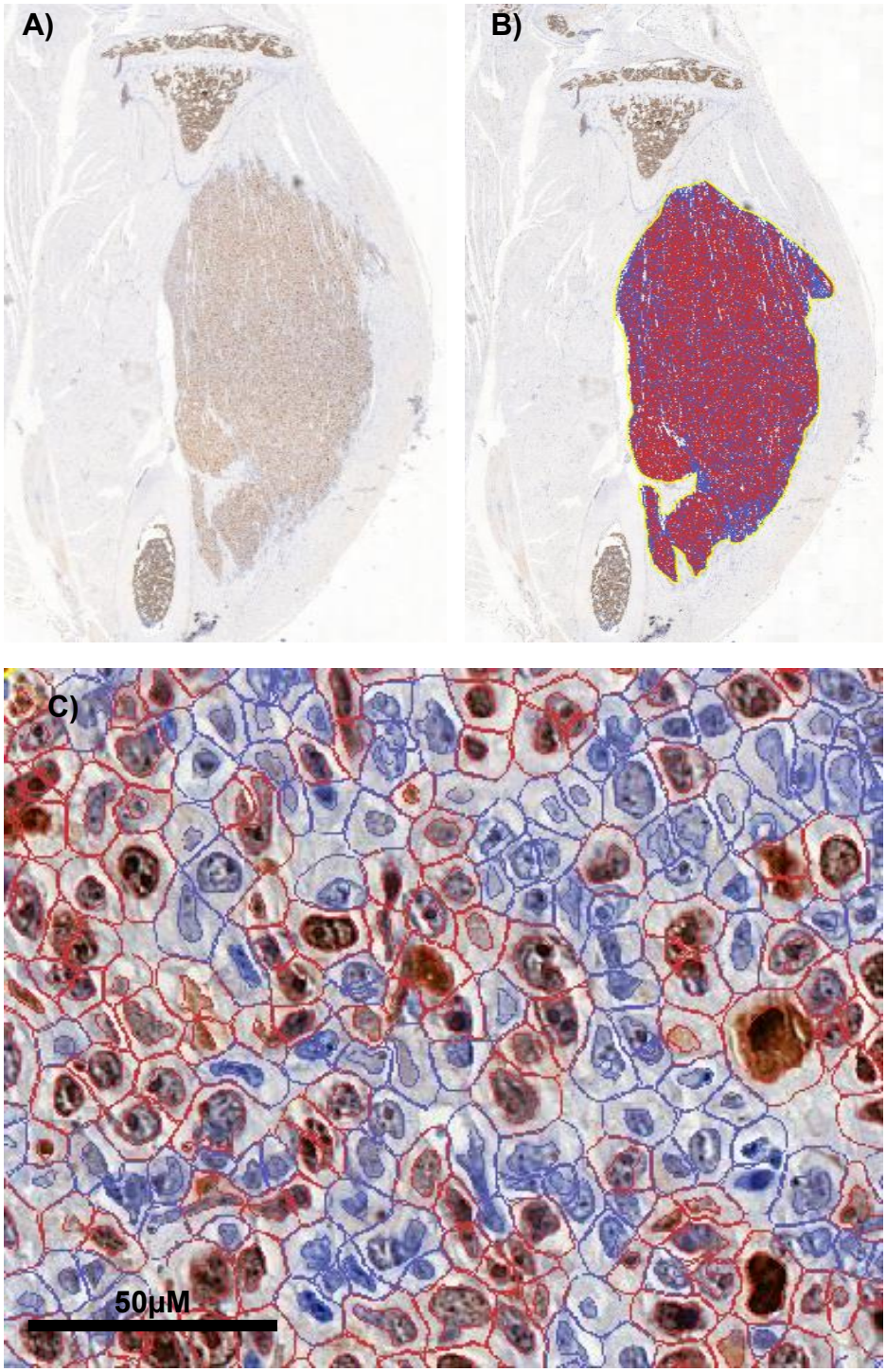

Figure 2.8: Example of a IHC ROI quantified using QuPath software. Each mouse was injected with 250,000 cells of either MNNG-HOS or MNNG-HOS+P2X7RB paratibially, they were then treated with either vehicle, A740003 or Ifosfamide every 2 days for 3 weeks via IP injection. The mice were then euthanised and dissected. The legs were collected processed, embedded into wax blocks and sections were taken to be stained for Ki-67 or annexin V. The sections were then analysed using QuPath. **A**) IHC staining **B)** Cells detected using Qupath **C)** The detection of positively stained cells red and the negatively stained cells blue.

2.3.8 Tartrate-resistant acid phosphate (TRAP) staining

Samples were dewaxed by passing them through xylene and graded alcohols, they were then incubated in pre-warmed acetate-tartrate buffer (0.1 M Sodium tartrate in 0.2 M acetate buffer [Both Sigma pH 5.2) at 37°C for 5 minutes. Followed by a 30 minute incubation at 37°C in 20 mg/mL Naphthol AS-BI phosphate Dimethylformamide (Sigma/Fisher Scientific) in acetate-tartrate buffer. The samples were then incubated in acetate-tartrate buffer hexazotised pararosaniline solution for 15 minutes at 37°C, counterstained in haematoxylin for 10 seconds, washed in tap water for 5 minutes, dehydrated by passing through graded alcohols and cleared with xylene. Coverslips were then mounted using DPX. Osteoclasts were analysed at the bone-tumour interface using an osteomeasure (Figure 2.9).

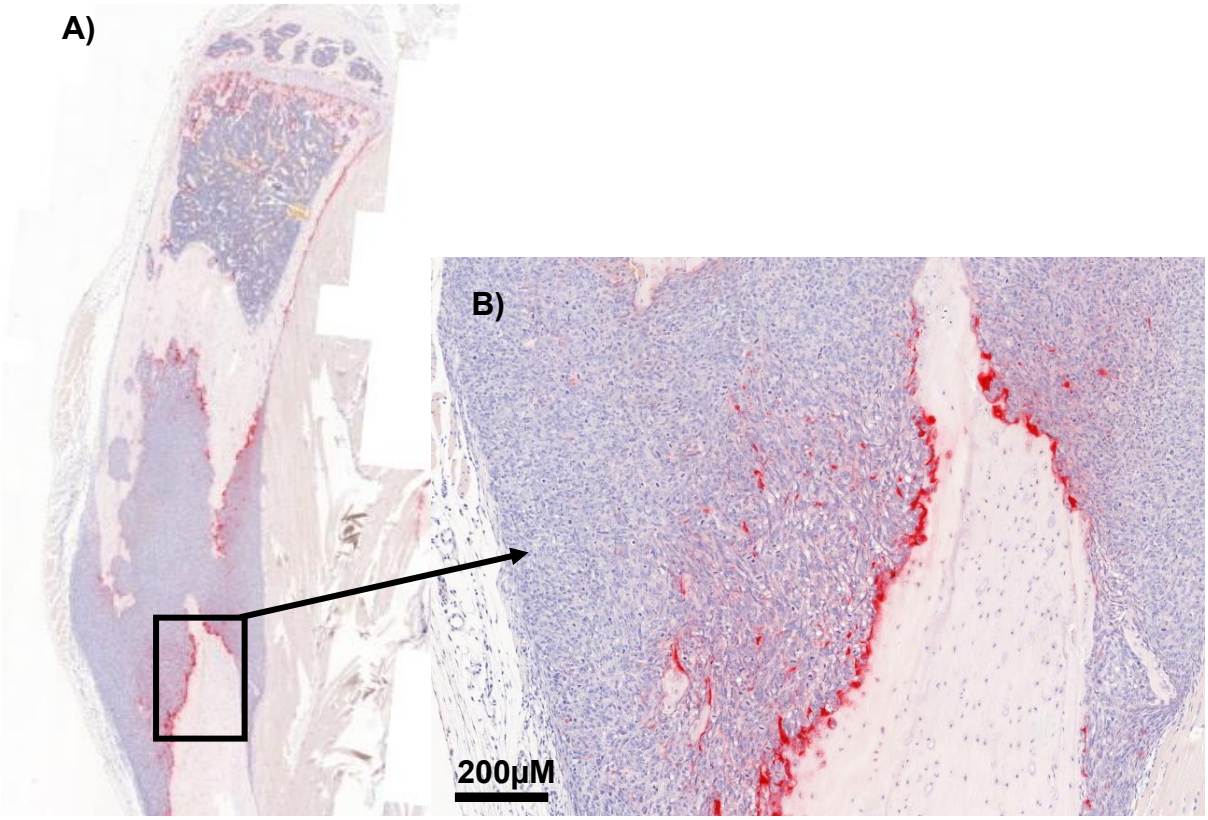

Figure 2.9: Representative TRAP stained tibia section showing osteoclasts in red. To visualize TRAP activity, Naphthol AS-BI phosphate is used as a substrate for TRAP. The product of this reaction can then react with a diazonium salt (hexazotised pararosalinine) which will leave a red precipitate and can be visualised. **A)** The tumour is shown forming at the surface of the bone **B)** Osteoclasts visibly stained red at the point in which the tumour cells meet the bone surface.

2.3.9 Haematoxylin & eosin staining

Sections were added to xylene twice for 5 minutes to remove the wax. They were rehydrated through graded alcohols for 5 minutes each and tap water for 1 minute. The nuclei were then stained by Gill's II haematoxylin (VWR). for 90 seconds and wash using tap water for 3 minutes. 1% aqueous eosin (VWR) with 1% calcium carbonate (Sigma) was used to stain the cytoplasm for 5 minutes. The slides were then quickly dehydrated through tap water (30 seconds) to remove eosin, 70% IMS (10 seconds), 95% IMS (10 seconds), 99% IMS (30 seconds), and 99% IMS (30 seconds). Finally, the slides were passed through xylene to remove IMS and mounted with coverslips using DPX.

2.3.10 Lung analysis

Lungs were collected and fixed in 10% neutral buffered formalin for 48 hours at 4 °C before been changed into 70% ethanol, they were then processed as above and embedded in wax cassettes. To section the lungs 6 µm sections were cut every 100 µm deep to cover the entire lung and stained using Gill's II haematoxylin and eosin as above. Lung sections were visualised under a light microscope and observed for the presence of any metastasis.

2.3.11 Statistics

All data was analysed using GraphPad Prism version 7.00 for Windows (GraphPad Software, La Jolla California, USA). Statistical outliers in the data were removed using the ROUT method, and normality tested using the D'Agostino and Pearson omnibus normality test. Statistical significance was tested using parametric or non-parametric tests as appropriate. For comparing two groups, either a paired or unpaired t-test was used depending upon the groups to be compared, with a Mann-Whitney test for non-parametric data. For comparing more than two groups, Ordinary One-way ANOVA was used with Tukey's multiple comparison test for parametric data and a Kruskal-Wallis test with Dunn's comparison for non-parametric data. Slopes were compared using linear regression. The difference was considered significant for $P<0.05$.

Chapter 3 – P2X7R expression and function in Te85 OS cells *in vitro*

3.1 Introduction

Investigation of the tumour microenvironment has gained great importance for the understanding of tumour formation and progression, with various processes playing a role in OS. P2X7R signalling is ubiquitous and found to influence almost every cell system in the human body (Morandini *et al*., 2014) with a variety of different cancers expressing P2X7Rs (Burnstock, 2017). The P2X7R is the least sensitive P2X receptor to ATP and requires a 100 fold greater level of ATP to activate than for other P2X receptors (North, 2002). Studies have identified ATP to be at a high concentration in the tumour microenvironment in the range of hundreds of micromoles (Adinolfi, 2013, Qiu *et al*., 2014), yet low (10-100 nM) in surrounding healthy tissue (Pellegatti *et al*., 2008). This is particularly pertinent in the case of the bone tumour microenvironment where mechanical loading can stimulate ATP release (Rumney *et al.,* 2012, Genetos *et al*., 2010). Additionally ATP can be released through tumour cell death caused by stresses such as inflammation, hypoxia, and non-targeted therapies (Gilbert *et al.*, 2019). Dependent upon its level of activation mediated by extracellular ATP the P2X7R plays a role in both cell apoptosis and cell proliferation, the pore formation ability is mediated by the C terminal (Smart *et al.,* 2003) and is responsible for the apoptosis activated with high concentrations of ATP (Roger *et al.,* 2015). Cells become capable of allowing molecules with a mass of up to 900 Da to enter the cell (Volonte *et al*., 2012). Without this feature P2X7Rs are referred to as having a non-functional phenotype (Figure 3.1) (Barden *et al.,* 2014). Changes in P2X7R expression and function can vary dependent on tissue type and stage of differentiation, or can occur through splice variants and single nucleotide polymorphisms (Worthington *et al.,* 2006*)*.

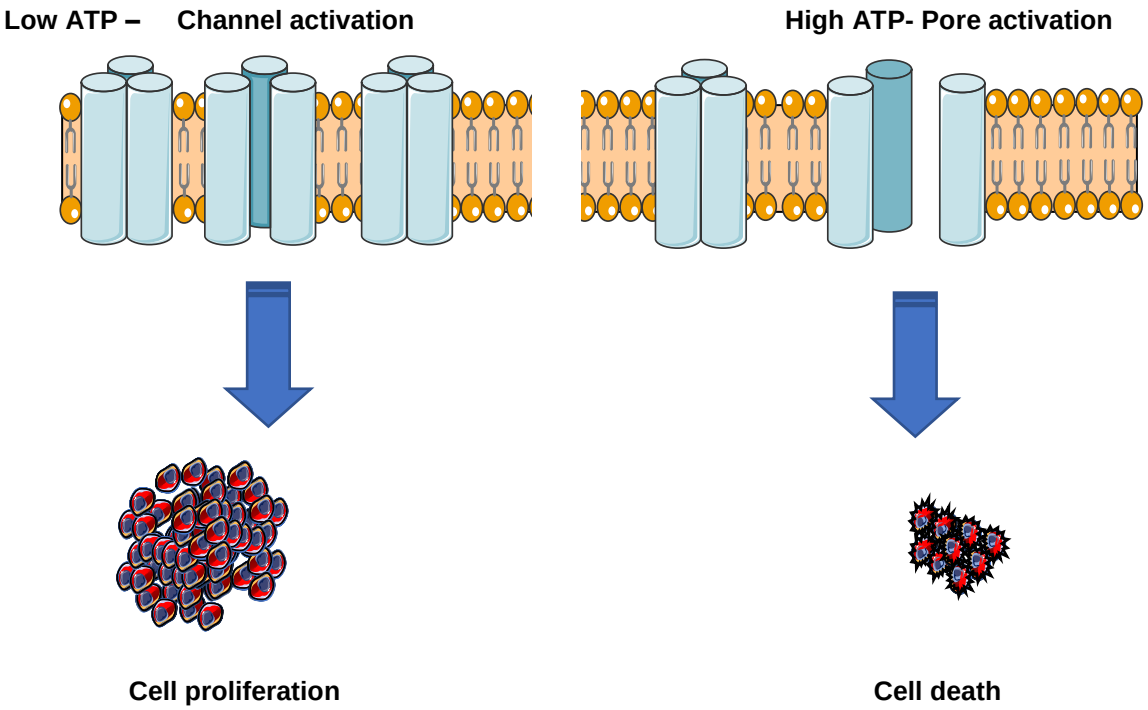

Figure 3.1 The contrasting roles played by the P2X7R in the cell microenvironment. P2X7R stimulation with low levels of ATP under tonic conditions can stimulate cell survival and proliferation, however when a high amount of ATP is present a large cytolytic pore can form and induce P2X7R-dependnt lysis.

Over-expression of a possible cytotoxic P2X7R by cancer cells is confusing, however, a non-functional receptor with oncogene-like properties may provide an explanation for this. The non-functional variants still retain the ability to signal with Ca2+, Na+ and K, and in a tumour setting leads to various morphological changes related to metastatic potential. This includes; membrane blebbing, loss of various adhesion proteins such as L-selectin, matrix metalloproteinase and cathepsins, influence cytokine release, increase cell survival, proliferation, migration and cancer cell invasion (Barden *et al*., 2014, Gilbert *et al.,* 2019). Expression of non-functional P2X7Rs has been demonstrated in a range of different cancer types and have been found to be upregulated when compared to corresponding healthy tissue. Expression of non-functional P2X7Rs have been examined using a specific non-functional specific P2X7R antibody in tissue originating from: Mesothelioma, lymphoma, thyroid papillary carcinoma, Hodgkin's lymphoma, oligodendrogliomas, glioblastomas, astrocytomas, bowel adenocarcinoma, ovarian serous tumour, cervical cancer, endometrial carcinoma of the uterus, small cell lung cancer, hepatocellular carcinoma, transitional cell carcinoma of the bladder and Barrett's mucosa with adenocarcinoma. Additionally,

tumours of mesenchymal origin express non-functional P2X7Rs including gastrointestinal stromal tumour, endometrial stromal tumour and Ewing's sarcoma (Barden *et al.*, 2014).

P2X7R expression and functional characteristics in OS and osteoblast cells is varied, one study showed P2X7R expression at the mRNA level for both Te85 and Saos-2 OS cell lines. In addition, P2X7R surface expression was detected in Saos-2 cells, but not Te85 OS cells (Gartland *et al.,* 2001). To further confirm the characteristics of the P2X7R in Saos-2 and Te85 OS cells pore formation was assessed and consistent with the P2X7R mRNA expression data, Saos-2 cells, but not Te85 OS cells, were found to form transmembrane pores when stimulated with BzATP (Gartland *et al.,* 2001). Other studies have found that P2X7R was expressed in bone marrow-derived stromal cells and in primary human trabecular osteoblasts, with only the mature cell type having fully functional P2X7R (Agrawal *et al*., 2017) however, they are also found on MSC cells (osteoblast precursors) and contribute towards cell differentiation and osteogenesis (Kaebisch *et al*. 2015).

To determine the role that P2X7Rs play in the pathology of OS, demonstration of their presence and of their functional characteristics is required for them to be targeted in the bone OS microenvironment therefore this chapter has the following aims:

- To determine if P2X7R mRNA is present in transfected Te85 OS cells, this will be assessed using end-point PCR and qPCR.
- To determine P2X7R intracellular calcium activation in the different Te85-P2X7R variant OS cells using Fluo-4AM.
- To determine if the transfected variants have P2X7R pore formation activity.

3.2 Expression of P2X7R variants in naïve and transfected Te85 OS cells using end-point PCR

The Te85 human OS cell line normally lacks endogenous P2X7R protein expression, therefore, this cell line acts as a suitable model to investigate the effects of expressing the receptor, which was achieved by stable transfection. Te85 OS cell lines were previously transfected with plasmids containing the full length P2X7RA, the truncated isoform P2X7RB and a co-transfected P2X7RAB variant, (courtesy of a previous Gartland Bone Group member Dr Eric Wang). HEK-293 cells were used as a positive control and had previously been transfected with the full length P2X7RA variant (courtesy of Dr Elena Adinolfi, Ferrara Italy).

RNA was isolated from the above cell lines and cDNA synthesized (Chapter 2 section 2.2). The success of the cDNA reactions was confirmed with the housekeeping gene beta actin with a clear band at 182 BP. RT+ve and a RT-ve control were used (Figure 3.2).

P2X7R mRNA expression was determined with two sets of primers for the P2X7R. The first primer set was designed early in the gene sequence with the forward primer on the exon boundary between exon 3 and 4 and the reverse between exon 7 and 8. This region is present on both the full length and truncated P2X7RB, (product length 413 BP). The second primer set was designed further along the gene sequence with the both the forward primer and reverse primer designed to bind to exon 13 (product length 399 BP) this region is only present on the full length P2X7RA and thereby unable to be detected in the cells with the truncated P2X7RB.

The results demonstrate that bands were produced in the HEK-293 positive control cells with very little P2X7R expression in Te85 naïve OS cells; this was increased in Te85 OS cells transfected with the P2X7R variants (A, B, and AB, Figure 3.3).

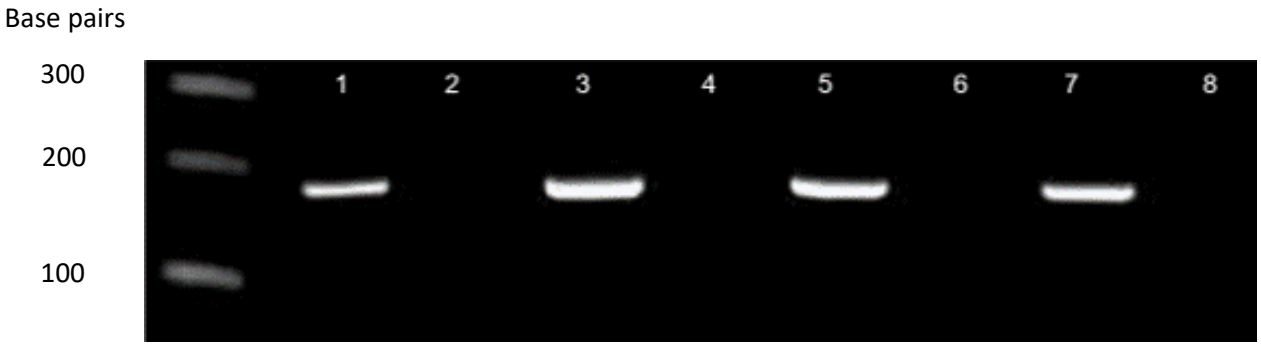

Figure 3.2: Confirmation of successful cDNA synthesis using the beta actin housekeeping gene in Te85 OS cells with different P2X7R variants. Lanes **1 & 2** Te85 naïve OS cells, RT+ve and RT-ve, lanes **3 & 4** Te85+P2X7RA OS cells, RT+ve and RT-ve, lanes **5 & 6** Te85+P2X7RB OS cells, RT+ve and RT-ve, lanes **7 & 8** Te85+P2X7RAB OS cells, RT+ve and RT-ve. All beta actin product lengths are at 182 BP.

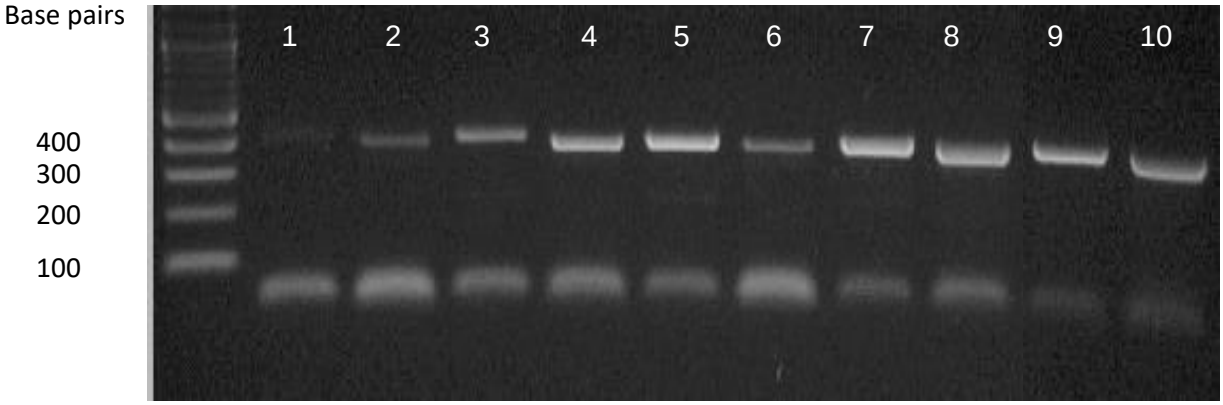

Figure 3.3: P2X7R expression in transfected Te85 OS cells with HEK-293+P2X7RA control. Expression of P2X7R mRNA in Te85 OS cells was determined with two different P2X7R sets of primers, one set binding to both P2X7RA and P2X7RB, the second set binding to a region on P2X7RA that is truncated on P2X7RB (product length 413 BP and 399 BP respectively). DNA from each cell type was amplified with both primer sets. Lane **1 & 2**: Te85 naïve OS cells, lane **3 & 4**: Te85+P2X7RA OS cells, lane **5 & 6**: Te85+P2X7RB OS cells, lane **7 & 8**: Te85+P2X7RAB OS cells, lane **9 & 10**: HEK-293+P2X7RA cells (control).

3.3 Expression of P2X7R variants in Te85 OS cells using qPCR

In addition to end-point PCR showing bands for P2X7R expression, qPCR was used to demonstrate gene expression changes in transfected cells. Delta cycle threshold (ΔCT) values were calculated by normalising target templates to HPRT a housekeeping gene, delta delta CT values and fold changes were then calculated. Transfected cells were compared to the untransfected Te85 naïve OS cells with results plotted as fold change. The human P2X7R Taqman® primer used is not isoform specific and will therefore detect both P2X7RA and P2X7RB.

The results demonstrate that there is a significantly increased P2X7RA average fold change expression in transfected Te85 OS cells (P=0.0148, Figure 3.4) a significantly increased P2X7RB expression in transfected Te85 OS cells (P=0.0027, Figure 3.4) and a significantly increased P2X7R expression in the P2X7RAB co-transfected variant (P=0.0012, Figure 3.4) compared to Te85 naïve OS cells. There was no significant difference in the levels of P2X7R expressions amongst the transfected cell lines.

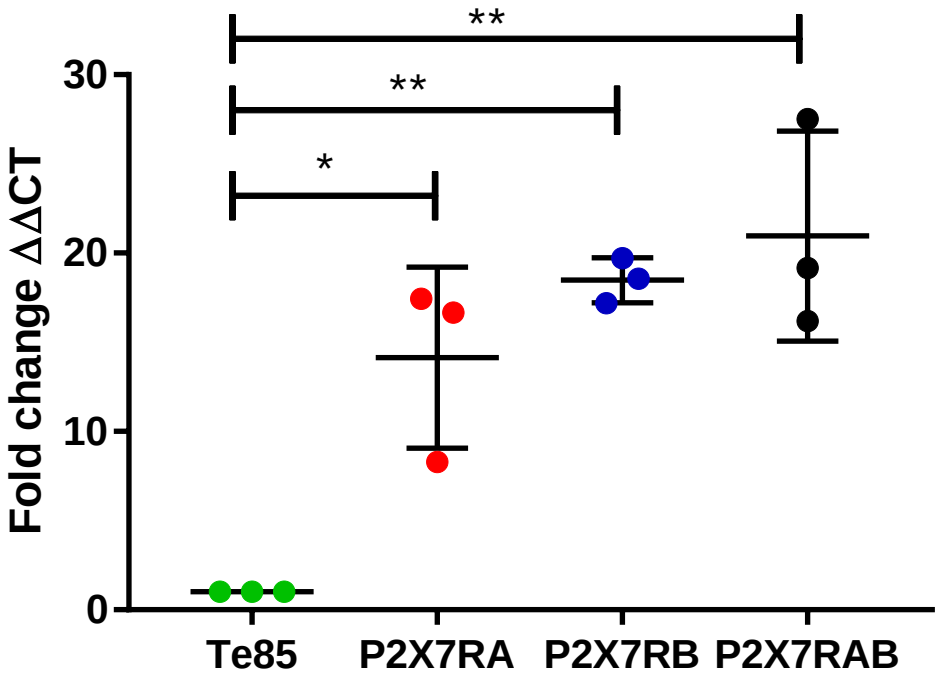

Figure 3.4: Quantification of P2X7RA, P2X7RB and P2X7RAB expression in Te85 OS cells. RNA was extracted from Te85 OS cells reverse transcribed to cDNA then amplified using qPCR, HPRT was used as a housekeeping gene with data expressed relative to this and the Te85 naïve P2X7R expression levels shown green, Te85+P2X7RA OS cells shown red, P2X7RB OS cells shown blue and P2X7RAB OS cells shown black. Data is from three biological repeats with six technical repeats per experiment with three technical repeats using the P2X7R Taqman probe and three using the HPRT Taqman probe. Results were analysed using a one-way ANOVA with Tukey's multiple comparisons test, * = P <0.05 ** = P <0.01.

3.4 Measurement of intracellular calcium activation in P2X7R transfected Te85 OS cells

Changes in cytosolic free calcium concentrations were measured in naïve and transfected cells. Cells were plated out at a density of 15,000 per well in 96-well plates and left overnight to adhere, the media was then changed into an equal solution of complete medium and 2X Fluo-4 Direct™ calcium reagent loading solution. Cells were incubated for 1 hour at 37°C before been stimulated with BzATP (100 µM) and then ionomycin (0.8 µM).

The results for calcium activation were plotted relative to its ionomycin response (Figure 3.5 A). The area under the curve (AUC) (Figure 3.5 B) and peak intensity (Figure 3.5 C) were plotted. The results demonstrate that there was a significantly increased AUC in cells when transfected with P2X7RA (Te85+P2X7RA 550.9 ± 22.13 SEM vs 378.4 ± 13.22 SEM Te85 naïve, $P<0.0001$, Figure 3.5 B) when transfected with P2X7RB (Te85+P2X7RB 470.9 ± 14.71 SEM vs 378.4 ± 13.22 SEM Te85 naïve, $P<0.0001$, Figure 3.5 B) and when transfected with P2X7RAB (Te85+P2X7RAB 542.7 ± 20.97 SEM vs 378.4 ± 13.22 SEM, Te85 naïve, $P<0.0001$, Figure 3.5 B) when compared to Te85 naïve OS cells.

The results for the peak intensity demonstrate that there was a significantly increased peak intensity in cells transfected with P2X7RA (Te85+P2X7RA 2.99 ± 0.1254 SEM vs 1.8 ± 0.6541 SEM Te85 naïve, $P<0.0001$, Figure 3.5 C) when transfected with P2X7RB (Te85+P2X7RB 2.486 ± 0.4863 SEM vs 1.8 ± 0.6541 SEM Te85 naïve, $P=0.0006$, Figure 3.5 C) and when transfected with P2X7RAB (Te85+P2X7RAB 3.239 ± 0.1458 SEM vs 1.8 ± 0.6541 SEM Te85 naïve, $P= <0.0001$, Figure 3.5 C) when compared to Te85 naïve OS cells.

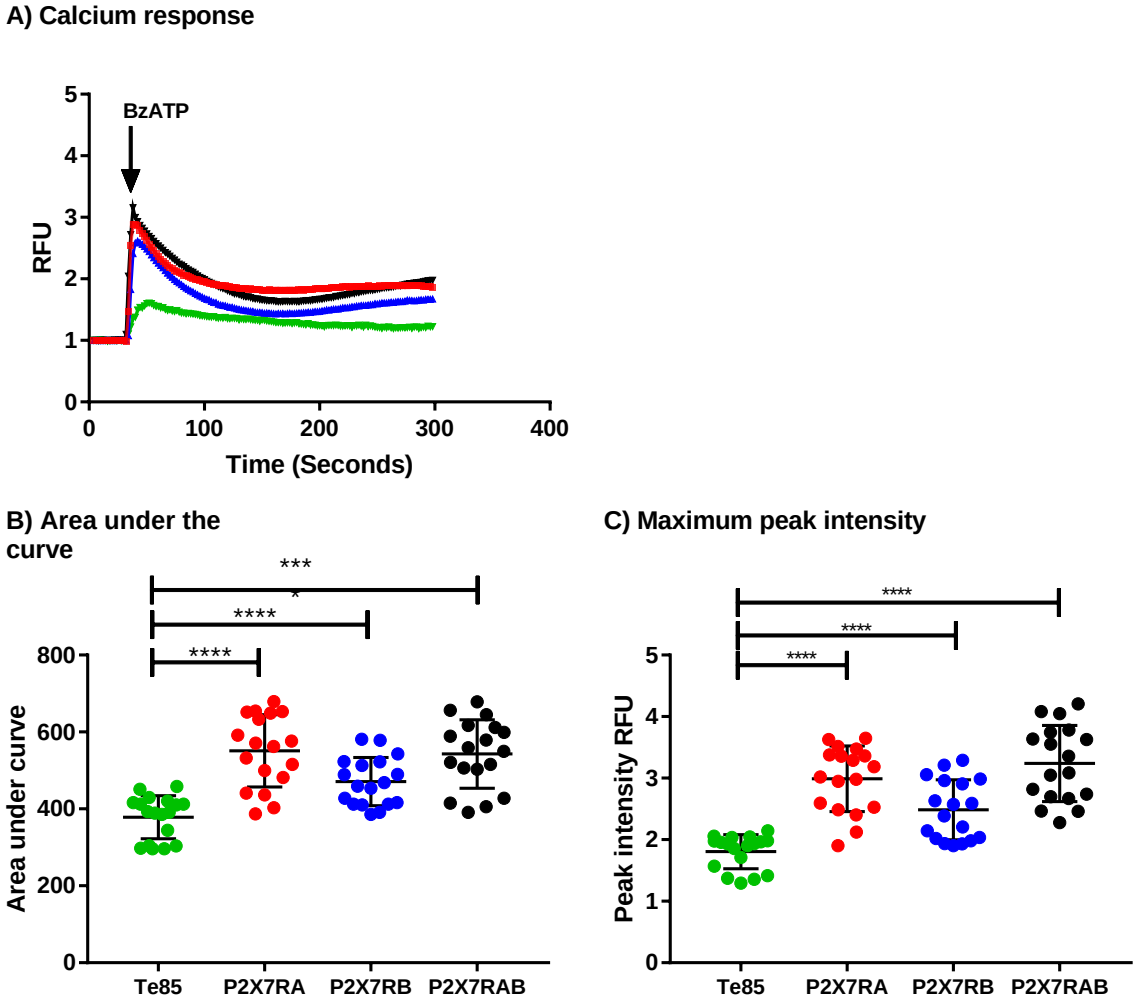

Figure 3.5: Measurement of intracellular calcium activation in P2X7R transfected Te85 OS cells after P2X7R stimulation with BzATP. Cells were seeded at 15,000 cells in 96-well plates and left overnight to adhere. The media was then changed into an equal solution of complete medium and 2X Fluo-4 Direct™ calcium reagent loading solution. Cells were then incubated for 1 hour at 37°C before been stimulated with BzATP (100 µM) and then ionomycin (0.8 µM) **A)** Calcium response for the different P2X7R variants, **B)** The AUC **C)** The maximum peak intensity. Te85 naïve OS cells are shown green, Te85+P2X7RA OS cells shown red, P2X7RB OS cells shown blue and P2X7RAB OS cells shown black. Results are from 3 biological repeats with 6 technical replicates. Results were analysed comparing each group to the Te85 naïve OS cells using an unpaired T-test **** = P <0.0001.

3.5 Measurement of P2X7R pore formation in transfected Te85 OS cells

Sustained stimulation of the P2X7R with its agonist ATP enables the P2X7R to form a large irreversible pore permeable to molecules with a molecular weight of up to 900 Daltons (Da) (Volonte *et al*., 2012). This includes large organic dyes such as ethidium bromide (molecular weight 394). This function is unique to the P2X7R subset of purinergic receptors and has a variety of roles. Therefore, this function was assessed in Te85 OS cells transfected with the different variants, with HEK-293 cells used as a positive control. A density of 15,000 cells/well were cultured in a 96 well plate, left overnight to form a monolayer and incubated in HBSS buffer for 1 hour prior to analysis. The pore formation function was then stimulated using 300 µM BzATP in the presence of 100 µM ethidium bromide and monitored for 45 minutes to assess the dye uptake by fluorescence emission at an excitation/emission wavelength couple of 360/580 nm. Cells were also treated with 10 µM of A740003, a P2X7R specific inhibitor, to confirm the pore was due to P2X7R expression.

The results demonstrate that as expected, activation with BzATP of the fully functional P2X7RA variant in HEK-293 cells led to uptake ethidium bromide, hence demonstrating pore formation and was used as a positive control to compare to pore formation in the Te85 OS cells, this effect was attenuated with the addition of A740003 shown in (Figure 3.6 A, C, E, G).

The assay demonstrated as expected, no functional pore formation ability in the untransfected Te85 naïve OS cells (Figure 3.6 B). However, the Te85 OS cells transfected with the full length P2X7RA variant also did not demonstrate functional pore formation, (Figure 3.6 D). There was no pore formation in the Te85+P2X7RB variant (Figure 3.6 F). The Te85+P2X7RAB variant did demonstrate the ability to produce a fully functional pore typical of the classical P2X7R, this effect was attenuated with the addition of A740003 (Figure 3.6 H).

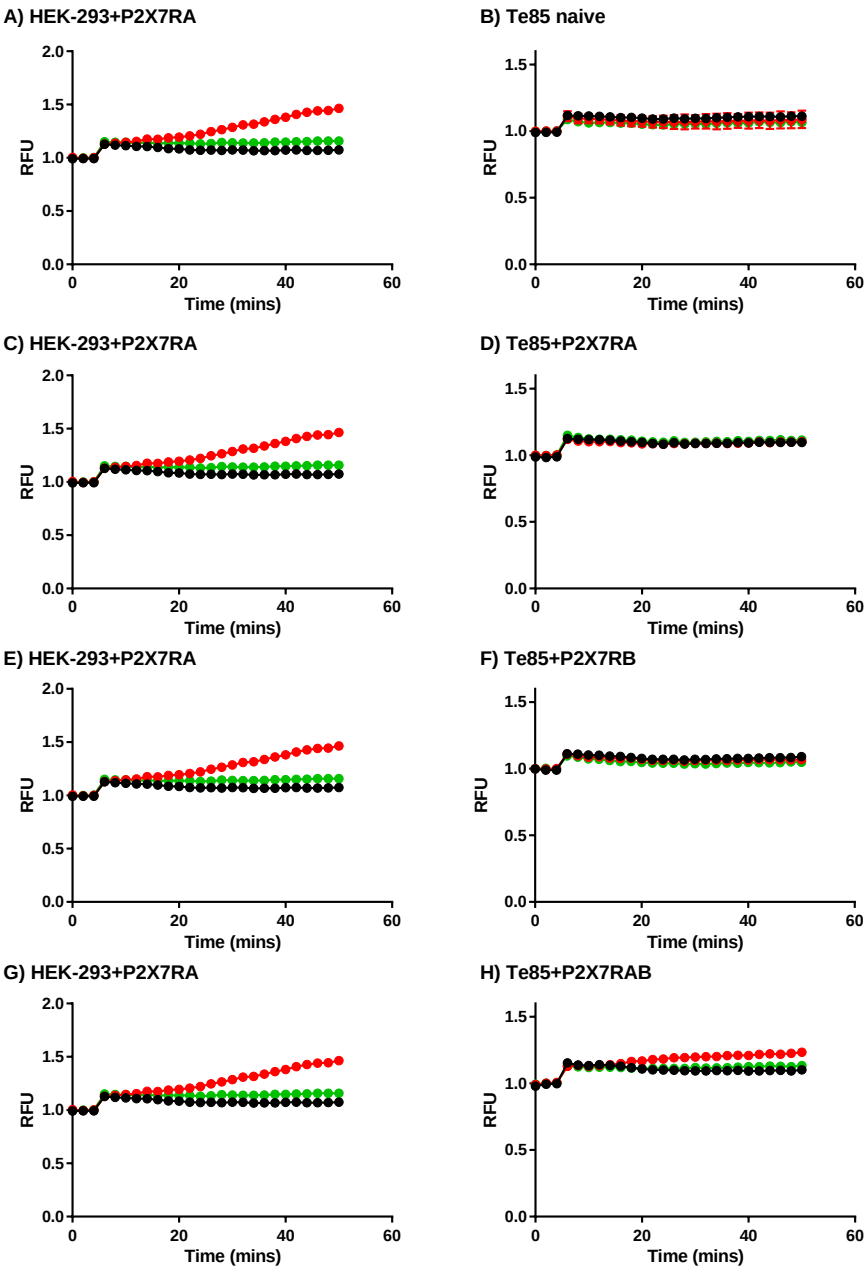

Figure 3.6: Ethidium bromide uptake in response to P2X7R activation in Te85 OS cells. Cells were plated out into 96-well plates and left overnight to adhere, the media was then changed to HBSS and incubated at 37°C with or without 10 µM of the P2X7R inhibitor A740003 for 1 hour. BzATP was diluted in ultra-pure ethidium bromide to a final concentration of 300 µM BzATP and 100 µM ethidium bromide. Induction of the P2X7R pore formation was detected for 45 minutes after an initial 5-minute baseline reading, with readings taken every 2 minutes. **A, C, E, G)** Transfected HEK-293+P2X7R cells known to form pores used as a positive control. **B)** Te85 naïve OS cells **D)** Te85+P2X7RA OS cells **F)** Te85+P2X7RB OS cells **H)** Te85+P2X7RAB OS cells. Red are cells stimulated with BzATP, green are stimulated with BzATP but containing the A740003 inhibitor, black indicates the cells incubated with ethidium bromide only and no BzATP stimulation. Results are from three biological repeats with six technical replicates.

3.6 Discussion

This purpose of this chapter was to demonstrate P2X7R expression and function in the Te85 OS cell line. Te85 naïve OS cells have a very negligible expression of P2X7R at mRNA level, don't have P2X7R calcium activation or the typical P2X7R pore formation response to stimulation with BzATP, this is in accordance with previous studies (Gartland *et al.,* 2001, Giuliani *et al*., 2014). In order to investigate the role that P2X7R plays in OS the full length P2X7RA and truncated P2X7RB were transfected into Te85 OS cells along with a co-transfected cell line expressing both P2X7RA and P2X7RB, the transfected variants were then checked for mRNA expression calcium activation, and pore formation.

After transfection there is a clear band for mRNA expression in all transfected Te85 variants. There is also an increased calcium response when stimulated with BzATP in P2X7R expressing cell lines. The Te85 OS cell line transfected with full length P2X7RA didn't demonstrate the pore formation, this was unexpected as the P2X7RA is usually capable of this response in other cell lines, such as the HEK-P2X7RA control cells (Adinolfi *et al.,* 2010).This is also the case for the Te85+P2X7RB OS cell line but this was an expected result as this isoform is truncated and missing the C terminal region responsible for pore formation. The co expressing P2X7RAB variant did produce the P2X7R pore, suggesting some subunit interactions, its again been shown in HEK-293 cells that co transfection with both variants produced a pore formation response higher than in P2X7RA expressing cells alone (Adinolfi *et al.,* 2010).

The results in this chapter provide a future basis to target P2X7R variants by confirming successful transfection of the Te85 OS cell line, thereby they can be used as a suitable *in vitro* model system. The increased level of ATP in tumour sites would be enough to stimulate P2X7R pore formation and could potentially be exploited to induce cancer cell death, drug delivery or chemotherapy loading. There is some evidence that P2X7R-dependent lysis could reduce cell proliferation of chronic lymphocytic leukaemia cells *in vitro* due to the cytotoxic effect of high ATP concentrations (Adinolfi *et al*., 2011). However the mechanism relating to pore formation isn't fully understood, whether pore formation even occurs *in vivo* is unknown, and the P2X7R pore function isn't always present depending upon cell type (Di Virgilio *et al.,* 2018). This chapter provides data demonstrating that the P2X7R

variants in the Te85 OS cells don't have the typical P2X7R pore formation and thereby they present a non-functional phenotype. Basal activation of P2X7Rs has previously been shown to contribute towards cell survival and proliferation by increasing internal ATP content and supporting mitochondrial activity whereas the pore formation function paradoxically contributes towards mitochondrial catastrophe and P2X7R-dependent lysis (Di Virgilio *et al.,* 2018). It could be the case that P2X7R expression may drive growth or cell survival and other important OS disease promoting properties when expressing the non-functional variants shown here. The effect that P2X7R variant expression has in the context of OS can be explored in future chapters now that the OS P2X7R cell lines have been generated and confirmed here.

Chapter 4 – The effect of P2X7R expression on Te85 OS cell properties *in vitro*

4.1 Introduction

Tumour survival and growth relies on the capability to acquire a phenotype displaying rapid uncontrolled proliferation of cells, which can be influenced by a variety of molecular, genetic and growth sustaining/promoting changes (Hanahan *et al*., 2000) OS tumours in most cases exhibit a highly aggressive and malignant phenotype of proliferating transformed osteoblasts, the underlying mechanisms of which are yet to be revealed and targeted (Evola *et al.,* 2017). Despite the expression of P2X7Rs in OS cell lines and implications in various other cancer models, the role of the P2X7R in the context of OS physiology has been minimal. However, in this chapter using the previously transfected Te85 OS cells with P2X7RA, P2X7RB, and P2X7RAB isoforms, investigations have been performed to determine if its expression affects various cancer properties in OS. Te85 OS cells expressing P2X7R variants have previously been shown to increase proliferation under serum free conditions (Giuliani *et al*., 2014), yet other properties that P2X7R variants may influence such as cell adhesion, cell migration and cell invasion have not been assessed previously. This chapter presents the results of these experiments and discusses the possible implications. P2X7R expression could potentially contribute to tumour progression, and metastasis. This chapter will demonstrate if the P2X7R can provide a viable target for inhibiting OS growth through receptor antagonism *in vitro* using A740003 and AZ11645373.

Although several studies have demonstrated the role of P2X7Rs in both diseased and normal physiological conditions both *in vitro* and *in vivo*, there are contrasting views in the cancer field of the role P2X7Rs plays in tumour growth and progression. On the one hand it can support cell growth and proliferation, and on other hand it can have a paradoxical cytolytic role in ATP mediated cell death/apoptosis through activation of a large non-selective pore (Di Virgilio & Adinolfi, 2017) This bi-functional phenotype has led to increasing debate over the part that P2X7Rs play in modulation of the tumour microenvironment. It is yet to be determined fully if P2X7R can be used as a therapeutic target for pharmacological intervention in cancer (Roger *et al*., 2015).

Increased proliferation of cell lines was initially attributed to P2Y receptors, the first study correlating P2X7R expression to an increase in proliferation was performed in 1999 using k562 and LG14 leukaemia cell lines (Baricordi *et al.,* 1999). Since this period a number of studies have shown that P2X7R expression can influence not only

cell proliferation but also adhesion, migration, and invasion, and that P2X7R antagonism can reduce these effects (Di Virgilio & Adinolfi, 2017).

To determine the role that P2X7Rs play in the pathology of OS a number of experiments were performed in this chapter, which has the following aims

- To determine if expression of the P2X7R variants can affect proliferation in Te85 OS cells *in vitro* in varying concentrations of FBS.
- To determine if antagonism of the P2X7R variants using A740003 and AZ11645373 can affect the proliferation of Te85 OS cells *in vitro.*
- To determine if expression of the P2X7R variants affect Te85 OS cell adhesion to a type 1 collagen matrix *in vitro*.
- To determine if expression of the P2X7R variants affects Te85 OS cell migration in various concentrations of FBS and when stimulated with BzATP *in vitro*.
- To determine if expression of the P2X7R variants affects Te85 OS cell invasion when stimulated with BzATP *in vitro*.

4.2 Effect of P2X7R expression on Te85 OS cell proliferation

Having established that the transfected Te85 OS cell lines do indeed contain mRNA for the P2X7R, and validated their typical P2X7R responses for each variant including intracellular calcium responses, and pore formation (Chapter 3), the effect of receptor expression on cell physiology was determined. The first parameter that was examined was the Te85 ability to grow in varying serum concentrations. Te85 OS cells were grown to 50% confluence then counted and seeded into 96 well plates at various cell densities (1250, 2500, and 5000). After 24 hours, the media was changed to either 0.5%, 2% or 10% FBS. Cell proliferation was assessed using an MTS assay at days 0, 1, 3, 5 and 7.

Te85 OS cells that had been transfected with either the P2X7RA isoform (Te85+P2X7RA) the P2X7RB isoform (Te85+P2X7RB) or both P2X7RA and P2X7RB (Te85+P2X7RAB) when cultured in 0.5% FBS had a significant increase in proliferation ($p<0.05$) compared to Te85 naïve OS cells across all seeding densities and at all the time points (Figure 4.1 A, B, C). At 2% FBS there was a significant increase in proliferation for Te85+P2X7RA OS cells on all days when seeded at 1250 cells, on day 3 and 5 at 2500 cells and on day 3 only at 5000 cells. This was the same for P2X7RB expressing cells. For P2X7RAB expressing cells there was an increase in proliferation on day 3 and 7 but not on day 5 across all seeding densities (Figure 4.1 D, E, F). At 10% FBS there was an increase in proliferation for Te85+P2X7RA and Te85+P2X7RB on days 3 and 5. However, the Te85 naïve OS cell proliferation reached similar levels by day 7 when the cell density became saturated and growth reached a plateau. Te85+P2X7RAB expressing cells had a significant increase in proliferation at day 3 across all seeding densities at day 5 and 7 with 1250 cells and day 7 at 5000 cells (Figure 4.1 G, H, I).

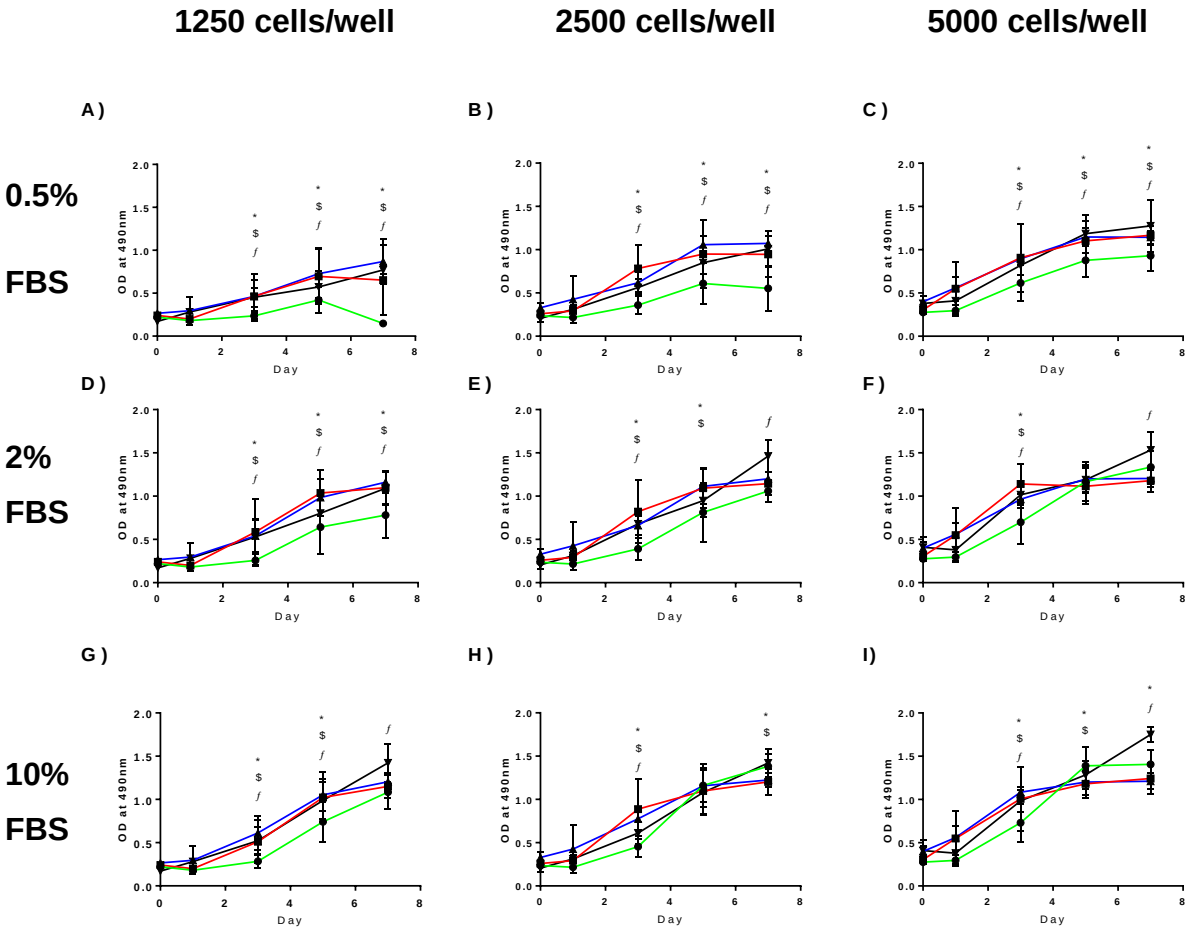

Figure 4.1: The effect of P2X7RA, P2X7RB or P2X7RAB expression on Te85 OS cell proliferation. Te85 OS cells were seeded into 96 well plates at various cell densities of 1250, 2500, and 5000 per well in either 0.5% **A-C)** 2% **D-F)** 10% FBS **G-I)**. Cell proliferation was assessed using an MTS assay with OD values plotted (absorbance measured at 490 nm) on days 0, 1, 3, 5 and 7. Te85 naïve OS cells are shown in green, Te85+P2X7RA OS cells in red, Te85+P2X7RB OS cells in blue, and Te85+P2X7RAB OS cells in black, data is from 3 biological repeats with 4 technical repeats per experiment and was analysed using a one-way ANOVA with Tukey's multiple comparisons test to compare days 3, 5 and 7. * = P<0.05 comparing Te85 naïve and Te85+P2X7RA OS cells **$** = P<0.05 comparing Te85 naïve and Te85+P2X7RB OS cells and *ƒ* = P<0.05 between Te85 naïve and P2X7RAB OS cells.

4.3 Effects of P2X7R variant inhibition using A740003 and AZ11645373 P2X7R antagonists on Te85 OS cells

As previously shown P2X7RA, B and AB all increased the growth of Te85 OS cells, therefore whether this increased growth could be attenuated using specific P2X7R antagonists was next investigated. By varying the cell seeding density and serum concentration in the previous experiments, optimum conditions were established to successfully detected cell growth in the linear range of the MTS assay. Based on these results, 5000 cells at 0.5% FBS was selected for inhibition studies with Te85 OS cells. The concentration of inhibitor used was 100 µM, derived from the previously used concentration (Giuliani *et al.,* 2014).

Treatment of Te85 naïve OS cells with A740003 or AZ11645373 had no significant effect on cell growth (A740003 1.106 ± 0.042 SEM vs 1 ± 0.002 SEM Te85 naïve, P=0.0506, Figure 4.2 A) and (AZ11645373 1.002 ± 0.002 SEM vs 1 ± 0.002 SEM Te85 naïve, P= 0.9576, Figure 4.2 A)

In Te85 OS cells transfected with P2X7RA, growth was significantly decreased by both A740003 and AZ11645373 (A740003 0.3583 ± 0.011 SEM vs 1 ± 0.002 SEM vehicle, P<0.0001, Figure 4.2 B) and (AZ11645373 0.3903 ± 0.008 SEM vs 1 ± 0.002 SEM vehicle, P<0.0001, Figure 4.2 B). This was the same for P2X7RB transfected Te85 OS cells (A740003 0.5977 ± 0.026 SEM vs 1 ± 0.180 SEM vehicle, P<0.0001, Figure 4.2 C) and (AZ11645373 0.6368 ± 0.044 SEM vs 1 ± 0.180 SEM vehicle, P<0.0001, Figure 4.2 C) Finally, this was the same for P2X7RAB transfected Te85 OS cells (A740003 0.5769 ± 0.025 SEM vs 1 ± 0.053 SEM vehicle P<0.0001, Figure 4.2 D) and (AZ116455373 0.5662 ± 0.045 SEM vs 1 ± 0.053 SEM vehicle, P<0.0001 Figure 4.2 D).

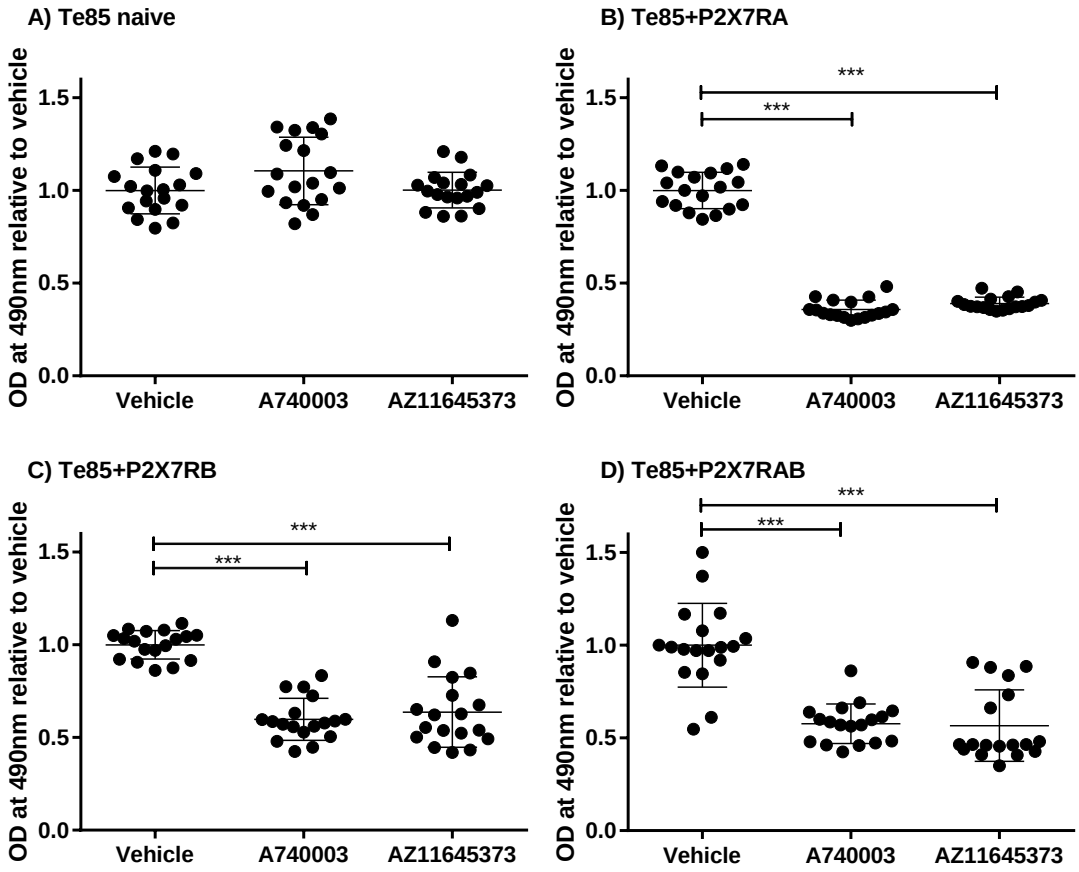

Figure 4.2: The effect of A740003 and AZ11645373 P2X7R inhibitors on the proliferation of Te85 OS cells. Cells were plated out in a 96 well plate at a density of 5000 cells in 0.5% FBS, and left to adhere for 24 hours, the medium was then changed to medium containing vehicle or 100 µM of either A740003 or AZ11645373. The cell activity was assessed using an MTS assay (absorbance measured at 490 nm) at 3 days. **A)** Te85 naïve OS cells **B)** Te85+P2X7RA OS cells **C)** Te85+P2X7RB **OS** cells **D)** Te85+P2X7RAB OS cells. Data is from 3 biological repeats with 6 technical repeats per experiment. Data was analysed comparing the treatment groups to Te85 naïve OS cells using an unpaired T-test, **** = P <0.0001.

4.4 The effects of P2X7R expression on Te85 OS cell adhesion

The loss of adhesion to an extracellular matrix is an essential step in OS metastasis, in order to measure this process, type 1 rat tail collagen was coated inside a 96 well plate and cells were left to adhere for a set period of 4 hours (previously determined empirically as an optimum time). The coated wells containing cells were then washed and the remaining cells quantified by lysing the cells with lysis buffer and detecting the DNA present using Quant-iT™ PicoGreen® dsDNA Reagent. Fluorescence was detected at excitation 485 nm and emission 530 nm with a cut off at 530 nm.

Cells expressing the P2X7RA or the P2X7RB variants had significantly decreased adhesion to the type I collagen matrix when compared to the Te85 naïve OS cells (Te85+P2X7RA 0.4815 ± 0.02322 SEM vs 1.008 ± 0.03864 SEM vehicle, $P<0.0001$) Figure 4.3 A) and (Te85+P2X7RB 0.5484 ± 0.02465 SEM vs 1.008 ± 0.03864 SEM vehicle, $P<0.0001$, Figure 4.3 B) This was in contrast to the cells expressing the P2X7RAB which had no significant difference in cell adhesion when compared to Te85 naïve OS cells (Te85+P2X7RAB 0.9775 ± 0.022 vs 1.000 ± 0.02287 SEM vehicle, $P= 0.4847$ Figure 4.3 C).

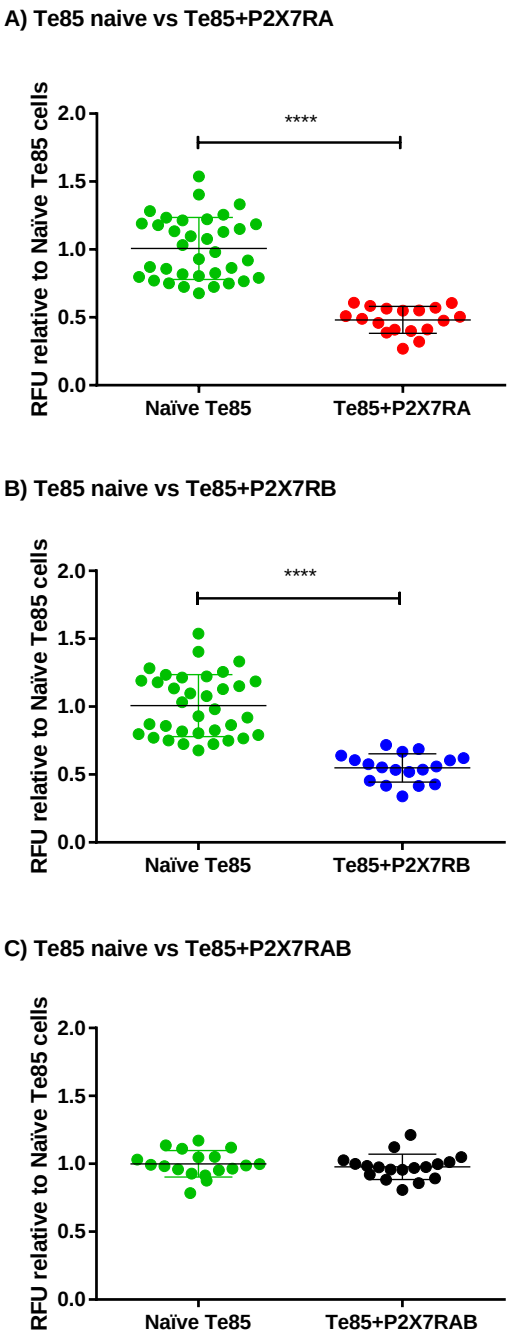

Figure 4.3: The effect of P2X7RA, P2X7RB and P2X7RAB on OS cell adhesion. For each experiment 7500 cells were plated into a 96 well plate pre-coated with type 1 rat tail collagen and left for 4 hours at 37°C. Wells were then washed 4 times with PBS to removed unattached cells. Remaining attached cells were lysed using lysis buffer and detected using Quant-iT™ PicoGreen® dsDNA Reagent. Fluorescence was detected at excitation 485 nm and emission 530 nm (cut off 530 nm). **A)** Te85+P2X7RA OS cells **B)** Te85+P2X7RB OS cells **C)** Te85+ P2X7RAB OS cells. All data is plotted relative to the Te85 naïve OS cells, which are shown in green, Te85+P2X7RA OS cells in red, Te85+P2X7RB OS cells in blue, and Te85+P2X7RAB OS cells in black. Data shown is from 3 biological repeats with 6 technical repeats per experiment and was analysed using an unpaired T-test. **** = P <0.0001.

4.5 The effect of P2X7R expression onTe85 OS cell migration

An important step in OS metastasis is the ability of the cells to migrate away from the primary site (Sahai., 2005). To determine the role of P2X7R on Te85 OS cell migration, a scratch assay was used. The OS cell lines were seeded into a 12 well plate at a density of 200,000 in complete medium and left overnight to adhere and form a monolayer. Cells were then changed over into complete medium containing 5 µg/ml mitomycin C and left for 2 hours at 37°C. After this, monolayers were scratched down the centre of each well using a 10 µL pipette tip. After washing twice with PBS the cells were left in either 10% FBS medium, 0.5% FBS medium or 0.5% FBS medium with 10 µM BzATP. Images were taken every 2 hours for 24 hours.

In 10% FBS medium, there was no significant difference in migration between Te85 naïve OS cells and Te85 OS cells expressing P2X7RA or P2X7RB (P= 0.3817 & 0.1974, Figure 4.4 & 4.5 A, B). However, cells expressing P2X7RAB migrated slower than Te85 naïve OS cells (P= <0.0001, Figure 4.4 & 4.5 C). In 0.5% FBS, there was no significant difference in migration between Te85 naïve OS cells and Te85 OS cells expressing P2X7RA (P= 0.053, Figure 4.6 & 4.7 A). However, both the P2X7RB and P2X7RAB variants migrated significantly faster than Te85 naïve OS cells (P= <0.0001, Figure 4.6 & 4.7 B, C). Finally, when cells were cultured in 0.5% FBS and stimulated with 10 µM BzATP to activate the P2X7R variants, there was a significant increase in migration in all Te85+P2X7R variants when compared to stimulated Te85 naïve OS cells. (P= <0.0001, Figure 4.8 and 4.9 A, B, C).

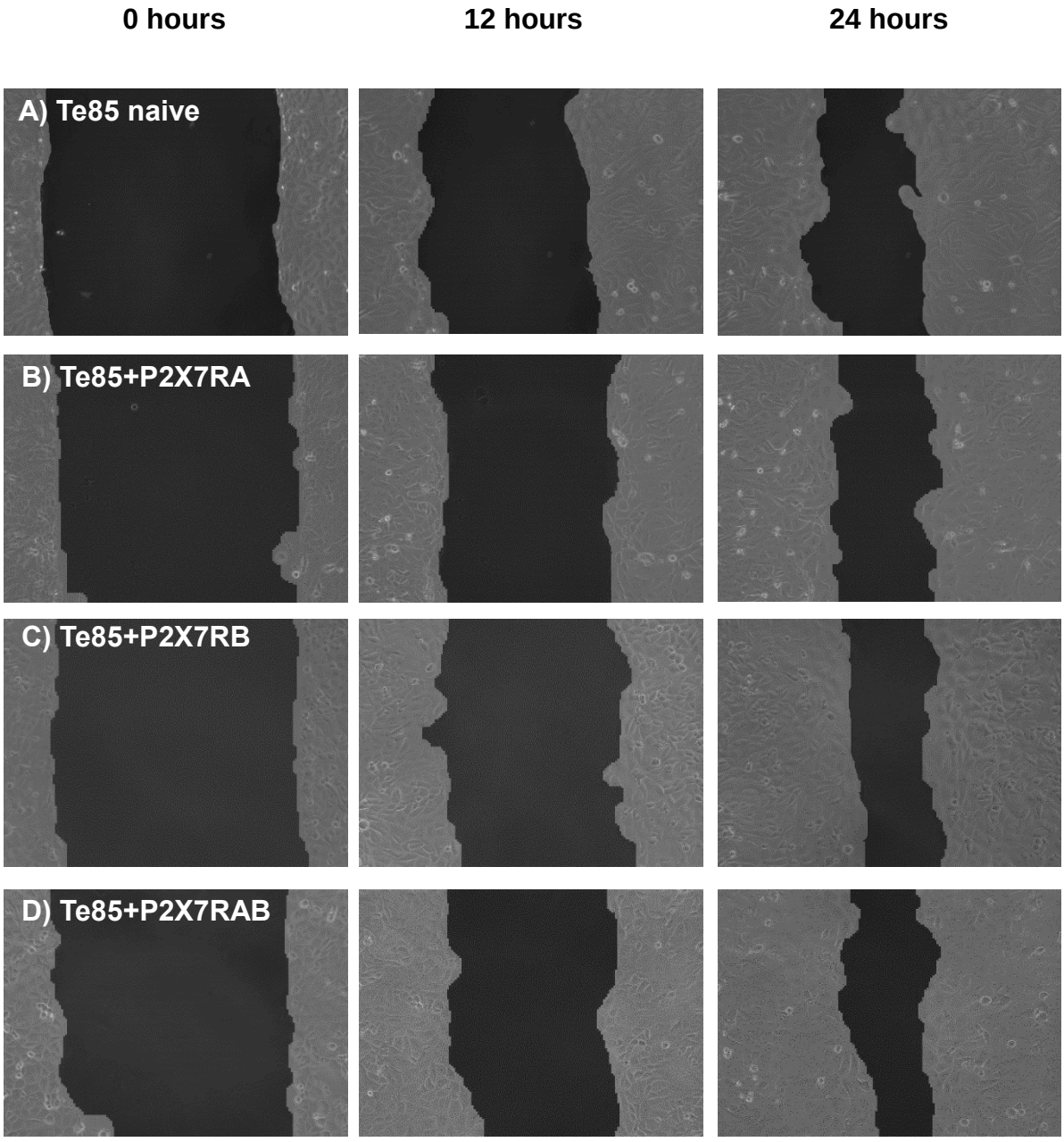

Figure 4.4: Representative images showing the effect of P2X7RA, P2X7RB or P2X7RAB expression on Te85 OS cell migration in 10% FBS medium. Cells were seeded into a 12 well plate at a density of 200,000 in complete medium and left overnight to adhere and form a monolayer. Cells were then changed over into complete medium containing 5 µg/ml mitomycin C and left for 2 hours at 37°C after this, monolayers were scratched down the centre of the well using a 10 µL pipette tip. After washing twice with PBS the cells were left in 10% FBS with images taken every 2 hours for 24 hours. The images are representative of 0 hours, 12 hours and 24 hours only. The images were analysed, and pseudo coloured using Tscratch software. **A)** Te85 naïve OS cells **B)** Te85+P2X7RA OS cells **C)** Te85+P2X7RB OS cells **D)** Te85+P2X7RAB OS cells

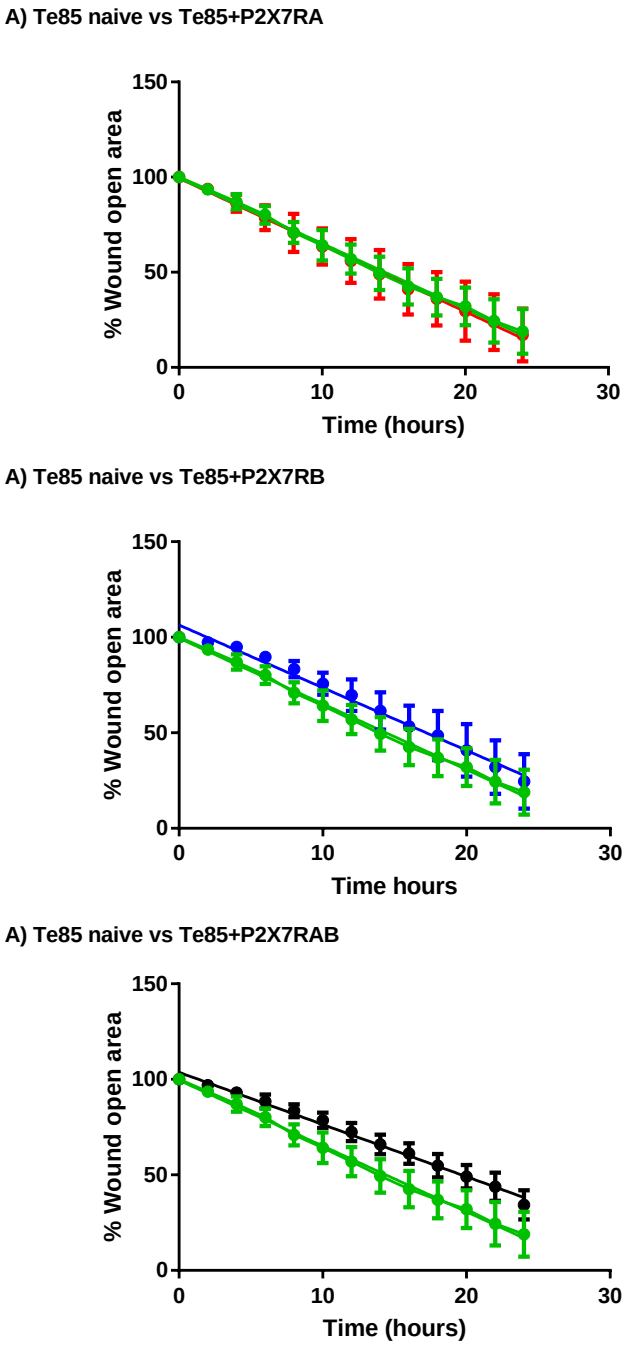

Figure 4.5: The effect of P2X7RA, P2X7RB or P2X7RAB expression on Te85 OS cell migration in 10% FBS medium. Cells were plated out into a 12 well plate at a density of 200,000 in complete medium and left overnight to adhere and form a monolayer. Cells were then changed over into complete medium containing 5 µg/ml mitomycin C and scratched down the centre of the well using a 10 µL pipette tip. After washing twice with PBS the cells were left in 10% FBS with images taken every 2 hours for 24 hours. **A)** Te85+P2X7RA OS cells shown red **B)** Te85+P2X7RB OS cells shown blue **C)** Te85+P2X7RAB OS cells shown black, data plotted compared to Te85 naïve OS cell migration shown green. The slopes were compared by linear regression. Data from 3 biological repeats with 3 technical repeats per experiment. **** = P <0.0001.

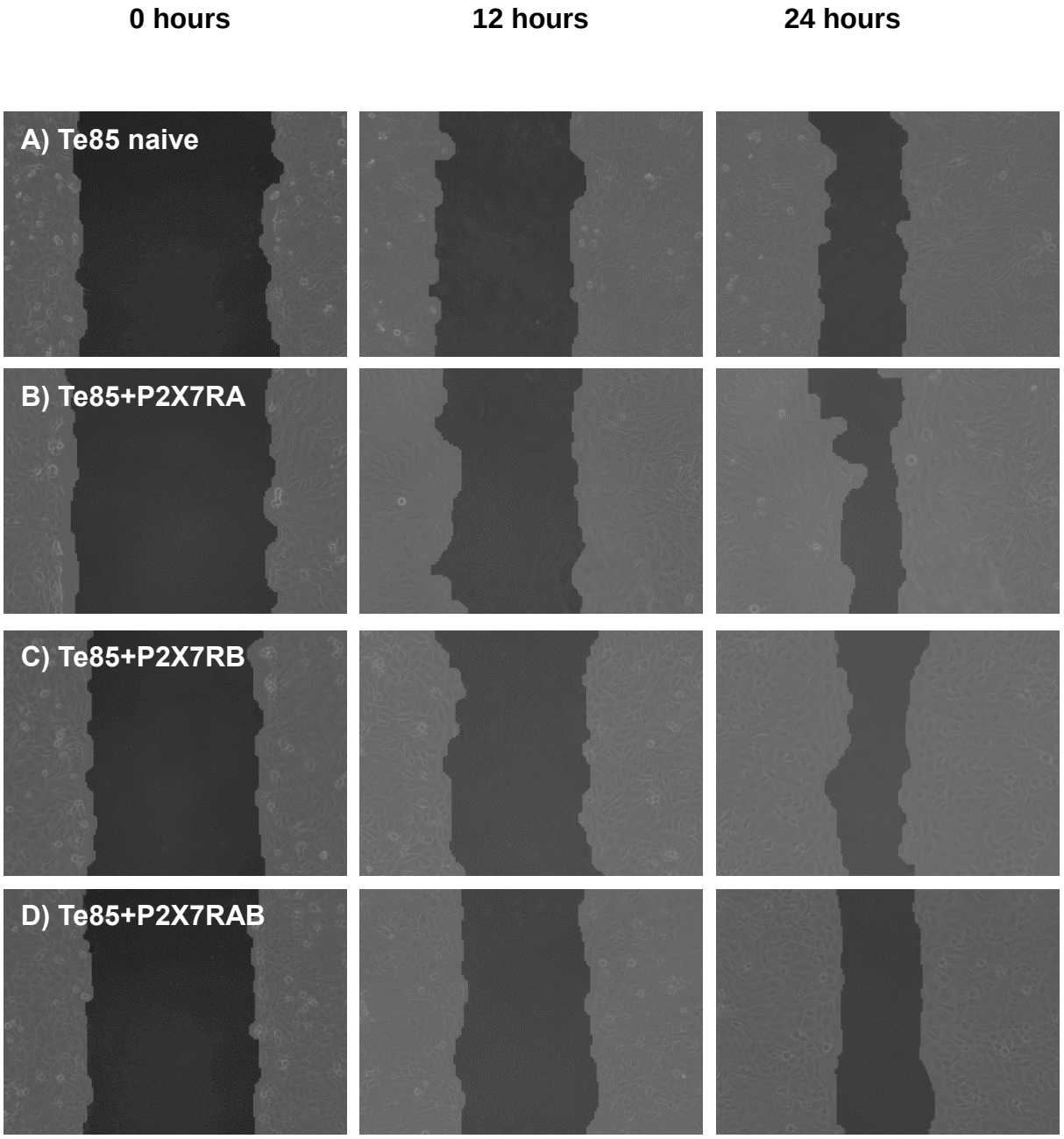

Figure 4.6: Representative images showing the effect of P2X7RA, P2X7RB or P2X7RAB expression on Te85 OS cell migration in 0.5% FBS medium. Cells were seeded into a 12 well plate at a density of 200,000 in complete medium and left overnight to adhere and form a monolayer. Cells were then changed over into complete medium containing 5 µg/ml mitomycin C and left for 2 hours at 37°C.After this, monolayers were scratched down the centre of the well using a 10 µL pipette tip. After washing twice with PBS the cells were left in 0.5% FBS medium with images taken every 2 hours for 24 hours. The images are representative of 0 hours, 12 hours and 24 hours only. The images were analysed, and pseudo coloured using Tscratch software. **A)** Te85 naïve OS cells **B)** Te85+P2X7RA OS cells **C)** Te85+P2X7RB OS cells **D)** Te85+P2X7RAB OS cells.

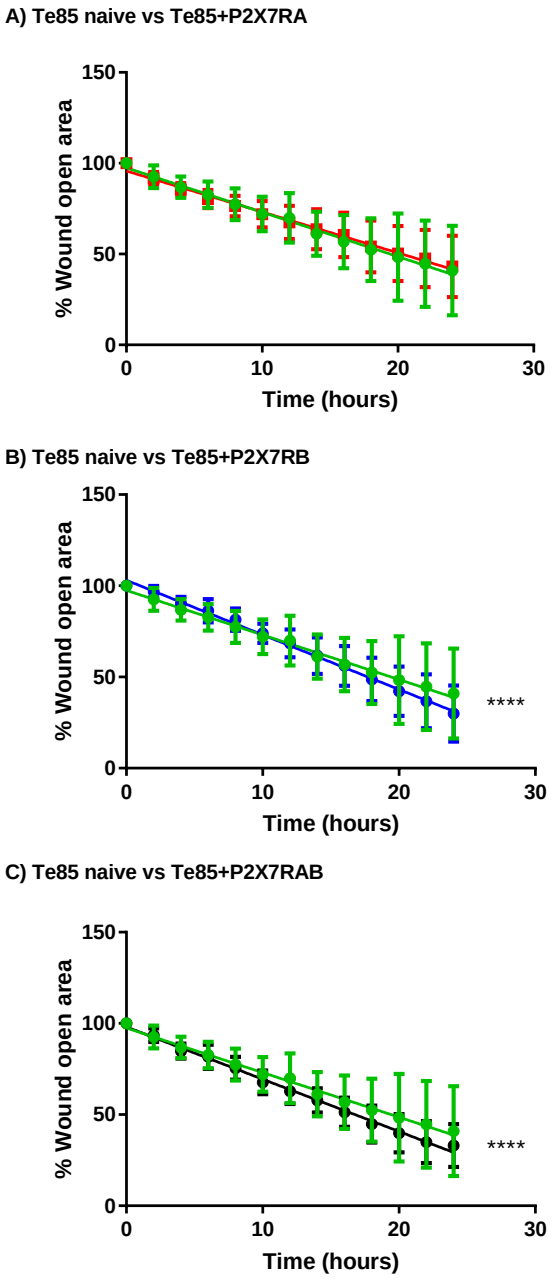

Figure 4.7 The effect of P2X7RA, P2X7RB or P2X7RAB expression on Te85 OS cell migration in 0.5% FBS medium. Cells were plated out into a 12 well plate at a density of 200,000 in complete medium and left overnight to adhere and form a monolayer. Cells were then changed over into complete medium containing 5 µg/ml mitomycin C and scratched down the centre of the well using a 10 µL pipette tip. After washing twice with PBS the cells were left in 0.5% FBS medium with images taken every 2 hours for 24 hours. **A)** Te85+P2X7RA OS cells shown red **B)** Te85+P2X7RB OS cells shown blue **C)** Te85+P2X7RAB OS cells shown black. Data plotted compared to Te85 naïve OS cell migration shown green. The slopes were compared by linear regression. Data from 3 biological repeats with 3 technical repeats per experiment **** = P <0.0001.

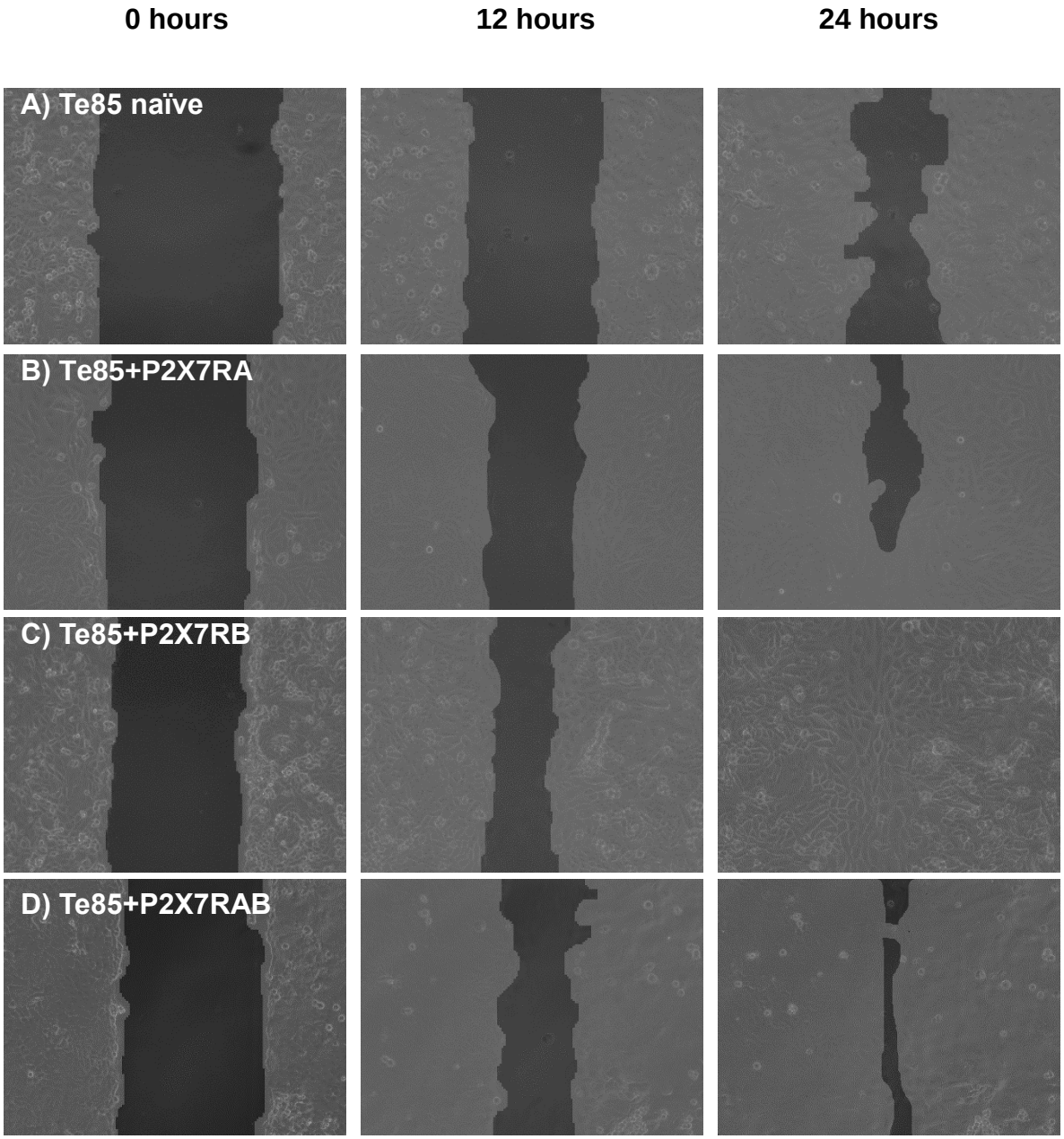

Figure 4.8: Representative images showing the effect of P2X7RA, P2X7RB or P2X7RAB expression on Te85 OS cell migration in 0.5% FBS medium stimulated with BzATP. Cells were plated out into a 12 well plate at a seeding density of 200,000 in complete medium and left overnight to adhere and form a monolayer. Cells were then changed over into complete medium containing 5 µg/ml mitomycin C and scratched down the centre of the well using a 10 µL pipette tip. After washing twice with PBS the cells were left in medium containing 0.5% FBS and 10 µM BzATP with images taken every 2 hours for 24 hours. The images are representative of 0 hours, 12 hours and 24 hours. The images were analysed and pseudocoloured using Tscratch software **A)** Te85 naïve OS cells **B)** Te85+P2X7RA OS cells **C)** Te85+P2X7RB OS cells **D)** Te85+ P2X7RAB OS cells.

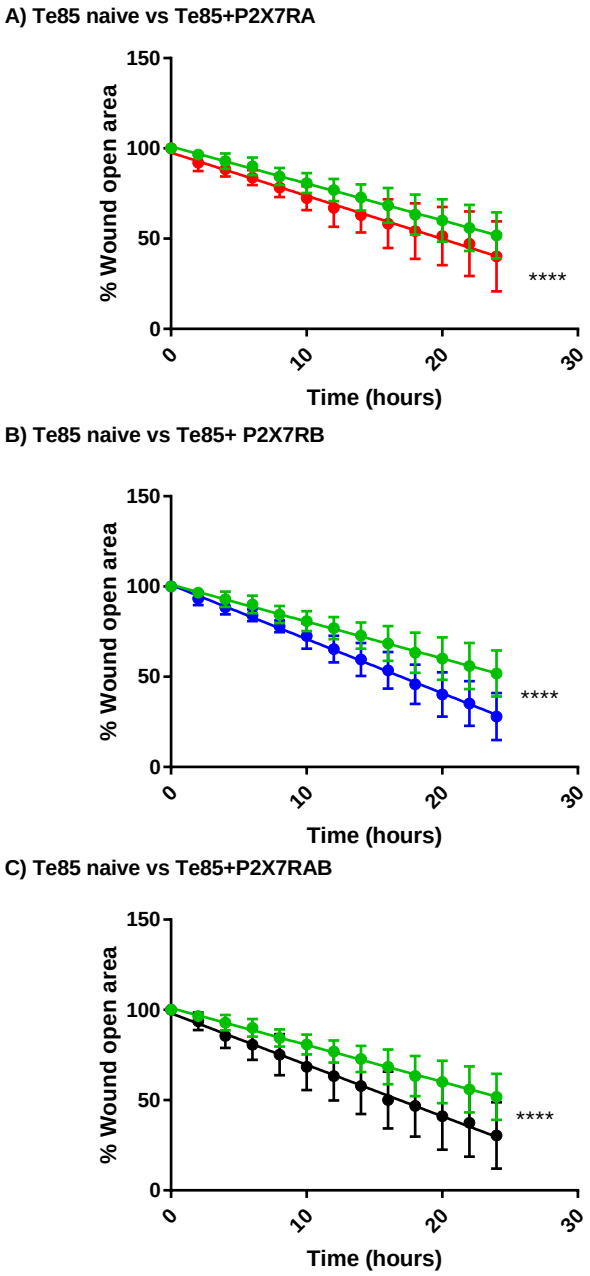

Figure 4.9: The effect of P2X7RA, P2X7RB or P2X7RAB expression on Te85 OS cell migration in 0.5% FBS medium stimulated with BzATP. Cells were plated out into a 12 well plate at a seeding density of 200,000 in complete medium and left overnight to adhere and form a monolayer. Cells were then changed over into complete medium containing 5 µg/ml mitomycin C and scratched down the centre of the well using a 10 µL pipette tip. After washing twice with PBS the cells were left in medium containing 0.5% FBS and 10 µM BzATP with images taken every 2 hours for 24 hours. **A)** Te85+P2X7RA OS cells shown red **B)** Te85+P2X7RB OS cells shown blue **C)** Te85+P2X7RAB OS cells shown black, data plotted compared to Te85 naïve OS cell migration shown green. The slopes were compared by linear regression. Data from 3 biological repeats with 3 technical repeats per experiment. **** = P <0.0001.

4.6 The effects of P2X7R expression on Te85 OS cell invasion

Before OS cells can migrate away from the primary site to metastasize to different parts of the body they must degrade the surrounding extracellular matrix and penetrate into surrounding tissue. Thereby, in addition to the migration assay which only tracks cell motility an invasion assay was performed to analyse ability to break down an extracellular matrix to facilitate invasion. Invasion is considered one of the first stages of metastasis (Sahai, 2005). In order to determine the effect of P2X7R expression on OS invasion *in vitro* the cells were cultured in mitomycin C to inhibit proliferation, before being plated into a pre-coated matrigel transwell FluoroBlok insert in serum free medium containing 10 μM BzATP. The lower chamber contained complete medium as a chemoattractant. After 24 hours the inserts were removed, washed in PBS and stained with Calcein AM cell permeant dye and imaged, these were then quantified using Image J and plotted as the amount of invaded cells detected.

The results show that there was no significant difference in invasion when Te85 OS cells were expressing P2X7RA when compared to Te85 naïve OS cells (Te85+P2X7RA 107.3 ± 33.41 SEM vs 49.11 ± 14.8 SEM Te85 naïve, P= 0.9098 Figure 4.10 E). However, there was significantly increased ability to invade the matrigel layer with the Te85+P2X7RB OS cells (Te85+P2X7RB 297.9 ± 49.74 SEM vs 49.11 ± 14.8 SEM Te85 naïve, P= 0.00374, Figure 4.10 E) and with the Te85+P2X7RAB OS cells (Te85+P2X7RAB 76.3 ± 107.6 SEM vs 49.11 ± 14.8 SEM Te85 naïve, P=0.0039, Figure 4.10 E).

There was no significant difference between Te85+P2X7RA and Te85+P2X7RB OS cells 107.3 ± 33.41 SEM vs 297.9 ± 49.74 SEM, P=0.1526, Figure 4.10 E) or between Te85+P2X7RB OS cells and Te85+P2X7RAB OS cells (297.9 ± 49.74 SEM vs 376.3 ± 107.6 SEM, P=0.8077 Figure 4.10 E). However, the Te85+P2X7RAB OS cells invaded significantly more than the Te85+P2X7RA OS cells 376.3 ± 107.6 SEM vs 107.3 ± 33.41 SEM, P=0.0216 Figure 4.10 E).

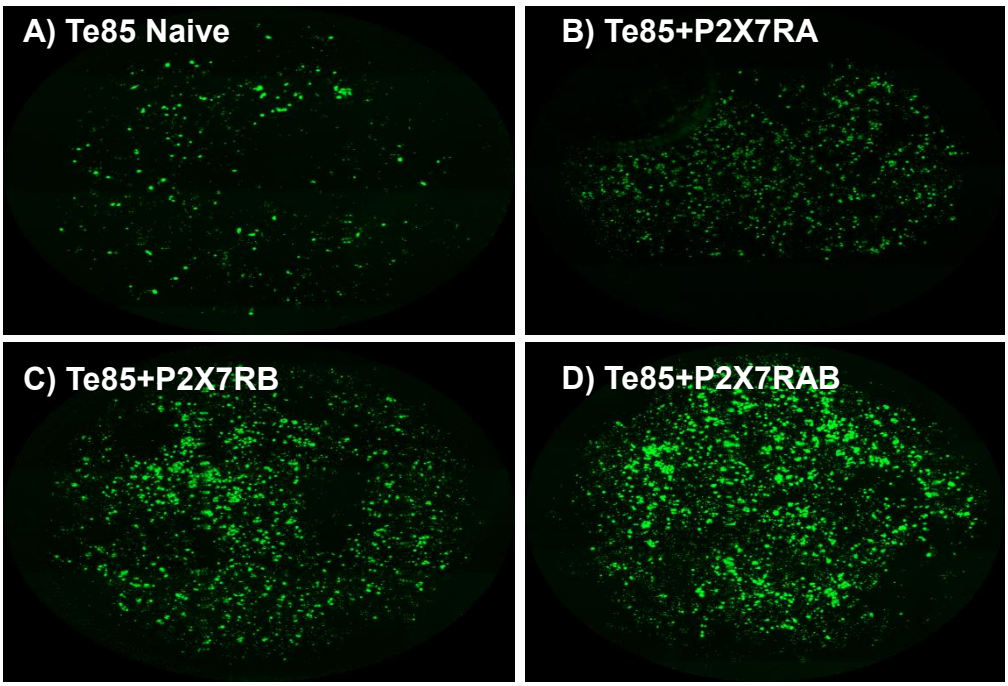

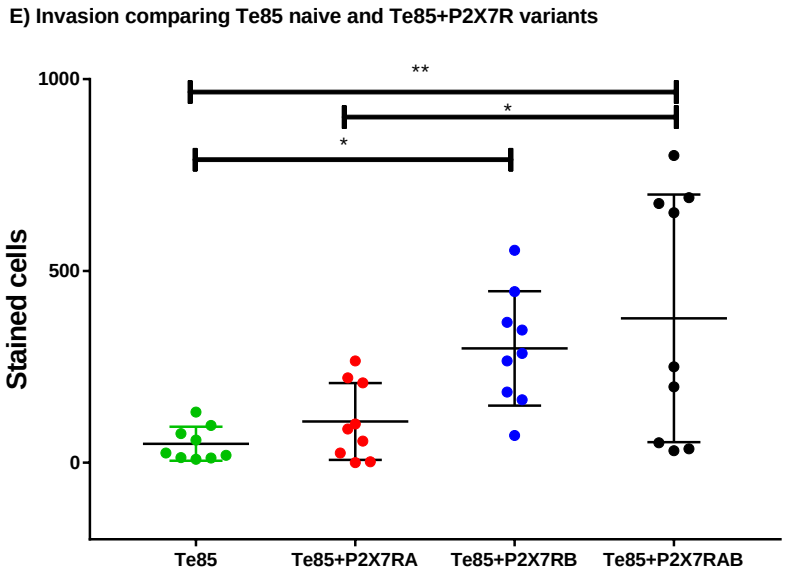

Figure 4.10: The effect of P2X7RA, P2X7RB and P2X7RAB on Te85 OS cell invasion. Cells were incubated in culture with 5 µg/ml mitomycin C and left for 2 hours at 37°C. They were seeded into a 24 well plate at a density of 100,000 cells in serum free medium containing 10 µM BzATP, in an upper fluoroblok chamber pre-coated with 1.5 mg/ml Matrigel. The lower chamber contained complete medium. After 24 hours the upper fluoroblok transwells were washed twice in PBS and left for 30 minutes at 37°C in Calcein AM cell permeant dye. Images were taken of underside of the smaller insert. For representative images **A)** Te85 naïve OS cells **B)** Te85+P2X7RA OS cells, **C)** Te85+P2X7RB OS cells **D)** Te85+P2X7RAB OS cells. **E)** Te85 naïve OS cells green, Te85+P2X7RA OS cells red, P2X7RB OS cells blue and P2X7RAB OS cells black. The data is from 3 biological repeats with 3 technical repeats per experiment, Data was analysed using a one-way ANOVA with Tukey's multiple comparisons test, * = P <0.05 ** = P <0.01.

4.7 Discussion

Although P2X7R expression and function has been studied in bone physiology and in other cancers there is minimal data relating to the role it plays in OS. This chapter examined the effect of P2X7RA, P2X7RB and P2X7RAB expression on important OS properties including proliferation, cell adhesion, migration, and invasion in Te85 OS cells *in vitro*. Specific P2X7R inhibitors A740004 and AZ11645373 were used in cell proliferation studies, along with BzATP (a potent P2X7R agonist) in migration and invasion studies. This chapter provides novel insights about the role P2X7R variants play in the OS microenvironment.

When the effect of P2X7R expression on proliferation was examined under normal *in vitro* conditions with 10% FBS over 7 days the proliferation was similar, this was also the case in 2% FBS. Under low 0.5% FBS conditions transfection with any P2X7R variant provided a strong growth stimulus. The blunted effect of P2X7R expression in the higher serum concentrations could be attributed to the fact that FBS in the *in vitro* culture contains ATPases (Michel *et al.,* 2001) which will rapidly degrade ATP and thereby making P2X7R activation in these conditions less likely to occur.

The results of the proliferation data are consistent with previously studies showing a growth increase in Te85 OS cells (Giuliani *et al*., 2014) and in a range of other cell types with various studies demonstrating the same findings. In a first study transfection of P2X7R increased the growth of K562 and LG14 leukemic cells under serum free conditions in comparison to mock transfected cells (Baricordi *et al.,* 1999). This was also the case in P2X7R transfected HEK-293 cells (Adinolfi *et al.,* 2005). In chronic B lymphocytic leukaemia it was found that when comparing the indolent slow growing cell type to a more aggressive type, the more aggressive type had increased cell proliferation correlating with increased P2X7R expression (Adinolfi *et al*., 2002). Further support for the role of P2X7R in cell proliferation has been shown in mesothelioma, P2X7R expressing malignant pleural mesothelioma cell lines showed increased growth when compared to healthy cells (Amoroso *et al.,* 2016). In neuroblastoma there was an increase in proliferation when stimulated with BZATP in ACN neuroblastoma cells (Raffaghello *et al*., 2006). Additionally, serum deprivation was shown to increase P2X7R transcript and protein levels in N2a and SHSY5Y cells. The P2X7R expression caused by serum deficiency enhanced neuroblastoma cell

proliferation through the PI3K/Akt signalling pathway (Gómez-Villafuertes *et al.,* 2015). P2X7R effect on proliferation was examined in pancreatic stellate cells and supports the findings in this chapter, when examining proliferation over an 8-day period *in vitro* comparing cells isolated from wild type or P2X7R KO mice the KO mice had approximately 50% less cell growth. Furthermore, they found that proliferation increased with exposure to ATP and was decreased when apyrase was added, (Haanes *et al.*, 2012).

To determine whether the increased growth seen in the transfected cells was due to receptor expression and if the P2X7R could provide a suitable therapeutic target two different P2X7R antagonists, A740003 and AZ11645373, were used in the proliferation assay. Due to the P2X7R providing the largest growth stimulus at low serum conditions this condition was used for the inhibition study. The results demonstrated that both antagonists had no effect on Te85 naïve OS cells, as would be expected given the previous evidence that Te85 OS cells do not expression functional P2X7R (Chapter 3 results and [Gartland *et al*., 2001). However, in all cell lines expressing P2X7R variants there was a decrease in cell growth when grown in the presence of the P2X7R antagonists.

The anti-proliferative effect of targeting P2X7R has been shown in Te85 OS cells, as treatment with A740003 or apyrase reduced the proliferation of the P2X7R expressing cells (Giuliani *et al*., 2014). The effects of targeting the P2X7R in other cancers also support the findings in this chapter. Two human ovarian cancer cell lines SKOV-3 and CAOV-3 express endogenous P2X7Rs, when treated with AZ10606120 *in vitro* had reduced growth compared to control cultures (Vázquez-Cuevas *et al*., 2014). This was also the case using AZ10606120 again but in fibrogenic pancreatic stellate cells (Haanes *et al.,* 2012), pancreatic ductal adenocarcinoma cells (Giannuzzo *et al.*, 2015) and PancTu-1 pancreatic cancer cells (Giannuzzo *et al.*, 2016) The results in this study confirm that the growth increase was P2X7R expression dependent and that targeting the P2X7R may be a viable therapeutic option in OS as is the case in other cancers *in vitro*.

Whilst proliferation is a key feature of OS, other characteristics were examined. The ability of the cells to break away from the primary site due to a loss of adhesion to an extracellular matrix is an initial stop towards metastasis.

The results suggest that the P2X7R could play a role in OS metastasis. The P2X7RA and P2X7RB expressing Te85 OS cells showed a decreased ability to anchor to the collagen extracellular matrix but the co-transfected P2X7RAB didn't. This decrease in adhesion suggests that single non-functional P2X7R variants are more likely to be metastatic and supports the idea that non-functional P2X7Rs have a pro tumour effect (Gilbert *et al*., 2019). This effect could be due to down regulation of cell adhesion proteins as previously P2X7R has been demonstrated to downregulate E-cadherin in breast cancer cells (Xia *et al.,* 2015). P2X7Rs also induce expression of various MMPs which are capable of digesting the extracellular matrix, allowing the cells to break away from the primary site. ATP acting on P2X7Rs has been shown to induce the release of MMP 9 in human peripheral-blood mononuclear cells which could be attenuated with P2X7R antagonists oATP and KN-62 (Gu & Wiley, 2006). P2X7Rs have additionally been shown to increase MMP-13 expression in the cartilage tissues of rats with osteoarthritis and was again reversed by P2X7R inhibitors (Hu *et al.,* 2016).

Another important feature of cancer cell behaviour is migration; cells migrate to other parts of the body during metastasis. The results in this chapter for migration show that in 10% FBS medium for P2X7RA expressing Te85 OS cells and P2X7RB expressing Te85 OS cells there was no difference, however P2X7RAB again showed a less aggressive phenotype as the expressing cells migrated slower than Te85 naïve OS cells. Under low 0.5% serum conditions, the P2X7RA expressing Te85 OS cells showed no difference compared to Te85 naïve OS cells but the P2X7RB and P2X7RAB expressing Te85 OS cells had increased migration. These results demonstrate that under low serum conditions, where ATP availability is increased possibly stimulating the P2X7R, an increase in migration is demonstrated. Finally, when Te85 OS cells were stimulated with 10 μM BzATP, all P2X7R expressing variants increased cell migration, with the cells expressing the P2X7RB migrating the most. Due to migration being increased when BzATP was present to activate P2X7R, invasion experiments were performed with BzATP added to the top transwell, this measures the ability of the Te85 OS cells to invade through a matrigel layer towards a chemoattractant. The results from this show that all the P2X7R variants increased the invasion of Te85 OS cells with the P2X7RAB and P2X7RB expressing cells displaying the most invasion compared to Te85 naïve OS cells. P2X7Rs playing a role in migration and invasion of cancer cells has not been demonstrated in OS but has

previously in other cancers, with various studies supporting the results from this chapter. Migration and invasion of MDA-MB-435S breast cancer cells was increased due to P2X7R activating cysteine cathepsins (Jelassi *et al.,* 2011) whilst in TD47 breast cancer cells P2X7R downregulated the protein level of E-cadherin and upregulated the production of MMP-13 and the AKT pathway (Xia *et al.,* 2015) driving migration and invasion. This was particularly increased when stimulated with ATP or BzATP (Jelassi *et al.,* 2011, Xia *et al., 2015)*. In a further study using MCF7 and MDA-231 breast cancer cells hypoxia was shown to upregulate P2X7R expression which then drove cell invasion through the phosphorylation of Akt and Erk1/2 resulting in a nuclear increase of NF-κB sustaining expression of MMPs (Tafani *et al*., 2011). Two studies have demonstrated the that the P2X7R can increase the migration of H292 and PC-9 lung cancer cells supporting the results in this chapter which was attenuated with the addition of P2X7R antagonists (Takai *et al.,* 2014). In a second study TGF-β1 stimulation evoked ATP release from A549 lung cancer cells which subsequently activated P2X7Rs and an increase in cell migration, this could again be attenuated with P2X7R antagonists (Takai *et al.*, 2012). Migration of glioma cells was assessed using a scratch assay and demonstrated that migration was increased when stimulated with BzATP using U87 and U251 cells and acts via the MEK/ERK pathway, treating the cells with BBG a P2X7R antagonist decreased this effect (Tafani *et al.,* 2011). The effect of P2X7R expression on migration and invasion has been explored in prostate cancer with results again supporting that P2X7R can increase migration and invasion, three prostate cancer cell lines 2B4, 1E8 and DU-145 were treated with ATP which caused an increase via ERK1/2 and PI-3 K/AKT pathways and increased expression of MMP-3 and MMP-13 (Zhang *et al.,* 2010). This was also the case when 22RV1 prostate cancer cells were transfected with P2X7R, these cells then had increased migration, invasion and decreased E-cadherin expression (Qiu *et al*., 2014). A final study that supports the results in this chapter shows that in pancreatic ductal adenocarcinoma using Panc-1 cells migration and invasion were both were increased when treated with BzATP or ATP, and subsequently reduced with AZ10606120 (Giannuzzo *et al*., 2015).

The results from this chapter demonstrate that OS cell behaviour including proliferation, adhesion, migration and invasion is influenced *in vitro* by expression and stimulation of the P2X7R variants. It also shows that of the P2X7R variants the

P2X7RB was implicated in affecting all of the parameters assessed and therefore targeting this variant could provide the most promising option. Finally, this chapter provides preliminary data to support the use of targeting the P2X7R in animal models in future OS studies, with the hope of exploiting P2X7R as a therapeutic option for patients in the future.

Chapter 5 – A pilot *in vivo* study to establish an OS xenograft model and the effect of P2X7R expression on OS tumorigenesis.

5.1 Introduction

The Te85 OS cell line has historically been shown not to form tumours in mice. However, modified derivatives of this cell line such as MNNG-HOS have (Luu *et al.,* 2005). In the previous chapters it has been demonstrated that the Te85 OS cells have the P2X7R variants transfected in, and that this can alter the *in vitro* properties of the cells including cell growth, cell adhesion, cell migration and cell invasion. Therefore, it is possible that modulation of the Te85 OS cell line by P2X7R variants could provide a strong stimulus to enhance Te85 OS cells into inducing tumour formation in immunocompromised BALB/c mice. This would then enable the cell line to be used as a suitable *in vivo* model. By establishing an OS xenograft model the P2X7R can be targeted *in vivo* in future studies. This will determine if inhibition of the receptor could be a viable therapeutic option and will provide a means to validate the previously shown *in vitro* data in OS. The OS model developed in this chapter should also ideally provide the ability to metastasize to the lungs, as this is an important aspect of OS progression with P2X7R expression has been linked to increasing metastasis in other cancers (Di Virgilio, 2016).

The effect of P2X7R expression on tumorigenesis in other cell lines *in vivo* has been explored. HEK-293 cells are only weakly tumorigenic *in vivo* as mock transfected cells produced tumours in approximately 50% of injected mice, this increased to 80-100% when transfected with human P2X7R (Adinolfi *et al.,* 2012). Tumours were also detected earlier at day 17 post inoculation for P2X7R transfected cells compared to 21 days for HEK-293-mock transfected cells. The P2X7R expressing HEK-293 tumours were also significantly larger in size with a higher cell density, decreased apoptosis and increased Ki-67 staining (Adinolfi *et al.,* 2012). In a second study J6-1 leukaemia cells that had a P2X7R mutant due to a A559-to-G substitution had a hypo-functional P2X7R receptor with reduced agonist sensitivity compared to the fully functional P2X7R. This P2X7R mutant when implanted into nude mice had significantly larger, heavier and faster growing tumours compared to wild type P2X7R (Chong *et al.*, 2010). This demonstrates how P2X7R variants can influence the progression of a tumour especially when displaying a more non-functional phenotype.

This chapter aims to determine:

- If Te85 OS cells can be used as a suitable *in vivo* model in BALB/c nude mice as they have previously been shown not to form tumours (Luu *et al.,* 2005).
- If transfection with P2X7R variants can modify Te85 OS cell behaviour causing tumorigenesis.
- If Te85+P2X7R OS cell variants have any effect on total bone volume or lung metastasis.
- If MNNG-HOS+GFP+LUC OS cells are different to the MNNG-HOS naïve OS cells.
- If the MNNG-HOS model can used as an OS model *in vivo* to target P2X7R.

5.2 The tumourgenicity of OS cell lines

MNNG-HOS+GFP+LUC, MNNG-HOS naïve, Te85 naïve, Te85+P2X7RA, Te85+P2X7RB, Te85+P2X7RAB, and were used, in this *in vivo* pilot study. For each cell line 500,000 cells were suspended in 20 µL PBS and injected paratibially into 3 7-9 week old female BALB/c nude mice per condition. Both MNNG-HOS+GFP+LUC and MNNG-HOS OS cells formed tumours in 6/6 mice, were palpable after 9 days. None of the Te85 OS cell lines formed tumours when left for 6 weeks.

5.3 Histological analysis on H&E stained mouse limb sections

Histological analysis assesses the tumour and surrounding architecture, itis the gold standard for a diagnosis in almost all types of cancer (Gurcan *et al.*, 2009) H&E staining can be used to assess characteristics such as the tumour grade, phenotype, nuclei, morphological appearance, size, and shape. At the end of the experiment, the mouse legs were collected processed, embedded, sectioned and H&E stained. The Te85 and Te85+P2X7R variants didn't form any detectable tumours in either bone or muscle tissue (Figure 5.1). The MNNG-HOS+GFP+LUC and MNNG-HOS OS cells formed tumours that were high-grade undifferentiated OS tumours, with very little osteoid matrix and collagen production (Figure 5.1).

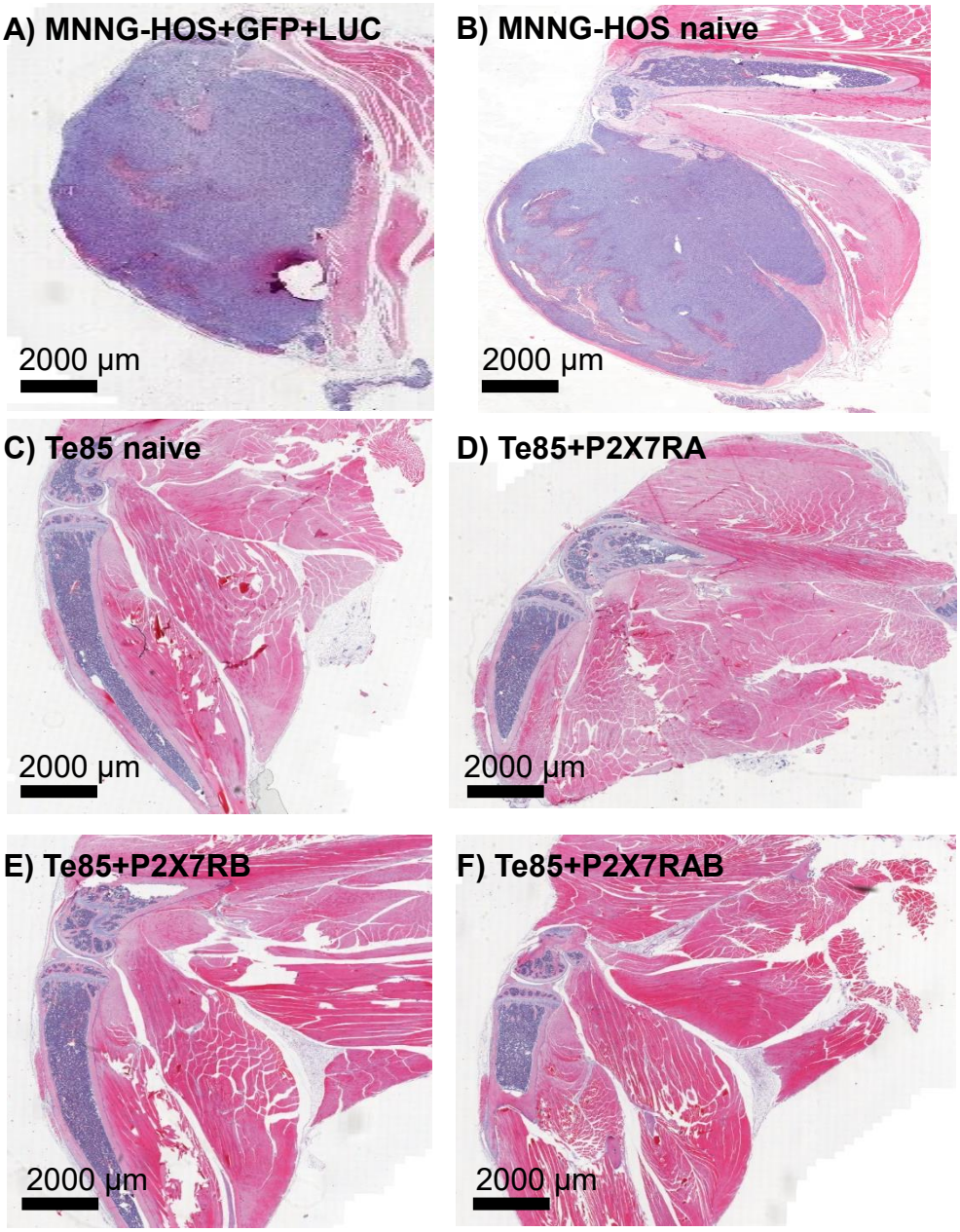

Figure 5.1: Representative H&E stained sections of mice legs injected with MNNG-HOS naïve OS cells or Te85+P2X7R variants. For each group 3 female BALB/c 7-9 week old mice were injected paratibially with 500,000 cells of either MNNG-HOS+GFP+LUC OS cells, MNNG-HOS naïve OS cells, Te85 naïve OS cells, Te85+P2X7RA OS cells, Te85+P2X7RB OS cells or Te85+P2X7RAB OS cells suspended in 20 µL PBS. The tumours were left to grow untreated. The mice were then euthanised and dissected. The legs were collected processed, embedded into wax blocks and sections were taken to be H&E stained **A)** MNNG-HOS+GFP+LUC OS cells **B)** MNNG-HOS OS cells **C)** Te85 OS cells **D)** Te85+P2X7RA OS cells **E)** Te85+P2X7RB OS cells **F)** Te85+P2X7RAB OS cells.

5.4 Ki-67 IHC staining for the detection of proliferating cells

Each female BALB/c 7-9 week old was injected with 500,000 cells of either MNNG-HOS+GFP+LUC, MNNG-HOS naïve, Te85 naïve, Te85+P2X7RA, Te85+P2X7RB or Te85+P2X7RAB paratibially and the tumours were left to grow untreated. The mice were then euthanised and dissected. The legs were collected processed, embedded into wax blocks and sections were taken to be stained for Ki-67, a marker for cell proliferation (Scotlandi *et al.,* 1995).

There was Ki-67 staining in the mice legs bearing the MNNG-HOS+GFP+LUC and MNNG-HOS tumours (Figure 5.2 A, B). The percentage of cells stained positive for Ki-67 in MNNG-HOS+GFP+LUC bearing mice was not statistically different from the mice bearing MNNG-HOS naïve OS cells (MNNG-HOS+GFP+LUC OS cells 67.24% ± 5.87 SEM vs 59.79% ± 3.324 SEM MNNG-HOS OS cells, P= 0.331, Figure 5.3). There was no Ki-67 staining of tumour cells in the mice legs containing Te85+P2X7R variants as there was no tumour formation, however, some staining was detected due to some proliferating cells in the bone marrow (Figure 5.2 C, D, E, F).

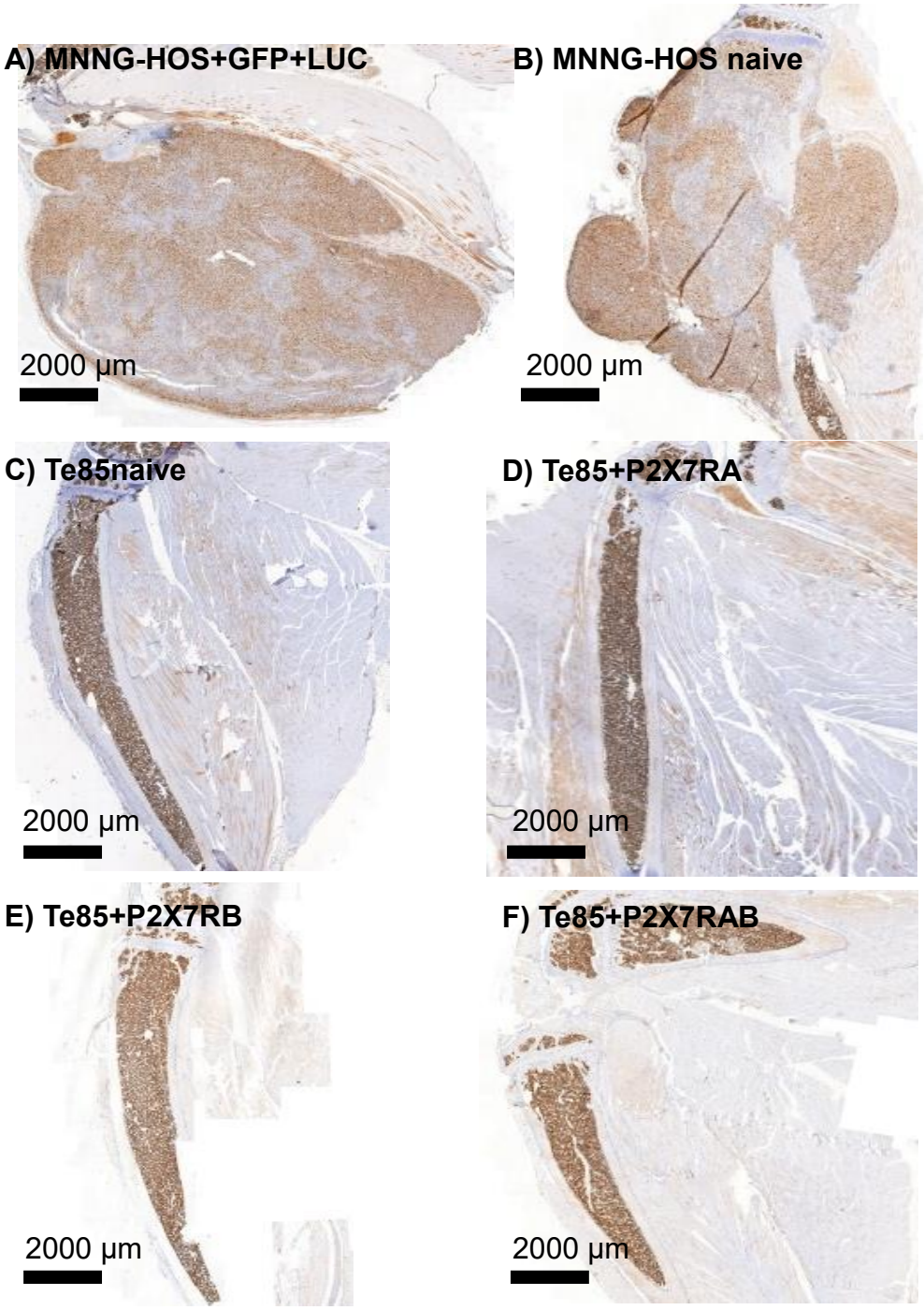

Figure 5.2: Representative Ki-67 stained sections of mice injected with MNNG-HOS naïve OS cells or Te85+P2X7R variants. For each group 3 female BALB/c 7-9 week old mice were injected paratibially with 500,000 cells of either MNNG-HOS+GFP+LUC OS cells, MNNG-HOS naïve OS cells, Te85 naïve OS cells, Te85+P2X7RA OS cells, Te85+P2X7RB OS cells or Te85+P2X7RAB OS cells suspended in 20 µL PBS. The tumours were left to grow untreated. The mice were then euthanised and dissected. The legs were collected processed, embedded into wax blocks and sections were taken to be Ki-67 stained. **A)** MNNG-HOS+GFP+LUC OS cells **B)** MNNG-HOS OS cells **C)** Te85 OS cells **D)** Te85+P2X7RA OS cells **E)** Te85+P2X7RB OS cells **F)** Te85+P2X7RAB OS cells.

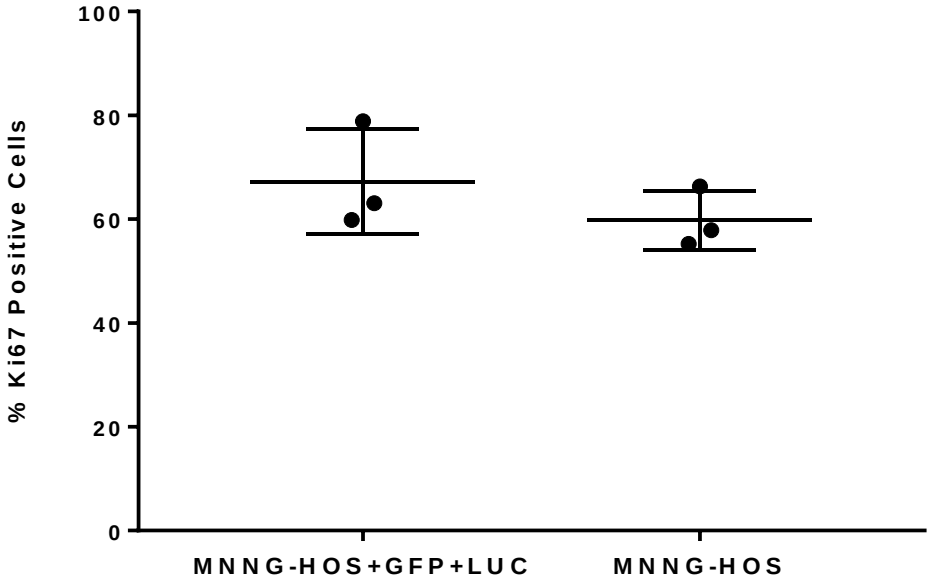

Figure 5.3: Ki-67 staining for proliferating cells comparing MNNG-HOS+GFP+LUC and MNNG-HOS mice. For each group 3 female BALB/c 7-9 week old mice were injected paratibially with 500,000 cells of either MNNG-HOS+GFP+LUC OS cells, MNNG-HOS naïve OS cells suspended in 20 µL PBS. The tumours were left to grow untreated. The mice were then euthanised and dissected. The legs were collected processed, embedded into wax blocks and sections were taken to be Ki-67 stained and analysed using QuPath. MNNG-HOS+GFP+LUC bearing mice were compared to MNNG-HOS bearing using an unpaired T-test. N= 3 mice per cell type.

5.5 The effect of MNNG-HOS and Te85 tumours on total bone volume

Micro-CT analysis was performed according to chapter 2 to determine the total bone volume on the left tumour bearing leg and the contralateral right leg (non-tumour). Of the 18 BALB/c nude mice used in this pilot study when viewing the 3D reconstruction of the legs there was clear osteolysis, and some ectopic bone formation in the tumour bearing injected legs of the MNNG-HOS+GFP+LUC and MNNG-HOS mice (Figure 5.5). Despite these findings, the total bone volume of the MNNG-HOS+GFP+LUC tumour bearing leg was not statistically different to the contralateral non-tumour bearing leg (tumour bearing leg 4.930 mm^3 ± 0.333 SEM vs 5.665 mm^3 ± 0.086 SEM contralateral leg, P= 0.155, Figure 5.4 A). Similarly, the average total bone volume of the MNNG-HOS tumour bearing leg was not statistically different to the non-tumour bearing leg (tumour bearing leg 4.242 mm^3 ± 0.428 SEM vs 4.701 mm^3 ± 0.332 SEM contralateral leg, P=0.250, Figure 5.4 B).

No bone lysis or ectopic bone formation was observed in the mice injected with Te85 OS cells, Te85+P2X7RA, P2X7RB or P2X7RAB when viewing the 3D reconstruction of the legs (Figure 5.6 & 5.7 A, B, C, D). The total bone volume of the Te85 tumour bearing leg was not statistically different to the contralateral non-tumour bearing leg (tumour bearing leg 5.921 mm^3 ± 0.169 SEM vs 6.117 mm^3 ± 0.244 SEM contralateral leg, P= 0.012, Figure 5.4 C). This was also the case for the mice injected with P2X7RA (tumour bearing leg 5.902 mm^3 ± 0.093 SEM vs 5.651 mm^3 ± 0.016 SEM contralateral leg, P= 0.143, Figure 5.4 D) with P2X7RB (tumour bearing leg 6.052 mm^3 ± 0.1061 SEM vs 6.138 mm^3 ± 0.113 SEM contralateral leg, P= 0.496, Figure 5.4 E) and with P2X7RAB (tumour bearing leg 5.516 mm^3 ± 0.255 SEM vs 5.414 mm^3 ± 0.182 SEM contralateral, P= 0.400, Figure 5.4 F)

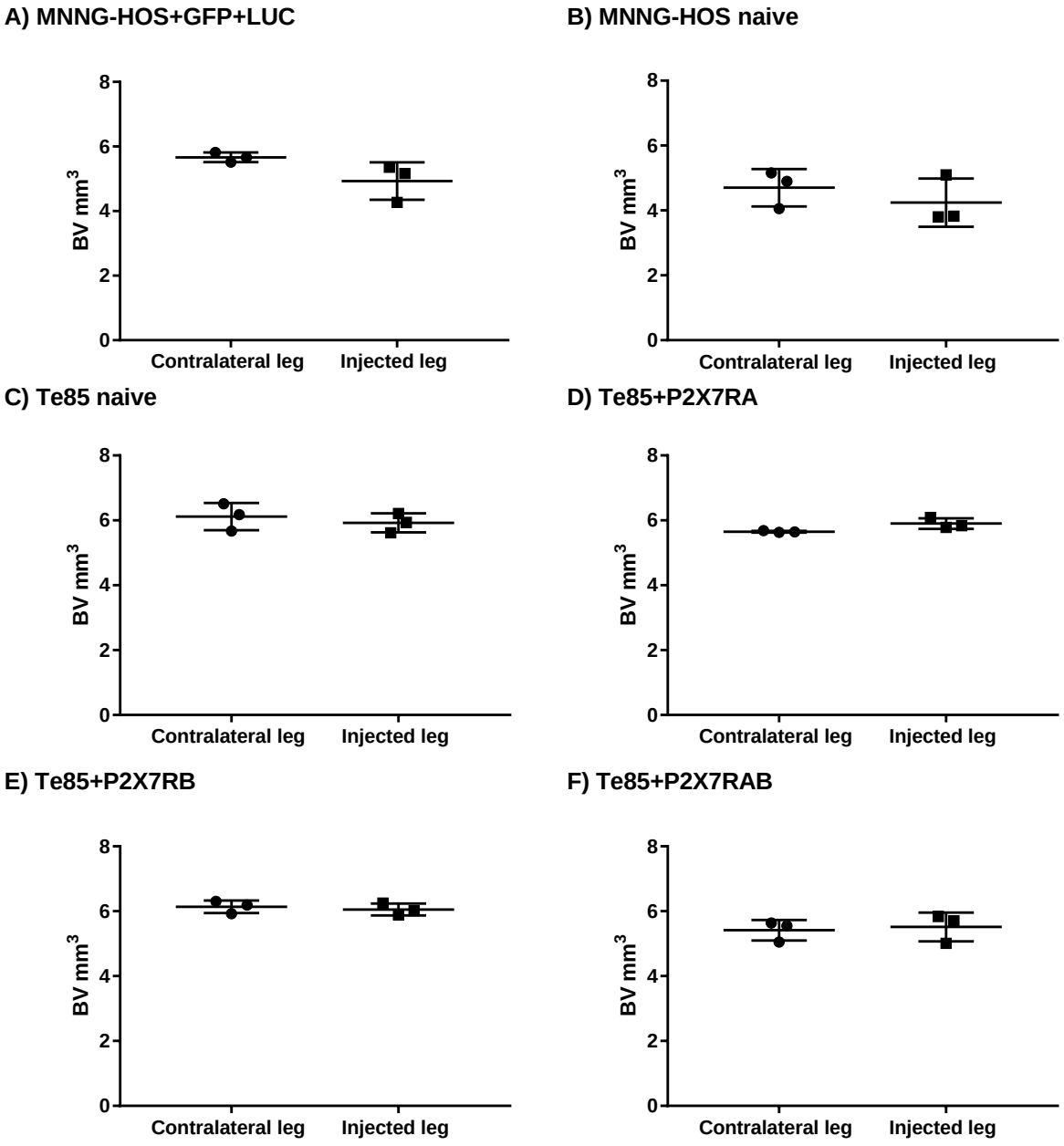

Figure 5.4: Micro-CT total bone volume of BALB/c nude mice legs injected with Te85 or MNNG-HOS OS cells compared to contralateral non-injected legs. For each group 3 female BALB/c 7-9 week old mice were injected paratibially with 500,000 cells of either MNNG-HOS+GFP+LUC OS cells, MNNG-HOS naïve OS cells, Te85 naïve OS cells, Te85+P2X7RA OS cells, Te85+P2X7RB OS cells or Te85+P2X7RAB OS cells suspended in 20 µL PBS. The tumours were left to grow untreated. The mice were then euthanised and dissected. Micro-CT was used to assess total bone volume **A)** MNNG-HOS+GFP+LUC **B)** MNNG-HOS naïve **C)** Te85 naïve **D)** Te85+P2X7RA **E)** Te85+P2X7RB **F)** Te85+P2X7RAB. No significant difference was observed when comparing tumour bearing legs to the it's contralateral leg using a paired T-Test. N=3 mice per group.

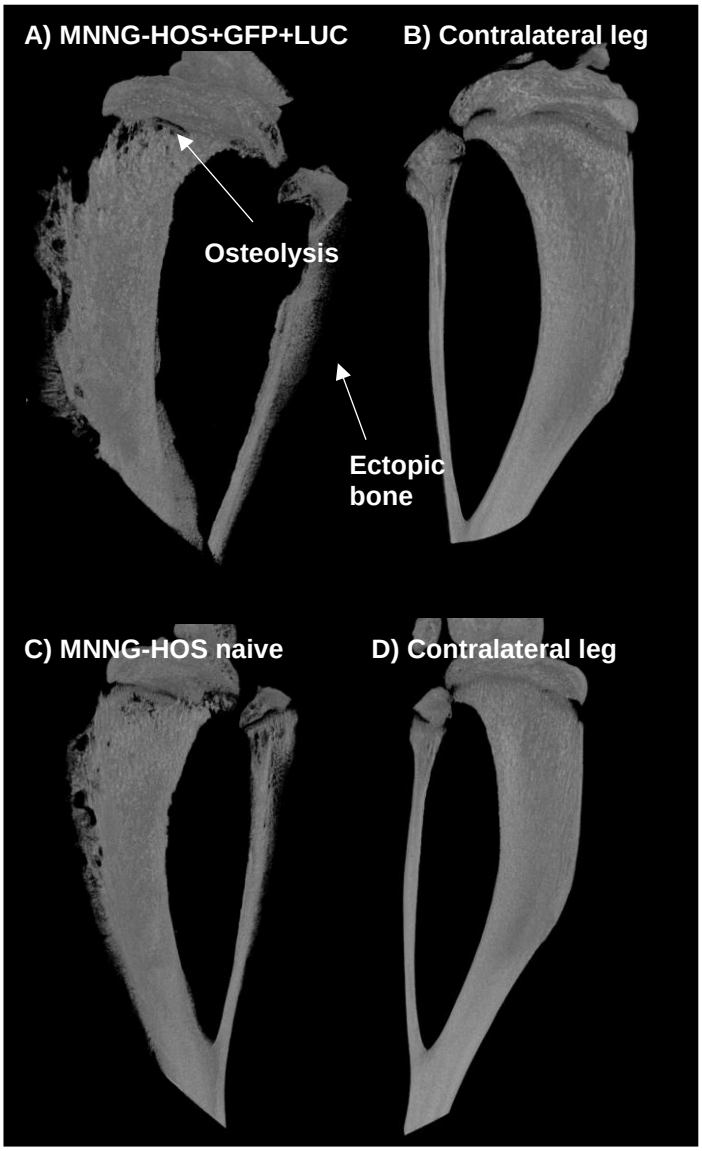

Figure 5.5: Representative 3D micro-CT images of BALB/c nude mice left legs injected with MNNG-HOS OS cells compared to contralateral legs: For each group 3 female BALB/c 7-9 week old mice were injected paratibially with 500,000 cells of either MNNG-HOS+GFP+LUC OS cells, MNNG-HOS naïve OS cells suspended in 20 µL PBS. The tumours were left to grow untreated. The mice were then euthanised and dissected. Micro-CT was used to assess total bone volume. **A)** MNNG-HOS+GFP+LUC tumour bearing left leg **B)** Contralateral right leg, **C)** MNNG-HOS tumour bearing left leg **D)** Contralateral right. The models demonstrate evidence of both ectopic bone formation and osteolysis in the tumour-bearing legs.

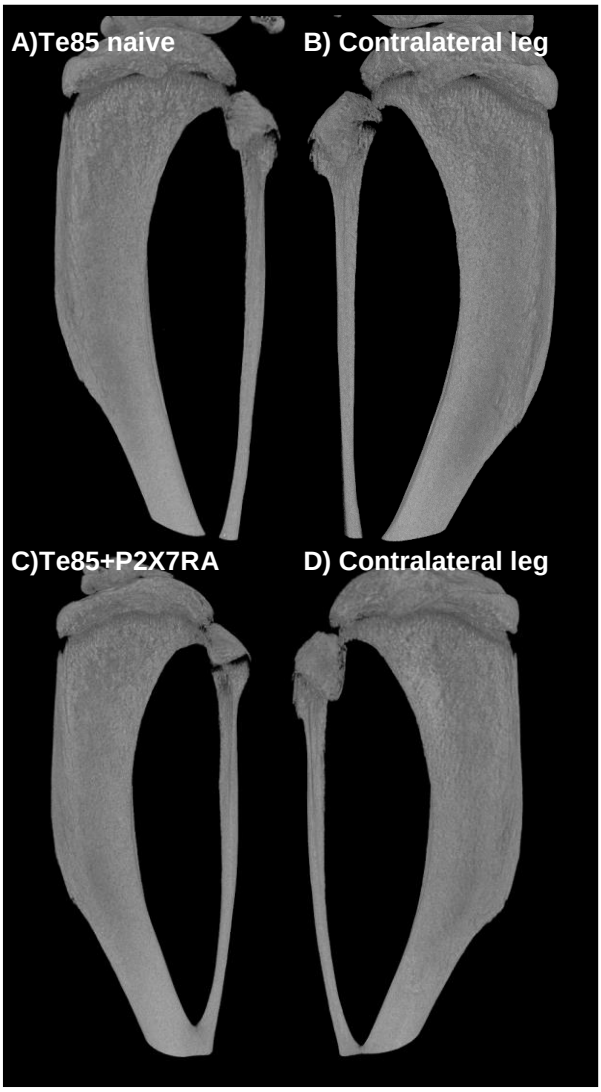

Figure 5.6: Representative 3D micro-CT reconstruction of a BALB/c nude mouse leg after injection of 500,000 of the Te85 +P2X7R variant OS cells: For each group 3 female BALB/c 7-9 week old mice were injected paratibially with 500,000 cells of either Te85 OS cells or Te85+P2X7RA OS cells suspended in 20 µL PBS. The tumours were left to grow untreated. The mice were then euthanised and dissected. Micro-CT was used to assess total bone volume. **A)** Te85 tumour bearing left leg **B)** Contralateral right leg, **C)** Te85+P2X7RA tumour bearing left leg **D)** Contralateral right leg. No evidence of ectopic bone formation or osteolysis is demonstrated.

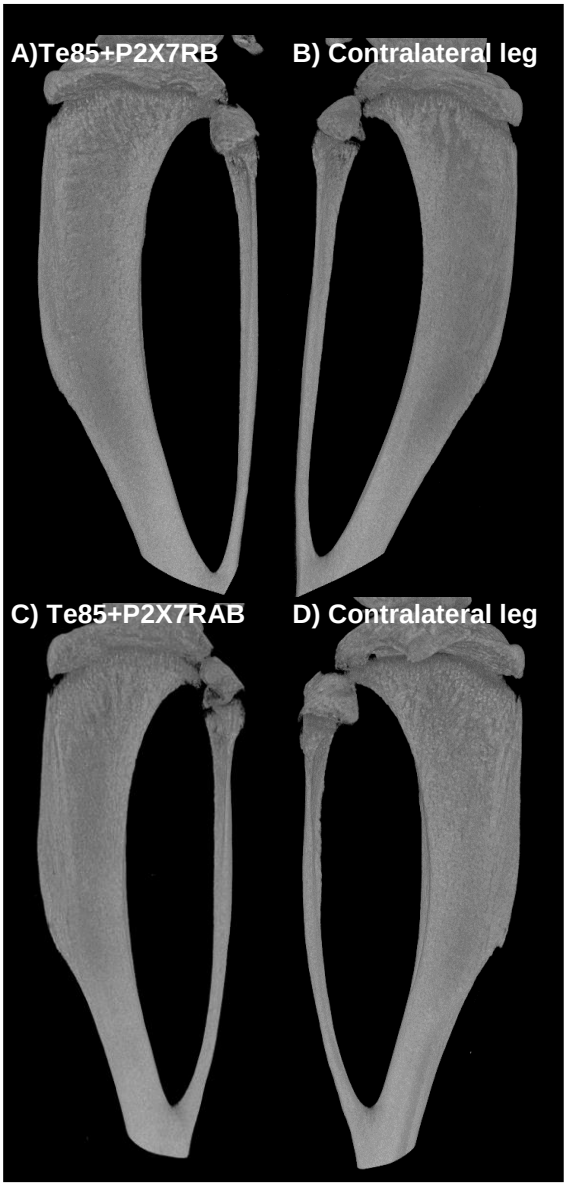

Figure 5.7: Representative 3D micro-CT reconstruction of a BALB/c nude mouse leg after injection of 500,000 of the Te85 +P2X7R variant OS cells. For each group 3 female BALB/c 7-9 week old mice were injected paratibially with 500,000 cells of either Te85+P2X7RB OS cells or Te85+P2X7RAB OS cells suspended in 20 µL PBS. The tumours were left to grow untreated. The mice were then euthanised and dissected micro-CT was used to assess total bone volume. **A)** Te85+P2X7RB tumour bearing left leg **B)** Contralateral right leg **C)** Te85+P2X7RAB tumour bearing left leg **D)** Contralateral right leg. No evidence of ectopic bone formation or osteolysis is demonstrated.

5.6 Lung analysis for OS metastasis

The lungs from each mouse were collected, processed, embedded into wax blocks, serial sectioned every 100 µm and H&E stained. The corresponding slides were then examined for the presence of OS metastasis.

In the mice inoculated with MNNG-HOS+GFP+LUC one mouse presented with an OS metastasis (Figure 5.8 A), this is distinct from normal lung tissue, it has a high amount of condensed chromatin, and a high cell density with a disorganised shape.

There was no metastasis in the mice inoculated with the MNNG-HOS OS cells (Figure 5.8 B). This was also the case in the mice inoculated with Te85 and Te85+P2X7R variants, in addition to no palpable tumour formation, no OS metastasis was present in any of the mice lungs (Figure 5.8 C, D, E, F).

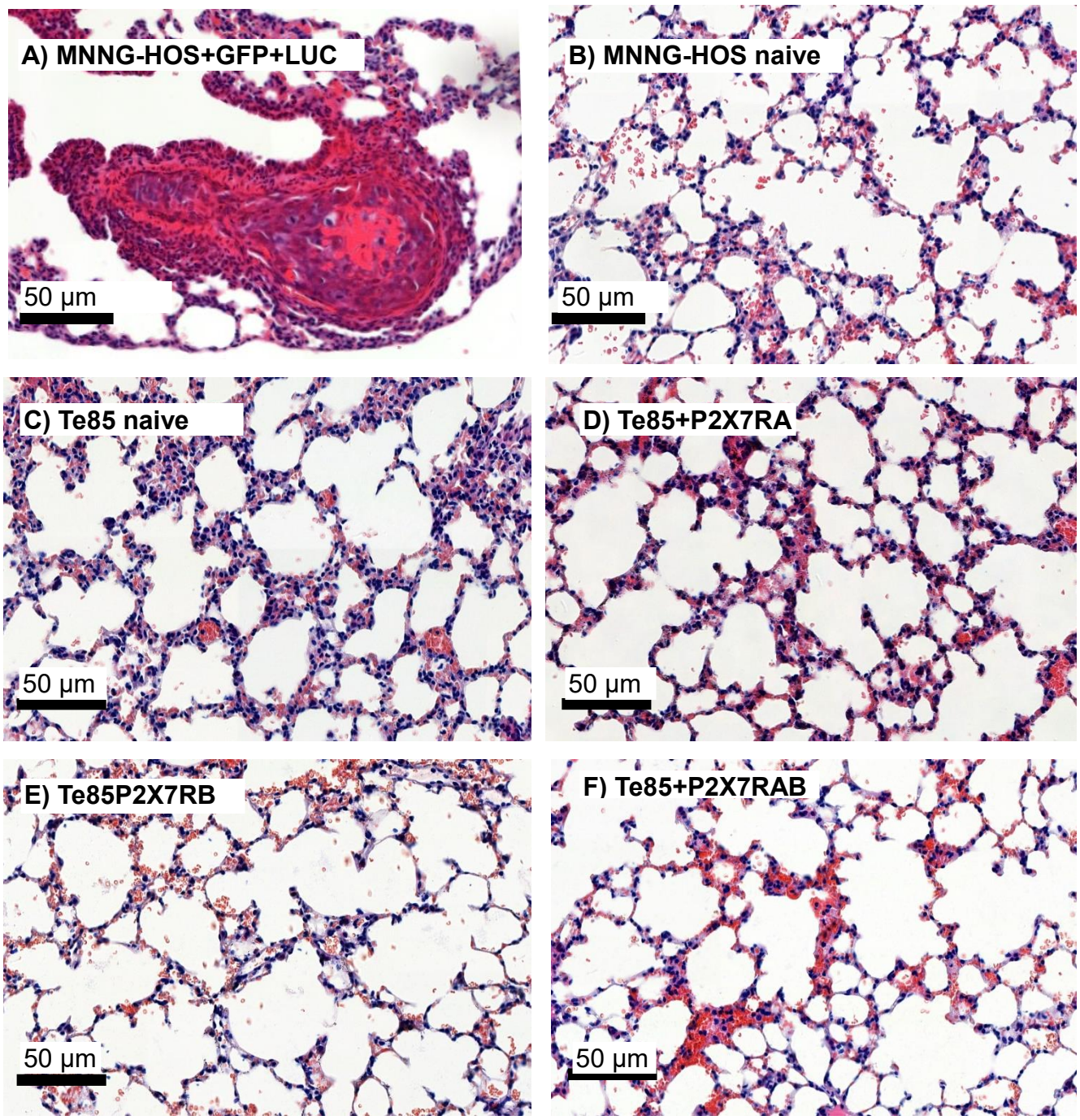

Figure 5.8: Representative histology images of lung tissue from tumour bearing MNNG-HOS+GFP+LUC, MNNG-HOS and Te85+P2X7R variant mice stained with H&E. For each group 3 female BALB/c 7-9 week old mice were injected paratibially with 500,000 cells of either MNNG-HOS+GFP+LUC OS cells, MNNG-HOS naïve OS cells, Te85 naïve OS cells, Te85+P2X7RA OS cells, Te85+P2X7RB OS cells or Te85+P2X7RAB OS cells suspended in 20 µL PBS. The tumours were left to grow untreated. The mice were then euthanised and dissected. The lungs were collected processed, embedded and sectioned, then stained with H&E. **A)** MNNG-HOS+GFP+LUC with an OS metastasis (1/3 mice) **B)** MNNG-HOS naïve mice lungs **C)** Te85 naïve mice lungs **D)** Te85+ P2X7RA mice lungs **E)** Te85+P2X7RB mice lungs **F)** Te85+P2X7RAB mice lungs.

5.7 Expression of P2X7RB in transfected MMNG-HOS cells using end-point PCR

The previously used Te85 OS cells did not form an OS model *in vivo* and therefore cannot be used further. An alternative model is subsequently required. In order to overcome this MNNG-HOS naïve OS cells were checked for endogenous P2X7R expression which was absent. This results in a P2X7R variant needing to be transfected. The P2X7RB variant was chosen as this led to an increase rate of proliferation, decreased cell adhesion and increased migration and invasion (when stimulated with BzATP) in Te85 OS cells previously. HEK-293 cells were used as a positive control and have previously been transfected with the full length P2X7RA variant (courtesy of Dr Elena Adinolfi, Ferrara Italy).

RNA was isolated from the above cell lines and cDNA synthesized (according to Chapter 2). The success of the cDNA reactions was confirmed with the housekeeping gene beta actin with a clear band at 182 BP RT+ve and a RT-ve controls were used (Figure 5.9).

P2X7R mRNA expression was determined with two sets of primers for the P2X7R. The first primer set was designed early in the gene sequence with the forward primer on the exon boundary between exon 3 and 4 and the reverse between exon 7 and 8. This region is present on both the full length and truncated P2X7RB, (product length 413 BP). The second primer set was designed further along the gene sequence with the both the forward primer and reverse primer designed to bind to exon 13 (product length 399 BP) this region is only present on the full length P2X7RA and thereby unable to be detected in the cells with the truncated P2X7RB.

The results demonstrate that bands were produced in the HEK-293+P2X7RA positive control cells. MNNG HOS naïve cells did not show P2X7R mRNA expression (Figure 5.10), however the MNNG-HOS OS cells transfected with the P2X7RB variant showed expression at the expected regions (Figure 5.10).

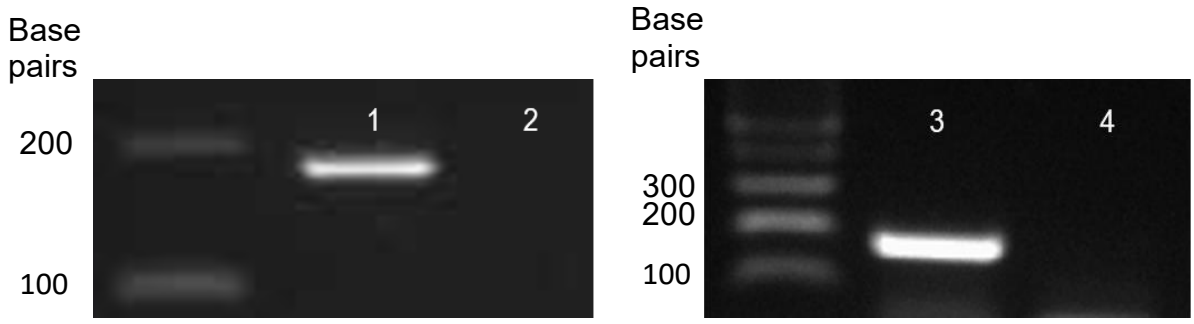

Figure 5.9: Confirmation of successful cDNA synthesis using the beta actin housekeeping gene in MNNG-HOS OS cells. The beta actin housekeeping gene was used to confirm cDNA synthesis for RT+ve and RT-ve samples in MNNG-HOS naïve OS cells and MNNG-HOS+P2X7RB OS cells. **Lanes 1 & 2** MNNG-HOS naïve OS cells RT+ve and RT-ve. **Lanes 3 & 4** MNNG-HOS+P2X7RB OS cells RT+ve and RT-ve. All beta actin product lengths are at 182 BP.

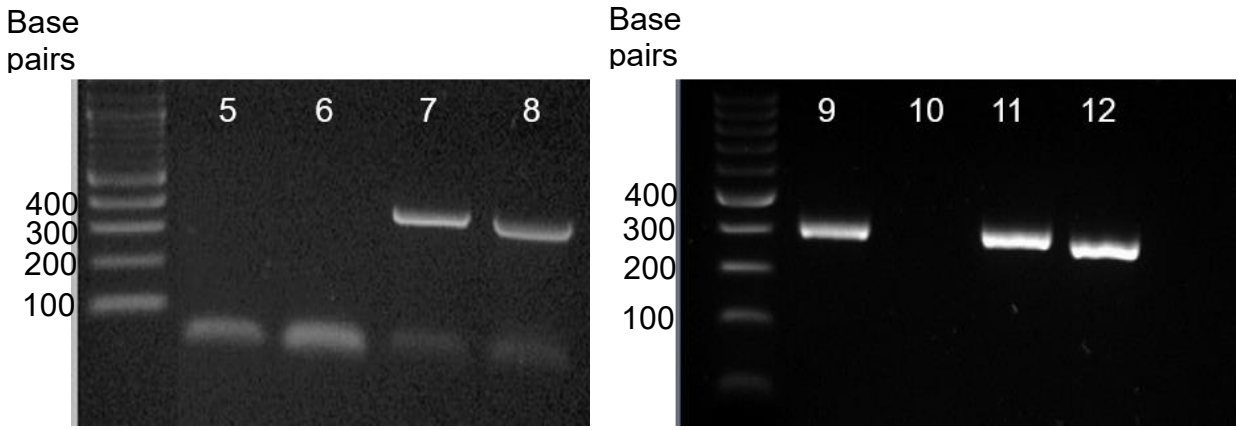

Figure 5.10: MNNG-HOS naïve and transfected MNNG-HOS+P2X7RB OS cells P2X7R expression with HEK-293+P2X7RA control. Expression of P2X7RB mRNA was determined with two different P2X7R sets of primers, one set binding to both P2X7RA and P2X7RB, the second set binding to a region on P2X7RA that is truncated on P2X7RB (product length 413 BP and 399 BP respectively). DNA from each cell type was amplified with both primer sets. **Lanes 5 & 6** MNNG-HOS naïve OS cells, **lanes 7 & 8** HEK-293+P2X7RA cells **lanes 9 & 10** MNNG-HOS+P2X7RB OS cells **lanes 11 & 12** HEK-293+P2X7RA cells.

5.8 Expression of P2X7RB in MNNG-HOS naïve OS cells confirmed using qPCR

In addition to end-point PCR showing bands for P2X7R expression, qPCR was used to demonstrate gene expression changes in transfected cells. ΔCT values were calculated by normalising target templates to HPRT a housekeeping gene, delta delta CT values and fold changes were then calculated. Transfected cells were compared to the untransfected MNNG-HOS naïve OS cells with results plotted as fold change. The human P2X7R Taqman® primer used is not isoform specific and will therefore detect the full length P2X7RA and P2X7RB

The results also demonstrate that there is a significant increase in P2X7RB expression in transfected MNNG-HOS OS cells when compared to MNNG-HOS naïve OS cells (P=0.0067, Figure 5.11).

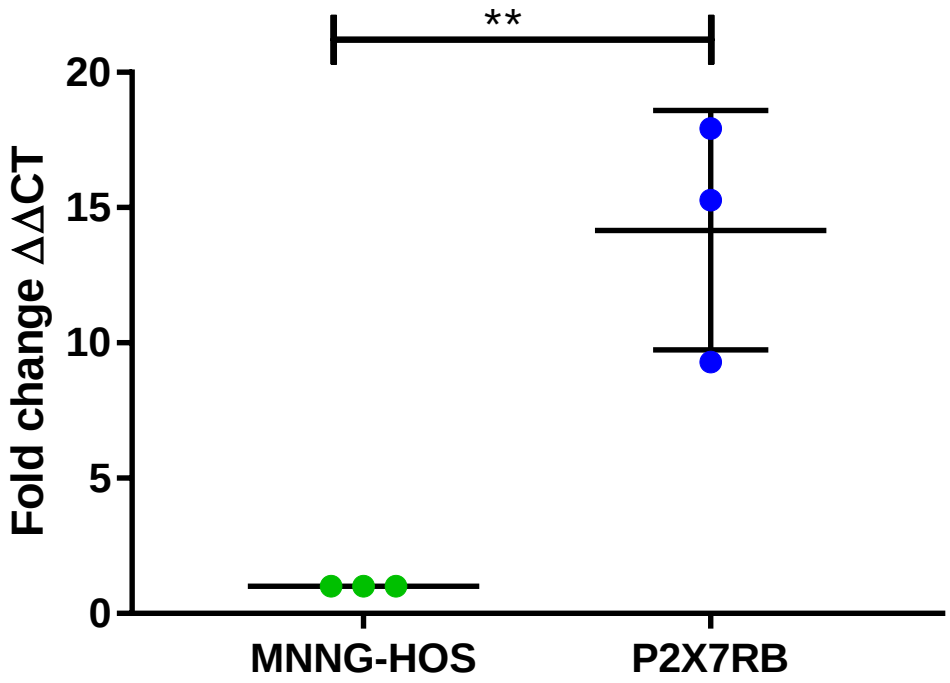

Figure 5.11: Quantification of P2X7RB expression in MNNG-HOS OS cells RNA was extracted from MNNG-HOS OS cells reverse transcribed to cDNA then amplified using qPCR, HPRT was used as a housekeeping gene with data expressed relative to this and the MNNG-HOS naïve P2X7R expression levels. MNNG-HOS naïve OS cells are shown in green and MNNG-HOS+P2X7RB OS cells are shown in blue. Data shown is from 3 biological repeats with 6 technical repeats per experiment 3 using P2X7R Taqman probe and 3 using HPRT Taqman probe. ** = P <0.01.

5.9 Measurement of intracellular calcium concentrations in P2X7R transfected MNNG-HOS OS cells

Changes in cytosolic free calcium concentrations were measured in naïve and transfected cells. Cells were plated out at a density of 15,000 into 96-well plates and left overnight to adhere, the media was then changed into an equal solution of complete medium and 2X Fluo-4 Direct™ calcium reagent loading solution. Cells were incubated for 1 hour at 37°C before been stimulated with BzATP (100 µM) and then ionomycin (0.8 µM).

The results for calcium concentrations were plotted relative to its ionomycin response which is shown in Figure 5.12 A) The AUC (Figure 5.12 B) and peak intensity (Figure 5.12 C) were plotted. The results demonstrate that there was a significantly increased AUC in cells when transfected with P2X7RB compared to MNNG-HOS naïve OS cells (MNNG-HOS+P2X7RB 480.4 ± 21.38 SEM vs 417.0 ± 22.03 SEM MNNG-HOS naïve, P= 0.0266, Figure 5.12 B) The results for the peak intensity demonstrate there was a significantly increased peak intensity in cells transfected with P2X7RB compared to MNNG-HOS naïve OS cells (MNNG-HOS+P2X7RB 2.556 ± 0.09239 SEM vs 2.045 ± 0.1052 SEM MNNG-HOS naïve, P=0.0018, Figure 5.12 C).

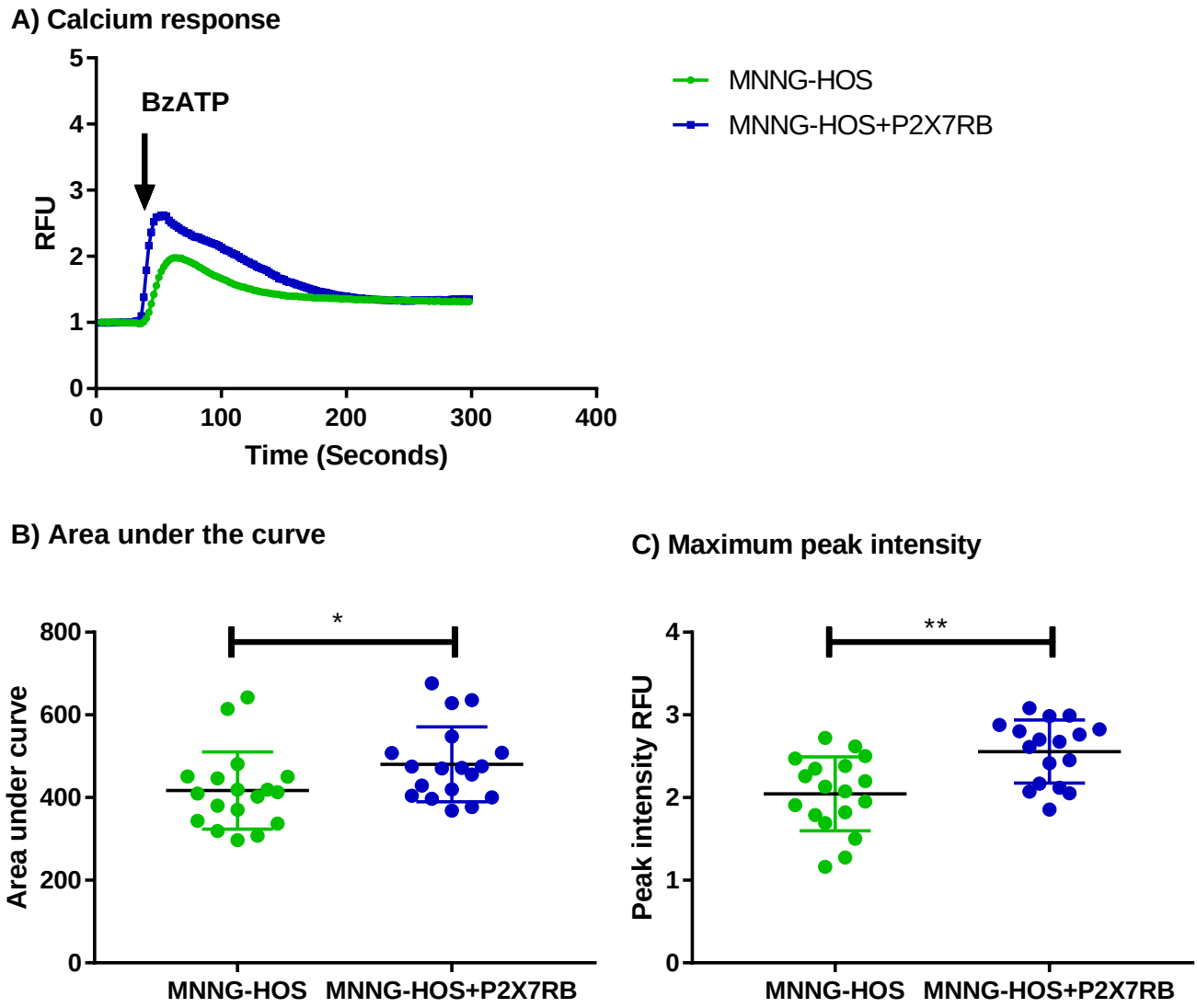

Figure 5.12: Measurement of intracellular calcium concentrations in P2X7RB transfected MNNG-HOS OS cells after P2X7R stimulation with BzATP. Cells were seeded at 15,000 cells in 96-well plates and left overnight to adhere. The media was then changed into an equal solution of complete medium and 2X Fluo-4 Direct™ calcium reagent loading solution. Cells were then incubated for 1 hour at 37°C before been stimulated with either BzATP (100 µM) or ionomycin (0.8 µM) **A)** Calcium response **B)** The area under the curve **C)** The maximum peak intensity. MNNG-HOS naïve are shown in green and MNNG-HOS+P2X7RB are shown in blue. Results are from 3 biological repeats with 6 technical replicates and were compared using an unpaired T-test. * = P <0.05 ** = P<0.01.

5.10 Measurement of P2X7R pore formation in transfected MNNG-HOS OS cells

Sustained stimulation of the P2X7R with its agonist ATP enables the P2X7R to form a large irreversible pore permeable to molecules with a molecular weight of up to 900 Da (Volonte *et al*., 2012). This includes large organic dyes such as ethidium bromide (molecular weight 394). This function is unique to the P2X7R subset of purinergic receptors and has a variety of roles. Therefore, this function was assessed in MNNG-HOS OS cells transfected with the P2X7RB variant with HEK-293 cells used as a positive control. A density of 15,000 cells/well were cultured in a 96 well plate, left overnight to form a monolayer and incubated in HBSS buffer for 1 hour prior to analysis. The pore formation function was then stimulated using 300 µM BzATP in the presence of 100 µM ethidium bromide and monitored for 45 minutes to assess the dye uptake by fluorescence emission at an excitation/emission wavelength couple of 360/580 nm. Cells were also treated with 10 µM of A740003, a P2X7R specific antagonist, to confirm if any pore formation was due to P2X7R expression. The MNNG-HOS naïve OS cells lack P2X7R expression but were checked for any non-specific pore formation. The P2X7RB is a naturally truncated isoform of the P2X7RA and lacks the typical pore function. Therefore, no ethidium bromide uptake was anticipated; however, this was still checked.

The results demonstrate that as expected, activation of with BzATP the fully functional P2X7RA variant in HEK-293 cells led to uptake ethidium bromide, hence demonstrating pore formation and was used as a positive control to compare to pore formation, this effect was attenuated with the addition of A740003 shown in (Figure 5.13).

The assay demonstrated no functional pore formation ability in the untransfected MNNG-HOS naïve OS cells or in the MNNG-HOS+P2X7RB expressing OS cells (Figure 5.13).

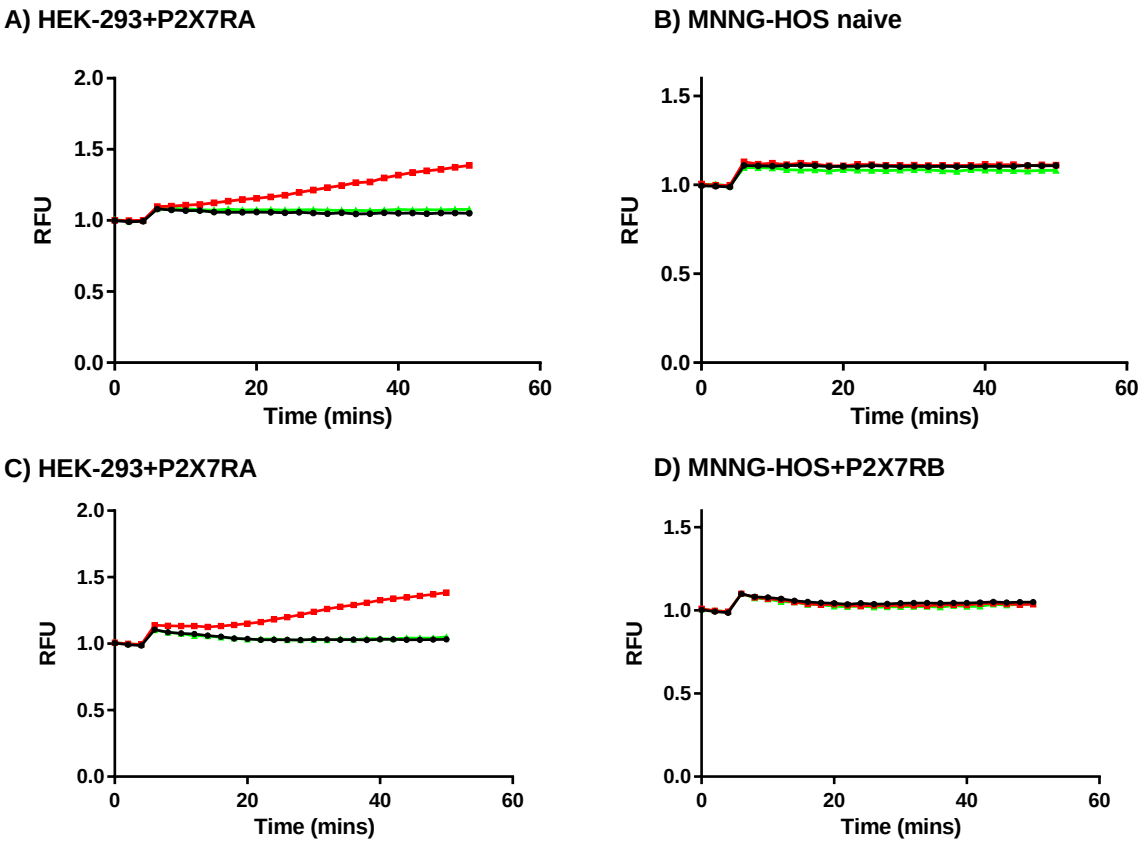

Figure 5.13: Ethidium bromide uptake in response to P2X7R activation in MNNG-HOS and MNNG-HOS+P2X7RB OS cells. Cells were plated out into 96-well plates and left overnight to adhere, the media was then changed to HBSS and incubated at 37°C with or without 10 µM of the P2X7R inhibitor A740003 for 1 hour. BzATP was diluted in ultra-pure ethidium bromide to a final concentration of 300 µM BzATP and 100 µM ethidium bromide. Induction of the P2X7R pore formation was detected for 45 minutes after an initial 5-minute baseline reading, with readings taken every 2 minutes. **A)** and **C)** Transfected HEK-293+P2X7RA cells known to form pores used as a positive control. **B)** MNNG-HOS naïve OS cells **D)** MNNG-HOS+P2X7RB OS cells. Red coloured lines indicate the cells stimulated with BzATP, green lines indicate cells stimulated with BzATP but containing the A740003 inhibitor, black coloured lines indicate the cells incubated with ethidium bromide and no BzATP stimulation. Results are from three biological repeats with six technical replicates.

5.11 Effect of P2X7R on MNNG-HOS OS cell proliferation

Having established that the transfected MNNG-HOS cell lines do indeed contain mRNA for the P2X7RB, and having validated the typical P2X7RB responses including intracellular calcium responses (Chapter 5, sections 5.7 – 5.10), the effect of receptor expression on cell physiology was determined. The first parameter that was examined was the MNNG-HOSs ability to grow in varying serum concentrations. MNNG-HOS OS cells were grown to 50% confluence then counted and seeded into 96 well plates at 2500 cells. After 24 hours, the media was changed to either 0.5%, 2% or 10% FBS medium. Cell proliferation was assessed using an MTS assay at days 0, 1, 3, 5 and 7.

MNNG-HOS OS cells that had been transfected with the P2X7RB isoform when cultured in 0.5%, 2% or 10% FBS had a significant increase in proliferation across all day 3 and 5 ($P = <0.0001$, Figure 5.14 A, B, C) and for day 7 ($P = 0.0008$ for 10% FBS, $P = 0.0006$ for 2% FBS and $P = <0.0001$ for 0.5% FBS Figure 5.14 A, B, C) compared to MNNG-HOS naïve OS cells.

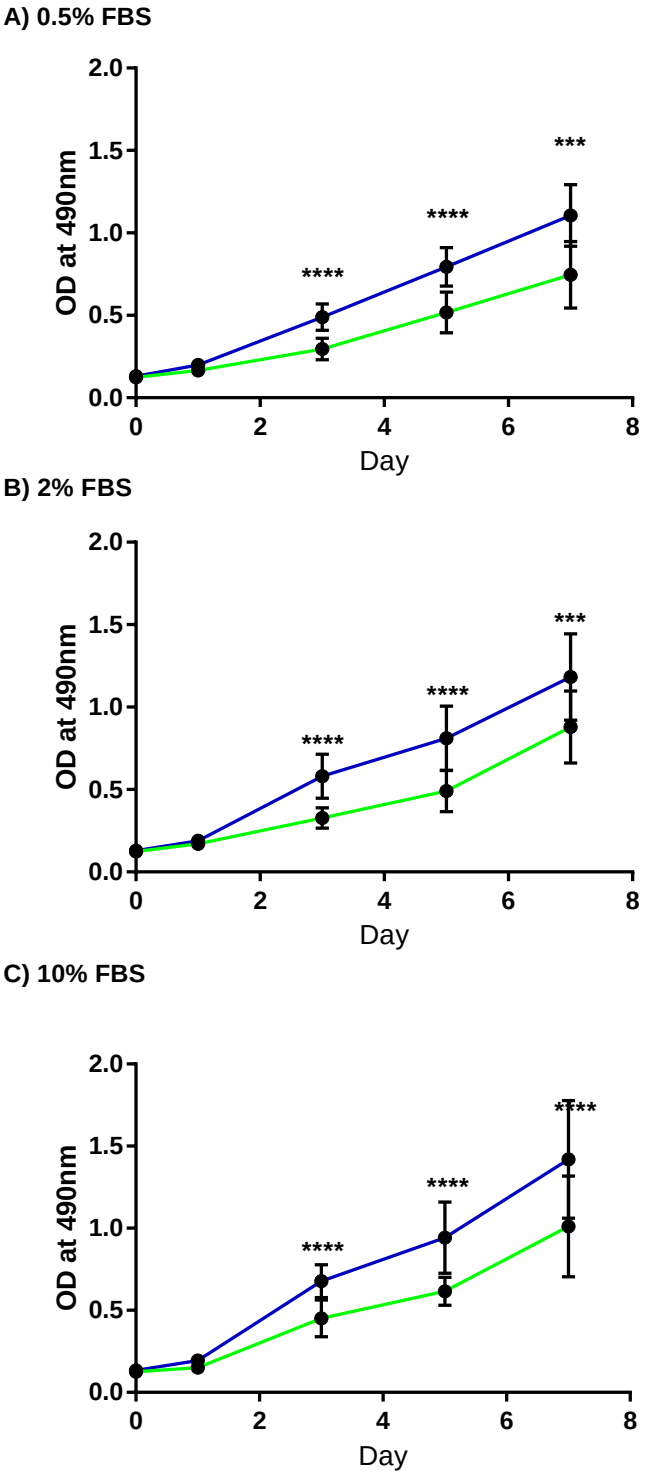

Figure 5.14: The effect of P2X7RB expression on MNNG-HOS OS cell proliferation. MNNG-HOS OS cells were seeded into 96 well plates at a density of 2500, in either **A)** 0.5% FBS) **B)** 2% FBS or **C)** 10% FBS Cell proliferation was assessed using an MTS assay (absorbance measured at 490 nm) on days 0, 1, 3, 5 and 7. MNNG-HOS naïve OS cells are shown in green with MNNG-HOS+P2X7RB OS cells in blue, data is from 3 biological repeats with 6 technical repeats per experiment. Data was analysed using an unpaired T test for days 3, 5, 7. *** = P< 0.001 **** = P < 0.0001.

5.12 Effect of A740003 and AZ11645373 on MNNG-HOS OS cell proliferation

As previously shown P2X7RB increased the growth of MNNG-HOS OS cells, therefore whether this increased growth could be attenuated using specific P2X7R antagonists was next investigated. The amount of cells used was 2500 in 0.5% FBS medium. The concentration of inhibitor used was 100 μM, derived from a previously used concentration (Giuliani *et al.,* 2014).

Treatment of MNNG-HOS naïve OS cells with A740003 or AZ11645373 had no significant effect on cell growth (A740003 0.735 ± 0.069 SEM vs 1.000 ± 0.087 SEM vehicle, P=0.060, Figure 5.15 A) and (AZ11645373 0.982. ± 0.080 SEM vs 1.000 ± 0.087 SEM vehicle, P= 0.912, Figure 5.15 A).

In MNNG-HOS OS cells transfected with P2X7RB, growth was significantly decreased by both A740003 and AZ11645373 (A740003 0.4831 ± 0.045 SEM vs 1.000 ± 0.079 SEM vehicle, P<0.0001, Figure 5.15 B) and (AZ11645373 0.650 ± 0.058 SEM vs 1.000 ± 0.079 SEM, P= 0.0007, Figure 5.15 B).

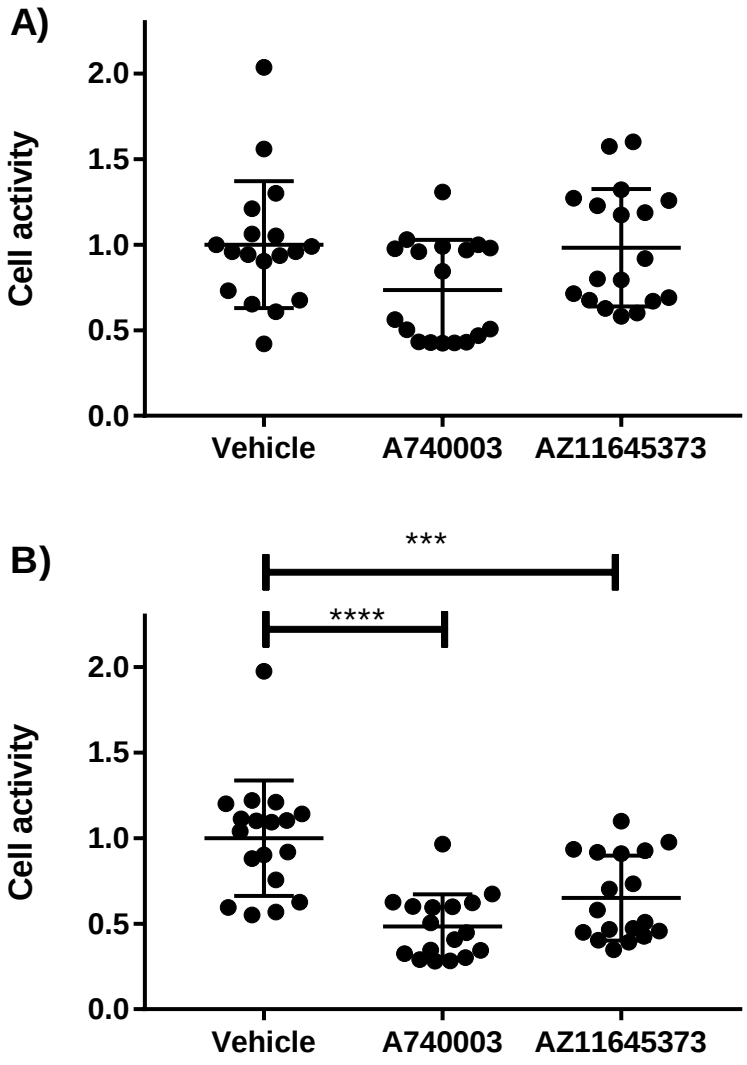

Figure 5.15: The effect of two different P2X7R inhibitors on the proliferation of MNNG-HOS and MNNG-HOS OS cells. Cells were plated out in a 96 well plate at a density of 2500 cells in 0.5% FBS, and left to adhere for 24 hours, the medium was then changed to medium containing vehicle or 100 µM of either A740003 or AZ11645373. The cell activity was assessed using an MTS assay (absorbance measured at 490 nm) at 3 days. **A)** MNNG-HOS naïve OS cells, **B)** MNNG-HOS+ P2X7RB OS cells. Data is from 3 biological repeats with 6 technical repeats per experiment. Data was analysed comparing the treatment groups to the vehicle control using a Mann Whitney test as data was considered non-parametric. ** = P< 0.01 ****= P<0.0001.

5.13 The effect of P2X7R expression on MNNG-HOS OS cell adhesion

For cell adhesion studies assessing the ability to adhere to type 1 collagen coated to a 96-well plate. The same experiment was performed for the MNNG-HOS OS cells as per the Te85 OS cells, a 4-hour time point used, the wells containing cells were washed and the remaining cells quantified by lysing the cells with lysis buffer and detecting the DNA present using Quant-iT™ PicoGreen® dsDNA Reagent. Fluorescence was detected at excitation 485 nm and emission 530 nm with a cut off at 530 nm.

MNNG-HOS OS cells expressing the P2X7RB had significantly decreased adhesion to the type I collagen matrix when compared to the MNNG-HOS naïve OS cells (MNNG-HOS+P2X7RB 0.724 ± 0.047 SEM vs 1.000 ± 0.042 SEM, MNNG-HOS naïve P= <0.0001, Figure 5.16).

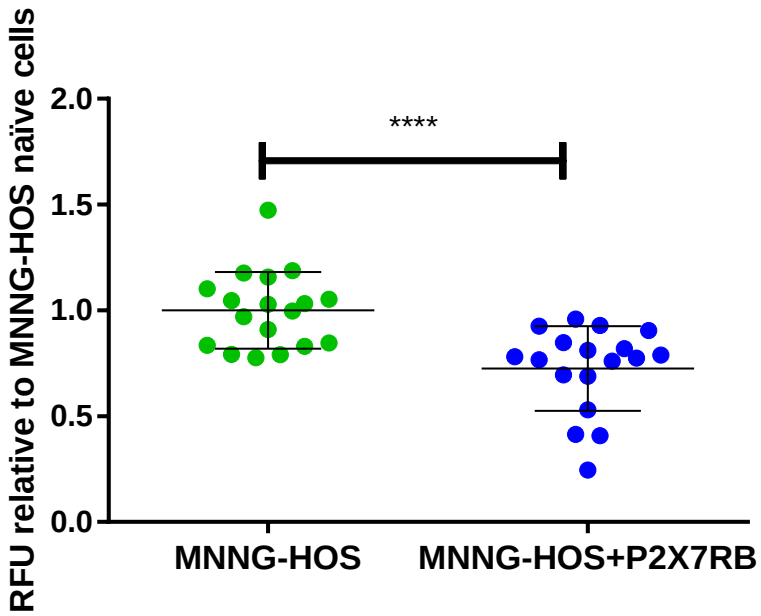

Figure 5.16: The effect of P2X7RB on OS cell adhesion. For each experiment 7500 cells were plated into a 96 well plate pre-coated with type 1 rat tail collagen and left for 4 hours at 37°C. Wells were then washed 4 times with PBS to removed unattached cells. Remaining attached cells were lysed using lysis buffer and detected using Quant-iT™ PicoGreen® dsDNA Reagent. Fluorescence was detected at excitation 485 nm and emission 530 nm. MNNG-HOS naïve vs MNNG+P2X7RB OS cells. data is plotted relative to the MNNG-HOS naïve OS cells which are shown in green, MNNG-HOS+P2X7RB OS cells in blue. Data shown is from 3 biological repeats with 6 technical repeats per experiment. Data was analysed using an unpaired T-test. **** = P <0.0001.

5.14 The effect of P2X7R expression on MNNG-HOS OS cell migration

Migration was performed using the same method as the Te85 OS cells, a scratch assay was used. The OS cell lines were seeded into a 12 well plate at a density of 200,000 in complete medium and left overnight to adhere and form a monolayer. Cells were then changed over into complete medium containing 5 µg/ml mitomycin C and left for 2 hours at 37°C. After this, monolayers were scratched down the centre of each well using a 10 µL pipette tip. After washing twice with PBS the cells were left in either 10% FBS, 0.5% FBS medium or 0.5% FBS medium with 10 µM BzATP. Images were taken every 2 hours for 24 hours.

In 10% FBS, there was no significant difference in migration between MNNG-HOS naïve OS cells and MNNG-HOS OS cells expressing P2X7RB (P= 0.058, Figure 5.17). In 0.5% FBS, there was no significant difference in migration between MNNG-HOS naïve OS cells and MNNG-HOS OS cells expressing P2X7RB (P= 0.123, Figure 5.18). However, when cells were cultured in 0.5% FBS and stimulated with 10 µM BzATP to activate the P2X7RB, there was a significant increase in migration in MNNG-HOS+P2X7RB OS cells when compared to stimulated MNNG-HOS naïve OS cells. (P= <0.002, Figure 5.19).

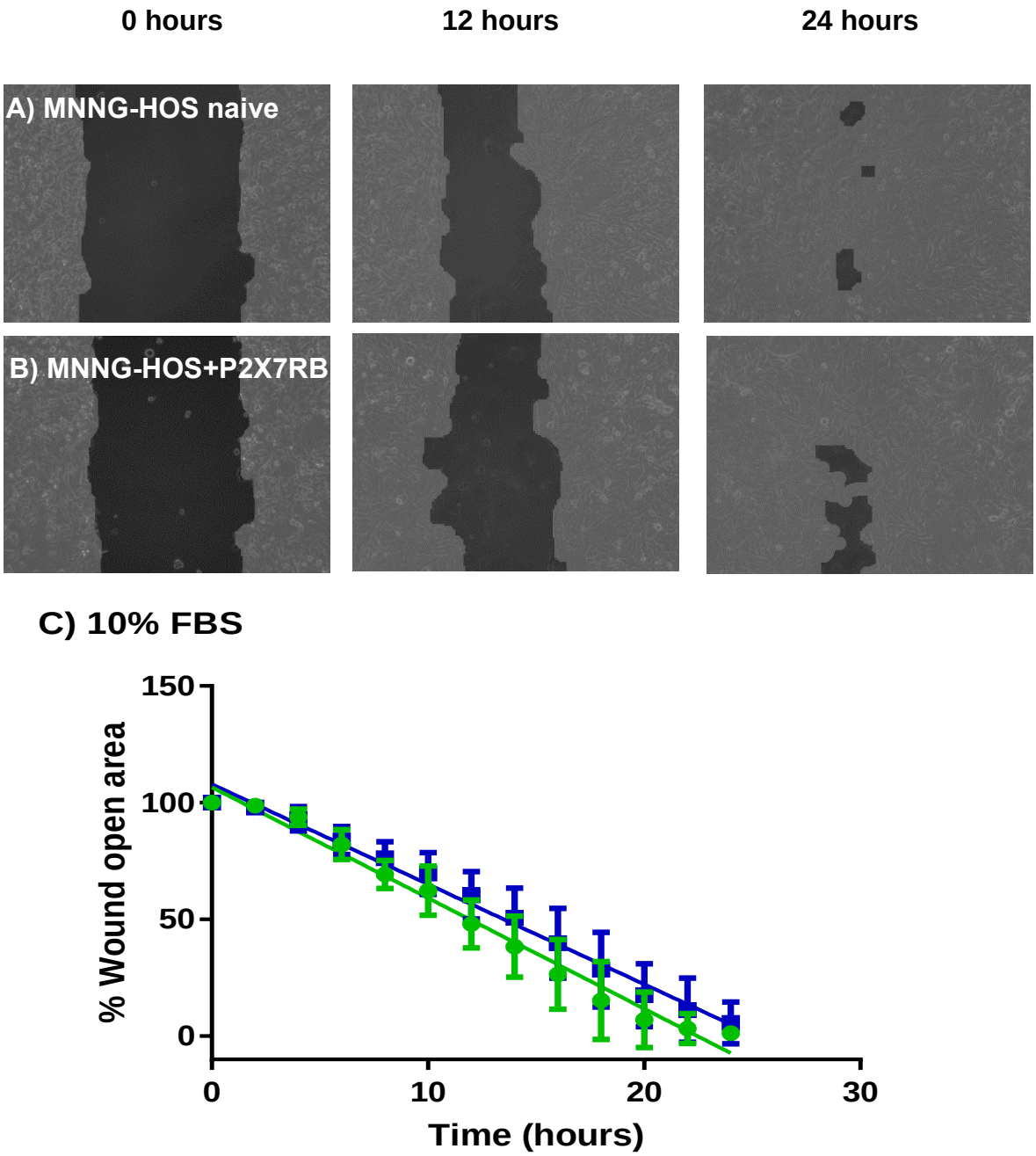

Figure 5.17: The effect of P2X7RB on MNNG-HOS OS cell migration in 10% FBS medium. Cells were plated out into a 12 well plate at a seeding density of 200,000 in complete medium and left overnight to adhere and form a monolayer. Cells were then changed over into complete medium containing 5 µg/ml mitomycin C and left for 2 hours at 37°C, monolayers were then scratched down the centre of the well using a 10 µL pipette tip, after washing twice with PBS the cells were left in 10% FBS with images taken every 2 hours for 24 hours. The images are representative of 0 hours, 12 hours and 24 hours only. The images were analysed and pseudocoloured using Tscratch software. Data from 3 biological repeats with 3 technical repeats per experiment. **A)** MNNG-HOS naïve OS cells **B)** MNNG-HOS+P2X7RB OS cells. **C)** MNNG-HOS naïve OS cells in green vs MNNG-HOS+P2X7RB OS cells blue. Linear regression was used to compare the slopes.

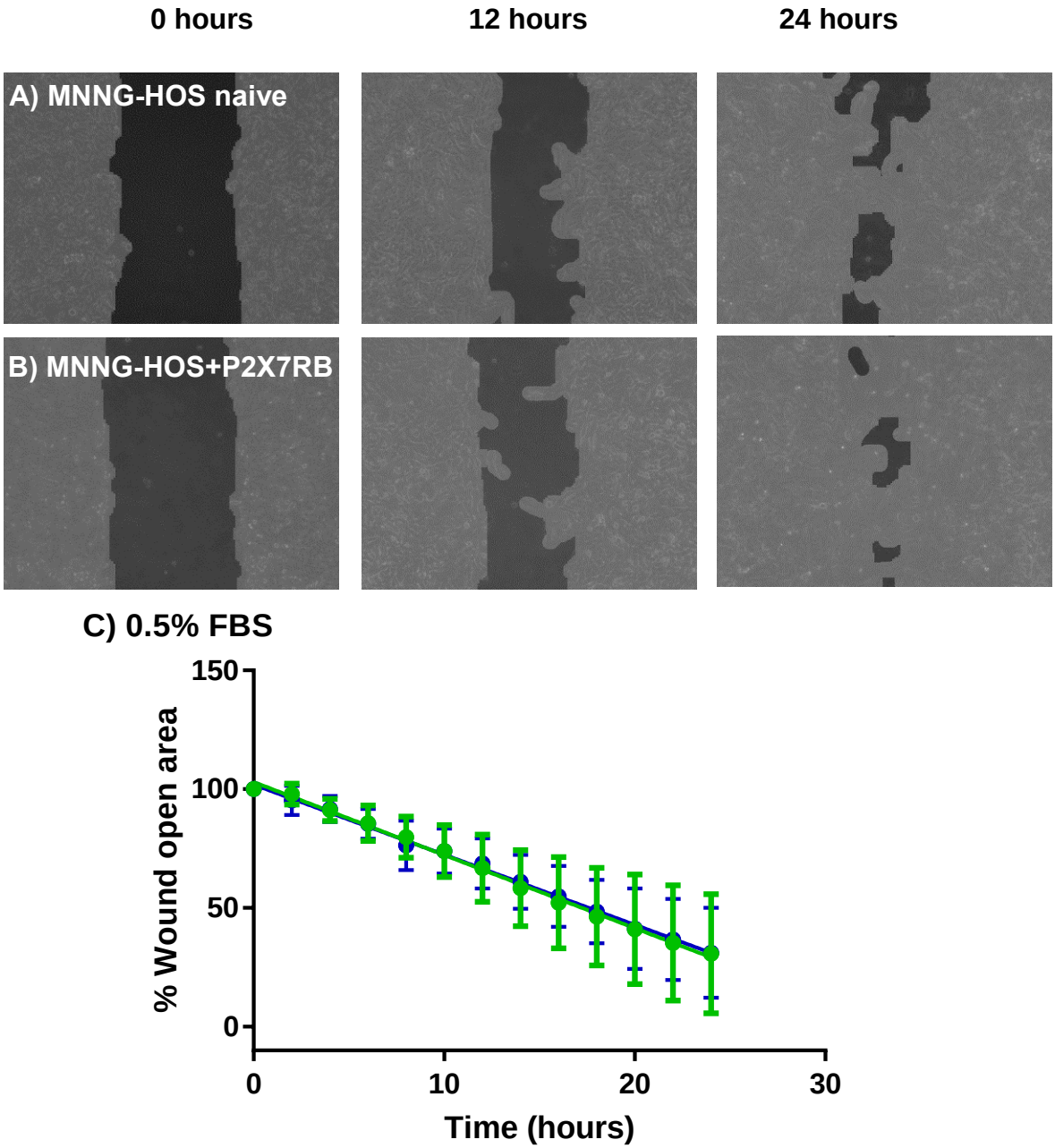

Figure 5.18: The effect of P2X7RB, on MNNG-HOS OS cell migration in 0.5% FBS medium. Cells were plated out into a 12 well plate at a seeding density of 200,000 in complete medium and left overnight to adhere and form a monolayer. Cells were then changed over into complete medium containing 5 µg/ml mitomycin C and left for 2 hours at 37°C, monolayers were then scratched down the centre of the well using a 10 µL pipette tip, after washing twice with PBS the cells were left in medium containing 0.5% FBS with images taken every 2 hours for 24 hours. The images are representative of 0 hours, 12 hours and 24 hours only. The images were analysed and pseudocoloured using Tscratch software. Data from 3 biological repeats with three technical repeats per experiment. **A)** MNNG-HOS naïve OS cells **B)** MNNG-HOS+P2X7RB OS cells. **C)** MNNG-HOS naïve OS cells in green vs MNNG-HOS+P2X7RB OS cells blue. Linear regression was used to compare the slopes.

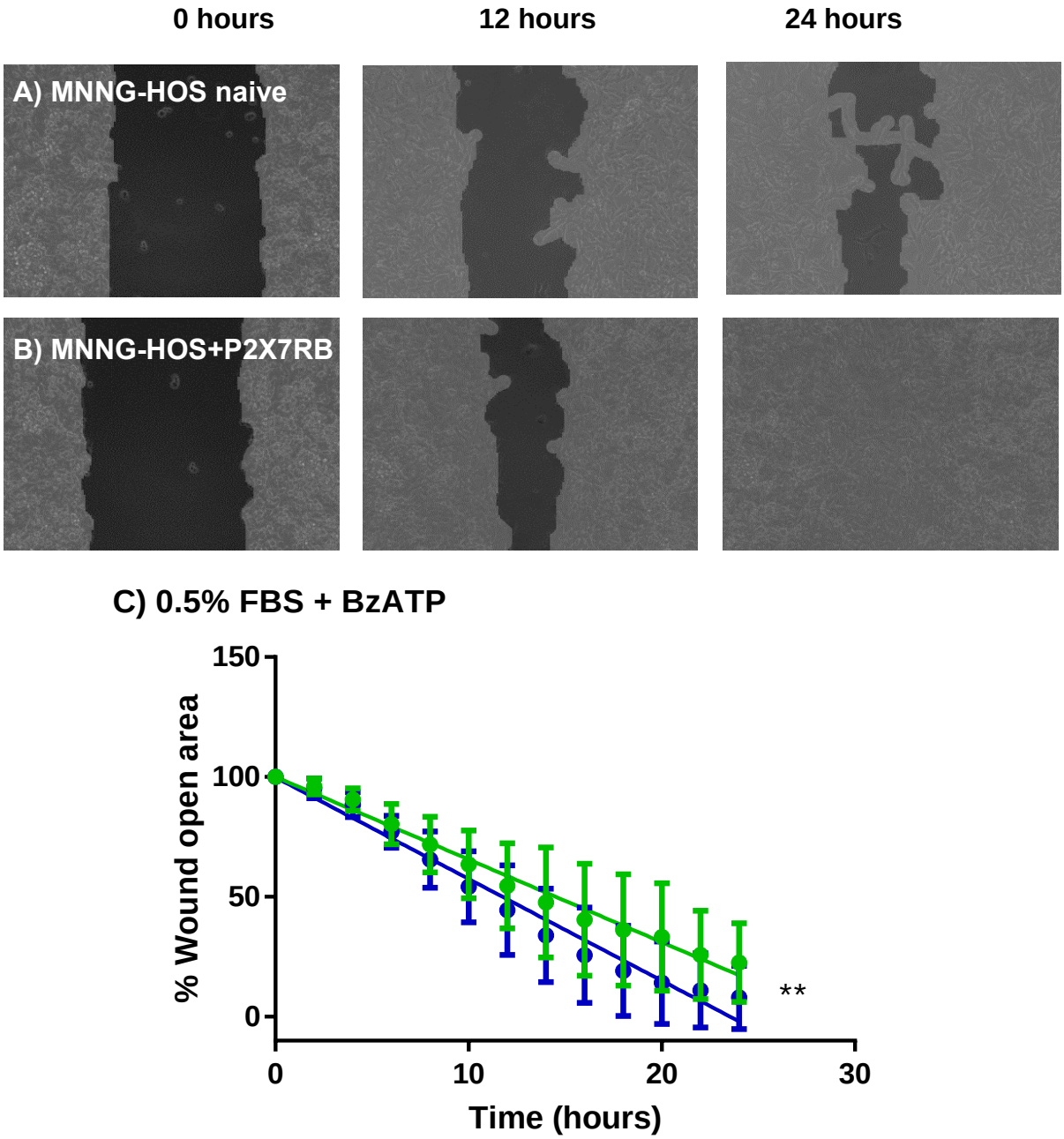

Figure 5.19: The effect of P2X7RB, on MNNG-HOS OS cell migration in 0.5% FBS medium stimulated with BzATP. Cells were plated out into a 12 well plate at a seeding density of 200,000 in complete medium and left overnight to adhere and form a monolayer. Cells were then changed over into complete medium containing 5 µg/ml mitomycin C and left for 2 hours at 37°C, monolayers were then scratched down the centre of the well using a 10 µL pipette tip, after washing twice with PBS the cells were left in medium containing 0.5% FBS and 10 µM BzATP with images taken every 2 hours for 24 hours. The images are representative of 0 hours, 12 hours and 24 hours only. All images were analysed, and pseudo coloured using Tscratch software. Data from 3 biological repeats with 3 technical repeats per experiment. **A)** MNNG-HOS naïve OS cells **B)** MNNG-HOS+P2X7RB OS cells **C)** MNNG-HOS naïve OS cells in green vs MNNG-HOS+P2X7RB OS cells in blue. Linear regression was used to compare the slopes. ** = P <0.01.

5.15 The effects of P2X7R expression on MNNG-HOS OS cell invasion

Invasion in MNNG-HOS OS cells was performed according to the same method used for Te85 OS cells. The cells were cultured in mitomycin C to inhibit proliferation, before being plated into a pre-coated matrigel transwell FluoroBlok insert in serum free medium containing 10 μM BzATP. The lower chamber contained 10% FBS medium as a chemoattractant. After 24 hours the inserts were removed, washed in PBS and stained with Calcein AM cell permeant dye and imaged, these were then quantified using Image J and plotted as the amount of invaded cells detected.

The results show that there was a significantly increased ability to invade the matrigel layer in the MNNG-HOS+P2X7RB OS cells compared to MNNG-HOS naïve OS cells (MNNG-HOS+P2X7RB 661.7 ± 173.0 SEM vs 180.9 ± 66.73 SEM MNNG-HOS, P= 0.025, Figure 5.20).

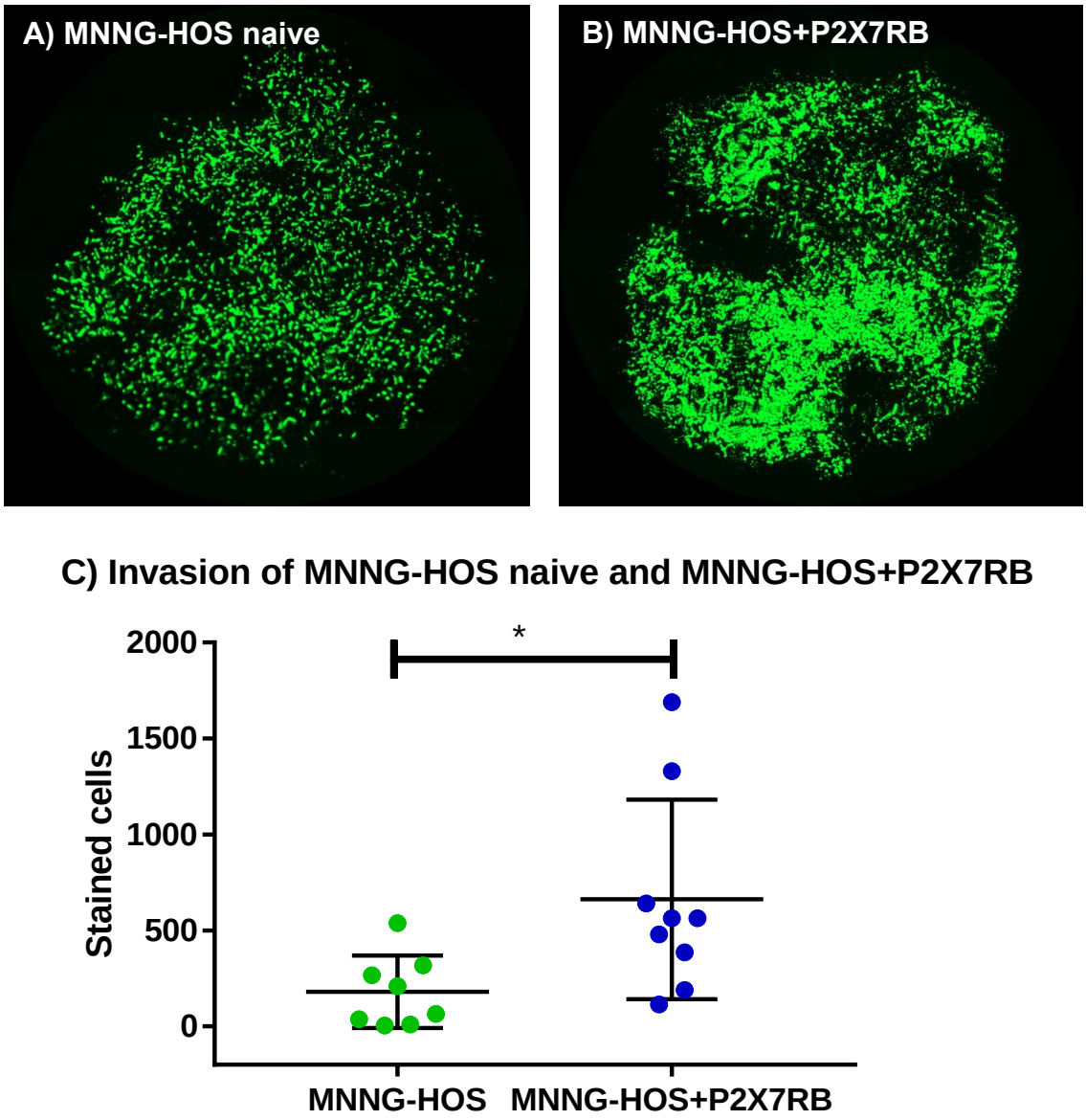

Figure 5.20: Representative images of the effect of P2X7RB on MNNG-HOS OS cell invasion and the analysed results. Cells were incubated in culture with 5 µg/ml mitomycin C and left for 2 hours at 37°C. They were seeded into a 24 well plate at a density of 100,000 cells in serum free medium containing 10 µM BzATP, in an upper fluoroblok chamber pre-coated with 1.5 mg/ml Matrigel. The medium in the lower chamber contained complete medium. After 24 hours the upper fluoroblok transwells were removed and washed twice in PBS and left for 30 minutes at 37°C in calcein AM cell permeant dye to stain live invaded cells. Images were taken covering 60% of the underside of the 24-well, this covered the entire surface of the smaller insert, these were analysed using Image J, shown are representative images of **A)** MNNG-HOS OS cells **B)** MNNG-HOS+P2X7RB OS cells **C)** MNNG-HOS naïve OS cells shown in green vs MNNG-HOS+P2X7RB OS cells shown in blue. Data is from 3 biological repeats with 3 technical repeats per experiment. * = P< 0.05 data was analysed using an unpaired T-test.

5.16 Discussion

The purpose of this chapter was to determine if Te85 OS cells could be used as an *in vivo* model of OS to target the P2X7R Due to the P2X7R providing a growth increase in Te85 OS cells (Chapter 4) and having previously been reported to increase the growth of cell lines injected *in vivo* (Adinolfi *et al.,* 2012) this chapter tested the hypothesis that P2X7R expression would increase the tumourgenicity of the Te85 OS cells *in vivo.* However, this was not the case and therefore the second aspect of the chapter was to determine if an alternative MNNG-HOS model could be used. The MNNG-HOS OS cell line is a derivative of the Te85 parental OS cell line which was treated with MNNG and increases the carcinogenesis of the cells (Rhim *et al.,*1975a).

The results from this *in vivo* pilot study demonstrate that the Te85 OS cell line when injected paratibially into 3 BALB/c nude mice do not form palpable tumours after 6 weeks, in addition no micro-tumours were detected in the H&E and Ki-67 stained leg sections. There was also no effect on bone phenotype, such as osteolysis or ectopic bone formation as determined using micro-CT reconstructions of the bones and total bone volume determination as there was no difference in total bone volume when comparing the Te85 injected limb to the contralateral limb in any variants. The cells didn't form any metastasis in the lungs when they were collected and analysed. The observed results are in accordance with previously reported findings regarding the use of Te85 OS cells *in vivo* (Luu *et al.,* 2005). This means that the Te85 OS cell line or Te85+P2X7R expressing variants cannot be used as a suitable *in vivo* model and an alternative OS cell line would need to be used to target P2X7R.

Mice injected with MNNG-HOS+GFP+LUC and MNNG-HOS naïve OS cells did form palpable tumours in all 6 mice 9 days' post injection. Tumours were shown clearly on the H&E and Ki-67 stained sections. Additionally, the bones had both osteolysis and ectopic bone formation which was visible on the 3D micro-CT reconstruction. The total bone volumes also showed an average decrease in the injected limbs, this was however considered not significant most likely due to the low N number used in the pilot study. There was only one incidence of pulmonary metastasis with MNNG-HOS+GFP+LUC mice and none in the MNNG-HOS mice suggesting this model may not provide the ability to study OS metastasis.

Due to the MNNG-HOS+GFP+LUC and MNNG-HOS naïve OS cells forming a reliable OS model when paratibially injected into BALB/c nude mice, which was palpable in a fast time frame, these cells could be used as an alternative to the Te85 OS cells as a xenograft model to be used to target the P2X7R.

P2X7R was found not to be expressed in MNNG-HOS naïve OS cells so a P2X7R isoform was required to be transfected. The P2X7RB is a naturally occurring splice variant of the full length P2X7RA, with a non-functional P2X7R phenotype lacking the pore formation function (Sluyter & Stokes, 2011). It is highly expressed in OS patient samples (Giuliani *et al.,* 2014) however, when P2X7R has been examined in various other cancers studies only focus on the full length receptor. Based on this and the data from chapter 4 showing that transfection with the P2X7RB increases OS proliferation, decreases cell adhesion, and increases migration and invasion, the P2X7RB isoform could provide a novel therapeutic target that has yet to be widely explored. MNNG-HOS naïve OS cells were subsequently transfected with P2X7RB and confirmed with end point PCR, qPCR and receptor functional assays. Its effect on cell proliferation adhesion migration and invasion were then further assessed. The results demonstrated transfection with the P2X7RB variant lead to an increase rate of proliferation, decreased cell adhesion and increased migration and invasion when stimulated with BzATP. These findings concur with the Te85 OS cell line when transfected with P2X7RB and has been discussed in the previous chapter.

In conclusion, the Te85 model cannot be used *in vivo,* however, this chapter demonstrates that a MNNG-HOS model can be used which has led to the formation of a MNNG-HOS+P2X7RB OS cell line which will now be used for further *in vivo* studies.

Chapter 6 - Targeting the P2X7RB *in vivo* using the MNNG-HOS OS xenograft mouse model

6.1 Introduction

The previous chapters have demonstrated that the expression of P2X7R contributes towards OS cell growth, adhesion, migration and invasion in both Te85 and MNNG-HOS cell lines *in vitro;* and that targeting the P2X7R with A740003 could provide a novel therapeutic target for the treatment of OS as it significantly reduced OS cell growth.

Previously, P2X7R targeting has been performed *in vivo* in different cancers, and the application of P2X7R antagonists has had encouraging effects on reducing tumour growth. In an orthotopic xenograft mouse model of pancreatic ductal adenocarcinoma the P2X7R antagonist AZ10606120 administered via IP injection was shown to decrease tumour size (Giannuzzo *et al.,* 2016) similar effects were also observed using the same antagonist *in vivo* on mesothelioma tumours (Amoroso *et al.,* 2016), although in the latter case the antagonist was delivered intra mass directly to the tumour. Another study showed a similar effect looking at three different cancer types. Growth of CT26 mouse colon cancer cells was reduced *in vivo* using the P2X7R antagonist oATP administered intra mass. The growth of B16 melanoma cells was reduced using the P2X7R antagonist AZ10606120 again administered intra mass. The study then further demonstrated that genetic silencing of the P2X7R using short hairpin RNA decreased tumour growth of the neuroblastoma cell line ACN *in vivo,* (Adinolfi *et al., 2012).*

In order to further validate the *in vitro* findings of P2X7R influencing OS growth and P2X7R antagonism reducing it (Chapter 4 & 5) a xenograft mouse model of OS was used. The Te85 OS cells used in previous *in vitro* studies were shown to be an unsuitable model to use *in vivo* as they didn't form any palpable tumours or pulmonary metastasis (Chapter 5). However, the MNNG-HOS cell line did provide a reliable model (Chapter 5). Therefore, the MNNG-HOS cell line was transfected with the P2X7RB variant as the *in vitro* data for P2X7RB transfected cells showing a consistent pro tumour effect (Chapter 4&5). P2X7R caused an increase in growth which was attenuated with A740003, a decrease in cell adhesion and an increase in migration and invasion when stimulated with BzATP. Due to its truncation it naturally doesn't have the pore forming ability related to cell apoptosis (Cheewatrakoolpong *et al.,* 2005). Additionally OS patient samples which express the P2X7RB have a higher cell

density possibly suggesting they are more aggressive and contribute towards disease progression (Giuliani *et al.,* 2014).

In this chapter BALB/c nude mice were paratibially injected in their left leg with either MNNG-HOS naïve OS cells or MNNG-HOS+P2X7RB OS cells. The mice were then treated every two days with either vehicle, Ifosfamide (a common chemotherapy drug used for human OS treatment) (Fan *et al.,* 2015) or A740003 (a competitive P2X7R antagonist) (Honore *et al.,* 2006). The mice were then euthanised and *ex vivo* analysis was performed assessing the primary tumour, bone phenotype and metastasis.

The aims of this chapter were to examine the following:

- The effect of P2X7RB expression and treatment with A740003 on tumour growth. This was measured using both external callipers and micro-CT imaging.
- The effect of P2X7RB and treatments on histology of the MNNG-HOS tumours using H&E staining.
- The effect of P2X7RB expression and A740003 treatment on tumour proliferation using Ki-67 IHC.
- The effect of P2X7RB expression and A740003 treatment on tumour apoptosis using annexin V IHC.
- The effect of P2X7RB expression and A740003 treatment on the total bone volume using micro-CT.
- The effect of P2X7RB expression and A740003 treatment on osteoclast coverage at the tumour-bone interface.
- The effect of P2X7RB expression and A740003 treatment on OS pulmonary metastasis.

6.2 Tumorigenicity of MNNG-HOS and MNNG-HOS+P2X7RB OS cells injected into BALB/c nude mice

Initially 72 mice were paratibially injected with 250,000 cells (MNNG-HOS or MNNG-HOS+P2X7RB) in 20μl PBS in order to replicate the OS tumour microenvironment by ensuring that cells were in close proximity to the bone. Mice were then randomised into 3 treatment groups (vehicle, Ifosfamide or A740003 via IP injection every 2 days) for each cell line. For each treatment group the N number was 12 mice. For the mice injected with MNNG-HOS naïve OS cells, the group treated with vehicle resulted in 9/12 mice with palpable tumours, with Ifosfamide 11/12 mice had palpable tumours and with A740003 10/12 mice had palpable tumours (Figure 6.1). For the mice injected with transfected MNNG-HOS+P2X7RB OS cells, the group treated with vehicle resulted in 6/12 mice with palpable tumours, with Ifosfamide 10/12 mice had palpable tumours and with A740003 8/12 mice had palpable tumours (Figure 6.1). In total of 54/72 mice had palpable OS tumours. An additional group of 12 mice were used as a paratibially injected control, these were scratched with the injection needle but not injected with any tumour cells and therefore did not have any palpable tumours.

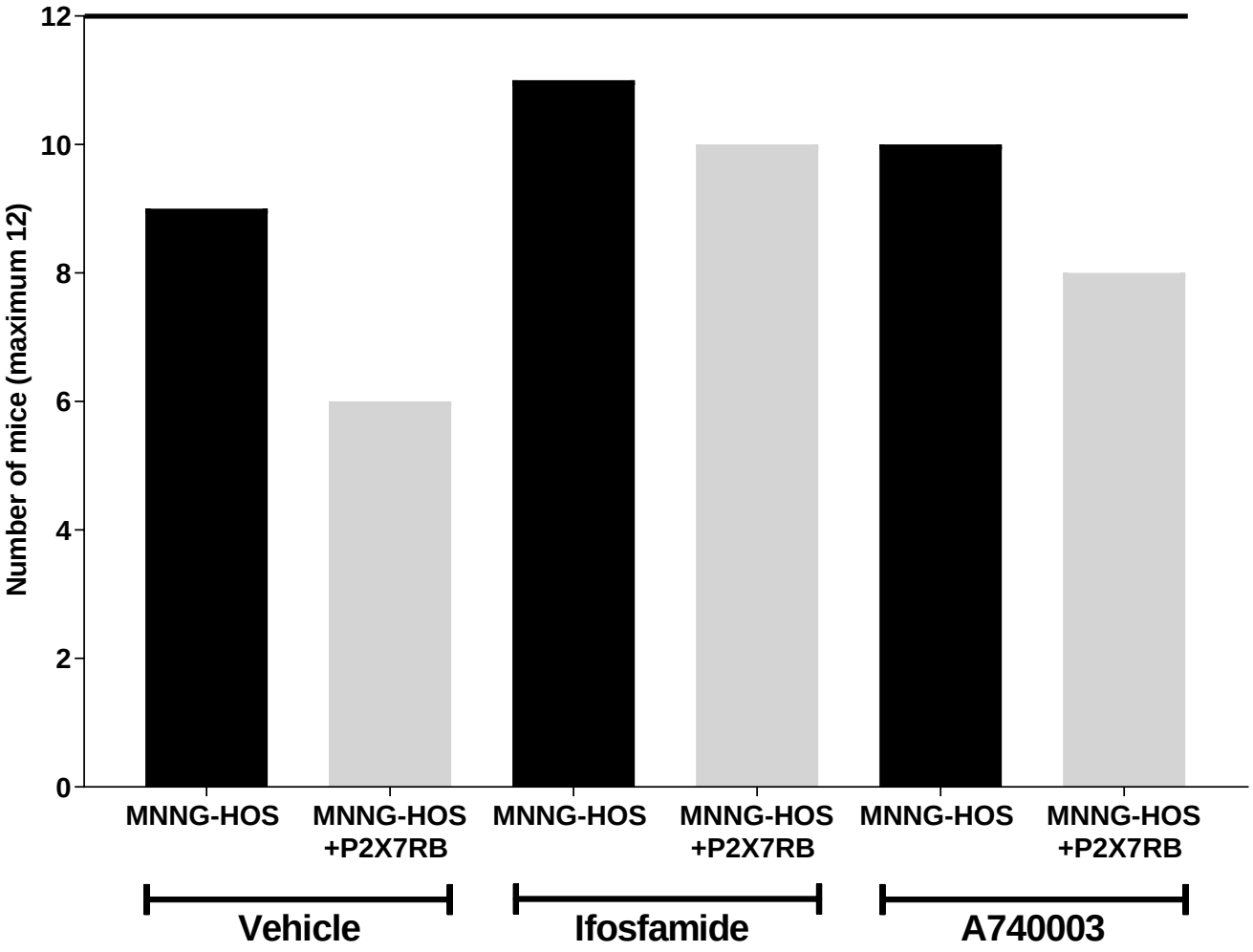

Figure 6.1: Tumourgenicity in the different *in vivo* conditions. For each treatment group 12 female BALB/c 7-9 week old mice were injected paratibially with 250,000 cells of either MNNG-HOS or MNNG-HOS+P2X7RB suspended in 20 µL PBS. Mice were then treated with vehicle, Ifosfamide or A740003 every 2 days for 3 weeks via IP injection and the number of mice with palpable tumours at the end of the procedure plotted. An additional group of 12 mice were used as a paratibially injected control, these were scratched with the injection needle but not injected with any tumour cells and therefore did not have any palpable tumours.

6.3 The effect of P2X7RB expression and drug treatments on primary tumour size measured using external callipers

External calliper measurements were taken at the end of the *in vivo* experiment. This was to determine if P2X7RB expression or if treatment with Ifosfamide or A740003 had an effect on tumour size.

The size of the MNNG-HOS+P2X7RB tumour bearing mice legs was not statistically different to the size of the MNNG-HOS tumour bearing mice legs (MNNG-HOS+P2X7RB 6.983 mm^3 ± 0.350 SEM vs 8.323 mm^3 ± 0.514 SEM MNNG-HOS, P= 0.071, Figure 6.2).

The average size of the MNNG-HOS tumour bearing mice tumours treated with Ifosfamide were not statistically different to the size when treated with vehicle (Ifosfamide 7.570 mm^3 ± 0.356 SEM, vs 8.323 mm^3 ± 0.514 SEM vehicle, P= 0.231, Figure 6.3 A) or when mice were treated with A740003 (A740003 7.083 mm^3 ± 0.404 SEM vs 8.323 mm^3 ± 0.514 SEM vehicle, P= 0.0725, Figure 6.3 A). This was similarly the case in the MNNG-HOS+P2X7RB tumour bearing mice, where mice treated with Ifosfamide did not have statistically different tumour sizes compared to mice treated with vehicle (Ifosfamide 6.739 mm^3 ± 0.1602 SEM, vs 6.983 mm^3 ± 0.3507 SEM vehicle, P= 0.4898, Figure 6.3 B) or when mice were treated with A740003 (A740003 7.001 ± 0.3418 SEM vs 6.983 mm^3 ± 0.3507 SEM vehicle, P= 0.9719, Figure 6.3 B).

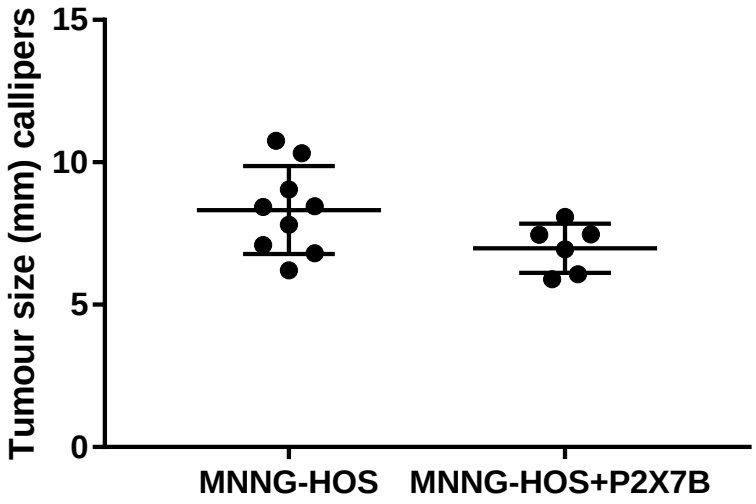

Figure 6.2: End-point primary tumour size comparing the MNNG-HOS and MNNG-HOS+P2X7RB OS bearing mice using external callipers. For each treatment group 12 female BALB/c 7-9 week old mice were injected paratibially with 250,000 cells of either MNNG-HOS or MNNG-HOS+P2X7RB suspended in 20 µL PBS. Mice were then treated with vehicle, Ifosfamide or A740003 every 2 days for 3 weeks via IP injection. Tumour size was determined at the end of the experiment using external callipers to measure the tumour bearing limb only (left leg). MNNG-HOS treated with vehicle was compared to MNNG-HOS+P2X7RB treated with vehicle using an unpaired T-test. N= 9 mice for MNNG-HOS and 6 mice for MNNG-HOS+P2X7RB.

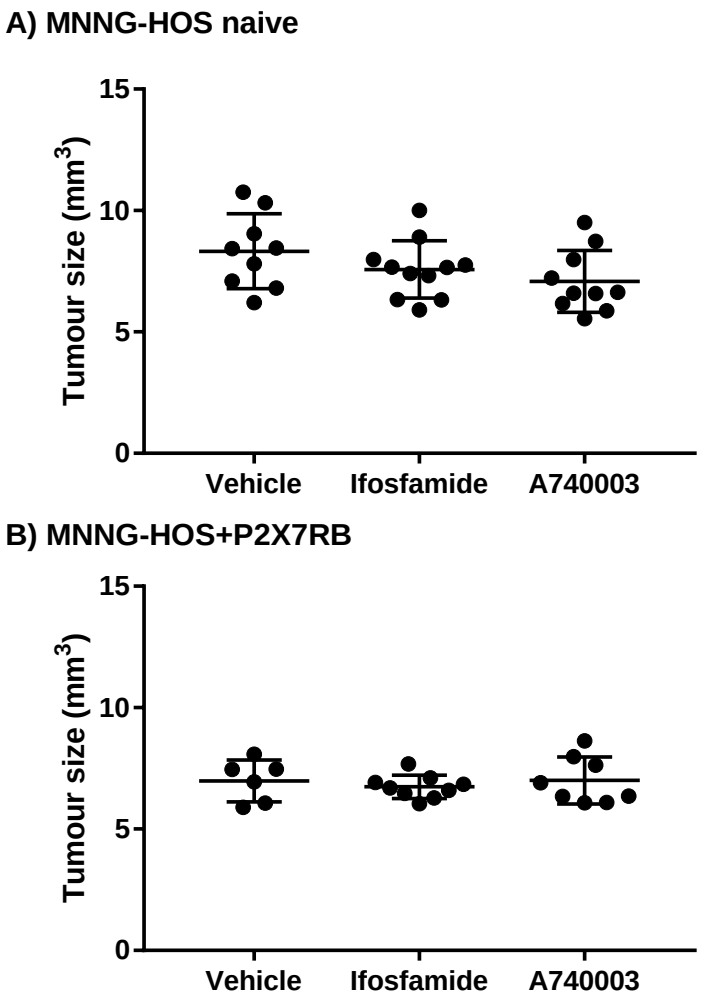

Figure 6.3: End-point primary tumour size in MNNG-HOS and MNNG-HOS+P2X7RB OS bearing mice receiving treatments measured using external callipers. For each treatment group 12 female BALB/c 7-9 week old mice were injected paratibially with 250,000 cells of either MNNG-HOS or MNNG-HOS+P2X7RB suspended in 20 µL PBS. Mice were then treated with vehicle, Ifosfamide or A740003 every 2 days for 3 weeks via IP injection. Tumour size was determined at the end of the experiment using external callipers to measure the tumour bearing limb only (left leg) **A)** MNNG-HOS tumour bearing mice treated with vehicle, Ifosfamide or A740003. **B)** MNNG-HOS+P2X7RB tumour bearing mice treated with vehicle, Ifosfamide or A740003 .The treatment groups were compared to vehicle using an unpaired T-test. N= 9-11 mice for MNNG-HOS groups and 6-9 mice for MNNG-HOS+P2X7RB groups.

6.4 The effect of P2X7RB expression and drug treatments on tumour size measured using the entire tissue size of the left leg from micro-CT scans

As no treatment group for both cell lines had a significant difference measured with external callipers (despite the presence of tumours) there were concerns with the accuracy of the measurements which can be influenced by observer subjectivity, tumour compressibility, skin thickness, subcutaneous fat level and differences in tumour shape (Kersemans *et al*., 2013) therefore micro-CT calliper measurements were also made. The micro-CT calliper measurements were made using Skyscan CTAn software by drawing across the width of the entire leg tissue including the tumour from the widest point in a straight line (see Chapter 2). Only tumour bearing left legs were analysed. To determine if this method would be able to detect a difference in tumour bearing legs.

Using this method, the tumour size of the legs injected with MNNG-HOS naïve OS cells had a significantly increased size compared to the scratched control leg sizes (vehicle 8.170 mm^3 ± 0.544 SEM vs 4.693 mm^3 ± 0.153 SEM scratched only leg, P= <0.0001, Figure 6.4 A). This was also the case for legs injected with MNNG-P2X7RB OS cells (vehicle 7.232 mm^3 ± 0.249 SEM, vs 4.693 mm^3 ± 0.153 SEM scratched only leg, P= <0.0001, Figure 6.4 B).

Similar to the external calliper measurement observations the MNNG-HOS+P2X7RB tumour bearing mice leg tissue was not statistically different to the size of the MNNG-HOS tumour bearing mice leg (MNNG-HOS+P2X7RB 7.232 mm^3 ± 0.249 vs 8.170 mm^3 ± 0.544 SEM vs SEM MNNG-HOS, P= 0.207, Figure 6.4 C). Next, there was no significant effect of either Ifosfamide or A740003 treatment on the average size of the MNNG-HOS bearing tumour size compared to vehicle (Ifosfamide 7.057 mm^3 ± 0.402 SEM vehicle 8.170 mm^3 ± 0.544 SEM vehicle, P=0.110 Figure 6.5 A) and (A740003 7.238 mm^3 ± 0.327 SEM vs 8.170 mm^3 ± 0.544 SEM vehicle, P= 0.151, Figure 6.5 A).

Finally, treatment of the MNNG-HOS+P2X7RB bearing mice with Ifosfamide significantly reduced tumour size compared to vehicle (Ifosfamide 6.339 mm^3 ± 0.276 SEM vs 7.232 mm^3 ± 0.249 SEM vehicle, P= 0.045 Figure 6.5 B) but not when treated with A740003 (A740003 6.621 mm^3 ± 0.371 SEM vs 7.232 mm^3 ± 0.249 SEM vehicle, P= 0.227, Figure 6.5 B).

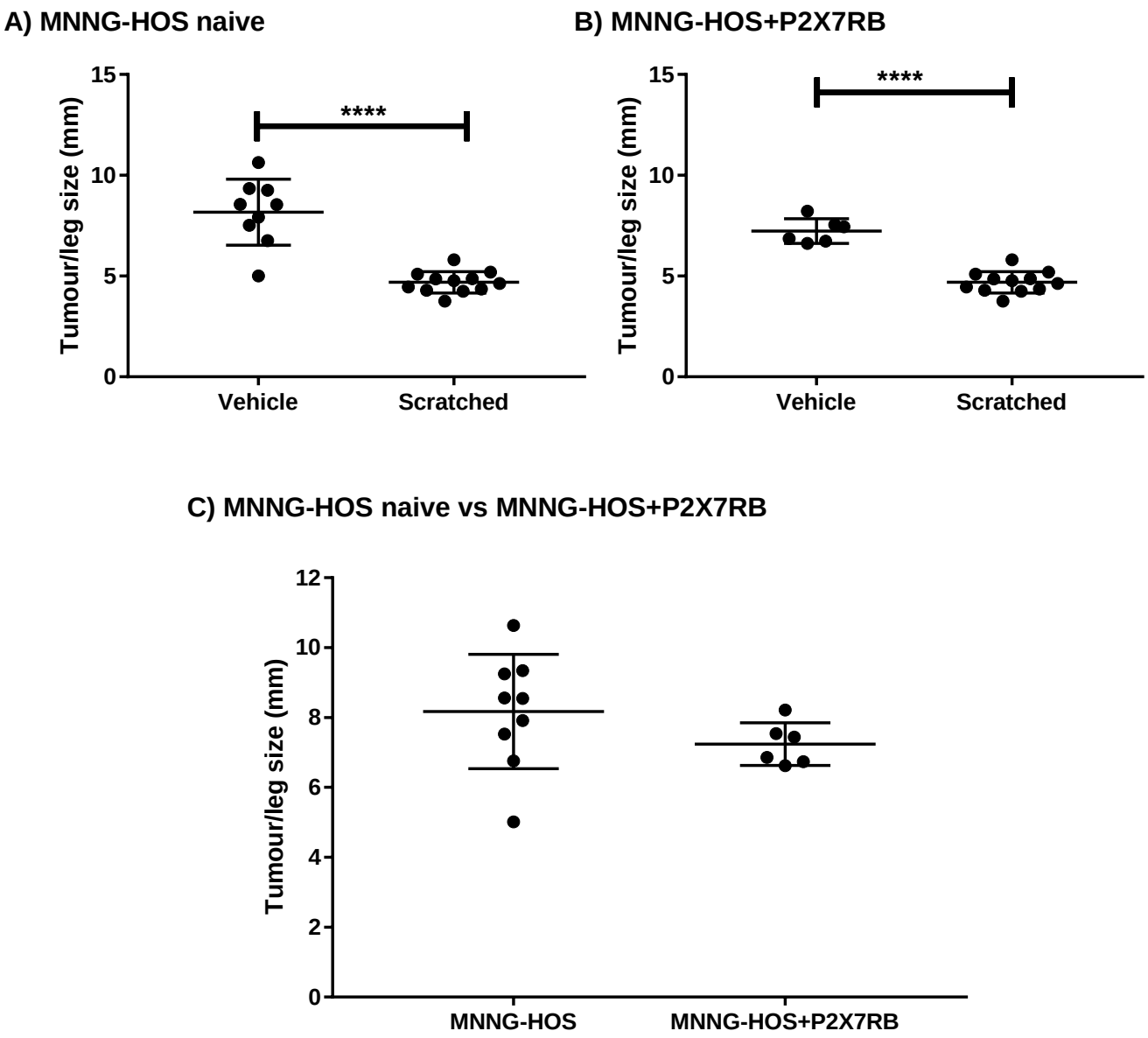

Figure 6.4: Measurement of tumour size using micro-CT scans comparing the MNNG-HOS and MNNG-HOS+P2X7RB performed on the BALB/c tumour bearing mice left legs. For each treatment group 12 female BALB/c 7-9 week old mice were injected paratibially with 250,000 cells of either MNNG-HOS or MNNG-HOS+P2X7RB suspended in 20 µL PBS. Mice were then treated with vehicle, Ifosfamide or A740003 every 2 days for 3 weeks via IP injection. Tumour size was determined using micro-CT images measuring the tumour bearing limb only and including the entire width of the leg. MNNG-HOS treated with vehicle were compared to MNNG-HOS+P2X7RB treated with vehicle using an unpaired T-test. N= 9 mice for MNNG-HOS and 6 mice for MNNG-HOS+P2X7RB.

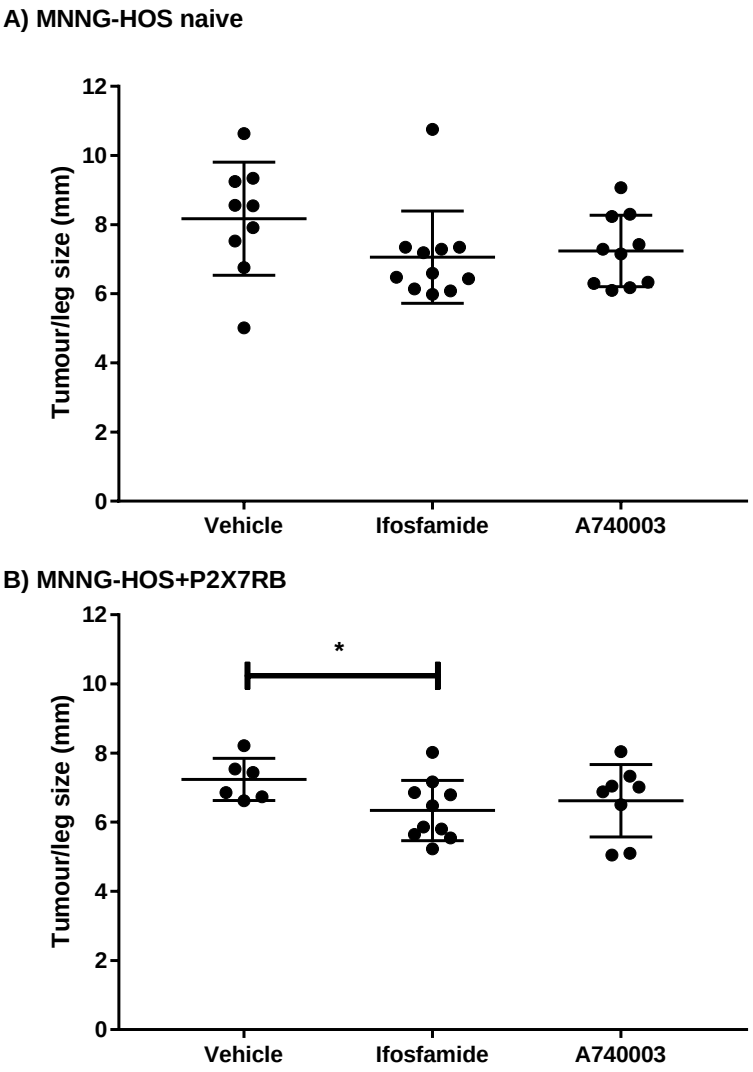

Figure 6.5: Measurement of tumour size in MNNG-HOS and MNNG-HOS+P2X7RB OS bearing mice receiving treatments using micro-CT scans performed on the BALB/c tumour bearing mice left legs. For each treatment group 12 female BALB/c 7-9 week old mice were injected paratibially with 250,000 cells of either MNNG-HOS or MNNG-HOS+P2X7RB suspended in 20 µL PBS. Mice were then treated with vehicle, Ifosfamide or A740003 every 2 days for 3 weeks via IP injection. Tumour size was determined using micro-CT images to measure the tumour bearing limb only measuring the entire width of the leg. Each group was compared to the vehicle and scratched control **A)** MNNG-HOS tumour bearing mice treated with vehicle, Ifosfamide or A740003 and the scratched only leg **B)** MNNG-HOS+P2X7RB tumour bearing mice treated with vehicle, Ifosfamide or A740003 and the scratched only leg. The groups were compared to using an unpaired T-test. N= 12 mice scratched only, 9-11 mice for MNNG-HOS and 6-10 mice for MNNG-HOS+P2X7RB.

6.5 The effect of P2X7RB expression and drug treatments on the histology of the OS tumours

Histological analysis is the gold standard for a diagnosis in almost all types of cancer including OS (Gurcan *et al.*, 2009), therefore, this was performed to assess the MNNG-HOS and MNNG-HOS+ P2X7RB OS tumours and surrounding bone architecture which can also have been affected. H&E staining was used to assess tumour characteristics such as the grade, phenotype, nuclei, morphological appearance, size and shape. At the end of the experiment mice legs were collected processed, embedded, sectioned and H&E stained. There was no overt difference in the histology of both the MNNG-HOS and MNNG-HOS+P2X7RB tumours, and no overt difference when Ifosfamide and A740003 were administered. Both cell lines formed tumours that were high-grade undifferentiated OS tumours with cells, with very little osteoid matrix and collagen production (Figure 6.6).

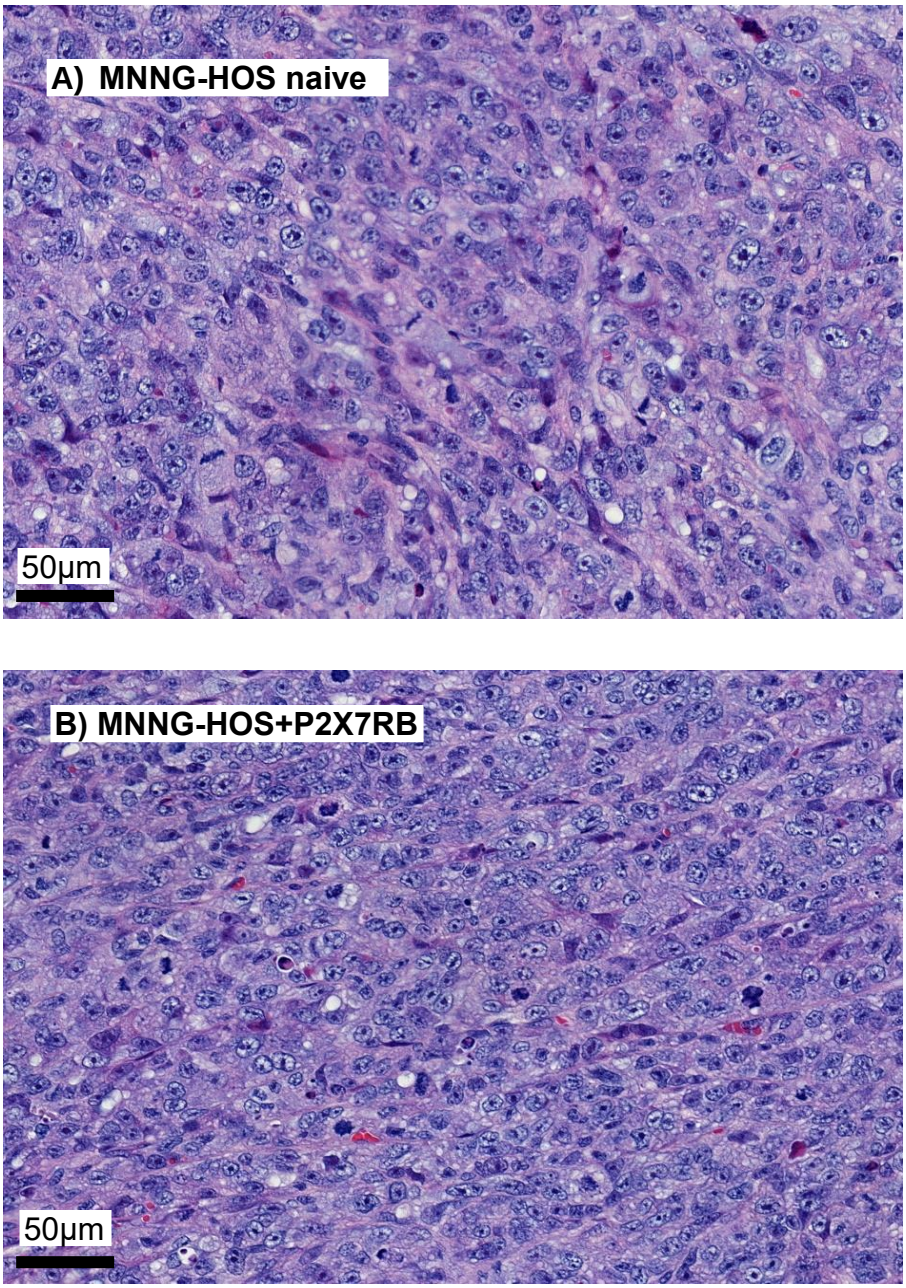

Figure 6.6: Representative H&E stained sections of mice legs injected with MNNG-HOS naïve and MNNG-HOS+P2X7RB OS cells. For each treatment group 12 female BALB/c 7-9 week old mice were injected paratibially with 250,000 cells of either MNNG-HOS or MNNG-HOS+P2X7RB suspended in 20 µL PBS. Mice were then treated with vehicle, Ifosfamide or A740003 every 2 days for 3 weeks via IP injection. The mice were then euthanised and dissected. The legs were collected processed, embedded into wax blocks and sections were taken to be H&E stained **A)** MNNG-HOS tumour **B)** MNNG-HOS+P2X7RB tumour.

6.6 The effect of P2X7RB expression and drug treatments on OS cell proliferation *in vivo* detected using Ki-76 IHC

To assess if any of the treatments had an effect on the primary tumour's rate of proliferation IHC was performed. Mice legs were collected, processed, embedded into wax blocks, sectioned and stained for Ki-67.

The amount of cells stained positive for Ki-67 in MNNG-HOS+P2X7RB tumours were not statistically different to the amount stained positive in MNNG-HOS tumours (MNNG-HOS+P2X7RB 37.98% ± 8.185 SEM vs 27.82% ± 2.288 SEM MNNG-HOS, P= 0.178, Figure 6.7).

The cells stained positive for Ki-67 in the tumours of mice injected with MNNG-HOS naïve OS cells showed no difference when treated with Ifosfamide (Figure 6.9) (Ifosfamide 30.26% ± 4.144 SEM vs 27.82% ± 2.288 SEM vehicle, P= 0.633, Figure 6.8 A) or when treated with A740003 (Figure 6.9) (A740003 26.49% ± 5.079 SEM vs 27.82% ± 2.288 SEM vehicle, P= 0.822, Figure 6.8 A).

The cells stained positive for Ki-67 in the tumours of mice injected with MNNG-HOS+P2X7RB OS cells showed no difference when treated with Ifosfamide (Figure 6.10) (Ifosfamide 25.88% ± 6.287 SEM, vs 37.98% ± 8.185 SEM vehicle, P= 0.259, Figure 6.8 B) or when treated with A740003 (Figure 6.10) (A740003 22.00% ± 7.654 SEM vs 37.98% ± 8.185 SEM vehicle, P= 0.183, Figure 6.8 B).

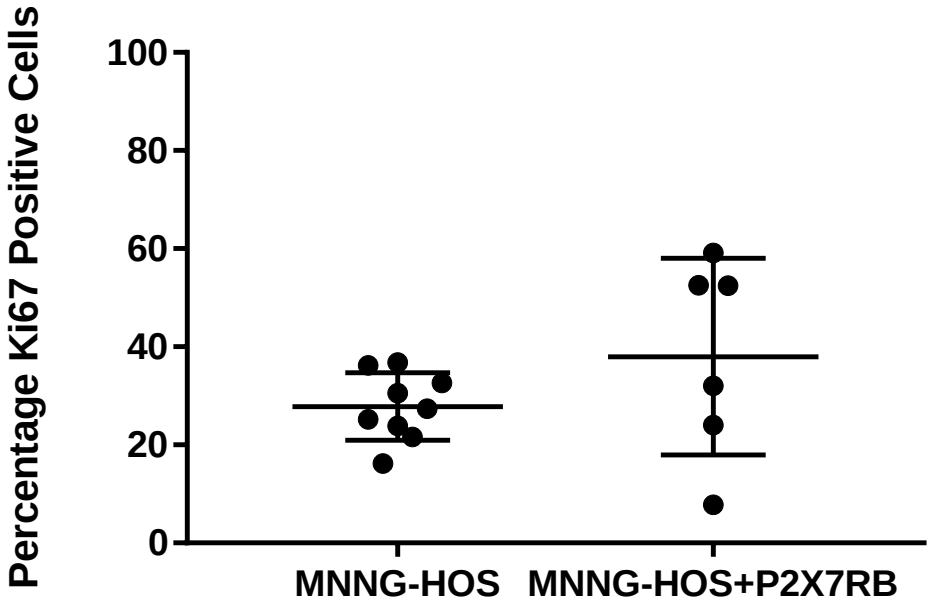

Figure 6.7: Measurement of proliferating cells in leg sections from MNNG-HOS and MNNG-HOS+P2X7RB OS bearing BALB/c mice using Ki-67 IHC. For each treatment group 12 female BALB/c 7-9 week old mice were injected paratibially with 250,000 cells of either MNNG-HOS or MNNG-HOS+P2X7RB suspended in 20 µL PBS. Mice were then treated with vehicle, Ifosfamide or A740003 every 2 days for 3 weeks via IP injection. The mice were then euthanised and dissected. The legs were collected processed, embedded into wax blocks and sections were taken to be stained for Ki-67. The sections were then analysed using QuPath. MNNG-HOS tumour bearing mice treated with vehicle were compared to MNNG-HOS+P2X7RB tumour bearing mice treated with vehicle. Results were compared using an unpaired T-Test. N= 9 mice for MNNG-HOS and 6 mice for MNNG-HOS+P2X7RB.

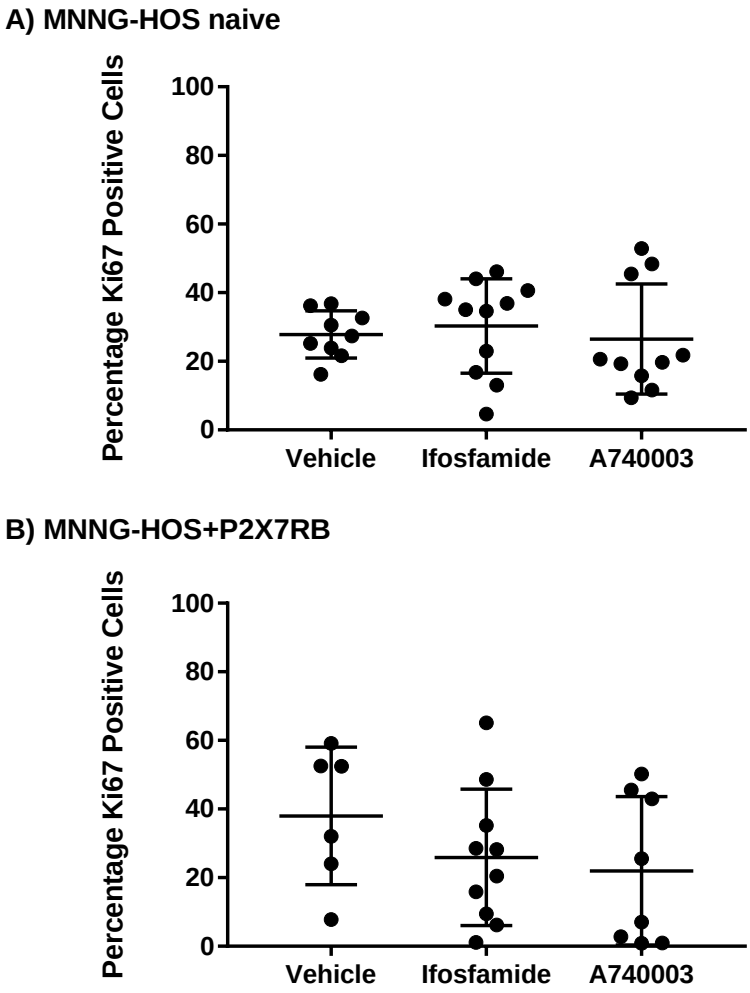

Figure 6.8: Measurement of proliferating cells in leg sections from MNNG-HOS and MNNG-HOS+P2X7RB OS bearing BALB/c mice receiving treatments using Ki-67 IHC. For each treatment group 12 female BALB/c 7-9 week old mice were injected paratibially with 250,000 cells of either MNNG-HOS or MNNG-HOS+P2X7RB suspended in 20 µL PBS. Mice were then treated with vehicle, Ifosfamide or A740003 every 2 days for 3 weeks via IP injection. The mice were then euthanised and dissected. The legs were collected, processed, embedded into wax blocks and sections were taken to be stained for Ki-67. The sections were then analysed using QuPath. Treatment groups Ifosfamide and A740004 were both compared to the vehicle control. **A)** MNNG-HOS tumour bearing mice. **B)** MNNG-HOS+P2X7RB tumour bearing mice. Groups were compared using an unpaired T-test. N= 9-11 mice for MNNG-HOS and 6-10 mice for MNNG-HOS+P2X7RB.

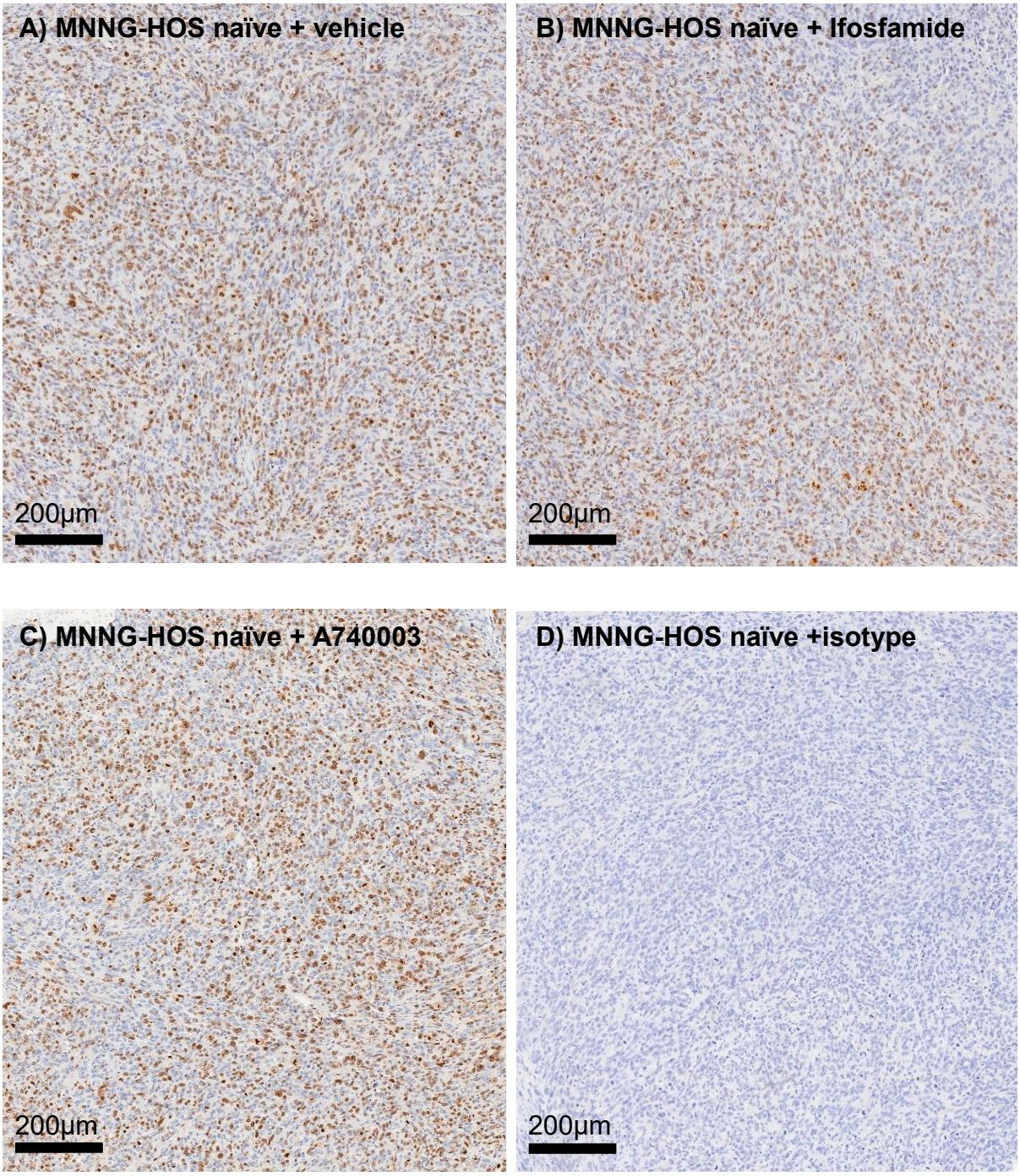

Figure 6.9: Representative images of Ki-67 stained MNNG-HOS tumour bearing left leg sections. For each treatment group 12 female BALB/c 7-9 week old mice were injected paratibially with 250,000 cells of either MNNG-HOS or MNNG-HOS+P2X7RB suspended in 20 µL PBS. Mice were then treated with vehicle, Ifosfamide or A740003 every 2 days for 3 weeks via IP injection. The mice were then euthanised and dissected. The legs were collected processed, embedded into wax blocks and sections were taken to be stained for Ki-67. **A)** Vehicle treatment **B)** Ifosfamide treatment **C)** A740003 treatment **D)** Isotype control.

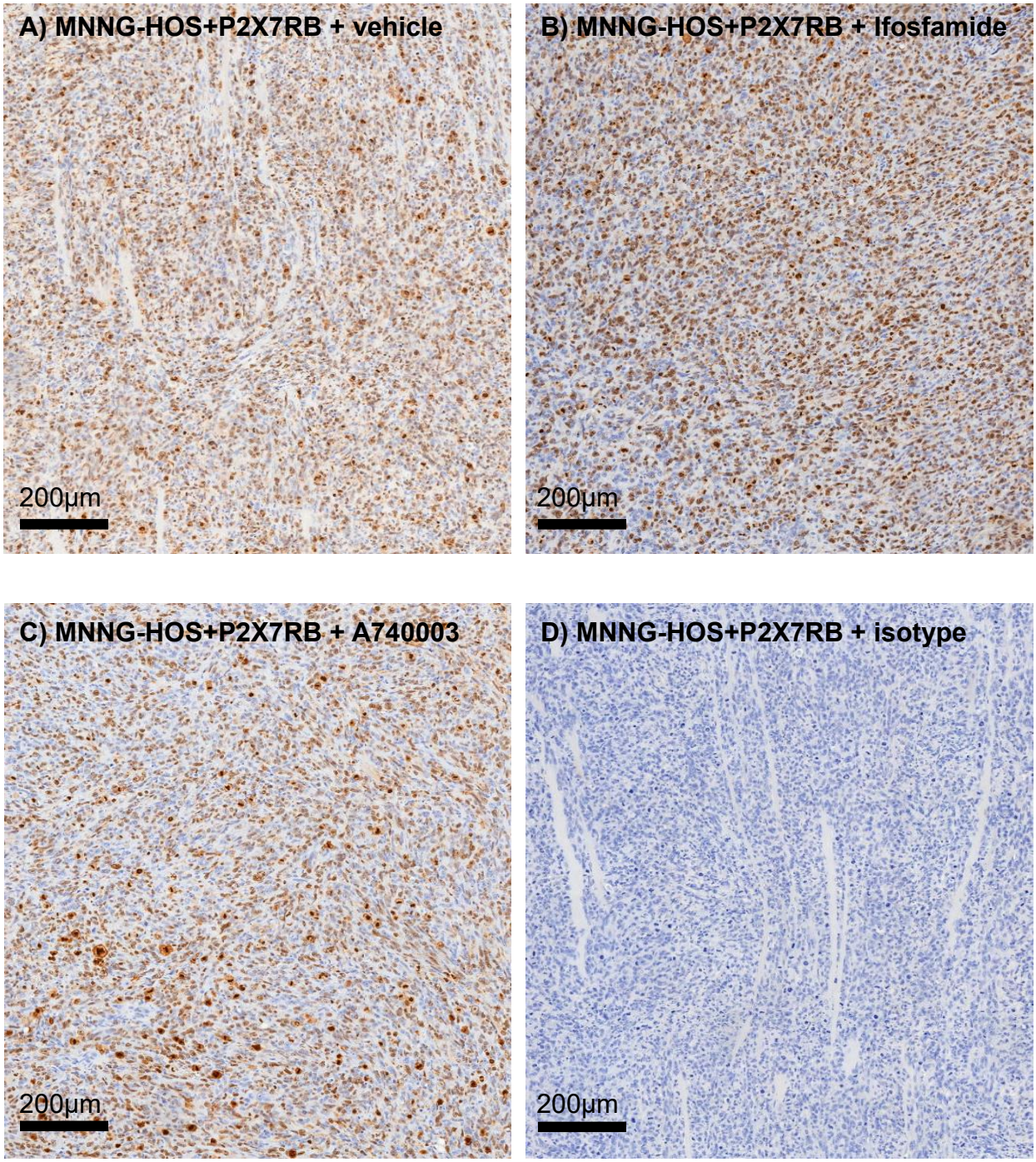

Figure 6.10: Representative image of Ki-67 stained MNNG-HOS+P2X7RB tumour bearing left leg sections. For each treatment group 12 female BALB/c 7-9 week old mice were injected paratibially with 250,000 cells of either MNNG-HOS or MNNG-HOS+P2X7RB suspended in 20 µL PBS. Mice were then treated with vehicle, Ifosfamide or A740003 every 2 days for 3 weeks via IP injection. The mice were then euthanised and dissected. The legs were collected processed, embedded into wax blocks and sections were taken to be stained for Ki-67. **A)** Vehicle treatment **B)** Ifosfamide treatment **C)** A740003 treatment **D)** Isotype control.

6.7 The effect of P2X7RB expression and drug treatments on cell apoptosis detected using annexin V IHC

Phosphatidylserine is externalised and expressed on early apoptotic cell membranes, annexin V binds to phosphatidylserine and therefore is routinely used to indicate cell death.

Mice legs were collected, processed, embedded into wax blocks, sectioned and IHC was performed to detect cells undergoing apoptosis to see if any of the treatments had an effect on the primary tumour or if MNNG-HOS and MNNG-HOS+P2X7RB tumour bearing mice had any difference.

The percentage of cells stained positive for annexin V in MNNG-HOS+P2X7RB tumour bearing mice was statistically higher than the amount stained positive in MNNG-HOS tumour bearing mice (MNNG-HOS+P2X7RB 97.15% ± 0.267 SEM vs 57.91% ± 12.620 SEM MNNG-HOS, P= 0.026, Figure 6.11).

The percentage of cells stained positive for annexin V in mice injected with MNNG-HOS OS cells showed a significant increase when treated with Ifosfamide (Figure 6.13) (Ifosfamide 98.25% ± 0.768 SEM vs 57.91% ± 12.620 SEM vehicle, P= 0.0008, Figure 6.12 A) there was no difference when treated with A740003 (Figure 6.13) (A740003 85.57% ± 4.954 SEM vs 57.91% ± 12.620 SEM, P= 0.112, Figure 6.12 A).

The percentage of cells stained positive for annexin V in mice injected with MNNG-HOS+P2X7RB OS cells showed no difference when treated with Ifosfamide (Figure 6.14) (Ifosfamide 96.75% ± 0.343 SEM vs 97.15% ± 0.267 SEM vehicle, P=0.5006, Figure 6.12 B) or when treated with A740003 (Figure 6.14) (A740003 97.10% ± 0.343 SEM vs 97.15% ± 0.267 SEM vehicle, P= 0.910, Figure 6.12 B).

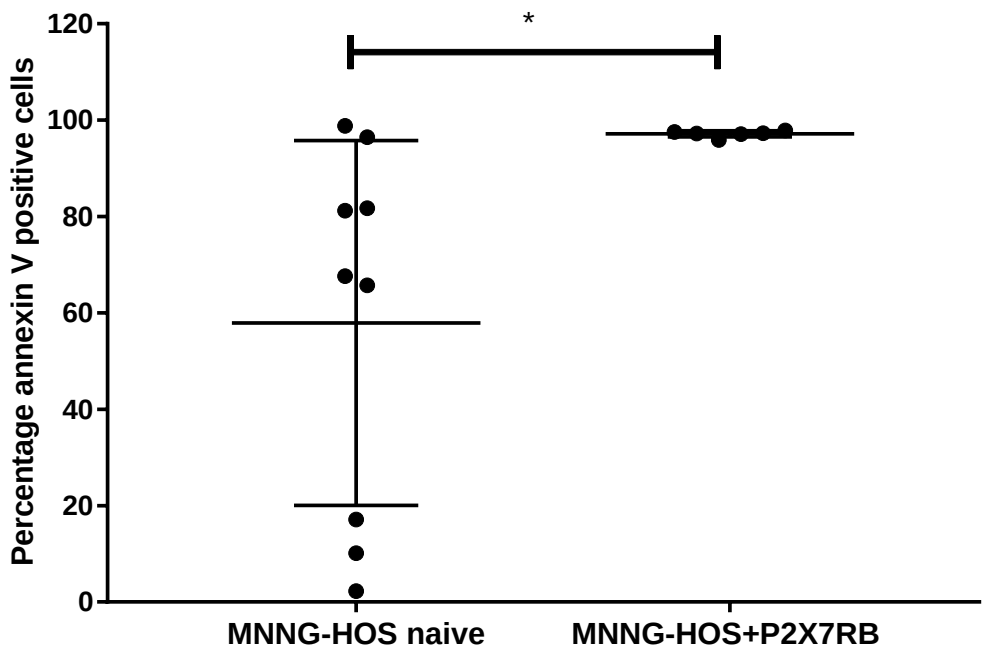

Figure 6.11: Measurement of cell death in leg sections from MNNG-HOS and MNNG-HOS+P2X7RB OS bearing BALB/c mice using annexin V IHC. For each treatment group 12 female BALB/c 7-9 week old mice were injected paratibially with 250,000 cells of either MNNG-HOS or MNNG-HOS+P2X7RB suspended in 20 µL PBS. Mice were then treated with vehicle, Ifosfamide or A740003 every 2 days for 3 weeks via IP injection. The mice were then euthanised and dissected. The legs were collected processed, embedded into wax blocks and sections were taken to be stained for annexin V. The sections were then analysed using QuPath**.** MNNG-HOS tumour bearing mice treated with vehicle were compared to MNNG-HOS+P2X7RB tumour bearing mice treated with vehicle. Results were compared using an unpaired T-Test. N= 9 mice for MNNG-HOS and 6 mice for MNNG-HOS+P2X7RB.

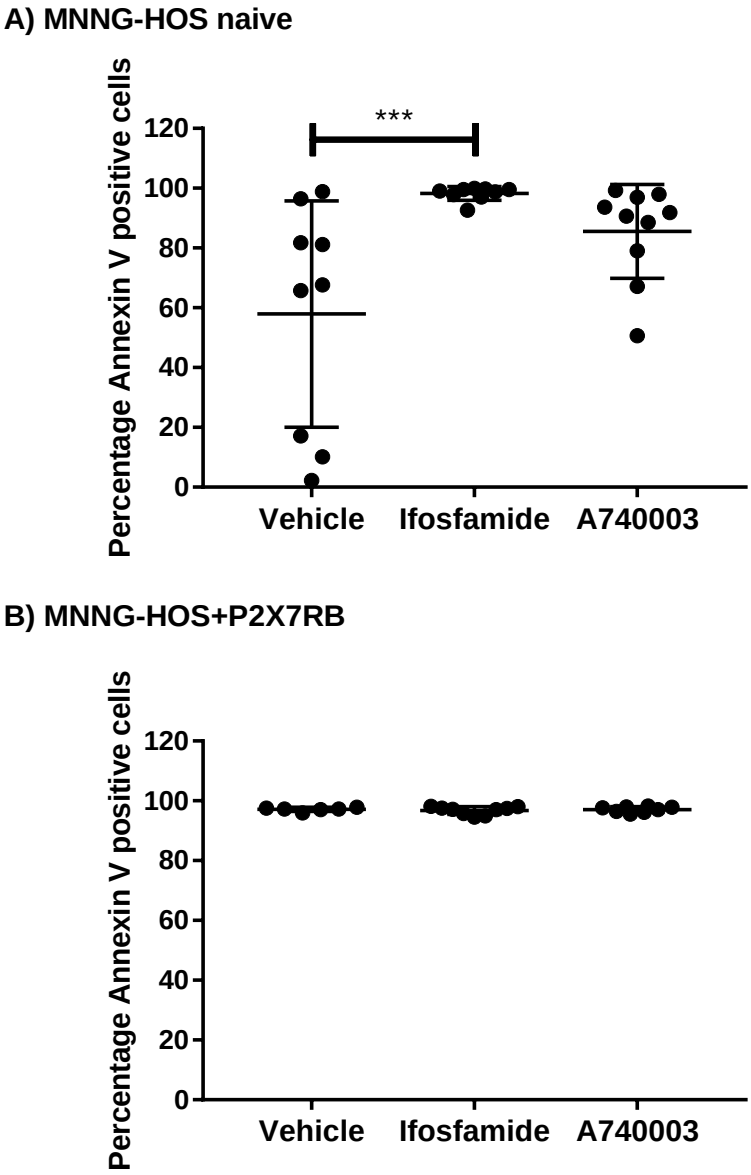

Figure 6.12: Measurement of cell death in leg sections from MNNG-HOS and MNNG-HOS+P2X7RB OS bearing BALB/c mice receiving treatments using annexin V IHC. For each treatment group 12 female BALB/c 7-9 week old mice were injected paratibially with 250,000 cells of either MNNG-HOS or MNNG-HOS+P2X7RB suspended in 20 µL PBS. Mice were then treated with vehicle, Ifosfamide or A740003 every 2 days for 3 weeks via IP injection. The mice were then euthanised and dissected. The legs were collected processed, embedded into wax blocks and sections were taken to be stained for annexin V. The sections were then analysed using QuPath. Treatment groups Ifosfamide and A740004 were both compared to the vehicle control. **A)** MNNG-HOS tumour bearing mice. **B)** MNNG-HOS+P2X7RB tumour bearing mice. Groups were compared using an unpaired T-test for parametric data and Mann-Whitney test for non-parametric data. N= 9-11 mice for MNNG-HOS and 6-10 mice for MNNG-HOS+P2X7RB

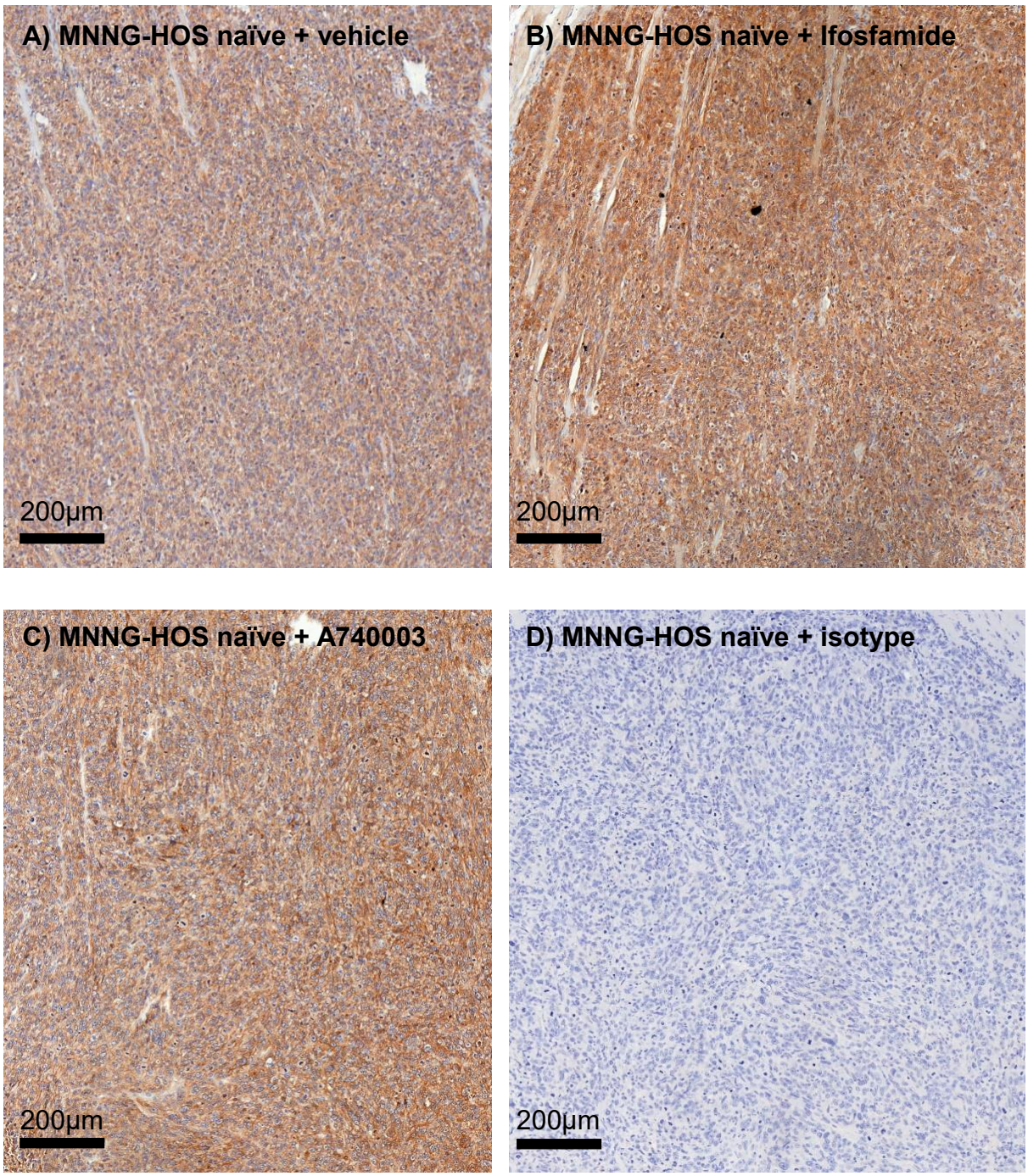

Figure 6.13: Representative image of annexin V stained MNNG-HOS tumour bearing left leg sections. For each treatment group 12 female BALB/c 7-9 week old mice were injected paratibially with 250,000 cells of either MNNG-HOS or MNNG-HOS+P2X7RB suspended in 20 µL PBS. Mice were then treated with vehicle, Ifosfamide or A740003 every 2 days for 3 weeks via IP injection. The mice were then euthanised and dissected. The legs were collected processed, embedded into wax blocks and sections were taken to be stained for annexin V. **A)** Vehicle treatment **B)** Ifosfamide treatment **C)** A740003 treatment **D)** Isotype control.

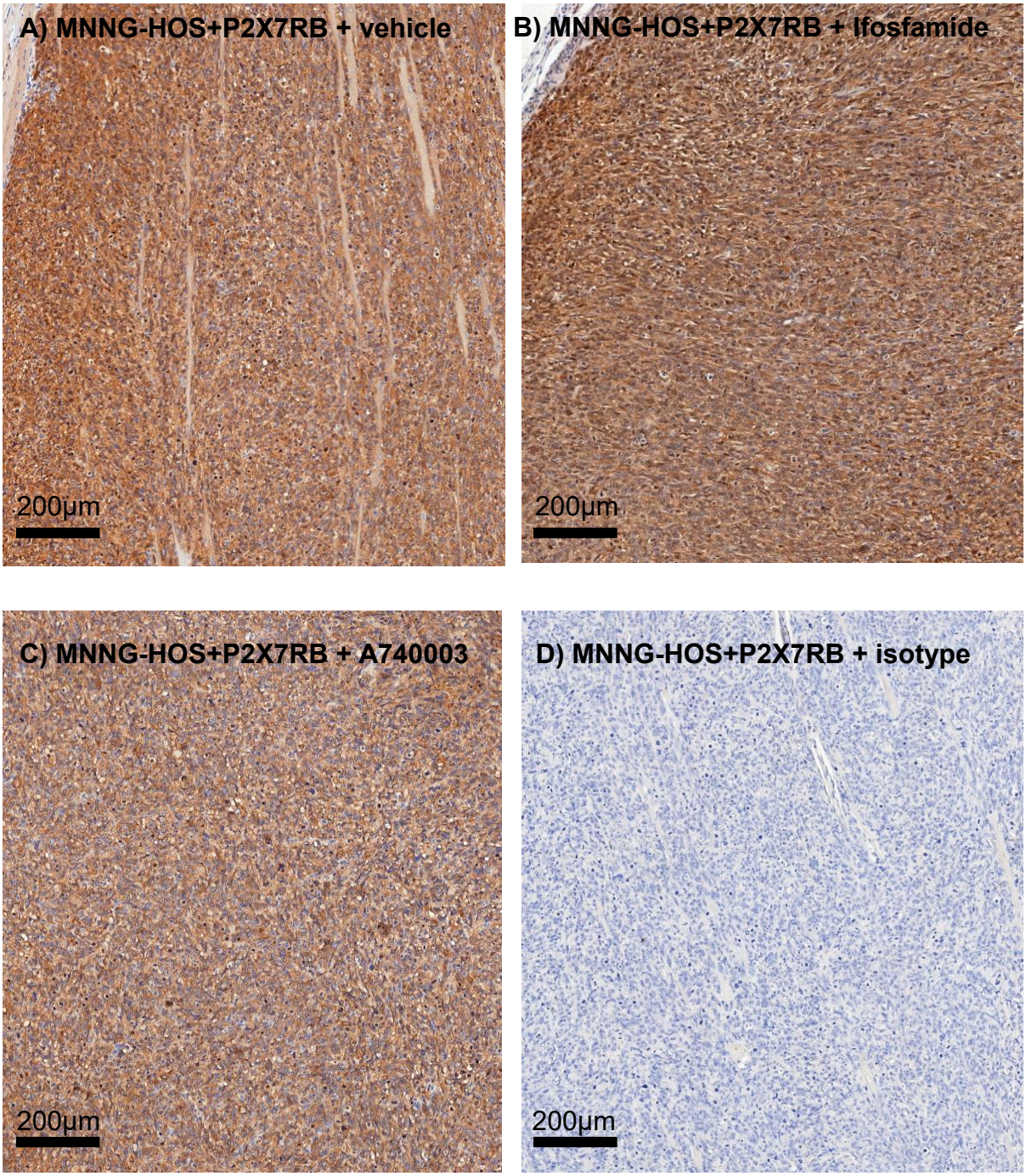

Figure 6.14: Representative image of annexin V stained MNNG-HOS+P2X7RB tumour bearing left leg. For each treatment group 12 female BALB/c 7-9 week old mice were injected paratibially with 250,000 cells of either MNNG-HOS or MNNG-HOS+P2X7RB suspended in 20 µL PBS. Mice were then treated with vehicle, Ifosfamide or A740003 every 2 days for 3 weeks via IP injection. The mice were then euthanised and dissected. The legs were collected processed, embedded into wax blocks and sections were taken to be stained for annexin V. **A)** Vehicle treatment **B)** Ifosfamide treatment **C)** A740003 treatment **D)** Isotype control.

6.8 The effect of P2X7RB expression and drug treatments on total bone volume determined by micro-CT analysis

Micro-CT analysis was performed according to chapter 2 to determine the total bone volume on the left tumour bearing leg and the contralateral right leg (non-tumour). However, since scratching the needle against the mouse bone when injecting the cell lines for the paratibial injection could potentially have an impact on the bone volume by affecting bone turnover, a group of 12 non-tumour bearing mice had the bone scratched and PBS injected as an external control (scratched only group).

On analysis, there was no significant effect of scratching the bone on the total bone volume compared to the contralateral right leg (Figure 6.16) (scratched leg 5.809 mm^3 ± 0.204 SEM vs 5.664 mm^3 ± 0.159 SEM contralateral leg, P= 0.158, Figure 6.15).

The total bone volume of the MNNG-HOS tumour bearing left leg was not statistically different to the contralateral non-tumour bearing right leg (MNNG-HOS tumour bearing 6.262 mm^3 ± 0.228 SEM vs 5.763 mm^3 ± 0.1401 SEM contralateral leg, P= 0.1030, Figure 6.17 A). The total bone volume of the MNNG-HOS+P2X7RB tumour bearing leg was statistically increased compared to the contralateral non-tumour bearing right leg (MNNG-HOS+P2X7RB tumour bearing 6.117 mm^3 ± 0.2358 SEM vs 5.507 mm^3 ± 0.1381 SEM contralateral leg, P= 0.0341, Figure 6.17 B). Despite the lack of a statistically significant effect on bone volume in the MNNG-HOS injected mice, when viewing the 3D reconstructions of the tumour-bearing limbs there was clearly an effect on the bone with a mixed phenotype of osteolysis and ectopic bone formation (Figure 6.19).

In order to compare total bone volume across the treatment groups each tumour bearing leg was normalised to its contralateral leg. The normalised total bone volume of the MNNG-HOS tumour bearing group wasn't statistically different to the scratched only group (MNNG-HOS vehicle 1.025 ± 0.01644 SEM vs 1.092 ± 0.048 SEM scratched leg, P= 0.1534, Figure 6.18 A). Ifosfamide had no significant effect on the total bone volume (Ifosfamide 1.061 ± 0.03162 SEM vs 1.092 ± 0.048 SEM vehicle, P= 0.5765, Figure 6.18 A) neither did A740003 (A740003 1.016 ± 0.03161 SEM vs 1.092 ± 0.048 SEM vehicle, P=0.1949, Figure 6.18 A).

The total bone volume of the MNNG-HOS+P2X7RB tumour bearing group was statistically higher than the scratched only group (MNNG-HOS+P2X7RB vehicle 1.118 ± 0.03238 SEM vs 1.025 ± 0.01644 SEM scratched leg, P= 0.0107, Figure 6.18 B). Ifosfamide had no effect on the increased bone volume (Ifosfamide 1.057 ± 0.01911 SEM vs 1.118 ± 0.03238 SEM vehicle, P= 1.069, Figure 6.18 B) but A740003 gave a statistically significant reduction in bone volume (A740003 0.9928 ± 0.03299 SEM vs 1.118 ± 0.03238 SEM vehicle, P= 0.0183, Figure 6.18 B).

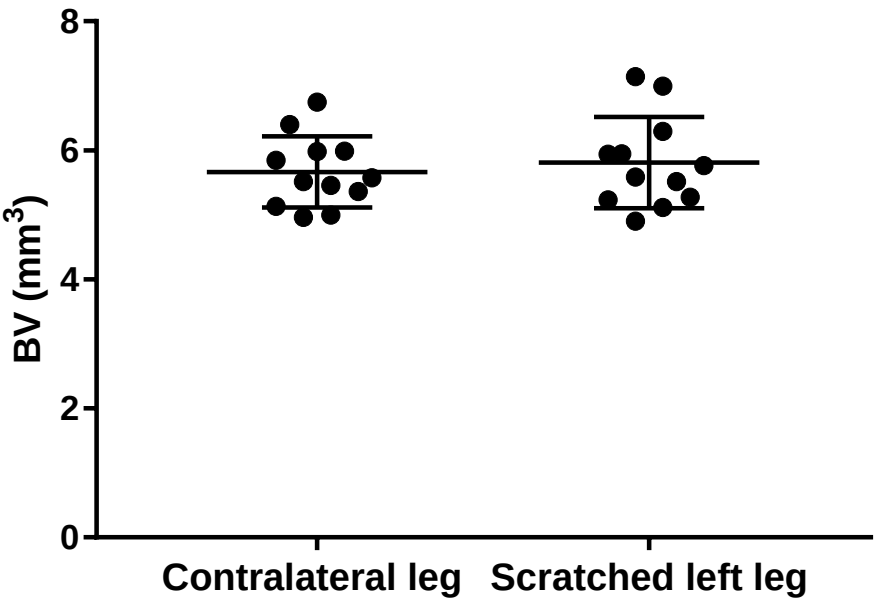

Figure 6.15: Micro-CT analysis to determine the total bone volume of the scratched control left legs and contralateral right legs. In order to demonstrate that a paratibial injection did not have an effect on the total bone volume 12 female 7-9 week old BALB/c mice were used as a scratched only control group where no tumour cells were injected but a paratibial injection was performed, after 3 weeks the mice were euthanised and both legs collected and micro-CT scanned. The total bone volume starting from the point at which the femur wasn't visible and the fibula meets the tibia was determined for each leg and compared to its contralateral leg. The groups were compared using a paired T-test. N= 12 mice per group.

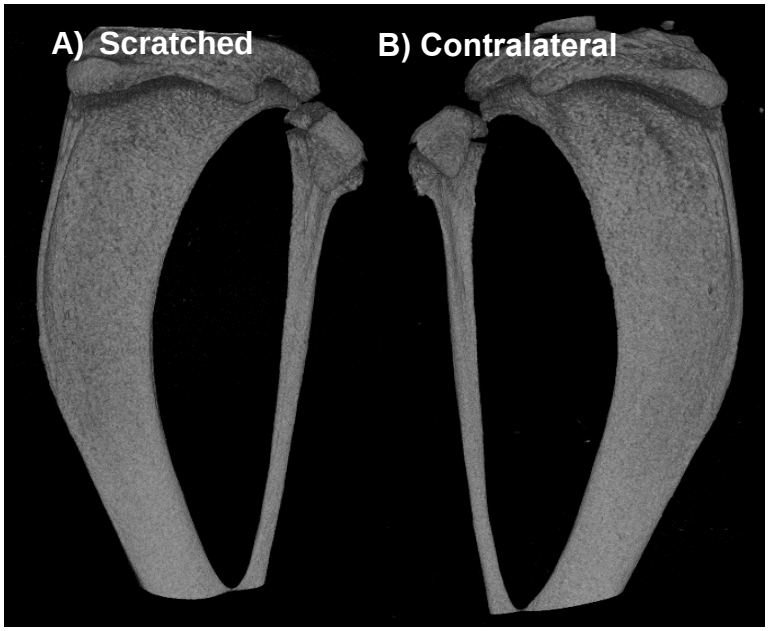

Figure 6.16: Representative 3D reconstructed models using micro-CT scanning to show the effects of a paratibial scratch on the total bone volume as a control group. In order to demonstrate that a paratibial injection did not have an effect on the total bone volume 12 female 7-9 week old BALB/c mice were used as a scratched only control group where no tumour cells were injected but a paratibial injection was performed, after 3 weeks the mice were euthanised and both legs were collected for micro-CT scanning and reconstruction. Representative micro-CT images of **A)** scratched left leg and **B)** contralateral leg.

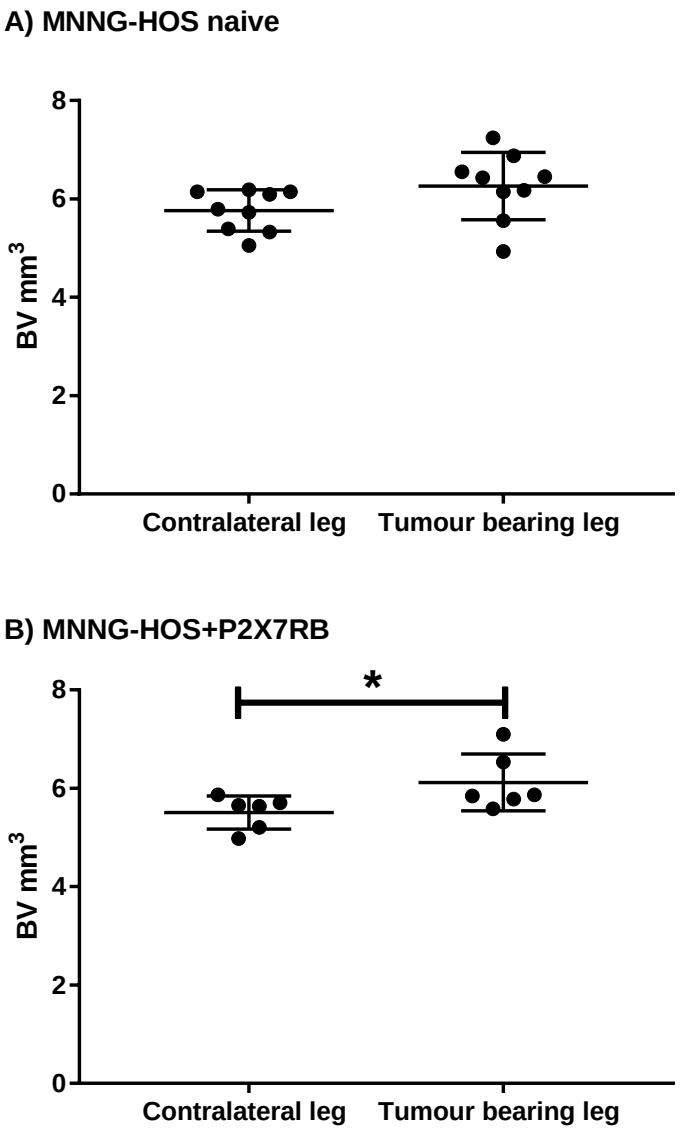

Figure 6.17: The total bone volume of the MNNG-HOS and MNNG-HOS+P2X7RB tumour bearing left legs compared to the contralateral right legs analysed by micro-CT. For each treatment group 12 female BALB/c 7-9 week old mice were injected paratibially with 250,000 cells of either MNNG-HOS or MNNG-HOS+P2X7RB suspended in 20 µL PBS. Mice were then treated with vehicle, Ifosfamide or A740003 every 2 days for 3 weeks via IP injection. The mice were euthanised and both legs collected and micro-CT scanned, the total bone volume starting from the point at which the femur wasn't visible and the fibula meets the tibia was determined for each leg and compared to its contralateral leg. **A)** MNNG-HOS left tumour bearing leg compared to its contralateral leg. **B)** MNNG-HOS+P2X7RB left tumour bearing leg compared to its contralateral right leg. Groups were compared using a paired T-test. N= 9 mice for MNNG-HOS and 6 mice for MNNG-HOS+P2X7RB.

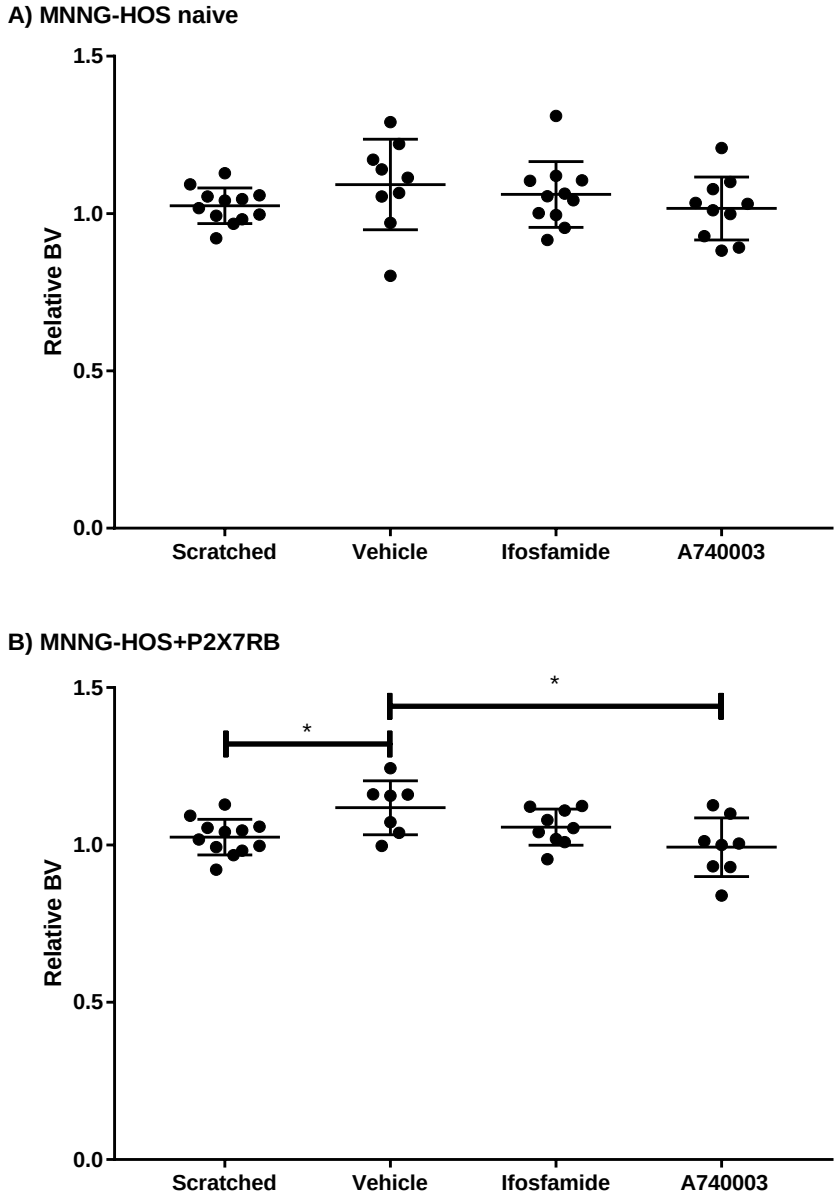

Figure 6.18: The total bone volume of the MNNG-HOS and MNNG-HOS+P2X7RB tumour bearing mice when receiving treatments analysed by micro-CT. For each treatment group 12 female BALB/c 7-9 week old mice were injected paratibially with 250,000 cells of either MNNG-HOS or MNNG-HOS+P2X7RB suspended in 20 µL PBS. Mice were then treated with vehicle, Ifosfamide or A740003 every 2 days for 3 weeks via IP injection. The mice were then euthanised and both legs were collected and micro-CT scanned, the total bone volume starting from the point at which the femur wasn't visible and the fibula meets the tibia was determined for each leg and normalised to its own contralateral leg. **A)** MNNG-HOS injected cells **B)** MNNG-HOS+P2X7RB injected cells. An unpaired T-test was used to compare groups. N= 12 mice for the scratched group, 9-11 mice for MNNG-HOS and 6-10 mice for MNNG-HOS+P2X7RB.

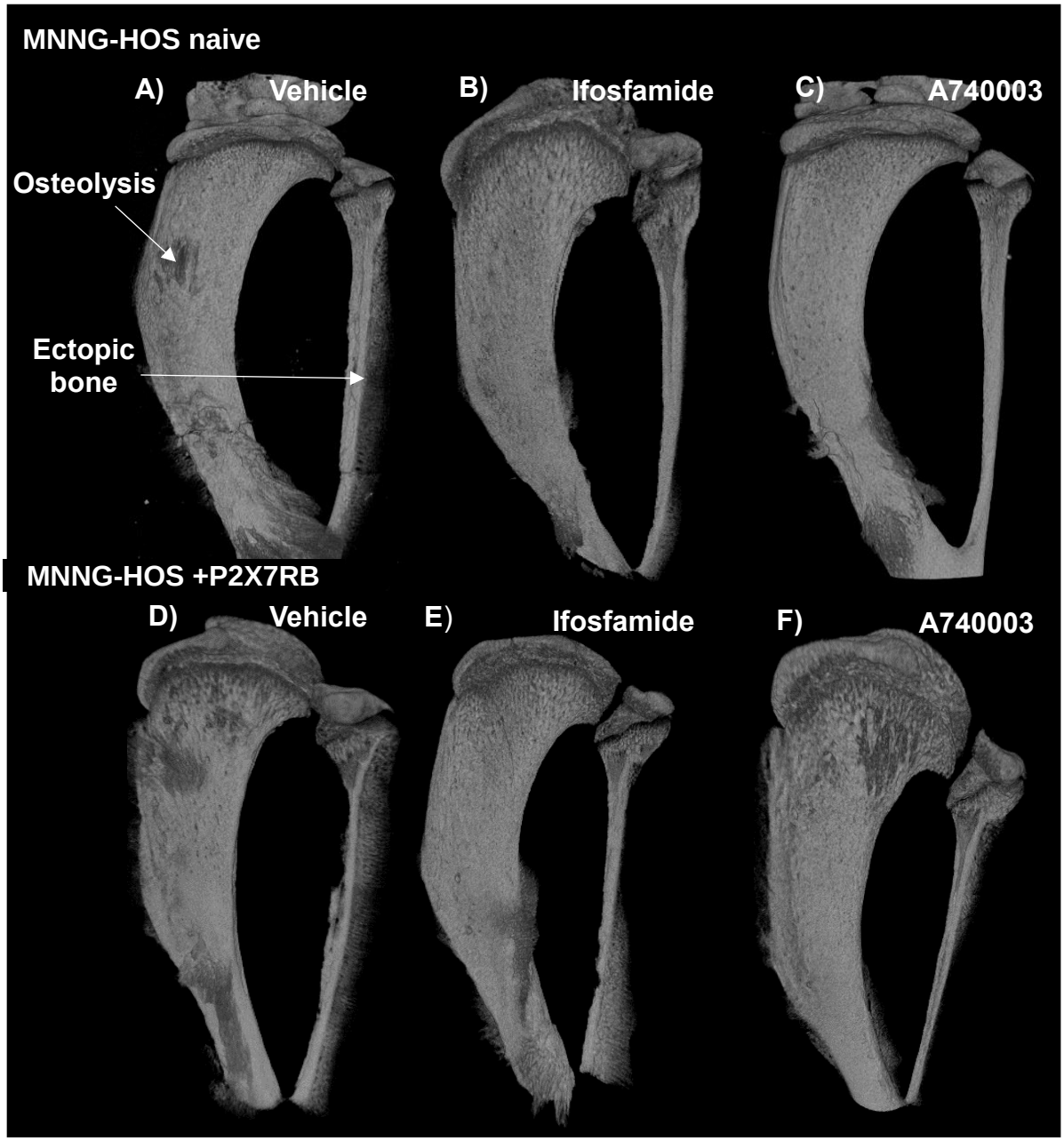

Figure 6.19: Representative 3D reconstructed models using micro-CT scanning show the effects of P2X7R expression on the total bone volume and the effects of treatment. For each treatment group 12 female BALB/c 7-9 week old mice were injected paratibially with 250,000 cells of either MNNG-HOS or MNNG-HOS+P2X7RB suspended in 20 µL PBS. Mice were then treated with vehicle, Ifosfamide or A740003 every 2 days for 3 weeks via IP injection. The mice were euthanised and both legs collected, micro-CT scanned and reconstructed. **A)** MNNG-HOS tumour bearing mice treated with vehicle **B)** Treated with Ifosfamide **C)** Treated with A740003 **D)** MNNG-HOS+P2X7RB tumour bearing mice treated with vehicle **E)** treated with Ifosfamide **F)** treated with A740003.

6.9 The effect of P2X7RB expression and drug treatment on osteoclasts at the tumour-bone interface

OS can cause, increased osteoclast activity which is associated with OS aggressiveness (Avnet *et al.*, 2008). The amount of osteoclasts in this study were detected using TRAP staining, the osteoclast perimeter was measured at the bone-tumour interface. This is where the tumour comes into contact with the bone as shown in chapter 2.

The percentage of the tumour-bone interface that is covered with osteoclasts in the vehicle treated MNNG-HOS+P2X7RB tumour bearing mice was not statistically different to the percentage of osteoclasts in the vehicle treated MNNG-HOS tumour bearing mice (MNNG-HOS+P2X7RB 48.3% ± 14.810 SEM vs 34.79% ± 5.440 SEM MNNG-HOS, P= 0.3337, Figure 6.20).

In the MNNG-HOS tumour bearing group treatment with Ifosfamide had no significant effect on the percentage of osteoclasts at the tumour-bone interface when compared to the vehicle group (Ifosfamide 39.66% ± 11.11 SEM vs 34.79% ± 5.44 SEM vehicle, P= 0.6769, Figure 6.21 A) treatment with A740003 also had no significant effect when compared to vehicle group (A740003 43.44% ± 8.133 SEM vs 34.79% ± 5.44 SEM vehicle, P= 0.3914, Figure 6.21 A). In the MNNG-HOS+P2X7RB tumour bearing group treatment with Ifosfamide had no significant effect on the percentage of osteoclasts at the tumour-bone interface when compared to the vehicle group (Ifosfamide 37.04% ± 5.378 SEM vs 48.3% ± 14.81 SEM vehicle, P= 0.4611, Figure 6.21 B) treatment with A740003 also had no significant effect when compared to vehicle group (A740003 32.59 ± 8.062 SEM vs 48.3% ± 14.81 SEM vehicle, P= 0.3384, Figure 6.21 B).

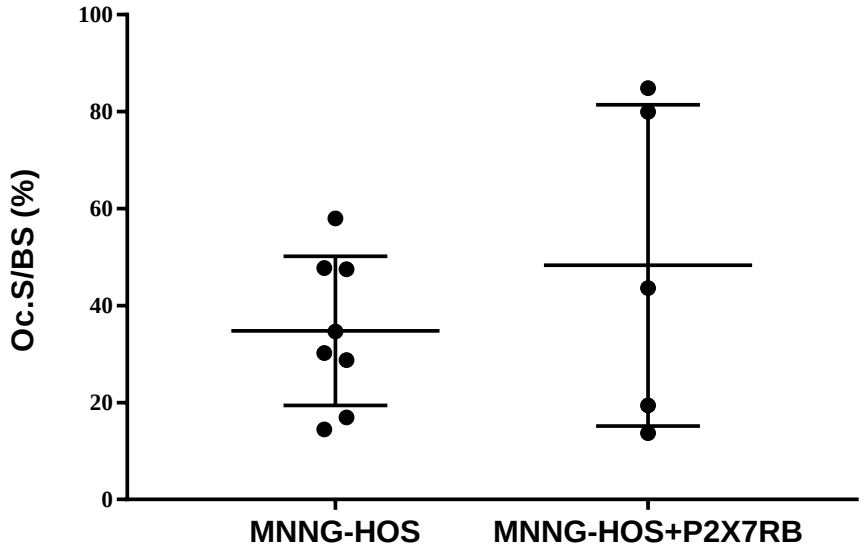

Figure 6.20: Osteoclast quantification at the bone tumour interface using TRAP staining comparing MNNG-HOS tumour bearing mice to MNNG-HOS+P2X7RB tumour bearing mice. For each treatment group 12 female BALB/c 7-9 week old mice were injected paratibially with 250,000 cells of either MNNG-HOS or MNNG-HOS+P2X7RB suspended in 20 µL PBS. Mice were then treated with vehicle, Ifosfamide or A740003 every 2 days for 3 weeks via IP injection. The mice were then euthanised and dissected. The legs were collected processed, embedded into wax blocks and sections were taken to be stained for TRAP. The osteoclasts at the tumour-bone interface were quantified and expressed as osteoclast percentage along the bone tumour surface. Groups were analysed using an unpaired T-test. N= 8 mice for MNNG-HOS and 5 mice for MNNG-HOS+P2X7RB.

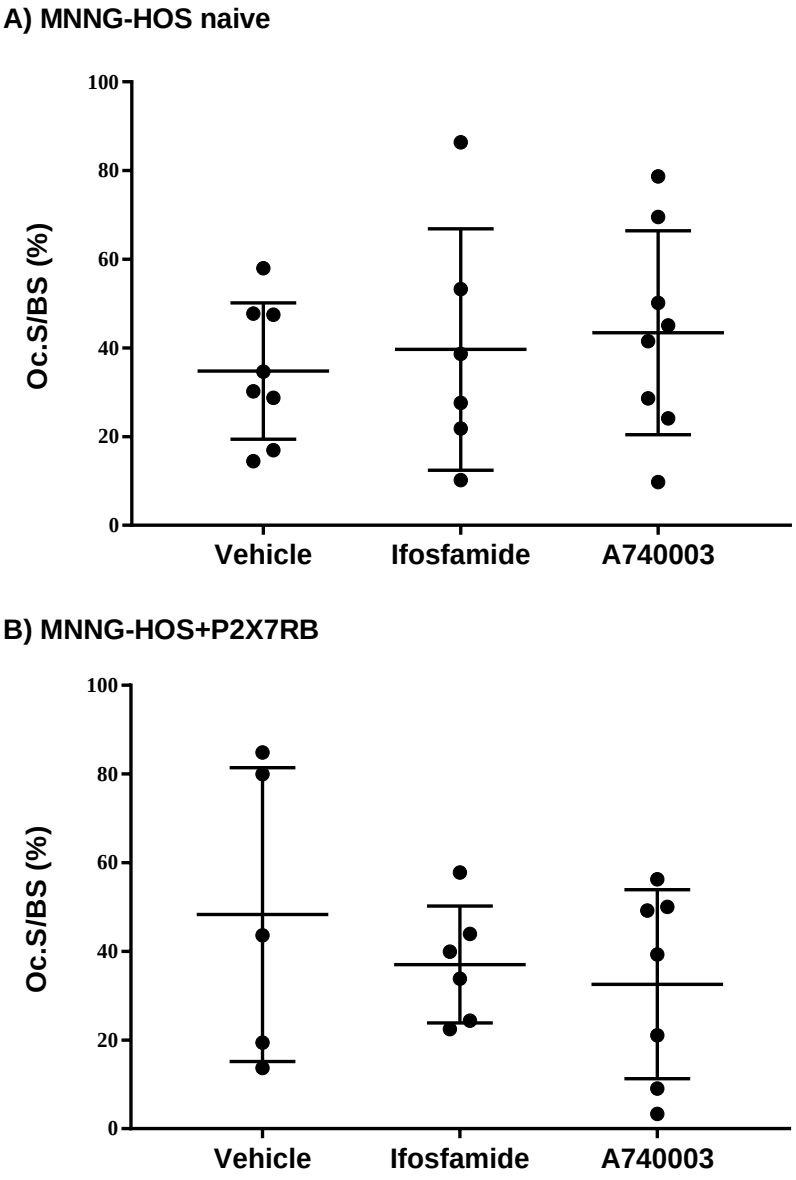

Figure 6.21: Osteoclast quantification at the bone tumour interface using TRAP staining comparing MNNG-HOS and MNNG-HOS+P2X7RB tumour bearing mice when receiving treatments. For each treatment group 12 female BALB/c 7-9 week old mice were injected paratibially with 250,000 cells of either MNNG-HOS or MNNG-HOS+P2X7RB suspended in 20 µL PBS. Mice were then treated with vehicle, Ifosfamide or A740003 every 2 days for 3 weeks via IP injection. The mice were then euthanised, legs collected processed, embedded into wax blocks and sections were stained for TRAP**.** Osteoclast perimeter was measured at the bone-tumour interface. **A)** MNNG-HOS tumour bearing mice treated with vehicle, Ifosfamide and A740003 **B)** MNNG-HOS+P2X7RB tumour bearing mice treated with vehicle, Ifosfamide and A740003. Groups were analysed using an unpaired T-test. N= 6-8 mice for MNNG-HOS and 5-7 mice for MNNG-HOS+P2X7RB.

MNNG-HOS naïve

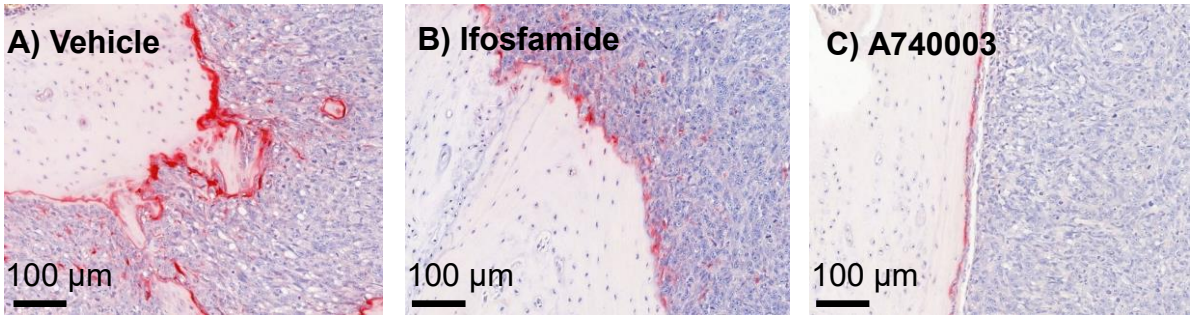

MNNG-HOS+P2X7RB

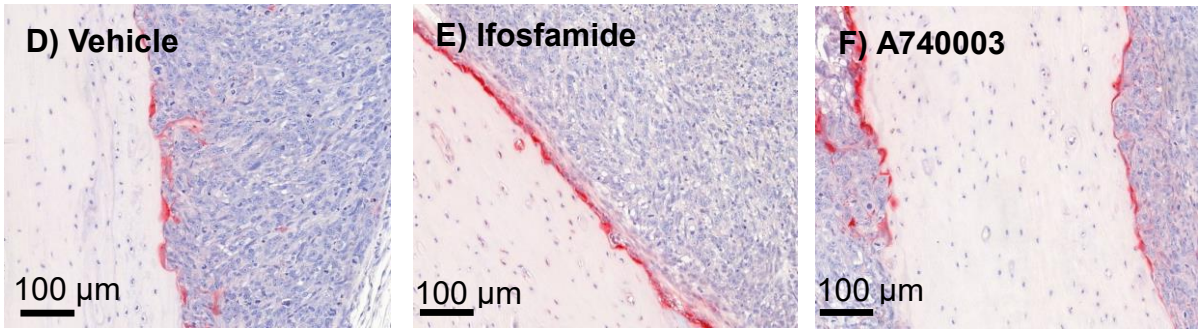

Figure 6.22: Representative images of TRAP stained MNNG-HOS and MNNG-HOS+P2X7RB tumour bearing left leg sections. For each treatment group 12 female BALB/c 7-9 week old mice were injected paratibially with 250,000 cells of either MNNG-HOS or MNNG-HOS+P2X7RB suspended in 20 µL PBS. Mice were then treated with vehicle, Ifosfamide or A740003 every 2 days for 3 weeks via IP injection. The mice were then euthanised and dissected. The legs were collected processed, embedded into wax blocks and sections were taken to be TRAP stained. Osteoclast perimeter was measured at the bone-tumour interface in MNNG-HOS bearing mice treated with **A)** MNNG-HOS vehicle **B)** MNNG-HOS Ifosfamide **C)** MNNG-HOS A740003 **D)** MNNG-HOS+P2X7RB vehicle **E)** MNNG-HOS+P2X7RB Ifosfamide and **F)** MNNG-HOS+P2X7RB A740003.

6.10 The effect of P2X7RB expression and drug treatment on OS pulmonary metastasis

The most common site for OS metastasis is the lungs accounting for 80% of all metastatic cases. Patients present with metastasis at initial diagnosis approximately 20% of the time (Zhu *et al.,* 2013, Lindsey *et al.,* 2017, Posthumadeboer *et al.,* 2011) and these patients have the worst prognosis (Lindsey *et al.*, 2017). Therefore, to investigate if the P2X7RB plays a role in OS metastasis the lungs were collected from each mouse then processed and embedded in wax cassettes. To section the lungs 6 µm sections were cut every 100 µm to cover the entire lung and stained using H&E. All slides were examined under a light microscope for any incidence of OS metastasis scored by two independent researchers. In all MNNG-HOS tumour bearing mice out of 20 with primary OS tumours there was no incidence of lung metastasis.

In mice bearing MNNG-HOS+P2X7RB tumours, out of 24 mice with primary OS tumours 5 had incidence of metastasis which was determined by two independent researchers: 1 in the vehicle treatment group, 2 each in the Ifosfamide and A740003 groups (Figure 6.23).

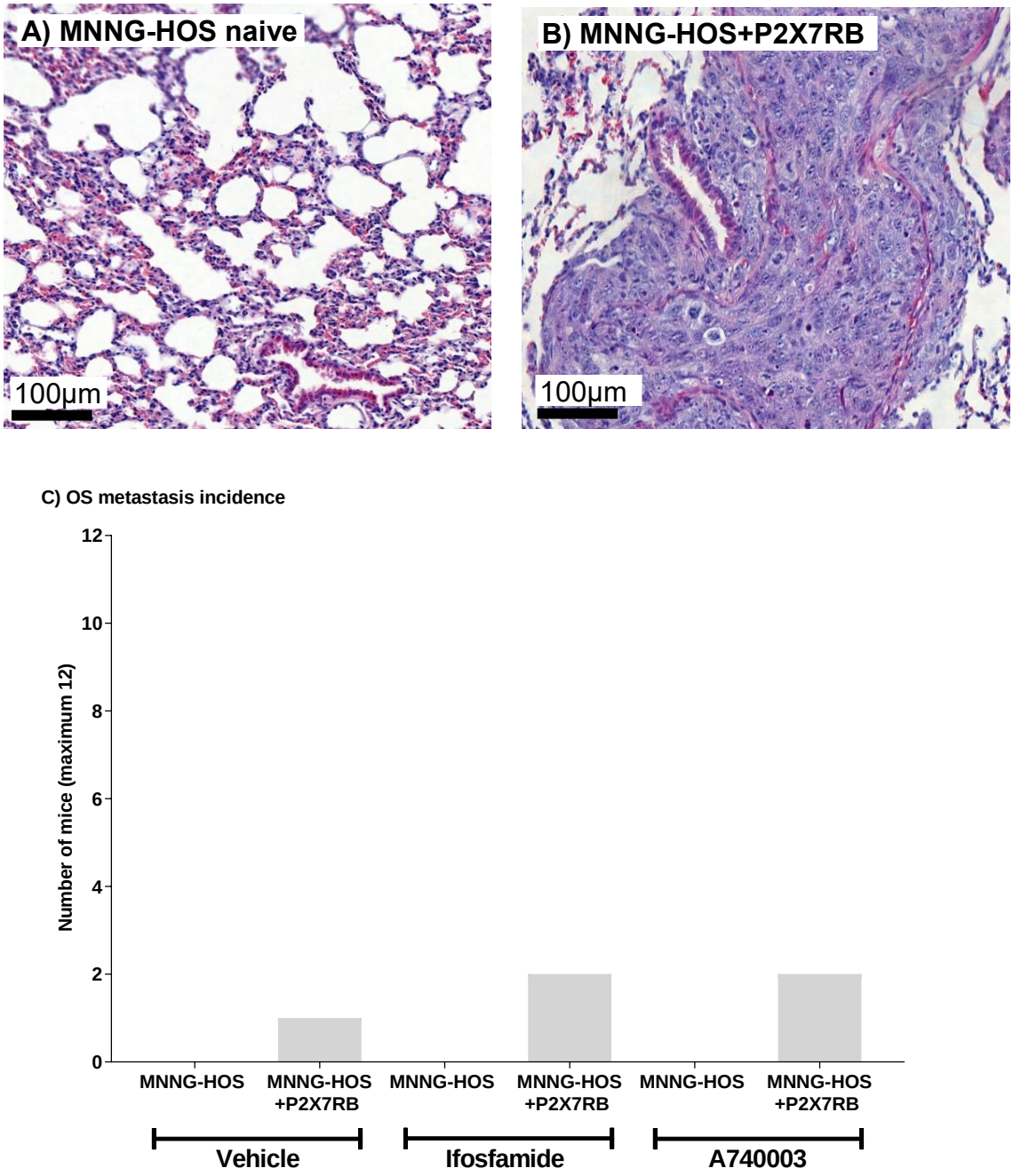

Figure 6.23: Detection of lung metastasis in MNNG-HOS and MNNG-HOS+P2X7RB tumour bearing mice including representative histological images. For each treatment group 12 female BALB/c 7-9 week old mice were injected paratibially with 250,000 cells of either MNNG-HOS or MNNG-HOS+P2X7RB suspended in 20 µL PBS. Mice were then treated with vehicle, Ifosfamide or A740003 every 2 days for 3 weeks via IP injection. The mice were then euthanised and dissected. The lungs were collected processed, embedded into wax blocks and sections were taken to be H&E to enable the detection of any OS metastasis. N= 9-11 mice for MNNG-HOS and 6-10 mice for MNNG-HOS+P2X7RB **A)** Lungs from MNNG-HOS naïve tumour bearing mice. **B)** Lungs from MNNG-HOS+P2X7RB tumour bearing mice **C)** OS metastasis incidence across each group.

6.11 Discussion

The aim of this chapter was to explore the role of P2X7RB in OS *in vivo*. Therefore, MNNG-HOS OS cells and MNNG-HOS+P2X7RB OS cells were injected paratibially into BALB/c nude mice. The mice were then treated with either vehicle, Ifosfamide a standard chemotherapy for OS patients (Fan *et al.,* 2015) or A740003 which is a competitive P2X7R antagonist (Honore *et al*., 2006).

The results from this chapter demonstrate that the MNNG-HOS model did not form tumours in all instances when injected paratibially. Out of 72 mice 54 formed a palpable tumour that could have their properties further assessed. This could be due to injecting only 250,000 cells, as the injection of 500,000 cells showed a take rate of 100% (Chapter 5). Some studies have used as much as 1-1.5 million MNNG-HOS OS cells *in vivo*, Chalopin *et al*., 2018). However, a lower seeding rate was chosen in order to extend the time that the cells were in the mouse to enable a suitable treatment regime to be administered and better facilitate lung metastasis.

Determination of tumour size in xenograft mice is used to evaluate tumour progression and response to treatment, the current standard technique is external calliper measurements (Kersemans *et al.,* 2013, Jensen *et al.,* 2008, Ayers *et al*., 2010). Therefore, in this study the tumour size was examined using this method at the end of the experiment. The results showed that there wasn't a difference between any of the treatment groups or between cell lines. This included the Ifosfamide chemotherapy positive control which has been previously shown to cause a decrease in tumour growth in MNNG-HOS tumour bearing mice (Chalopin *et al*., 2018). Although calliper measurements have the advantage of been non-invasive, cheap and quick (Kersemans *et al.,* 2013) they have been shown to be susceptible to inaccuracy. This can be due to observer subjectivity, tumour compressibility, skin thickness, subcutaneous fat level and differences in tumour shape (Kersemans *et al*., 2013) with one study finding there could be up to 25% inter operator variability between measurements (Delgado San Martin *et al.,* 2015).

With regards to osteosarcoma, the developing tumour disrupts local architecture resulting in the loss of an anatomical landmark producing unreliable calliper placement and further inaccuracy (Cole *et al*., 2011). In order to avoid this two studies have

determined tumour growth by drawing, using Image-J, around the entire tissue volume of the leg defined by soft tissue silhouettes show on radiographs, (Cole *et al.,* 2011, Cole *et al.,* 2014). This proved to be more precise than external calliper measurements (Cole *et al.,* 2011, Cole *et al.,* 2014). Studies have further demonstrated that micro-CT scanning can be used to determine tumour size for other cancers in mice, such as lung cancer (Haines *et al*., 2009) and gliomas (Crespigny *et al.,* 2009), additionally micro-CT has been used to image tumour dimensions in patient breast lumpectomy specimens (Tang *et al.,* 2016). As the external calliper measurements demonstrated no effect on tumour size even with Ifosfamide treatment, in an attempt to improve this, mice legs were assessed using micro-CT scans. Due to not been able to distinguish between normal tissue and tumour, the entire leg tissue was measured at the widest part. The calliper measurements performed using micro-CT showed an increased leg tissue size in all groups compared to the scratched control legs, demonstrating that this was a valid way to measure the tumour. It also demonstrated that the positive control Ifosfamide chemotherapy drug had an effect on the leg tissue size of tumour bearing MNNG-HOS+P2X7RB mice. Consistent with the external calliper measurements, there was no difference between MNNG-HOS tumour size and MNNG-HOS+P2X7RB tumour size using micro-CT measurements. Whilst this is inconsistent with the results of the *in vitro* data (Chapter 5), it is consistent with another similar study using a xenograft model of pancreatic ductal adenocarcinoma. In that study P2X7R antagonist administration *in vivo* was shown not to affect tumour size when measured with external callipers, although a difference in tumour size was determined using bioluminescent imaging (Giannuzzo *et al.*, 2016).

After these measurements demonstrated no effect with the treatments on tumour size, other lines of investigation were performed that assessed the primary tumour. This included histology which showed that the tumours in all groups correlate to other *in vivo* studies which have shown MNNG-HOS OS cells have a high grade (Mohseny *et al*., 2011), undifferentiated (Avril *et al*., 2016) phenotype. They also produced osteolytic lesions and ectopic bone, all of these characteristics are often found in human OS cases (Yuan *et al*. 2010, Casali *et al*., 2014, Mohseny *et al*., 2011). Ki-67 IHC staining was performed on the primary tumour; due to its presence during active phases of the cell cycle (G1, S, G2 and mitosis) and its absence from quiescent cells (G0). Ki-67 is considered a marker of cell proliferation (Mussig *et al.,* 2012) and it has

been used as a biomarker for identification of cancer subtypes and their prognosis. It was shown that in both breast cancer and non-Hodgkin's lymphoma patients that with a higher Ki-67 value there was a worse overall survival rate (Soliman & Yussif, 2016, Kim *et al*., 2007), additionally Ki-67 staining correlated with increased incidence of metastasis in breast cancer (Soliman & Yussif, 2016) and was able to distinguish between high grade and low grade lung cancer (Soomro *et al,* 1998).

In a study that analysed Ki-67 expression in 205 samples from various bone tumours; a higher Ki-67 value compared to high grade and malignant tumours, whereas a lower Ki-67 score compared to benign and low grade tumours. A further correlation was demonstrated in both chondrosarcoma and osteosarcoma histological grades. After a 24 month follow up a worse prognosis was associated with higher Ki-67 scores. (Scotlandi *et al.,* 1995). This has been supported in an independent study of 56 osteosarcoma cases, which showed that the expression of Ki-67 correlated with reduced disease-free rates and reduced overall survival (Mardanpour *et al.,* 2016). In the current study Ki-67 was used as a proliferation biomarker to assess the effect of P2X7RB expression and the effect of treatment with Ifosfamide and A740003. The results again demonstrated no statistically significant difference between the treatment groups. However, there was a slight trend towards a reduction in the treated MNNG-HOS+P2X7RB mice for both drugs suggesting that the Ifosfamide positive control may have reduced proliferation as expected and P2X7RB antagonism could also potentially reduce OS cell proliferation. There was also no statistical difference in Ki-67 expression when comparing MNNG-HOS to MNNG-HOS+P2X7RB tumours. However, there was again a slight trend towards MNNG+P2X7RB having increased Ki67 staining meaning that the transfected cells could potentially display a more aggressive phenotype. This could potentially correlate to the *in vitro* findings which showed that expression of the P2X7RB variant increased proliferation rates.

A final parameter that was assessed on the primary tumour was annexin V staining. Annexin V is a phospholipid binding protein that binds to phosphatidylserine which is externalised and expressed on early apoptotic cell membranes as a cell death signal. Therefore, the amount of annexin V binding to phosphatidylserine correlates with cell apoptosis (Kenis *et al.,* 2007, Cummings *et al.*, 2004). The MNNG-HOS+P2X7RB bearing mice did have an increased amount of cells expressing annexin V when

compared to MNNG-HOS tumour bearing mice. This could potentially demonstrate that there was a higher cell density in these tumours resulting in them growing out of control and developing regions of hypoxia with apoptosis occurring due to the tumour being unable to sustain itself. This is due to not been able to meet the necessary nutritional and oxygen demands (Eales *et al.,* 2016). This process results in cancer cell adaptation and increased metastasis (Muz *et al.,* 2015). This could correlate to the increased incidence of metastasis in MNNG-HOS+P2X7RB tumour bearing mice. Due to the high level of annexin V staining in the vehicle MNNG-HOS+P2X7RB bearing mice there was no further increase in staining possible for the treatment groups. However, in MNNG-HOS bearing mice treatment with Ifosfamide increased the amount of cell death which you would anticipate due to it been the positive control, but A740003 showed no difference.

The formation of ectopic bone is a characteristic of human OS and the MNNG-HOS model does recapitulate this phenotype (Jacques *et al.,* 2018). This means that this important parameter can be examined in this study using micro-CT scanning. The total bone volume in MNNG-HOS bearing mice did not have an increased bone volume compared with its contralateral leg however, the MNNG-HOS+P2X7RB mice did. This means that P2X7RB potentially contributes towards more of an ectopic bone formation phenotype. Treatment with the P2X7R antagonist A740003 reduced the production of ectopic bone in MNNG-HOS-P2X7RB mice. It's been previously shown in OS cells that when the P2X7RA and P2X7RB were co-transfected into Te85 OS cells mineralisation is increased, however, this wasn't the case for P2X7RB alone *in vitro* (Giuliani *et al.,* 2014). P2X7Rs are expressed on osteoblasts both *in vitro* and in primary *in vivo* tissue (Gartland *et al.,* 2001, Panupinthu *et al.,* 2008, Grol *et al.,* 2009) with less differentiated osteoblasts producing less bone formation and expressing less P2X7Rs (Panupinthu *et al.,* 2008). In rat calvarial cell cultures treatment with BzATP increased mineralization and ALP activity by approximately 40%. It also up-regulated osterix and osteocalcin which are markers of osteoblast differentiation and bone production (Grol *et al.,* 2009) this data supports the total bone volume results for the MNNG-HOS-P2X7RB mice in this study. Additionally, cultures from P2X7R KO mice when compared to control cultures had 33% less mineralization and less ALP activity (Panupinthu *et al.,* 2008). This was also shown in a similar study where the bone phenotype from KO P2X7R mice and WT mice showed that deletion of the P2X7R

reduced periosteal bone formation, periosteal mineralizing surface, mineral apposition rate and bone formation rates with decreased periosteal osteoblast number and activity. There was also significantly lower total bone content and higher trabecular bone resorption in KO mice (Ke *et al.,* 2003) supporting the total bone volume results that P2X7R expression can increase bone formation. An additional consideration is that P2X7R KO mice have accelerated bone loss in an osteoporosis model. They demonstrate fewer osteoblasts and increased osteoclasts covering the bone surface (Wang *et al.,* 2018). Furthermore, SNPs can downregulate P2X7R function and have been linked to low lumbar spine bone mineral density and accelerated bone loss in post-menopausal women (Gartland *et al.,* 2012). These studies support the role of the P2X7R in bone formation it is therefore possible that expression of this receptor contributes towards the ectopic bone phenotype in the OS microenvironment. As demonstrated in this study P2X7R antagonism may provide a novel therapeutic to prevent ectopic bone build up in OS.

OS can disrupt bone remodelling due to increased osteoclast activity, this is associated with OS aggressiveness (Avnet *et al.*, 2008). In this study, the osteoclasts at the tumour-bone interface were analysed to examine if P2X7RB expression or treatments had an effect on osteoclast number. P2X7Rs in bone can modulate osteoclast formation and activity (Gartland *et al.,* 2003), application of P2X7R antagonists have been shown to inhibit osteoclast formation and reduce the amount of resorption *in vitro* (Agrawal *et al.,* 2010) this study suggests you would anticipate an increase in osteoclasts with P2X7R expression and a decrease with A740003. There were no differences in osteoclast numbers in P2X7RB expressing tumours, or with Ifosfamide and A740003 treatment. In another previous *in vitro* study using Te85 OS cells transfected with P2X7RB osteoprotegerin (OPG) mRNA was significantly increased (Giuliani *et al.,* 2014). OPG regulates osteoclast function and inhibits bone resorption (Sisay *et al.,* 2017) Additionally RANKL was reduced, (Giuliani *et al.,* 2014) this binds to RANK on osteoclasts and initiates cell fusion and formation of mature multinucleated osteoclasts, this is essential for osteoclast function and survival (McClung., 2007). This suggests that P2X7RB may not have the same effect on increasing osteoclast activity that the full length P2X7R has and therefore the results not showing an increase in osteoclast number, and the A740003 having no effect could

be due to the P2X7RB been the isoform that was examined *in vivo* rather than the fully functional P2X7R.

Metastatic dissemination is considered the final step in primary tumour development, (Hanahan & Weinberg, 2000). This process involves invasion through the extracellular matrix at the primary site, travel and survival in the blood stream, evasion of the host immune system, extravasation into foreign tissue and finally colonisation/growth at the secondary site (Zhu *et al.,* 2013, Posthumadeboer *et al.,* 2011, Hanahan & Weinberg, 2011). The most common site for OS metastasis is the lungs accounting for 80% of all metastasis cases. Patients present with metastasis at initial diagnosis approximately 20% of the time, Posthumadeboer *et al.,* 2011) these have the worst prognosis (Lindsey *et al.*, 2017). Prior to the mid-1960s presence of any lung metastasis resulted in death in under a year (Mittal *et al.,* 2013). Currently the five year survival rate for OS is around 60-70% which decreases to 20-30% with metastasis (Posthumadeboer *et al.,* 2011, Zhu *et al.,* 2013 Mittal *et al.,* 2013). Therefore, anything that promotes metastasis could be a potential therapeutic target.

To examine this process in the current study, the lungs were collected from the mice at the end of the experiment and examined for the presence of pulmonary metastasis. Studies using MNNG-HOS *in vivo* have reported a low incidence of pulmonary metastasis with no macroscopic surface metastases (Luu *et al.,* 2005). However, they have been detected in some instances, one study showed that in MNNG-HOS+LUC injected mice there was bioluminescent signals in the lungs 34 days after injecting 2 million cells (Avril *et al.,* 2016). In another study, cell bioluminescent signals were detected in excised lung lobes at day 28 with a total of 26/56 mice having pulmonary metastasis, this was after the injection of 1 million cells (Le Nail *et al*., 2018). The results from the current study demonstrated no pulmonary metastasis in 30 MNNG-HOS tumour bearing mice when injected with 250,000 cells and observed for three weeks. In contrast to this, in 24 MNNG-HOS+P2X7RB tumour bearing mice a total of 5 mice had OS pulmonary metastasis. This demonstrates that P2X7R could play a role in promoting OS metastasis. P2X7R expression has previously been linked to metastasis of other cancers. One study demonstrated that in a neuroblastoma mouse model, when injecting cells I.V and looking at the dissemination to the bone marrow and liver, P2X7R antagonism with BBG drastically reduced metastasis (Ulrich *et al.*,

2018). In a prostate cancer *in vivo* model in control cells metastasis was detected in the kidney in 3/8 mice and the lymph nodes in 7/8 mice. However, in P2X7R knockdown cells using shRNA no metastasis was detected in the kidney, and only in 1/8 mice for the lymph nodes. In breast cancer using a zebrafish model of metastasis MDA-MB-435s cell metastasis was reduced with the P2X7R antagonist A438079 (Jelassi *et al.,* 2011). In a lymphoma study P388D1 cells were injected into the foot pad of mice and metastasis was detected in the lymph nodes (Ren *et al.,* 2010), in the P2X7R knockdown condition the metastasis was reduced and overall survival was increased compared to control cells. The amount of metastasis was also reduced when a P2X7R antibody was administered (Ren *et al.,* 2010). These studies demonstrate P2X7R expression increases metastasis and that targeting may potentially provide a therapeutic option. The results in this chapter demonstrate a novel finding that P2X7RB increases metastasis to the lungs in an OS *in vivo* model, however P2X7RB antagonism with A740003 didn't prevent this, which could suggest a higher concentration is needed.

To conclude, the parameters assessed in this study have demonstrated various novel findings, P2X7RB may play a role in the formation of ectopic bone in OS which could be abolished with A740003 administration. Finally, expression of P2X7RB increased incidence of OS pulmonary metastasis and could therefore be a novel drug target to prevent this.

Chapter 7 – Discussion

7.1 Thesis findings

In this thesis the role of the P2X7R and targeting it therapeutically with a P2X7R antagonist has been explored in the OS microenvironment both *in vitro* and *in vivo*. The overall hypothesis is that the P2X7R enhances OS progression and metastasis, and that it could provide a novel therapeutic target to treat OS.

The findings in this thesis *in vitro* include:

- Confirmation of P2X7R expression in Te85 and MNNG-HOS OS cells, Te85 OS cells had negligible P2X7R expression at mRNA level and MNNG-HOS naïve OS cells completely lacked P2X7R expression. This was increased when transfected with P2X7R variants.
- Confirmation of P2X7R function when transfected with P2X7R variants in Te85 and MNNG-HOS OS cells, calcium activation was increased in all variants when stimulated with BzATP. However, only a co-transfected A+B variant in Te85 OS cells had the typical P2X7R pore formation.
- P2X7R increased the proliferation of both Te85 and MNNG-HOS OS cells *in vitro* in 10%, 2% and 0.5% FBS concentrations. This increase in proliferation was reduced with the application of A740003 and AZ11645373.
- Expression of P2X7RA and P2X7RB in Te85 OS cells and P2X7RB in MNNG-HOS OS cells reduced cell adhesion to an extracellular collagen matrix.
- P2X7RA, P2X7RB and P2X7RAB in Te85 OS cells and P2X7RB in MNNG-HOS OS cells increased cell migration when in low FBS concentrations and stimulated with BzATP.
- P2X7RA, P2X7RB and P2X7RAB in Te85 OS cells and P2X7RB in MNNG-HOS OS cells increased cell invasion when stimulated with BzATP.

The findings in this thesis *in vivo* include:

- Te85 OS cells were unable to form tumours when paratibially injected into BALB/c nude mice.
- P2X7R expression did not provide enough of a stimulus in Te85 OS cells to induce tumour formation *in vivo.*

- There was no difference in tumour size between MNNG-HOS and MNNG-HOS+P2X7RB injected mice, measured either with external callipers or micro-CT.
- There was no effect of the drug treatments on either MNNG-HOS or MNNG-HOS+P2X7RB tumours when measured with external callipers. However, tumour size could be detected by micro-CT and a significant decrease in size was detected in MNNG-HOS+P2X7RB tumour bearing mice treated with Ifosfamide.
- Histologically tumours formed from both cell lines were high-grade undifferentiated OS tumours with very little osteoid matrix and collagen production.
- There was no difference in Ki-67 staining between MNNG-HOS and MNNG-HOS+P2X7RB tumours, and treatment with Ifosfamide or A740003 had no effect.
- MNNG-HOS+P2X7RB had higher expression of annexin V than MNNG-HOS tumours with neither treatment further increasing this level. MNNG-HOS tumours treated with Ifosfamide increased annexin V staining, whilst there was no effect of A740003 treatment.
- MNNG-HOS and MNNG-HOS+P2X7RB both produced tumours with ectopic bone formation and osteolysis.
- MNNG-HOS+P2X7RB tumours had an increased total bone volume which could be decreased with A740003 treatment.
- MNNG-HOS and MNNG-HOS+P2X7RB tumours did not have a difference in osteoclast coverage at the tumour-bone interface when untreated or when treated with Ifosfamide or A740003.
- MNNG-HOS tumours after 3 weeks demonstrated no presence of pulmonary metastasis, whereas MNNG-HOS+P2X7RB tumours had incidence in ~20% of the mice.

7.2 Limitations of this study

This thesis provides some understanding of the role of the P2X7R in OS progression, but the studies performed do have some limitations. The cell lines used were transfected cells and thereby have P2X7R overexpression. Although this does allow

a link to be made between protein expression and phenotypic changes, it is an artificial system and may not be completely representative of normal physiology. Transfection of cells with a stable vector and an antibiotic resistance gene can cause off target effects and stress to the cells which can then cause genomic, transcriptomic and phenotypic changes (Jacobsen *et al.,* 2009, Stepanenko & Heng., 2017). Some of the experiments performed in this thesis were done *in vitro* using cell lines. This possesses a number of limitations: the cells are not in their natural environment and therefore can contain genetic changes from the original tumour losing its natural heterogenicity. They can also have genetic drift over long periods in culture or contain cross contamination with other cell lines or mycoplasma (Ferreira *et al.,* 2013). They are cultured individually, without considering the other cell types that contribute to the tumour microenvironment. A final consideration of the cell lines used *in vitro* was the Te85 OS cells only represent one subtype of OS. When compared with primary human bone cell cultures Te85 OS cells exhibit a low amount of alkaline phosphatase activity and low amount of osteocalcin, these are both used as markers of bone formation and therefore the low amount of these are not representative of human OS, as patients often have an osteogenic phenotype (Clover & Gowen, 1994). In order to overcome this, PDOX models are now emerging in OS research and could be used in future studies to fully recapitulate the heterogeneity of OS tumours and potentially offer personalised responses to drugs.

Animal models have been essential in the development of novel cancer therapeutics; however, they do have a number of limitations in this study. The animals used are BALB/c nude mice, these lack T cells in order to overcome recognition of the implanted cells as foreign. They therefore don't mount an immune response and reject the cells enabling successful engraftment (De La Rochere *et al.,* 2018). Although this allows the model system to be used it lacks an immune response. This is an important aspect of the tumour microenvironment, osteoimmunology is an emerging field in OS research with phase I and phase II trials in progress using immunotherapy as a potential treatment (Heymann & Heymann, 2017) this process has been overlooked in this study. It could therefore benefit from the use of a syngeneic mouse model of which there are numerous available for OS and are described in chapter 1. The type of injection and injection site can influence tumour growth (Holen *et al.*, 2017). In this study the cells were injected paratibially, this requires a high technical level of skill and

can suffer reproducibility problems (Guijarro *et al.,* 2014). The majority of *in vivo* results failed to reach statistical significance although showed some trends. A limitation that may have contributed to this was the drug dose, administration and regime. The treatment regime was started two days after cell injection, treatment could however be administered when the palpable tumour had already formed. This is clinically relevant as tumours are treated after it has already formed and been detected. This could potentially improve the study N number. An N of 12 mice per group was used, however, no group had the full 12 form a palpable tumour, with one group having an N of 6. This therefore should be repeated to determine fully if any of the trends were novel findings. The tumours additionally had a high amount of annexin V staining meaning that the tumours were undergoing cell death. This could have again contributed to the low N number meaning the cells did not take in the mice due to dying, and could be overcome by not leaving the tumours too long to grow, using a lower amount of initial cells or an alternative OS *in vivo* model such as the 143B OS cell line or syngeneic model.

The chemotherapy drug Ifosfamide failed to have a significant effect for many of the *in vivo* results, an alternative chemotherapy could have been used such as Methotrexate, Cisplatin or Doxorubicin or a higher Ifosfamide dose could have been used, this was also the case for A740003, which again could have been increased or given more frequently. It could also have been delivered intra mass which has shown an effect in other cancer types (Adinolfi *et al.,* 2012, Amoroso *et al.,* 2016).

As the Ifosfamide and A740003 wasn't showing a decrease in tumour size in this study using calliper measurements, bioluminescent techniques could have been used to provide a more accurate measurement of tumour size. In a previous study into pancreatic ductal adenocarcinoma P2X7R antagonist administration *in vivo* was shown not to affect tumour size when measured with external callipers, but a difference in tumour size was determined using bioluminescent imaging (Giannuzzo *et al.,* 2016).

A further limitation of the MNNG-HOS model used is that it only has a low incidence of pulmonary metastasis (Luu *et al.,* 2005) (Chapter 5 & 6). Therefore, this important parameter wasn't fully examined, the mice were unable to be left longer due to restrictions limiting the size of the primary tumour and therefore a different OS cell line

that has increased metastasis could be used in future OS studies, such as the 143B OS cell line. The MNNG-HOS model failed to show a significant increase in total bone volume despite having a high amount of ectopic bone formation when viewing the reconstructed model image. This could again be repeated to improve the N number. The total bone volume can be complicated by the presence of osteolytic lesions therefore, a method to measure only the ectopic bone could be developed using micro-CT rather than the entire total bone volume.

The limitations described can be addressed by repeating the *in vivo* investigations with an improved N number and the slight modifications mentioned. This will then fully elucidate the potential to target the PX7R in OS.

7.3 Future studies

This thesis suggests that P2X7R expression may contribute towards OS progression and metastasis, however it does require further future investigation. P2X7R expression *in vitro* showed many effects that contribute towards OS disease. This includes increased growth, decreased cell adhesion and increased migration and invasion. However, the reason for this is unknown and therefore details of the mechanism and pathways that P2X7R expression affects is needed. It is likely that P2X7R expression will upregulate and downregulate various genes related to OS progression, in a previous study using Te85 OS cells the increased growth was due to 1 NFATc1 activation (Giuliani *et al.,* 2014). However, there is no known mechanism for the adhesion, migration or invasion differences caused by P2X7R in OS. However, these have been linked to processes in other cancers which have been discussed in chapter 4. There are various other cancer properties that could have been examined *in vitro* which P2X7R expression may affect, or be affected by. This includes angiogenesis and hypoxia which have been shown in other cancers (Virgilio & Adinolfi, 2017) these are additional important aspects of OS which haven't been examined here.

With regards to the *in vivo* study, some initial trends could be examined further. P2X7RB expressing MNNG-HOS tumours metastasised to the lungs whereas MNNG-HOS tumours did not. In order to really determine if this effect is significant the experiment could be repeated or done with an alternative OS cell line which produces

more pulmonary metastasis such as the 143B human OS cell line, the mouse LM8, K7M2 and MOS-J, a final alternative model could also include the use of PDOXs from metastatic patients.

The P2X7RB expressing cells also appeared to have an increase in ectopic bone formation, this could be again repeated or a method developed to detect just ectopic bone rather than the entire total bone volume, which may result in the detection of slight changes and can account for the any osteolysis changing the overall total bone volume.

P2X7R antagonists are always improving in specificity and potency with the intention of human therapeutic use (Young & Górecki, 2018, Bartlett *et al.,* 2014) they can therefore be exploited in future studies. It could also be possible to develop P2X7R antagonists that are targeted to the bone so therefore become more specific for OS. This could potentially be done by conjugating the antagonists to bisphosphonates. Bisphosphonates have a high affinity to bone and specifically bind to hydroxyapatite (Farrell *et al.,* 2018) they are used to treat a variety of bone disorders individually but have been previously conjugated to small molecule drugs, proteins, antibiotics, and imaging agents. This results in reduced systemic contact and increased target exposure (Farrell *et al.,* 2018). This could therefore provide a suitable method to improve drug potency when targeting the P2X7R in OS and may result in seeing an improved effect. Additionally, P2X7R antagonists could be used as a combination therapy with currently available chemotherapy treatments or rather than only using antagonists, gene editing technologies could be used to knockout P2X7R in OS cells. This has had success in breast cancer cells (Xia *et al.,* 2015) and in pancreatic ductal adenocarcinoma cells (Giannuzzo *et al.,* 2016) using siRNA but could also use recently developed clustered regularly interspaced short palindromic repeats (CRISPR). This technology originated from a prokaryotic adaptive immune system defence mechanism, where it protects against invading nucleic acids such as viruses (Martinez-Lage *et al.,* 2018). It has now been developed and utilised as a gene editing technique whereby a guide RNA binds to the target DNA to be modified and is attached an endonuclease (such as Cas9) which recognises and then cuts the DNA at the desired location (Richter *et al.,* 2013). A new custom sequence can then be integrated where the cut is made and repaired using DNA repair mechanisms already present in

the cells (Richter *et al.,* 2013, Martinez-Lage *et al.,* 2018). This technique has now emerged at the forefront of gene editing technology and is fast and affordable (Martinez-Lage *et al.,* 2018). Due to genomic instability and mutations occurring in all cancers, the potential to edit genes that may be causing cancer cells to proliferate more, or become resistant to treatment is now being explored (Tian *et al.,* 2019). CRISPR could therefore be potentially used to target the P2X7R gene. There are limited studies exploring the use of CRISPR to knockout P2X7R, however, a recent study generated P2X7R deficient cells using a mouse BV-2 microglial cell line (Dhuna *et al.,* 2019) and P2X7R CRISPR/CAS9 knockout plasmids are commercially available for future use.

The P2X7R could potentially be exploited using its pore formation function as a drug delivery system, the formation of the larger pore could facilitate the entry of hydrophilic molecules into the cell (Pacheco *et al.,* 2016, Alves *et al.,* 2018). This has been demonstrated in a study to increase methylene blue (319 Da) uptake into the cytoplasm of macrophage cells treatment with only methylene blue resulted in a 4.7% rate of entry. However, treatment with methylene blue and ATP increased this rate to 90.2% (Pacheco *et al.,* 2016). This process could be applied in OS.

Patient samples for OS are rare, however, in a previous study P2X7R expression was found in 80% of OS cases examined (Giuliani *et al.,* 2014), this finding could be built upon and performed in a larger number of samples, correlated with stage of the disease, or the presence of metastasis. Overall, the final future goal of this research would be to reach a clinical trial stage for P2X7R targeting in OS and use of P2X7R antagonists as a novel therapeutic.

A final consideration of P2X7R targeting could be to apply it to other types of bone sarcoma such as Ewing's sarcoma, chondrosarcoma or chordoma, this could be done using the techniques presented in this thesis and may be a translatable therapy in addition to OS.

References

Abbracchio, M.P. & Burnstock, G., 1994. Purinoceptors: Are there families of P2X and P2Y purionceptors? *Pharmac Ther*, 64, pp. 445-475.

Adinolfi, E., Callerari, G., Ferrari, D., Bolognesi, C., Minelli, M., Wieckowski, R.M., Pinton, P., Rizzuto R., Di Virgilio, F., 2005. Basal Activation of the P2X7 ATP Receptor Elevates Mitochondrial Calcium and Potential, Increases Cellular ATP Levels, and Promotes Serum-independent Growth. *Molecular biology of the cell*, 16, pp. 3260–3272.

Adinolfi, E., Melchiorri, L., Falzoni, S., Chiozzi, P., Morelli, A., Tieghi, A., Cuneo, A., Castoldi, G., Di Virgilio, F., Di & Baricordi, O.R., 2002. Brief report P2X7 receptor expression in evolutive and indolent forms of chronic B lymphocytic leukemia. *Blood*, 99 (2), pp.706–709.

Adinolfi, E., Raffaghello, L., Giuliani, A.L., Cavazzini, L., Capece, M., Chiozzi, P., Bianchi, G., Kroemer, G., Pistoia, V. & Di Virgilio, F., 2012. Expression of P2X7 Receptor Increases In Vivo Tumor Growth. *Cancer Research*, 72(12), pp. 2957–2969.

Adinolfi, E., 2013. New intriguing roles of ATP and its receptors in promoting tumor metastasis. *Purinergic Signalling*, 9(4), pp. 487–490.

Adinolfi, E., Melchiorri, L., Falzoni, S., Chiozzi, P., Morelli, A., Tieghi, A., Cuneo, A., Castoldi, G., Di Virgilio, F., Baricordi, O.R., 2011. P2X7 receptor expression in evolutive and indolent forms of chronic B lymphocytic leukemia., 15(2), pp. 706–708.

Adinolfi, E., Cirillo, M., Woltersdorf, R., Falzoni, S., Chiozzi, P., Pellegatti, P., Callegari, M.G., Sandona, D., Markwardt, F. & Di Virgilio, F., 2010. Trophic activity of a naturally occurring truncated isoform of the P2X7 receptor., 24(9), pp.3393–3404.

Adinolfi, E., Amoroso, F. & Giuliani, A.L., 2012. P2X7 Receptor Function in Bone-Related Cancer. *Journal of Osteoporosis*, 2012, pp.1–10.

Agrawal, A., Henriksen, Z., Syberg, S., Petersen, S., Aslan, D., Solgaard, M., Nissen, N., Larsen, T.K., Schwarz, P., Steinberg, T.H. & Jørgensen, N.R., 2017. P2X7Rs are involved in cell death, growth and cellular signaling in primary human osteoblasts. *Bone*, 95, pp.91–101.

Agrawal, A., Buckley, K.A., Bowers, K., Furber, M., Gallagher, J.A. & Gartland, A., 2010. The effects of P2X7 receptor antagonists on the formation and function of human osteoclasts *in vitro. Purinergic Signalling*, 6(3), pp.307–315.

Agrawal, A. & Gartland, A., 2013. P2X7 receptors: role in bone cell formation and function., 54(2), pp.75–88.

Agteresch, H.J., Dagnelie, P.C., van der Gaast, A., Stijnen, T. & Wilson, J.H., 2000. Randomized clinical trial of adenosine 5'-triphosphate in patients with advanced non-small-cell lung cancer. *Journal of the National Cancer Institute*, 92(4), pp.321–328.

Alberto, A.V.P., Faria, R.X., Couto, C.G.C., Ferreira, L.G.B., Souza, C.A.M., Teixeira,

P.C.N., Fróes, M.M. & Alves, L.A., 2013. Is pannexin the pore associated with the P2X7 receptor? *Naunyn-Schmiedeberg's Archives of Pharmacology*, 386(9), pp.775–787.

Alqallaf, S., Evans, B. & Kidd, E., 2009. Atypical P2X7 receptor pharmacology in two human osteoblast-like cell lines. *British Journal of Pharmacology*, 156(7), pp.1124–1135.

Alves, L.A., Ferreira, L.B., Pacheco, P.F., Mendivelso, E.A.C., Teixeira, P.C.N. & Faria, R.X., 2018. Pore forming channels as a drug delivery system for photodynamic therapy in cancer associated with nanoscintillators. *Oncotarget*, 9(38), pp.25342–25354.

Amoroso, F., Salaro, E., Falzoni, S., Chiozzi, P., Giuliani, A.L., Cavallesco, G., Maniscalco, P., Puozzo, A. Bononi, I., Martini, F, Tognon, M., Di Virgilio, F., 2016. P2X7 targeting inhibits growth of human mesothelioma. *Oncotarget*. 7(31), pp.49664-49676.

Amoroso, F., Capece, M., Rotondo, A., Cangelosi, D., Ferracin, M., Franceschini, A., Raffaghello, L., Pistoia, V., Varesio, L. & Adinolfi, E., 2015. The P2X7 receptor is a key modulator of the PI3K / GSK3 β / VEGF signaling network : evidence in experimental neuroblastoma., *Oncogene,* pp.5240–5251.

Ando, K., Heymann, M.-F., Stresing, V., Mori, K., Redini, F. & Heymann, D., 2013. Current Therapeutic Strategies and Novel Approaches in Osteosarcoma. *Cancers*, 5, pp.591–616.

Asai, T., Ueda, T., Itoh, K., Yoshioka, K., Aoki, Y., Mori, S. & Yoshikawa, H., 1998. Establishment and characterization of a murine osteosarcoma cell line (LM8) with high metastatic potential to the lung. *International Journal of Cancer*, 76(3), pp.418–422.

Avnet, S., Longhi, A., Manuela, S., Halleen, J.M., Francesca, P., Granchi, D., Ferrari, S., Bertoni, F., Giunti, A. & Baldini, N., 2008. Increased osteoclast activity is associated with aggressiveness of osteosarcoma. *International Journal of Oncology*, 33, pp.1231–1238.

Avril, P., Le Nail, L.R., Brennan, M., Rosset, P., De Pinieux, G., Layrolle, P., Heymann, D., Perrot, P. & Trichet, V., 2016. Mesenchymal stem cells increase proliferation but do not change quiescent state of osteosarcoma cells: Potential implications according to the tumor resection status. *Journal of Bone Oncology*, 5(1), pp.5–14.

Ayers, G.D., McKinley, E.T., Zhao, P., Fritz, J.M., Metry, R.E., Deal, B.C., Adlerz, K.M., Coffey, R.J. & Manning, H.C., 2010. Volume of preclinical xenograft tumors is more accurately assessed by ultrasound imaging than manual caliper measurements. *Journal of Ultrasound in Medicine*, 29(6), pp.891–901.

Bacci, G., Ferrari, S., Longhi, A., Picci, P., Mercuri, M., Alvegard, T.A., Saeter, G., Donati, D., Manfrini, M., Lari, S., Briccoli, A. & Forni, C., 2002. High Dose Ifosfamide in Combination with High Dose Methotrexate, Adriamycin and Cisplatin in the Neoadjuvant Treatment of Extremity Osteosarcoma: Preliminary Results of an Italian Sarcoma Group/Scandinavian Sarcoma Group Pilot Study. *Journal of Chemotherapy*,

14(2), pp.198–206.

Barden, J.A., Yuksel, A., Pedersen, J., Danieletto, S. & Delprado, W., 2014. Non-Functional P2X7 : A Novel and Ubiquitous Target in Human Cancer Journal of Clinical & Cellular Immunology 5(237) pp.1-5.

Baricordi, O.R., Melchiorri, L., Adinolfi, E., Falzoni, S., Chiozzi, P., Buell, G. & Di Virgilio, F., 1999. Increased proliferation rate of lymphoid cells transfected with the P2X7 ATP receptor. *Journal of Biological Chemistry*, 274(47), pp.33206–33208.

Bartlett, R., Stokes, L. & Sluyter, R., 2014. The P2X7 Receptor Channel: Recent Developments and the Use of P2X7 Antagonists in Models of Disease. *Pharmacological reviews*, 66(3) pp.638-675.

Baumhoer, D., Brunner, P., Eppenberger-Castori, S., Smida, J., Nathrath, M. & Jundt, G., 2014. Osteosarcomas of the jaws differ from their peripheral counterparts and require a distinct treatment approach. Experiences from the DOESAK Registry. *Oral Oncology*, 50(2), pp.147–153.

Beijer, S., Gielisse, E.A.R., Hupperets, P.S., van den Borne, B.E.E.M., van den Beuken-van Everdingen, M., Nijziel, M.R., van Henten, A.M.J. & Dagnelie, P.C., 2007. Intravenous ATP infusions can be safely administered in the home setting: a study in pre-terminal cancer patients. *Investigational new drugs*, 25(6), pp.571–579.

Benedetti, M.G., Okita, Y., Recubini, E., Mariani, E., Leardini, A. & Manfrini, M., 2016. How Much Clinical and Functional Impairment do Children Treated With Knee Rotationplasty Experience in Adulthood? *Clinical Orthopaedics and Related Research*, 474(4), pp.995–1004.

Blattmann, C., Thiemann, M., Stenzinger, A., Roth, E.K., Dittmar, A., Witt, H., Lehner, B., Renker, E., Jugold, M., Eichwald, V., Weichert, W., Huber, P.E. & Kulozik, A.E., 2015. Establishment of a patient-derived orthotopic osteosarcoma mouse model. *Journal of Translational Medicine*, 13(1), pp.1–10.

Blumenfeld, Z., 2012. Best Practice & Research Clinical Obstetrics and Gynaecology. *Best Practice & Research Clinical Obstetrics & Gynaecology*, 26(3), pp.379–390.

Brake A.J., Wagenbach, M.J., & Julius, D., 1994. New structural motif for ligand-gated ion channels defined by an ionotropic ATP receptor. *Nature*. 371 pp. 519–523

Broadhead, M.L., Clark, J.C.M., Myers, D.E., Dass, C.R. & Choong, P.F.M., 2011. The Molecular Pathogenesis of Osteosarcoma : A Review. *Sarcoma* , pp.1-12

Brown, H., Schiavone, K., Tazzyman, S., Heymann, D. & Chico, T., 2017. Zebrafish xenograft models of cancer and metastasis for drug discovery. Expert opinion on Drug discovery, Informa Healthcare, Epub ahead of print.

Bruheim, S., Bruland, O.S., Breistol, K., Maelandsmo, G.M. & Fodstad, Ø., 2004. Human osteosarcoma xenografts and their sensitivity to chemotherapy. *Pathology and Oncology Research*, 10(3), pp.133–141.

Buckley, K.A., Hipskind, R.A., Gartland, A., Bowler, W.B. & Gallagher, J.A., 2002.

Adenosine triphosphate stimulates human osteoclast activity via upregulation of osteoblast-expressed receptor activator of nuclear factor-kappa B ligand. *Bone*, 31(5), pp.582–590.

Burnstock, G., 1972. Purinergic nerves. *Pharmacol Rev,* 24(3), pp. 509-581

Burnstock, G., 2012. Discovery of purinergic signalling, the initial resistance and current explosion of interest. *British Journal of Pharmacology*, 167(2), pp.238–255.

Burnstock, G., 2017. Purinergic signalling: Therapeutic developments. *Frontiers in Pharmacology*, 8:661, pp.1-55.

Campione-Piccardo, J., Rawls W.E., Bacchetti, S., 1979. Selective assay for herpes simplex viruses expressing thymidine kinase. *J Virol*, 31(2), pp.281–7.

Carloni, G., Venuat, A.M., Daya-Grosjean, L., Nardeux, P., Rhim, J.S. & Azzarone, B., 1988. Integration and loss of a single v-Ki-ras gene affects tumorigenic potential of human osteosarcoma cells. *Febs Lett.*, 229(2), pp.333–339.

Casali, P.G., Blay, J.Y., Bertuzzi, A., Bielack, S., Bjerkehagen, B., Vleggert-Lankamp, C.L.A., et al., 2014. Bone sarcomas: ESMO clinical practice guidelines for diagnosis, treatment and follow-up. *Annals of Oncology*, 25, pp.113-123.

Chalopin, A., Tellez-Gabriel, M., Brown, H.K., Vallette, F., Heymann, M.F., Gouin, F. & Heymann, D., 2018. Isolation of circulating tumor cells in a preclinical model of osteosarcoma: Effect of chemotherapy. *Journal of Bone Oncology*, 12, pp.83–90.

Cheewatrakoolpong, B., Gilchrest, H., Anthes, J.C. & Greenfeder, S., 2005. Identification and characterization of splice variants of the human P2X7 ATP channel. *Biochemical and Biophysical Research Communications*, 332(1), pp.17–27.

Chitty, J.L., Filipe, E.C., Lucas, M.C., Herrmann, D., Cox, T.R., & Timpson, P., 2018 Recent advances in understanding the complexities of metastasis, *F1000 Research* 7:1169 pp 1-18

Chong, J.H., Zheng, G.G., Ma, Y.Y., Zhang, H.Y., Nie, K., Lin, Y.M. & Wu, K.F., 2010. The hyposensitive N187D P2X7 mutant promotes malignant progression in nude mice. *Journal of Biological Chemistry*, 285(46), pp.36179–36187.

Clover, J. & Gowen, M., 1994. Are MG-63 and HOS TE85 human osteosarcoma cell lines representative models of the osteoblastic phenotype? *Bone*, 15(6), pp.585–591.

Cobb, L.M., 1970. Radiation-induced osteosarcoma in the rat as a model for osteosarcoma in man. *British Journal of Cancer*, 24(2), pp.294–299.

Cole, H.A., Ohba, T., Ichikawa, J., Nyman, J.S., Cates, J.M.M., Haro, H., Schwartz, H.S. & Schoenecker, J.G., 2014. Micro-Computed Tomography Derived Anisotropy Detects Tumor Provoked Deviations in Bone in an Orthotopic Osteosarcoma Murine Model. , 9(6), pp.1–7.

Cole, H.A., Ichikawa, J., Colvin, D.C., O'Rear, L. & Schoenecker, J.G., 2011. Quantifying intra-osseous growth of osteosarcoma in a murine model with

radiographic analysis. *Journal of Orthopaedic Research*, 29(12), pp.1957–1962.

Cotterill, S.J., Wright, C.M., Pearce, M.S. & Craft, A.W., 2004. Stature of young people with malignant bone tumors. *Pediatric blood & cancer*, 42(1), pp.59–63.

Crespigny, A. De, Bou-reslan, H., Nishimura, M.C., Phillips, H., Richard, A., Carano, D. & Arceuil, H.E.D., 2009. NIH Public Access. , 171(2), pp.207–213.

Cummings, B.S., Wills, L.P. & Schneellmann, R.G., 2004. Measurement of Cell Death in Mammalian Cells. *Current Protocols in Pharmacology*, pp.1–30.

Czekanska, E., Stoddart, M., Richards, R. & Hayes, J., 2012. In search of an osteoblast cell model for *in vitro* research. *European Cells and Materials*, 24, pp.1–17.

Dass, C.R. & Choong, P.F.M., 2007. Zoledronic acid inhibits osteosarcoma growth in an orthotopic model. *Molecular cancer therapeutics*, 6(12 Pt 1), pp.3263–70.

De La Rochere, P., Guil-Luna, S., Decaudin, D., Azar, G., Sidhu, S.S. & Piaggio, E., 2018. Humanized Mice for the Study of Immuno-Oncology. *Trends in Immunology*, 39(9), pp.748–763.

Delgado San Martin, J.A., Worthington, P. & Yates, J.W.T., 2015. Non-invasive 3D time-of-flight imaging technique for tumour volume assessment in subcutaneous models. *Laboratory Animals*, 49(2), pp.168–171.

Dhuna, K., Felgate, M., Bidula, S.M., Walpole, S., Bibic, L., Cromer, B.A., Angulo, J., Sanderson, J., Stebbing, M.J., Stokes, L., 2019. Ginsenosides Act As Positive Modulators of P2X4 Receptors. *Mol Pharmacol* 95: pp.210–221.

Di Virgilio, F., 2016. P2RX7: A receptor with a split personality in inflammation and cancer. *Molecular and Cellular Oncology*, 3(2), pp.14–16.

Di Virgilio, F. & Adinolfi, E., 2017. Extracellular purines, purinergic receptors and tumor growth. *Oncogene*, 36(3) pp.293–303.

Di Virgilio, F., Ferrari, D. & Adinolfi, E., 2009. P2X7: a growth-promoting receptor—implications for cancer. *Purinergic Signalling*, 5(2), pp.251–256.

Di Virgilio, F., Schmalzing, G. & Markwardt, F., 2018. The Elusive P2X7 Macropore. *Trends in Cell Biology*, 28(5), pp.392–404.

Drury, A.N. & Szent-Györgyi, A., 1929. The physiological activity of adenine compounds with especial reference to their action upon the mammalian heart. *The Journal of Physiology*, 68(3), pp.213–237.

Dunn, T.B. & Andervont, H.B., 1963. Histology of some neoplasms and non-neoplastic lesions found in wild mice maintained under laboratory conditions. *Journal of the National Cancer Institute*, 31, pp.873–901.

Eales, K.L., Hollinshead, K.E.R. & Tennant, D.A., 2016. Hypoxia and metabolic adaptation of cancer cells. *Oncogenesis*, 5(1), p.e190.

Elkeles, A., Juven-Gershon, T., Israeli, D., Wilder, S., Zalcenstein, A. & Oren, M., 1999. The c-fos proto-oncogene is a target for transactivation by the p53 tumor suppressor. *Molecular and cellular biology*, 19(4), pp.2594–600.

Errani, C., Traina, F., Perna, F., Calamelli, C. & Faldini, C., 2013. Current concepts in the biopsy of musculoskeletal tumors. *The Scientific World Journal*, 2013, pp.1–6.

Evola, F.R., Costarella, L., Pavone, V., Caff, G., Cannavò, L., Sessa, A., Avondo, S. & Sessa, G., 2017. Biomarkers of osteosarcoma, chondrosarcoma, and ewing sarcoma. *Frontiers in Pharmacology*, 8, pp.1–14.

Fan, X.L., Cai, G.P., Zhu, L.L. & Ding, G.M., 2015. Efficacy and safety of ifosfamide-based chemotherapy for osteosarcoma: A meta-analysis. *Drug Design, Development and Therapy*, 9, pp.5925–5932.

Farrell, K.B., Karpeisky, A., Thamm, D.H. & Zinnen, S., 2018. Bisphosphonate conjugation for bone specific drug targeting. *Bone Reports*, 9, pp.47–60.

Feng, Y.H., Li, X., Wang, L., Zhou, L. & Gorodeski, G.I., 2006. A truncated P2X7 receptor variant (P2X7-j) endogenously expressed in cervical cancer cells antagonizes the full-length P2X7 receptor through hetero-oligomerization. *Journal of Biological Chemistry*, 281(25), pp.17228–17237.

Fenger, J.M., London, C.A. & Kisseberth, W.C., 2014. Canine osteosarcoma: A naturally occurring disease to inform pediatric oncology. *ILAR Journal*, 55(1), pp.69–85.

Ferrari, D., Malavasi, F. & Antonioli, L., 2016. Review A Purinergic Trail for Metastases. *Trends in Pharmacological Sciences*, pp.1–14.

Ferreira, D., Adega, F. & Chaves, R., 2013. The Importance of Cancer Cell Lines as in vitro Models in Cancer Methylome Analysis and Anticancer Drugs Testing. *Oncogenomics and Cancer Proteomics- Novel Approaches in Biomarkers Discovery and Therapeutic Targets in Cancer*, pp.139–166.

Florea, A.-M. & Büsselberg, D., 2011. Cisplatin as an Anti-Tumor Drug: Cellular Mechanisms of Activity, Drug Resistance and Induced Side Effects. *Cancers*, 3(4), pp.1351–1371.

Fogh, J., Fogh, J.M. & Orfeo, T., 1977. One hundred and twenty-seven cultured human tumor cell lines producing tumors in nude mice. *Journal of the National Cancer Institute*, 59(1), pp.221–6.

Gartland, A., Buckley, K.A., Hipskind, R.A., Perry, M.J., Tobias, J.H., Buell, G., Chessell, I., Bowler, W.B., & Gallagher J.A., 2003 Multinucleated osteoclast formation *in vivo* and *in vitro* by P2X7 receptor-deficient mice. *Critical Reviews in Eukaryotic Gene Expression,* 13 pp. 243–253.

Gartland, A., Buckley, K.A., Bowler, W.B. & Gallagher, J.A., 2003. Blockade of the Pore-Forming P2X7 Receptor Inhibits Formation of Multinucleated Human Osteoclasts *In Vitro. Calcified Tissue International*, 73(4), pp.361–369.

Gartland, A., Hipskind, R.A., Gallagher, J.A. & Bowler, W.B., 2001. Expression of a P2X7 receptor by a subpopulation of human osteoblasts. *J Bone Miner Res*, 16(5), pp.846–856.

Gartland, A., Buckley, K.A., Hipskind, R.A., Bowler, W.B. & Gallagher, J.A., 2003. P2 receptors in bone-modulation of osteoclast formation and activity via P2X7 activation. *Crit. Rev. Eukaryotic Gene Expression*, 13(2–4), pp.237–242.

Gartland, A., Skarratt, K.K., Hocking, L.J., Parsons, C., Stokes, L., Jørgensen, N.R., Fraser, W.D., Reid, D.M., Gallagher, J.A. & Wiley, J.S., 2012. Polymorphisms in the P2X7 receptor gene are associated with low lumbar spine bone mineral density and accelerated bone loss in post-menopausal women. *European Journal of Human Genetics*, 20(5), pp.559–564.

Gelderblom, H., Jinks, R.C., Sydes, M., Bramwell, V.H.C., van Glabbeke, M., Grimer, R.J., Hogendoorn, P.C.W., McTiernan, A., Lewis, I.J., Nooij, M.A., Taminiau, A.H. & Whelan, J., 2011 Survival after recurrent osteosarcoma: data from 3 European Osteosarcoma Intergroup (EOI) randomized controlled trials. 2011. *European journal of cancer* 47(6), pp.895–902.

Genetos, D.C., Geist, D.J., Dawei, L., Donahue, H.J. & Randall, L., 2005. Fluid Shear-Induced ATP secretion Mediates Prostaglandin Release in MC3T3-E1 Osteoblasts, *J Bone Miner Res.* 20(1), pp.41–49.

Gerrand, C., Athanasou, N., Brennan, B., Grimer, R., Judson, I., Morland, B., Peake, D., Seddon, B. & Whelan, J., 2016. UK guidelines for the management of bone sarcomas. *Clinical Sarcoma Research*, 6(1), p.7.

Giannuzzo, A., Saccomano, M., Napp, J., Ellegaard, M., Alves, F. & Novak, I., 2016. Targeting of the P2X7 receptor in pancreatic cancer and stellate cells. *International Journal of Cancer*, 139(11), pp.2540–2552.

Giannuzzo, A., Pedersen, S.F. & Novak, I., 2015. The P2X7 receptor regulates cell survival, migration and invasion of pancreatic ductal adenocarcinoma cells. *Molecular Cancer*, 14(1), pp.203-218.

Gilbert, S., Oliphant, C., Hassan, S., Peille, A., Bronsert, P., Falzoni, S., Di Virgilio, F., McNulty, S. & Lara, R., 2019. ATP in the tumour microenvironment drives expression of nfP2X7, a key mediator of cancer cell survival. *Oncogene*, 38(2) pp.194-208.

Gisselsson, D., Palsson, E., Hoglund, M., Domanski, H., Mertens, F., Pandis, N., Sciot, R., Dal Cin, P., Bridge, J.A. & Mandahl, N., 2002. Differentially amplified chromosome 12 sequences in low- and high-grade osteosarcoma. *Genes, chromosomes & cancer*, 33(2), pp.133–140.

Giuliani, A.L., Colognesi, D., Ricco, T., Roncato, C., Capece, M., Amoroso, F., Wang, Q.G., De Marchi, E., Gartland, A., Di Virgilio, F. & Adinolfi, E., 2014. Trophic Activity of Human P2X7 Receptor Isoforms A and B in Osteosarcoma. *PLoS ONE*, 9(9), p.e107224.

Gobin, B., Gatien, M., Ory, B., Charrier, C., Brion, R., Blanchard, F., Redini, F. & Heymann, D., 2014. Imatinib Mesylate Exerts Anti-Proliferative Effects on

Osteosarcoma Cells and Inhibits the Tumour Growth in Immunocompetent Murine Models. PLoS ONE, 9(3) e90795.

Gómez-Villafuertes, R., García-huerta, P. Díaz-hernández, J.I., & Miras-Portugal, M.T., 2015. PI3K / Akt signaling pathway triggers P2X7 receptor expression as a pro-survival factor of neuroblastoma cells under limiting growth conditions. *Scientific Reports*, 5:18417, pp.1–15.

Goorin, A.M., Schwartzentruber, D.J., Devidas, M., Gebhardt, M.C., Ayala, A.G., Harris, M.B., Helman, L.J., Grier, H.E. & Link, M.P., 2003. Presurgical chemotherapy compared with immediate surgery and adjuvant chemotherapy for nonmetastatic osteosarcoma: Pediatric Oncology Group Study POG-8651. *Journal of Clinical Oncology*, 21(8), pp.1574–1580.

Greig, H., Linge, C., Healy, V., Lim, P., Clayton, E., Rustin, M.H.A., Mcgrouther, D.A. & Burnstock, G., 2003. Expression of Purinergic Receptors in Non-melanoma Skin Cancers and Their Functional Roles in A431 Cells., pp.315–327.

Grigoriadis, A.E., Schellander, K., Wang, Z.Q. & Wagner, E.F., 1993. Osteoblasts are target cells for transformation in c-fos transgenic mice. *Journal of Cell Biology*, 122(3), pp.685–701.

Grol, M.W., Panupinthu, N., Korcok, J., Sims, S.M. & Dixon, S.J., 2009. Expression, signaling, and function of P2X7 receptors in bone. *Purinergic Signalling*, 5(2), pp.205–221.

Gu, B.J. & Wiley, J.S., 2006. Rapid ATP-induced release of matrix metalloproteinase 9 is mediated by the P2X7 receptor. *Blood*, 107(12), pp.4946–4953.

Guijarro, M. V., Ghivizzani, S.C. & Gibbs, C.P., 2014. Animal Models in Osteosarcoma. *Frontiers in Oncology*, 4, pp.1–7.

Gurcan, M.N., Boucheron, L.E., Can, A., Madabhushi, A., Rajpoot, N.M. & Yener, B., 2009. Histopathological Image Analysis: A Review. *IEEE Reviews in Biomedical Engineering*, 2, pp.147–171.

Gvozdenovic, A., Arlt, M.J.E., Campanile, C., Brennecke, P., Husmann, K., Li, Y., Born, W., Muff, R. & Fuchs, B., 2013. CD44 enhances tumor formation and lung metastasis in experimental osteosarcoma and is an additional predictor for poor patient outcome. *Journal of Bone and Mineral Research*, 28(4), pp.838–847.

Haanes, K.A., Schwab, A. & Novak, I., 2012. The P2X7 Receptor Supports Both Life and Death in Fibrogenic Pancreatic Stellate Cells., PLoS ONE., 7(12) e51164.

Haines, B.B., Bettano, K.A., Chenard, M., Sevilla, R.S., Ware, C., Angagaw, M.H., Winkelmann, C.T., Tong, C., Reilly, J.F., Sur, C. & Zhang, W., 2009. A Quantitative Volumetric Micro-Computed Tomography Method to Analyze Lung Tumors in Genetically Engineered Mouse Models. *Neoplasia*, 11(1), pp.39–47.

Hanahan, D., Weinberg, R.A. & Francisco, S., 2000. The Hallmarks of Cancer Review University of California at San Francisco., 100, pp.57–70.

Hanahan, D. Weinberg, R., 2011. Hallmarks of Cancer: The Next Generation. *Cell*, 144, pp.P646-674.

He, H., Ni, J. & Huang, J., 2014. Molecular mechanisms of chemoresistance in osteosarcoma (Review). *Oncology letters*, 7(5), pp.1352–1362.

Heremans, H., Billiau, A., Cassiman, J.J., Mulier, J.C. & de Somer, P., 1978. In vitro cultivation of human tumor tissues. II. Morphological and virological characterization of three cell lines. *Oncology*, 35(6), pp.246–52.

Heymann, D., 2010. Bone Cancer Progression and Therapeutic Approaches 1st Edition

Heymann, D. & Rédini, F., 2011. Bone sarcomas: pathogenesis and new therapeutic approaches. *IBMS BoneKEY*, 8(9), pp.402–414.

Heymann, M.-F. & Heymann, D., 2017. Immune Environment and Osteosarcoma. *Osteosarcoma - Biology, Behavior and Mechanisms*, pp.105–120.

Hoebertz, A., Mahendran, S., Burnstock, G., Arnett, T.R., 2002. ATP and UTP At Low Concentrations Strongly Inhibit Bone Formation by Osteoblasts: A Novel Role for the P2Y2 Receptor in Bone Remodelling. *Journal of Cellular Biochemistry* 86: pp. 413-419.

Holen, I., Speirs, V., Morrissey, B. & Blyth, K., 2017. *In vivo* models in breast cancer research: progress, challenges and future directions. *Disease Models & Mechanisms*, 10(4), pp.359–371.

Honore, P., Donnelly-Roberts, D., Namovic, M., Hsieh, G., Zhu, C., Mikusa, J., Hernandez, G., Zhong, C., Gauvin, D., Chandran, P., Harris, R., Medrano, A., Carroll, W., Marsh, K., Sullivan, J., Faltynek, C. & Jarvis, M., 2006.) methyl] amino}-2, 2-dimethylpropyl)-2-(3, 4-dimethoxyphenyl) acetamide], a novel and selective P2X7 receptor antagonist, dose-dependently reduces neuropathic pain in the rat. *Pharmacology and Experimental therapeutics*, 319(3), pp.1376–1385.

Howe, K., Clark, M., Torroja, C., Torrance, J., Berthelot, C., Muffato, M., Collins, J.E., Humphray, S., McLaren, K., Matthews, L., McLaren, S., Sealy, I., Caccamo, M., Churcher, C., Scott, C., Barrett, J.C., Koch, R. & Al., E., 2013. The zebrafish reference genome sequence and its relationship to the human genome. *Nature*, 496(7446), pp.498–503.

Hu, H., Yang, B., Li, Y., Zhang, S. & Li, Z., 2016. Blocking of the P2X7 receptor inhibits the activation of the MMP-13 and NF-κB pathways in the cartilage tissue of rats with osteoarthritis. *International Journal of Molecular Medicine*, 38(6), pp.1922–1932.

Igarashi, K., Murakami, T., Kawaguchi, K., Kiyuna, T., Miyake, K., Zhang, Y., Nelson, S.D., Dry, S.M., Li, Y., Yanagawa, J., Russell, T.A., Singh, A.S., Tsuchiya, H., Elliott, I., Eilber, F.C., Hoffman, R.M., Igarashi, K., Murakami, T., Kawaguchi, K., Kiyuna, T., Miyake, K., Zhang, Y., Nelson, S.D., Dry, S.M., Li, Y., Yanagawa, J., Russell, T.A., Singh, A.S., Tsuchiya, H., Elliott, I., Eilber, F.C., Hoffman, R.M., Igarashi, K., Murakami, T., Kawaguchi, K., Kiyuna, T., Miyake, K., Zhang, Y., Nelson, S.D., Dry,

S.M., Li, Y., Yanagawa, J., Russell, T.A., Singh, A.S., Tsuchiya, H., Elliott, I., Eilber, F.C. & Hoffman, R.M., 2017. A patient-derived orthotopic xenograft (PDOX) mouse model of a cisplatinum-resistant osteosarcoma lung metastasis that was sensitive to temozolomide and trabectedin: implications for precision oncology. *Oncotarget*, 8(37), pp.62111–62119.

Ihara, H., Hirukawa, K., Goto, S. & Togari, A., 2005. ATP-stimulated interleukin-6 synthesis through P2Y receptors on human osteoblasts. *Biochemical and biophysical research communications*, 326(2), pp.329–334.

Jacobsen, L.B., Calvin, S.A. & Lobenhofer, E.K., 2009. Transcriptional effects of transfection: The potential for misinterpretation of gene expression data generated from transiently transfected cells. *BioTechniques*, 47(1), pp.617–624.

Jacques, C., Renema, N., Lezot, F., Ory, B., Walkley, C.R., Grigoriadis, A.E. & Heymann, D., 2018. Small animal models for the study of bone sarcoma pathogenesis:characteristics, therapeutic interests and limitations. *Journal of Bone Oncology*, 12, pp.7–13.

Janeway, K.A. & Walkley, C.R., 2010. Modeling human osteosarcoma in the mouse: From bedside to bench. *Bone*, 47(5), pp.859–865.

Jelassi, B., Alcaraz-Perez, F., Baroja-Mazo, A., Cayuela, M.L., Pelegrin, P., Surprenant, A. & Roger, S., 2011. P2X 7 receptor activation enhances SK3 channels- and cystein cathepsin-dependent cancer cells invasiveness. *oncogene*, 30, pp.2108–2122.

Jensen, M.M., Jørgensen, J.T., Binderup, T. & Kjær, A., 2008. Tumor volume in subcutaneous mouse xenografts measured by micro-CT is more accurate and reproducible than determined by 18F-FDG-microPET or external caliper. *BMC Medical Imaging*, 8, pp.1–9.

Jia, S.F., Worth, L.L. & Kleinerman, E.S., 1999. A nude mouse model of human osteosarcoma lung metastases for evaluating new therapeutic strategies. *Clinical & experimental metastasis*, 17(6), pp.501–6.

Joliat, M.J., Umeda, S., Lyons, B.L., Lynes, M.A. & Shultz, L.D., 2002. Establishment and characterization of a new osteogenic cell line (MOS-J) from a spontaneous C57BL/6J mouse osteosarcoma. *In vivo*, 16(4), pp.223–8.

Kaan, T.K.Y., Yip, P.K., Patel, S., Davies, M., Marchand, F., Cockayne, D. a., Nunn, P. a., Dickenson, A.H., Ford, A.P.D.W., Zhong, Y., Malcangio, M. & McMahon, S.B., 2010. Systemic blockade of P2X3 and P2X2/3 receptors attenuates bone cancer pain behaviour in rats. *Brain*, 133(9), pp.2549–2564.

Kaebisch, C., Schipper, D., Babczyk, P. & Tobiasch, E., 2015. The role of purinergic receptors in stem cell differentiation. *Computational and Structural Biotechnology Journal*, 13, pp.75–84.

Kanaya, K., Iba, K., Dohke, T., Okazaki, S., Yamashita, T., 2016. TRPV1, ASICs and P2X2/3 expressed in bone cells simultaneously regulate bone metabolic markers in ovariectomized mice. *Musculoskelet Neuronal Interact* 16(2): pp.145-151.

Ke, H.Z., Qi, H., Weidema, A.F., Zhang, Q., Panupinthu, N., Crawford, D.T., Grasser, W.A., Paralkar, V.M., Li, M., Audoly, L.P., Gabel, C.A., Jee, W.S.S., Dixon, S.J., Sims, S.M. & Thompson, D.D., 2003. Deletion of the P2X7 Nucleotide Receptor Reveals Its Regulatory Roles in Bone Formation and Resorption. *Molecular Endocrinology*, 17(7), pp.1356–1367.

Kenis, H., Hofstra, L. & Reutelingsperger, C.P.M., 2007. Annexin A5: Shifting from a diagnostic towards a therapeutic realm. *Cellular and Molecular Life Sciences*, 64(22), pp.2859–2862.

Kersemans, V., Cornelissen, B., Allen, P.D., Beech, J.S. & Smart, S.C., 2013. Subcutaneous tumor volume measurement in the awake, manually restrained mouse using MRI. *Journal of Magnetic Resonance Imaging*, 37(6), pp.1499–1504.

Khanna, C., Prehn, J., Yeung, C., Caylor, J., Tsokos, M. & Helman, L., 2000. An orthotopic model of murine osteosarcoma with clonally related variants differing in pulmonary metastatic potential. *Clinical and Experimental Metastasis*, 18(3), pp.261–271.

Kim, S.J., Kim, B.S., Choi, C.W., Choi, J., Kim, I., Lee, Y.H. & Kim, J.S., 2007. Ki-67 expression is predictive of prognosis in patients with stage I/II extranodal NK/T-cell lymphoma, nasal type. *Annals of Oncology*, 18(8), pp.1382–1387.

Kugelgen, I.V., Hoffman, K., 2016. Pharmacology and Structure of P2Y receptors. *Neuropharmacology.* 104, pp. 50-61

LaRue, S.M., Withrow, S.J., Powers, B.E., Wrigley, R.H., Gillette, E.L., Schwarz, P.D., Straw, R.C. & Richter, S.L., 1989. Limb-sparing treatment for osteosarcoma in dogs. *Journal of the American Veterinary Medical Association*, 195(12), pp.1734–44.

Le Nail, L.R., Brennan, M., Rosset, P., Deschaseaux, F., Piloquet, P., Pichon, O., Le Caignec, C., Crenn, V., Layrolle, P., Hérault, O., De Pinieux, G.D. & Trichet, V., 2018. Comparison of tumor-and bone marrow-derived mesenchymal stromal/stem cells from patients with high-grade osteosarcoma. *International Journal of Molecular Sciences*, 19(3) e.707.

Lenertz, L.Y., Baughman, C.J, Waldschmidt, N.V, Thaler, R., van Wijnen, A.J., 2015. Control of bone development by P2X and P2Y receptors expressed in mesenchymal and hematopoietic cells. *Gene*, 1:570 (1) pp.1-7.

Li, F.P. & Fraumeni, J.F., 1969. Soft-tissue sarcomas, breast cancer, and other neoplasms. A familial syndrome? *Annals of Internal Medicine*, 71(4), pp.747–752.

Li, J., Liu, D., Ke, H.Z., Duncan, R.L, & Turner, C.H., 2005 The P2X7 nucleotide receptor mediates skeletal mechanotransduction. *Journal of Biological Chemistry,* 280 pp. 42952–42959

Li, J., Meyer, R., Duncan, R.L., & Turner, C.H., 2009 P2X7 nucleotide receptor plays an important role in callus remodelling during fracture repair. *Calcified Tissue International* 84 pp. 405–412.

Lin, D., Qiming, F., Bing, T., Wei, Y. & Tingting, T., 2014. Establishment and characterization of a new highly metastatic human osteosarcoma cell line. *Clin Exp Metastasis*, 7(6), pp.2871–2882.

Lindsey, B.A., Markel, J.E. & Kleinerman, E.S., 2017. Osteosarcoma Overview. *Rheumatology and Therapy*, 4(1), pp.25–43.

Lisle, J.W., Choi, J.Y., Horton, J.A., Allen, M.J. & Damron, T.A., 2008. Metastatic osteosarcoma gene expression differs in vitro and in vivo. *Clinical Orthopaedics and Related Research*, 466(9), pp.2071–2080.

Longhi, A., Errani, C., De Paolis, M., Mercuri, M. & Bacci, G., 2006. Primary bone osteosarcoma in the pediatric age: State of the art. *Cancer Treatment Reviews*, 32(6), pp.423–436.

Luderman, L.N., Unlu, G. & Knapik, E.W., 2017. Zebrafish Developmental Models of Skeletal Diseases. *Current Topics in Developmental Biology*, 124, pp.81–124.

Lustig, K.D., Shiau, A.K., Brake, A.J., & Julius, D., 1993. Expression cloning of an ATP receptor from mouse neuroblastoma cells. *Proc Natl Acad Sci USA,* 90(11), pp. 5113-5117.

Luu, H.H., Kang, Q., Park, J.K., Si, W., Luo, Q., Jiang, W., Montag, A.G., Simon, M.A., Peabody, T.D., Haydon, R.C., Rinker-schaeffer, C.W. & He, T., 2005. An orthotopic model of human osteosarcoma growth and spontaneous pulmonary metastasis., pp.319–329.

Mardanpour, K., Rahbar, M. & Mardanpour, S., 2016. Coexistence of HER2, Ki67, and p53 in osteosarcoma: A strong prognostic factor. *North American Journal of Medical Sciences*, 8(5), pp.210–214.

Martin, D.S., Bertino, J.R. & Koutcher, J.A., 2000. Perspectives in Cancer Research ATP Depletion ⁄ Pyrimidine Depletion Can Markedly Enhance Cancer Therapy : Fresh Insight for a New Approach 1., pp.6776–6783.

Martin, J.W., Squire, J.A. & Zielenska, M., 2012. The Genetics of Osteosarcoma. *Sarcoma*, 2012, pp.1–11.

Martin, T.J., Ingleton, P.M., Underwood, J.C., Michelangeli, V.P., Hunt, N.H. & Melick, R.A., 1976. Parathyroid hormone-responsive adenylate cyclase in induced transplantable osteogenic rat sarcoma. *Nature*, 260(5550), pp.436–8.

Martinez-Lage, M., Puig-Serra, P., Menendez, P., Torres-Ruiz, R., Rodriguez-Perales, S., 2018. CRISPR/Cas9 for Cancer Therapy: Hopes and Challenges. *Biomedicines* 12;6 (4) pp.E105.

Mayordomo, E., Machado, I., Giner, F., Kresse, S.H., Myklebost, O., Carda, C., Navarro, S. & Llombart-Bosch, A., 2010. A tissue microarray study of osteosarcoma: histopathologic and immunohistochemical validation of xenotransplanted tumors as preclinical models. *Applied immunohistochemistry & molecular morphology : AIMM*, 18(5), pp.453–61.

McAllister, R.M., Gardner, M.B., Greene, A.E., Bradt, C., Nicholas, W.W. & Landing, B.H., 1971. Culltivation *in Vitro* of Cells Derived From a Human Osteosarcoma. *Cancer*, 27, pp.397–402.

McClung, M., 2007. Role of RANKL inhibition in osteoporosis. *Arthritis Research and Therapy*, 9, pp.1–6.

Michel, A.D., Ng, S.W., Roman, S., Clay, W.C., Dean, D.K. & Walter, D.S., 2009. Mechanism of action of species-selective P2X 7 receptor antagonists. *British Journal of Pharmacology*, 156(8), pp.1312–1325.

Michel, A.D., Xing, M. & Humphrey, P.P.A., 2001. potency at P2X7 receptors. , pp.1501–1508.

Minotti, G., Menna, P., Salvatorelli, E., Cairo, G., Gianni, L., 2004. Anthracyclines: Molecular Advances and Pharmacologic Developments in Antitumor Activity and Cardiotoxicity. *Pharmacological Reviews*, 56(2), pp.185–229.

Mirabello, L., Troisi, R.J. & Savage, S.A., 2009. Osteosarcoma incidence and survival rates from 1973 to 2004: Data from the surveillance, epidemiology, and end results program. *Cancer*, 115(7), pp.1531–1543.

Misdorp, W. (Netherlands C.I., 1980. Animal model of human disease: Skeletal Osteosarcoma. *American Journal of Pathology*, 96(1), pp.2–5.

Mittal, N., Kent, P.M. & Ording, J., 2013. Metastatic and recurrent bone primary bone cancers. *Current Problems in Cancer*, 37(4), pp.215–224.

Mohseny, A.B., Xiao, W., Carvalho, R., Spaink, H.P. & Hogendoorn, P.C.W., 2012. An osteosarcoma zebrafish model implicates Mmp-19 and Ets-1 as well as reduced host immune response in angiogenesis and migration. *J Pathol*, 227, pp.245–253.

Mohseny, A.B., MacHado, I., Cai, Y., Schaefer, K.L., Serra, M., Hogendoorn, P.C.W., Llombart-Bosch, A. & Cleton-Jansen, A.M., 2011. Functional characterization of osteosarcoma cell lines provides representative models to study the human disease. *Laboratory Investigation*, 91(8), pp.1195–1205.

Morandini, A.C., Eduardo, L. & Savio, B., 2014. The Role of P2X7 Receptor in Infectious Inflammatory Diseases and the Influence of Ectonucleotidases. *Biomed J,* 37 (4) pp169-177

Muff, R., Nigg, N., Gruber, P., Walters, D., Born, W. & Fuchs, B., 2007. Altered morphology, nuclear stability and adhesion of highly metastatic derivatives of osteoblast-like SAOS-2 osteosarcoma cells. *Anticancer Research*, 27(6 B), pp.3973–3979.

Muff, R., Ram Kumar, R.M., Botter, S.M., Born, W. & Fuchs, B., 2012. Genes regulated in metastatic osteosarcoma: Evaluation by microarray analysis in four human and two mouse cell line systems. *Sarcoma,* pp.1-13

Mussig, K., Wehrmann, T., Dittmann, H., Wehrmann, M., Ueberberg, B., Schulz, S., Bares, R. & Petersenn, S., 2012. Expression of the proliferation marker Ki-67

associates with tumour staging and clinical outcome in differentiated thyroid carcinomas. *Clinical Endocrinology*, 77(1), pp.139–145.

Muz, B., de la Puente, P., Azab, F. & Azab, A.K., 2015. The role of hypoxia in cancer progression, angiogenesis, metastasis, and resistance to therapy. *Hypoxia*, 3, pp.83–92.

Nakamura, E.I., Uezono, Y., Narusawa, K.I., Shibuya, I., Oishi, Y., Tanaka, M., Yanagihara, N., Nakamura, T & Izumi F., 2000. ATP activates DNA synthesis by acting on P2X receptors in human osteoblast-like MG-63 cells *Am J Physiol Cell Physiol*, *279,* pp.510–519.

Nicolaidou, V., Wong, M.M., Redpath, A.N., Ersek, A., Baban, D.F., Williams, L.M., Cope, A.P.,Horwood, N.J., 2012. Monocytes induce STAT3 activation in human mesenchymal stem cells to promote osteoblast formation. *PLos ONE* 7, e39871.

North, R., 2002. Molecular physiology of P2X receptors. *Physiological reviews*, 82(4), p.1013–67.

Orimo, H., Goseki-Sone, M., Hosoi, T. & Shimada, T., 2008. Functional assay of the mutant tissue-nonspecific alkaline phosphatase gene using U2OS osteoblast-like cells. *Molecular Genetics and Metabolism*, 94(3), pp.375–381.

Orriss, I.R., 2015. The role of purinergic signalling in the musculoskeletal system. *Autonomic Neuroscience*, 191, pp.124–134.

Orriss, I.R., & Arnett, T.R., 2012. P2Y receptors in bone. *WIREs Membr Transp Signal*, 1:pp.805–814.

Orriss, I.R., Burnstock, G. & Arnett, T.R., 2010. Purinergic signalling and bone remodelling. *Current Opinion in Pharmacology*, 10(3), pp.322–330.
Orriss, I.R., Knight, G.E., Ranasinghe, S., Burnstock, G. & Arnett, T.R., 2006. Osteoblast responses to nucleotides increase during differentiation. *Bone*, 39(2), pp.300–309.

Orriss, I.R., Syberg, S., Wang, N., Robaye, B., Gartland, A., Jorgensen, N., Arnett, T.R., Boeynaems, J.M., 2011. Bone phenotypes displayed by P2 receptor knockout mice. *Front Biosci*, S3:pp.1038–1046.

Oryan, A., Alidadi, S. & Moshiri, A., 2015. Osteosarcoma. *Current Orthopaedic Practice*, 26(2), pp.181–198.

Pacheco, P., Ferreira, L., Mendonça, L., Ferreira, D., Salles, J., Faria, R., Teixeira, P.C. & Alves L.A, 2016. P2X7 receptor as a novel drug delivery system to increase the entrance of hydrophilic drugs into cells during photodynamic therapy. *J Bioenerg Biomembr.*, 48(4), pp.397–411.

Panupinthu, N., Rogers, J.T., Zhao, L., Solano-Flores, L.P., Possmayer, F., Sims, S.M. & Dixon, S.J., 2008. P2X7 receptors on osteoblasts couple to production of lysophosphatidic acid: A signaling axis promoting osteogenesis. *Journal of Cell Biology*, 181(5), pp.859–871.

Partridge, N.C., Alcorn, D., Michelangeli, V.P., Ryan, G., Martin, T.J., Partridge, N.C., Alcorn, D., Michelangeli, V.P., Ryan, G. & Martin, T.J., 1983. Morphological and Biochemical Characterization of Four Clonal Osteogenic Sarcoma Cell Lines of Rat Origin. *Cancer Research*, 43(9), pp.4308–4314.

Pautke, C., Schieker, M., Tischer, T., Kolk, A., Neth, P., Mutschler, W. & Milz, S., 2004. Characterization of osteosarcoma cell lines MG-63, Saos-2 and U-2 OS in comparison to human osteoblasts. *Anticancer Research*, 24(6), pp.3743–3748.

Pelegrín, P., 2011. Many ways to dilate the P2X7 receptor pore. *British Journal of Pharmacology*, 163(5), pp.908–911.

Pellegatti, P., Raffaghello, L., Bianchi, G., Piccardi, F., Pistoia, V. & Di Virgilio, F., 2008. Increased Level of Extracellular ATP at Tumor Sites: In Vivo Imaging with Plasma Membrane Luciferase. *PLoS ONE*, 3(7), p.e2599.

Piperno-Neumann, S., Le Deley, M.C., Rédini, F., Pacquement, H., Marec-Bérard, P., Petit, P., Brisse, H., Lervat, C., Gentet, J.C., Entz-Werlé, N., Italiano, A., Corradini, N., Bompas, E., Penel, N., Tabone, M.D., Gomez-Brouchet, A., Guinebretière, J.M., Mascard, E., Gouin, F., Chevance, A., Bonnet, N., Blay, J.Y. & Brugières, L., 2016. Zoledronate in combination with chemotherapy and surgery to treat osteosarcoma (OS2006): a randomised, multicentre, open-label, phase 3 trial. *The Lancet Oncology*, 17(8), pp.1070–1080.

Pontén, J. & Saksela, E., 1967. Two established *in vitro* cell lines from human mesenchymal tumours. *International journal of cancer*, 2(5), pp.434–47.

Pittenger, M.F., Mackay, A.M., Beck, S.C., Jaiswal, R.K., Douglas, R., Mosca, J.D., Moorman, M.A., Simonetti, D.W., Craig, S., Marshak, D.R., 1999. Multilineage potential of adult human mesenchymal stem cells. *Science*, 284, pp.143-147.

Posthumadeboer, J., Witlox, M.A., Kaspers, G.J.L. & Van Royen, B.J., 2011. Molecular alterations as target for therapy in metastatic osteosarcoma: A review of literature. *Clinical and Experimental Metastasis*, 28(5), pp.493–503.

Potter, B.K., 2016. CORR Insights®: How Much Clinical and Functional Impairment do Children Treated With Knee Rotationplasty Experience in Adulthood? *Clinical orthopaedics and related research*, 474(4), pp.1005–7.

Pradhan, a, Reddy, K.I. a, Grimer, R.J., Abudu, a, Tillman, R.M., Carter, S.R. & Jeys, L., 2015. Osteosarcomas in the upper distal extremities: are their oncological outcomes similar to other sites? *European journal of surgical oncology : the journal of the European Society of Surgical Oncology and the British Association of Surgical Oncology*, 41(3), pp.407–12.

Qiu, Y., Li, W.H., Zhang, H. Q., Liu, Y., Tian, X. X. & Fang, W. G., 2014. P2X7 mediates ATP-driven invasiveness in prostate cancer cells. *PloS one*, 9(12), pp.e114371.

Raffaghello, L., Chiozzi, P., Falzoni, S., Virgilio, F. Di & Pistoia, V., 2006. The P2X 7 Receptor Sustains the Growth of Human Neuroblastoma Cells through a Substance P – Dependent Mechanism., (2), pp.907–915.

Ren, S., Zhang, Y., Wang, Y., Lui, Y., Wei, W., Huang, X., Mao, W. & Zuo, Y., 2010. Targeting P2X7 receptor inhibits the metastasis of murine P388D1 lymphoid neoplasm cells to lymph nodes. *Cell biology international*, 34(12), pp.1205–11.

Ren, W. & Gu, G., 2015. Prognostic implications of *RB1* tumour suppressor gene alterations in the clinical outcome of human osteosarcoma: a meta-analysis. *European Journal of Cancer Care*, 1.

Rhim JS, Park DK, Arnstein P, Huebner RJ, Weisburger EK, N.-R.W., 1975a. Transformation of human cells in culture by N-methyl-N'-nitro-N-nitrosoguanidine. *Nature*, 256(5520), pp.751–3.

Rhim JS, Cho HY, Vernon ML, Arnstein P, Huebner RJ, G.R., 1975b. Characterization of non-producer human cells induced by Kirsten sarcoma virus. *Int J Cancer.*, 15(1), pp.23–9.

Richter, H., Randau, L., Plagens, A., 2013. Exploiting CRISPR/Cas: Interference Mechanisms and Applications. *Int. J. Mol. Sci.*14 (7) pp.14518-31.

Roger, S., Jelassi, B., Couillin, I., Pelegrin, P., Besson, P. & Jiang, L.H., 2015. Understanding the roles of the P2X7 receptor in solid tumour progression and therapeutic perspectives. *Biochimica et Biophysica Acta - Biomembranes*, 1848(10), pp.2584–2602.

Rowell, J.L., McCarthy, D.O. & Alvarez, C.E., 2011. Dog models of naturally occurring cancer. *Trends in Molecular Medicine*, 17(7), pp.380–388.

Rumney, R.M.H., Sunters, A., Reilly, G.C. & Gartland, A., 2012. Application of multiple forms of mechanical loading to human osteoblasts reveals increased ATP release in response to fluid flow in 3D cultures and differential regulation of immediate early genes. *Journal of Biomechanics*, 45(3), pp.549–554.

Rumney, R.M.H., Wang, N., Agrawal, A. & Gartland, A., 2012. Purinergic signaling in bone. Front Endocrinol, 3, pp.1–7.

Sahai, E., 2005. Mechanisms of cancer cell invasion. *Current Opinion in Genetics and Development*, 15(1), pp.87–96.

Saraf, A.J., Fenger, J.M. & Roberts, R.D., 2018. Osteosarcoma: Accelerating Progress Makes for a Hopeful Future. *Frontiers in Oncology*, 8, pp.1–7.

Savage, S.A. & Mirabello, L., 2011. Using Epidemiology and Genomics to Understand Osteosarcoma Etiology. *Sarcoma*, 2011, pp.1–13.

Schmidt, J., Strauß, G.P., Schön, A., Luz, A., Murray, A.B., Melchiori, A., Aresu, O. & Erfle, V., 1988. Establishment and characterization of osteogenic cell lines from a spontaneous murine osteosarcoma. *Differentiation*, 39(3), pp.151–160.

Schrader, M., Mu, M., Straub, B. & Miller, K., 2001. The impact of chemotherapy on male fertility : a survey of the biologic basis and clinical aspects., 15, pp.611–617.

Scotlandi, K., Serra, M., Manara, M.C., Maurici, D., Benini, S., Nini, G., Campanacci,

M. & Baldini, N., 1995. Clinical relevance of Ki-67 expression in bone tumors. *Cancer*, 75(3), pp.806–814.

Silverman, M.H., Strand, V., Markovits, D., Nahir, M., Reitblat, T., Molad, Y., Rosner, I., Rozenbaum, M., Mader, R., Adawi, M., Caspi, D., Tishler, M., Langevitz, P., Rubinow, A., Friedman, J., Green, L., Tanay, A., Ochaion, A., Cohen, S., Kerns, W.D., Cohn, I., Fishman-Furman, S., Farbstein, M., Yehuda, S.B. & Fishman, P., 2008. Clinical evidence for utilization of the A3 adenosine receptor as a target to treat rheumatoid arthritis: data from a phase II clinical trial. *The Journal of rheumatology*, 35(1), pp.41–8.

Simpson, S., Dunning, M.D., de Brot, S., Grau-Roma, L., Mongan, N.P. & Rutland, C.S., 2017. Comparative review of human and canine osteosarcoma: morphology, epidemiology, prognosis, treatment and genetics. *Acta veterinaria Scandinavica*, 59(1), p.71-81.

Sisay, M., Mengistu, G. & Edessa, D., 2017. The RANK/RANKL/OPG system in tumorigenesis and metastasis of cancer stem cell: Potential targets for anticancer therapy. *OncoTargets and Therapy*, 10, pp.3801–3810.

Sitcheran, R., Cogswell, P.C., Baldwin Jr, A.S., 2003. NF-KappaB mediates inhibition of mesenchymal cell differentiation through a posttranslational gene silencing mechanism. *Genes Dev*, 17, pp.2368-2373.

Skarin, A.,& Canellos, G.P., 2002. Atlas of Diagnostic Oncology*,* Mosby 3rd Edition.

Sluyter, R. & Stokes, L., 2011. Significance of P2X7 receptor variants to human health and disease. *Recent Pat DNA Gene Seq*, 5, pp.41–54.

Smart, M.L., Gu, B., Panchal, R.G., Wiley, J., Cromer, B., Williams, D.A. & Petrou, S., 2003. P2X7 receptor cell surface expression and cytolytic pore formation are regulated by a distal C-terminal region. *Journal of Biological Chemistry*, 278(10), pp.8853–8860.

Soliman Nahed, A. & Yussif Shaimaa, M., 2016. Ki-67 as a prognostic marker according to breast cancer molecular subtype. *Cancer Biology & Medicine*, 13(4), pp.496-504.

Solle, M., Labasi, J., Perregaux, D.G., Stam, E., Petrushova, N., Koller, B.H., Griffiths, R.J., Gabel, C.A., 2001. Altered cytokine production in mice lacking P2X7 receptors. *J. Biol. Chem.* 276, pp.125–132.

Soomro, I.N., Holmes, J. & Whimster, W.F., 1998. Predicting Prognosis in Lung Cancer : Use of Proliferation marker Ki-67 monoclonal antibody. *J Pak Med Assoc* 48 (3) pp.66-69.

Spangrude, G.J., Heimfeld, S., Weissman, I.L., 1988. Purification and characterization of mouse hematopoietic stem cells. *Science* 241, pp.58–62.

Spitsbergen, J.M., Tsai, H.-W., Reddy, A., Miller, T., Arbogast, D., Hendricks, J.D. & Bailey, G.S., 2000. Neoplasia in Zebrafish (Danio rerio) Treated with 7,12-Diniethylbenz[a]anthracene by Two Exposure Routes at Different Developmental Stages. *Toxicol Pathol*, 28, pp.705–15.

Spoorendonk, K.M., Hammond, C.L., Huitema, L.F.A., Vanoevelen, J. & Schulte-Merker, S., 2010. Zebrafish as a unique model system in bone research: the power of genetics and *in vivo* imaging. *Journal of Applied Ichthyology*, 26(2), pp.219–224.

Stebbing, J., Paz, K., Schwartz, G.K., Wexler, L.H., Maki, R., Pollock, R.E., Morris, R., Cohen, R., Shankar, A., Blackman, G., Harding, V., Vasquez, D., Krell, J., Ciznadija, D., Katz, A. & Sidransky, D., 2014. Patient-derived xenografts for individualized care in advanced sarcoma. *Cancer*, 120(13), pp.2006–2015.

Stepanenko, A., & Dmitrenko., 2015. HEK293 in cell biology and cancer research: phenotype, karyotype, tumorigenicity and stress induced genome-phenotype evolution. *Gene* 569(2), pp. 182-190.

Stepanenko, A. & Heng, H., 2017. Transient and stable vector transfection: Pitfalls, off-target effects, artifacts. *Mutation Research*, 773, pp.91–103.

Stewart, E., Federico, S.M., Chen, X., Shelat, A.A., Bradley, C., Gordon, B., Karlstrom, A., Twarog, N.R., Clay, M.R., Bahrami, A., Freeman, B.B., Xu, B., Zhou, X., Wu, J., Honnell, V., Ocarz, M., Blankenship, K., Dapper, J., Mardis, E.R., Wilson, R.K., Downing, J., Zhang, J., Easton, J., Pappo, A. & Dyer, M.A., 2017. Orthotopic patient-derived xenografts of paediatric solid tumours. *Nature*, 549(7670), pp.96–100.

Stiller, C., Craft, A. & Corazziari, I., 2001. Survival of children with bone sarcoma in Europe since 1978: results from the EUROCARE study. *European Journal of Cancer*, 37(6), pp.760–766.

Sun, D., Junger, W.G., Yuan, C., Zhang, W., Bao, Y., Qin, D., Wang, C., Tan, L., Qi, B., Zhu, D., Zhang, X., Yu, T., 2013. Shockwaves induce osteogenic differentiation of human mesenchymal stem cells through ATP release and activation of P2X7 receptors. *Stem Cells* 31, pp.1170–1180.

Syberg, S., Petersen, S., Beck Jensen, J.E., Gartland, A., Teilmann, J., Chessell, I., Steinberg, T.H., Schwarz, P., & Jorgensen, N.R., 2012 Genetic background strongly influences the bone phenotype of P2X7 receptor knockout mice. *Journal of Osteoporosis,* 391097.

Syed, N. i H. & Kennedy, C., 2012. Pharmacology of P2X receptors. *Wiley Interdisciplinary Reviews: Membrane Transport and Signaling*, 1(1), pp.16–30.

Tafani, M., Schito, L., Pellegrini, L., Villanova, L., Marfe, G., Anwar, T., Rosa, R., Indelicato, M., Fini, M., Pucci, B. & Russo, M.A., 2011. Hypoxia-increased RAGE and P2X7R expression regulates tumor cell invasion through phosphorylation of Erk1 / 2 and Akt and nuclear translocation of NF- k B. , 32(8), pp.1167–1175.

Takahashi, N., Akatsu, T., Udagawa, N., Sasaki, T., Yamaguchi, A., Moseley, J.M., Martin, T.J., Suda, T., 1988. Osteoblastic cells are involved in osteoclast formation. *Endocrinology* 123, pp.2600–2602.

Takai, E., Tsukimoto, M., Harada, H., Sawada, K., Moriyama, Y. & Kojima, S., 2012. Autocrine regulation of TGF- 1-induced cell migration by exocytosis of ATP and activation of P2 receptors in human lung cancer cells. *Journal of Cell Science*, 125(21), pp.5051–5060.

Takai, E., Tsukimoto, M., Harada, H. & Kojima, S., 2014. Autocrine signaling via release of ATP and activation of P2X7 receptor influences motile activity of human lung cancer cells., *Purinergic Signalling*, 10 (3) pp.487–497.

Tang, R., Saksena, M., Coopey, S.B., Fernandez, L., Buckley, J.M., Lei, L., Aftreth, O., Koerner, F., Michaelson, J., Rafferty, E., Brachtel, E. & Smith, B.L., 2016. Intraoperative micro-computed tomography (micro-CT): A novel method for determination of primary tumour dimensions in breast cancer specimens. *British Journal of Radiology*, 89(1058), pp.1–7.

Taran, S., Taran, R. & Malipatil, N., 2017. Pediatric osteosarcoma: An updated review. *Indian Journal of Medical and Paediatric Oncology*, 38(1), p.33.

Taupin, T., Decouvelaere, A. V., Vaz, G. & Thiesse, P., 2016. Accuracy of core needle biopsy for the diagnosis of osteosarcoma: A retrospective analysis of 73 patients. *Diagnostic and Interventional Imaging*, 97(3), pp.325–329.

Thaler, R., Sturmlechner, I., Spitzer, S., Riester, S.M., Rumpler, M., Zwerina, J., Klaushofer,K., van Wijnen, A.J., Varga, F., 2014. Acute-phase protein serum amyloid A3 is a novel paracrine coupling factor that controls bone homeostasis. *Federation of American Societies for Experimental Biology.* 29, pp.1344–1359.

Thomas, D.M., Carty, S.A., Piscopo, D.M., Lee, J.-S., Wang, W.-F., Forrester, W.C. & Hinds, P.W., 2001. The Retinoblastoma Protein Acts as a Transcriptional Coactivator Required for Osteogenic Differentiation. *Molecular Cell*, 8(2), pp.303–316.

Tian, X., Gu, T., Patel, S., Bode, A.M., Lee, M., Dong, Z., 2019. CRISPR/Cas9 - An evolving biological tool kit for cancer biology and oncology. *NPJ Precision oncology* 18;3:8, eCollection 2019.

Ulrich, H., Ratajczak, M.Z., Schneider, G., Adinolfi, E., Orioli, E., Ferrazoli, E.G., Glaser, T., Corrêa-Velloso, J., Martins, P.C.M., Coutinho, F., Santos, A.P.J., Pillat, M.M., Sack, U. & Lameu, C., 2018. Kinin and purine signaling contributes to neuroblastoma metastasis. *Frontiers in Pharmacology*, 9, pp.1–17.

Uluçkan, Ö., Segaliny, A., Botter, S., Santiago, J.M. & Mutsaers, A.J., 2015. Preclinical mouse models of osteosarcoma., *Bonekey Rep,* 6 (4), pp.670-676.

Valera, S., Hussy, N., Evans, R.J., Adami, N., North, R.A., Suprenant, A., & Buell, G., 1994. A new class of ligand-gated ion channel defined by P2X receptor for extracellular ATP. *Nature.* 371(6497) pp. 516-519.

Vázquez-Cuevas, F.G., Martínez-Ramírez, A.S., Robles-Martínez, L., Garay, E., García-Carrancá, A., Pérez-Montiel, D., Castañeda-García, C. & Arellano, R.O., 2014. Paracrine Stimulation of P2X7 Receptor by ATP Activates a Proliferative Pathway in Ovarian Carcinoma Cells. *Journal of Cellular Biochemistry*, 115(11), pp.1955–1966.

Volonte, C., Apolloni, S., Skaper, S.D., 2012. P2X7 Receptors : Channels, Pores and More. CNS *Neurol Disord Drug Targets,* 11(6) pp705-721.

von Kugelgen, I., 2006. Pharmacological profiles of cloned mammalian P2Y-receptor sub-types. *Pharmacology & Therapeutics*. 110, pp.415–432.

Wagner, E.F., 2010. Bone development and inflammatory disease is regulated by AP-1(Fos/Jun). Ann. Rheum. Dis. 69 (Suppl. 1), pp.i86–i88.

Walkley, C.R., Qudsi, R., Sankaran, V.G., Perry, J.A., Gostissa, M., Roth, S.I., Rodda, S.J., Snay, E., Dunning, P., Fahey, F.H., Alt, F.W., McMahon, A.P. & Orkin, S.H., 2008. Conditional mouse osteosarcoma, dependent on p53 loss and potentiated by loss of Rb, mimics the human disease. *Genes & development*, 22(12), pp.1662–76.

Wang, J., Sun, Q., Morita, Y., Jiang, H., Gross, A., Lechel, A., Hildner, K., Guachalla, L.M., Gompf, A., Hartmann, D., Schambach, A., Wuestefeld, T., Dauch, D., Schrezenmeier, H., Hofmann, W.K., Nakauchi, H., Ju, Z., Kestler, H.A., Zender, L., Rudolph, K.L., 2012. A differentiation checkpoint limits hematopoietic stem cell self-renewal in response to DNA damage. *Cell* 148, pp.1001–1014.

Wang, N., Agrawal, A., Jørgensen, N.R. & Gartland, A., 2018. P2X7 receptor regulates osteoclast function and bone loss in a mouse model of osteoporosis. *Scientific Reports*, 8(1), pp.1–10.

Wang, N., Robaye, B., Gossiel, F., Boeynaems, J.M., Gartland, A., 2014. The P2Y13 receptor regulates phosphate metabolism and FGF-23 secretion with effects on skeletal development. *FASEB J.: Off. Publ. Fed. Am. Soc. Exp. Biol.* 28, pp.2249–2259.

Wang, Z., Liang, J., Schellander, K., Wang, Z., Liang, J., Schellander, K., Wagner, E.F. & Grigoriadis, A.E., 1995. c- fos -induced Osteosarcoma Formation in Transgenic Mice : Cooperativity with c- jun and the Role of Endogenous c-fos. *Cancer Res*, 55(24), pp.6244–6251.

Webb, T.E., Joseph., S., Krishek, B.J., Alan., B., Trevor.G, S., King, B.F., Burnstock, G., Bateson, A.N. & Barnarda, E.A., 1993. Cloning and functional expression of a brain G-protein-coupled receptor ATP. *Federation of European Biochemtcal Societies*, 324(2), pp.219–225.

Weinberg, R.A., 1995. The retinoblastoma protein and cell cycle control. *Cell*, 81(3), pp.323–330.

Weissman, I.L., 2000.Translating stem and progenitor cell biology to the clinic: barrier sand opportunities. *Science* 287, pp.1442–1446.

White, N. & Butler, P.E.M., 2005. Human melanomas express functional P2X7 receptors., pp.411–418.

Worthington, R.A., Smart, M.L., Gu, B.J., Williams, D.A., Petrou, S., Wiley, J.S. & Barden, J.A.Y., 2006. Point mutations confer loss of ATP-induced human P2X7 receptor function. , 512(2002), pp.43–46.

Wu, J.X., Xu, M.Y., Miao, X.R., Lu, Z.J., Yuan, X.M., Li, X.Q. & Yu, W.F., 2012. Functional up-regulation of P2X3 receptors in dorsal root ganglion in a rat model of bone cancer pain. *European journal of pain*, 16, pp.1378–88.

Wunder, J.S., Gokgoz, N., Parkes, R., Bull, S.B., Eskandarian, S., Davis, A.M., Beauchamp, C.P., Conrad, E.U., Grimer, R.J., Healey, J.H., Malkin, D., Mangham, D.C., Rock, M.J., Bell, R.S. & Andrulis, I.L., 2005. TP53 mutations and outcome in

osteosarcoma: A prospective, multicenter study. *Journal of Clinical Oncology*, 23(7), pp.1483–1490.

Xia, J., Yu, X., Tang, L., Li, G. & He, T., 2015. P2X7 receptor stimulates breast cancer cell invasion and migration via the AKT pathway. *Oncology Reports*, 34(1), pp.103–110.

Young, C.N.J. & Górecki, D.C., 2018. P2RX7 Purinoceptor as a Therapeutic Target—The Second Coming? *Frontiers in Chemistry*, 6, pp.1–14.

Yu, Z., Sun, H., Fan, Q., Long, H., Yang, T. & Ma, B., 2009. Establishment of reproducible osteosarcoma rat model using orthotopic implantation technique. *Oncology Reports*, 21(5), pp.1175–1180.

Yuan, J., Ossendorf, C., Szatkowski, J.P., Bronk, J.T., Yaszemski, M., Bolander, M.E., Sarkar, G. & Fuchs, B., 2010. Osteoblastic and Osteolytic Human Osteosarcomas can be Studied with a new Xenograft Mouse Model Producing Spontaneous Metastases. , 27(4), pp.435–442.

Zhang, Y., Gong, L.H., Zhang, HQ., Du, Q., You, J.F., Tian, X.X. & Fang, W.G., 2010. Extracellular ATP enhances in vitro invasion of prostate cancer cells by activating Rho GTPase and upregulating MMPs expression. *Cancer Letters*, 293(2), pp.189–197.

Zhu, L., McManus, M.M. & Hughes, D. P. M., 2013. Understanding the Biology of Bone Sarcoma from Early Initiating Events through Late Events in Metastasis and Disease Progression. *Frontiers in Oncology*, 3, pp.1–17.

List of awards, publications and presentations

Awards:

Bone Research Society – Travel Bursary to attend the International Purine Meeting 'Basic and translational science on purinergic signalling and its components for a healthy and better world' in Foz Do Iguazu, Brazil (2018).

Bone Research Society – The Barbara Mawer Travelling Fellowship awarded for a project entitled: *'Investigating extracellular ATP in the tumour microenvironment of osteosarcoma using the plasma membrane-targeted luciferase (pmeLUC) probe'* carried out in the laboratory of Dr Elena Adinolfi at Università degli Studi di Ferrara, Department of Morphology, Surgery and Experimental Medicine, Section of Pathology, Oncology and Experimental Biology, Italy, (2017).

Bone Research Society – Best Research Poster awarded for '*P2X7RA or P2X7RB expression confers a growth advantage to Te85 osteosarcoma cells in vitro'* at the Bone Research Society Annual Meeting, Liverpool, UK, (2016).

Publications:

Tattersall. L, Davison. Z, Gartland. A: Osteosarcoma, Encyclopaedia of Bone Biology, Elsevier, In Press

Accepted presentations:

2018 **Oral Presentation** at the International Purine Meeting 'Basic and translational science on purinergic signalling and its components for a healthy and better world' Foz Do Iguazu, Brazil. *'P2X7R in primary bone cancer'* **L. Tattersall**, E. De Marchi, A. Williamson, F. Di Virgilio, M.A. Lawson, E. Adinolfi, A. Gartland

2018 **Poster Presentation** at the Bone Research Society Annual Meeting, Winchester, UK. *'Bone Research Society Barbara Mawer Travelling Fellowship update: Investigating extracellular ATP in the tumour microenvironment of osteosarcoma using the plasma membrane-targeted*

luciferase (pmeLUC) probe' **L. Tattersall,** E. De Marchi, F. Di Virgilio, M.A Lawson, E. Adinolfi, A. Gartland

2017 **Oral Presentation** at the 8th Annual UK Purine Club Symposium, Warwick, UK, *'A pilot study to establish an osteosarcoma in vivo model to target the P2X7R'.* **L. Tattersall,** M.A. Lawson & A. Gartland

2017 **Snap Oral Poster Presentation** at the 8th Annual Mellanby Centre Research day, Sheffield UK, *'Investigating extracellular ATP in the tumour microenvironment of osteosarcoma using the plasma membrane-targeted luciferase (pmeLUC) probe'.* **L. Tattersall,** E. De Marchi, F Di Virgilio, M.A. Lawson, E Adinolfi, A. Gartland

2017 **Oral Presentation** at the Bone Cancer Research Trust Annual Conference, 'United until there's a cure' Birmingham UK. '*Purinergic signalling in osteosarcoma'* **L. Tattersall**, M.A. Lawson & A. Gartland

2017 **Oral Presentation** at the first European Workshop of Translational Research in Bone Sarcoma, Sheffield, UK. *'P2X7R confers a growth advantage and increases metastatic potential of osteosarcoma cells'* **L. Tattersall,** K.M. Shah, M.A. Lawson & A. Gartland

2016 **Poster Presentation** at the 7th annual Mellanby Centre Research day, Sheffield UK, '*Inhibition of P2X7RA isoform with the allosteric inhibitor AZ11645373 decreases proliferation of Te85 osteosarcoma cells*' L. **Tattersall,** K.M Shah, M.A Lawson & A Gartland

2016 **Poster Presentation** at the Bone Research Society Annual Meeting, Liverpool, UK. '*P2X7RA or P2X7RB expression confers a growth advantage to Te85 osteosarcoma cells in vitro'* **L. Tattersall,** K.M. Shah, F.M. Ismail, M.A. Lawson & A. Gartland

Accepted conference abstracts

The International Purine Meeting 'Basic and translational science on purinergic signalling and its components for a healthy and better world' Foz Do Iguazu, Brazil 2018

P2X7R in primary bone cancer

Tattersall. L[1], De Marchi. E[2], Williamson. A[1], Di Virgilio. F[2], Lawson. M.A[1], Adinolfi. E[2], Gartland. A[1]

1 The Mellanby Centre for Bone Research, the University of Sheffield, Sheffield, UK.
2 Department of Morphology, Surgery and Experimental Medicine, Section of Pathology, Oncology and Experimental Biology, University of Ferrara

Osteosarcoma is the most common type of primary bone cancer affecting adolescents attributed to rapid bone growth and turnover. The 5-year survival rate remains 65% and with metastasis this decreases to 20%. This highlights the need for development of novel therapeutics to treat osteosarcoma. In this study we have investigated the role of purinergic signalling in osteosarcoma, as this is particularly pertinent in the bone tumour microenvironment which could contribute towards disease progression.

When Te85 osteosarcoma cells were transfected with P2X7R variants *in vitro,* we observed increased growth compared to naïve cells ($p<0.05$) which was attenuated upon treatment with P2X7R inhibitors ($P<0.0001$). Te85 cell adhesion to collagen was significantly reduced ($P<0.0001$) and migration was significantly increased when cells were treated with BzATP ($P<0.0001$). As Te85 cells have historically not formed osteosarcoma tumours in mice, we next looked at the effect of P2X7RB expression in an MNNG-HOS cell line, an aggressive tumorigenic derivative of Te85 cells. As with the parental Te85 cells, P2X7RB expression decreased cell adhesion ($P<0.0001$) and migration was increased when treated with BzATP ($P<0.0025$).

Next, we injected 250,000 MNNG-HOS+P2X7RB cells paratibially into 7-week old female BALB/c mice. Two-days after cell inoculation treatment with 50 µg/kg of A740003 or PBS vehicle control was administered by IP injection 3 times a week for 3 weeks. All groups developed palpable tumours which did not vary in size as measured by basic calliper measurement at the end of the experiment. Analysis of the tibia using micro-CT scanning demonstrated that the MNNG-HOS+P2X7RB cells resulted in a significant 12% increase in total bone volume in the tumour bearing tibia

when compared to its corresponding leg ($P<0.0123$). This increased bone volume, which consists of ectopic bone formation, was ablated when mice were treated with A740003 ($P<0.0183$).

In conclusion, P2X7R variants were found to influence osteosarcoma cell behaviour *in vitro*. P2X7RB expression in the tumour inducing MNNG-HOS model resulted in a significant increase in total bone volume from ectopic bone formation typical of osteosarcoma tumours. P2X7R antagonism reduced this bone disease. This study provides promising data to support the use of P2X7R inhibitors as a novel therapy for osteosarcoma, however, future studies are required to identify the exact role P2X7RB has in tumour growth and metastasis.

The Bone Research Society Annual Meeting, Winchester, UK 2018.

Bone Research Society Barbara Mawer Travelling Fellowship update: Investigating extracellular ATP in the tumour microenvironment of osteosarcoma using the plasma membrane-targeted luciferase (pmeLUC) probe.

Tattersall. L[1], De Marchi. E[2], Di Virgilio. F[2], Lawson. M.A[1], Adinolfi. E[2], Gartland. A[1]

1 The Mellanby Centre for Bone Research, the University of Sheffield, Sheffield, UK.
2 Department of Morphology, Surgery and Experimental Medicine, Section of Experimental Pathology, Oncology and Biology, University of Ferrara, Ferrara, Italy.

Osteosarcoma is the most common type of primary bone cancer affecting adolescents, attributed to rapid bone growth and turnover, it is a rare incurable disease. The 5-year survival rate remains 65%, which reduces to 20% with metastasis. This highlights the need for development of novel therapeutics to treat osteosarcoma. One potential avenue to explore in the setting of osteosarcoma treatment is purinergic signalling, involving extracellular nucleotides binding to purinergic receptors expressed in many cancers and present on osteoblasts. ATP is at a high concentration in the tumour microenvironment but absent from surrounding healthy tissue. This is particularly pertinent in the bone tumour microenvironment where mechanical loading stimulates ATP release. ATP release from osteosarcoma cells which may depend on the P2X7R isoform expressed, could contribute towards disease progression. Current techniques that quantify ATP levels in biological systems are limited to measuring it in serum or cell supernatants which may be orders of magnitude lower than the levels at the cellular surface. However, pmeLUC is a novel plasmid that allows the measurement of ATP concentrations at the cellular membrane. pmeluc was produced by attaching membrane targeting sequences (N-terminal leader sequence and C-terminal GPI anchor) derived from a folate receptor to a full-length firefly luciferase sequence and was cloned into a pcDNA3 plasmid. Expression of this construct at the outer plasma membrane enables ATP released from cells to be detected in the immediate extracellular space. During a Bone Research Society Barbara Mawer Travelling Fellowship, pmeLUC was transfected into two osteosarcoma cell lines - MNNG-HOS and Te85. Successful transfections were confirmed by measuring ATP levels; and

these cells are currently being used to assess the effect of ATP and P2X7R isoforms on osteosarcoma both *in vitro* and *in vivo*. More sensitive and accurate quantification of ATP levels at the cell surface would better inform us about P2 receptor activation and improve our understanding of the role of purinergic signalling in the tumour microenvironment.

The UK Purine Club Symposium, Warwick, UK, 2017

A pilot study to establish an osteosarcoma *in vivo* model to target the P2X7R

Authors: Tattersall. L, Lawson. M.A, Gartland. A

The Mellanby Centre for Bone Research, the University of Sheffield, Sheffield, UK.

Osteosarcoma is the most common type of primary bone cancer affecting adolescents attributed to rapid bone growth and turnover. The 5-year survival rate remains 65% and with metastasis this decreases to 20%. This highlights the need for development of novel therapeutics to treat osteosarcoma. One potential avenue to explore in the setting of osteosarcoma treatment is purinergic signalling, involving extracellular nucleotides binding to purinergic receptors present on osteoblasts and many cancers. Previous *in vitro* data demonstrates P2X7R expression in Te85 cells results in increased growth which can be attenuated with P2X7R inhibitors. Te85 cells have historically not formed osteosarcoma tumours in mice, however aggressive derivatives of these cells such as MNNG-HOS have. As P2X7R expression can change osteosarcoma cell behaviour it could provide a strong stimulus to enhance Te85 cells into inducing tumour formation. The aim of this study is to see if P2X7R expression can increase tumorigenesis of the Te85 osteosarcoma cell line in nude mice, this can then be used as a model to target the P2X7R *in vivo* in the future.

Seven-week-old BALB/c nude mice were used to assess tumour formation, 3 mice were used for the following cell lines: Te85, Te85+P2X7RA, Te85+P2X7RB, and Te85+P2X7RAB, in addition MNNG-HOS cells known to form tumours were used as a positive control. The mice were injected with 500,000 cells in 20 μl PBS paratibially.

MNNG-HOS cells as expected formed palpable tumours after 9 days, mice were euthanised after three weeks. Micro-CT analysis demonstrated massive bone loss in the injected leg. Te85 cells expressing P2X7R variants did not form palpable tumours after a period of 6 weeks. Micro-CT analysis did however demonstrate a significant reduction in the trabecular bone volume of the Te85+P2X7RAB cells. Further analysis is underway to determine the reason for this loss.

The first European Workshop of Translational Research in Bone Sarcoma, Sheffield, UK, 2017

P2X7R confers a growth advantage and increases metastatic potential of osteosarcoma cells

L. Tattersall, KM. Shah, MA. Lawson & A. Gartland

The Mellanby Centre for Bone Research, the University of Sheffield, Sheffield, UK

Purinergic signalling, the process of ATP binding to extracellular purinergic receptors, is found to be involved in a variety of bone functions such as differentiation, apoptosis and remodelling. Purinergic receptors, in particular the ligand gated ion channel P2X7R, has been found to be highly expressed by a variety of tumours with implications in progression and metastasis. High expression of P2X7R has previously been shown in osteosarcoma tumours. In this study, we provide further data to support P2X7R as a potential new target in osteosarcoma as it confers a growth advantage and increases metastatic potential of osteosarcoma cells *in vitro*.

P2X7R expression was confirmed in transfected Te85 cells by PCR, and function confirmed through pore formation. The naïve and transfected cells were seeded at $5x10^3$ cells and changed into media with 10%, 2% or 0.5% FCS. Proliferation was assessed by MTS assay at day 0,1, 3, 5 and 7. For inhibition studies, cells were seeded at $5x10^3$ in 0.5% FCS and treated with two P2X7R specific antagonists (A740003 and AZ11645373). Proliferation was measured at day 3. For cell adhesion $7.5x10^3$ cells were added to collagen coated 96-well plates and unattached cells were washed away after 4 hours. Cells were lysed and dsDNA quantified using Quant-iT™ PicoGreen® dsDNA Reagent. Statistical analysis was performed in Graphpad Prism® using One-way ANOVA with Tukeys post-hoc test and an unpaired T test for inhibition and cell adhesion studies.

Cells expressing the P2X7R had increased growth rates compared to naïve cells ($P<0.0001$), and both P2X7R inhibitors significantly decreased this ($P<0.0001$). Te85 cell adhesion to collagen was significantly reduced when transfected with the P2X7R ($P<0.0001$).

Our data suggests inhibition of P2X7R may provide a target for treating osteosarcoma.

The inhibitors have proven to be safe in clinical trials for other diseases and therefore could benefit osteosarcoma patients quickly.

The Bone Research Society Annual Meeting, Liverpool, UK, 2016

‘P2X7RA or P2X7RB expression confers a growth advantage to Te85 osteosarcoma cells *in vitro’*

L. Tattersall, K.M. Shah, F.M. Ismail, M.A. Lawson & A. Gartland

The Mellanby Centre for Bone Research, the University of Sheffield, Sheffield, UK

Osteosarcoma is the most common type of primary bone cancer mainly affecting adolescents, it is a rare incurable disease with current treatments including chemotherapy and amputation. Survival statistics have remained constant for a number of years suggesting the need for new treatments. Purinergic signalling involves the binding of extracellular nucleotides including ATP to purinergic receptors and has been found to play a role in many cellular processes. Purinergic signalling acting on bone cells has been demonstrated with roles in differentiation, apoptosis, and bone remodelling. Additionally, purinergic receptors have been found across a variety of cancers with implications in tumour formation, progression and metastasis. High concentrations of ATP have been observed within the tumour microenvironment which could act on the P2X7 receptor, a type of purinergic receptor that acts as a ligand-gated ion channel and plays a role in cell behaviour, including increased cell proliferation. This receptor has been previously found on osteosarcoma tumours. In this study we provide evidence that expression of P2X7R isoforms modulate proliferation of osteosarcoma cells particularly under low serum conditions.

Te85 osteosarcoma cells, either naïve or previously transfected with the P2X7RA or P2X7RB isoform, were seeded at various cell densities (1.25, 2.5 and 5 $x10^3$). After 24 hours, the media was changed to either 10%, 2% or 0.5% FCS. Cell proliferation was assessed using an MTS assay at days 0, 1, 3, 5 and 7. Statistical analysis was performed in Graphpad Prism® using One-way ANOVA with Tukeys post-hoc test and linear regression compared slopes of the growth curves.

At all serum concentrations and cell seeding densities, P2X7RA and P2X7RB had significantly increased growth rates compared to naïve cells ($P<0.0001$ for both), with no difference between the growth rates of P2X7RA and P2X7RB.

The naïve cells had a longer lag phase and caught up with the transfected cells towards day 5 and 7 under 10% serum conditions only.

These results suggest that P2X7RA and P2X7RB expression confers a growth advantage to Te85 osteosarcoma cells in low serum conditions which may contribute to tumour growth and invasiveness. Thus, P2X7R could be a potential new target for treating osteosarcoma.